Circadian regulation of human skeletal muscle function in physiology and insulin resistance

Perrin, Laurent

UNIVERSITÉ DE GENÈVE
Département de biologie moléculaire

FACULTÉ DES SCIENCES
Professeur Robbie Loewith

HÔPITAUX UNIVERSITAIRES DE GENÈVE
Département des spécialités de médecine

FACULTÉ DE MÉDECINE
Professeur Jacques Philippe

UNIVERSITÉ DE GENÈVE
Département de physiologie cellulaire et métabolisme

FACULTÉ DE MÉDECINE
Docteure Charna Dibner

Circadian regulation of human skeletal muscle function in physiology and insulin resistance

THÈSE

présentée à la Faculté des sciences de l'Université de Genève
pour obtenir le grade de Docteur ès sciences, mention biologie

par

Laurent PERRIN
de Genève

Thèse n° 5151

Genève
11 décembre 2017

UNIVERSITÉ DE GENÈVE

FACULTÉ DES SCIENCES

DOCTORAT ÈS SCIENCES, MENTION BIOLOGIE

Thèse de Monsieur Laurent PERRIN

intitulée :

«Circadian Regulation of Human Skeletal Muscle Function in Physiology and Insulin Resistance»

La Faculté des sciences, sur le préavis de Monsieur J. PHILIPPE, professeur ordinaire et directeur de thèse (Faculté de médecine, Département de médecine interne - spécialités), Madame C. DIBNER, docteure et codirecteur de thèse (Faculté de médecine, Département de médecine interne - spécialités), Monsieur R. LOEWITH, professeur ordinaire et codirecteur de thèse (Département de biologie moléculaire), Monsieur E. LEFAI, docteur (Institut National de la Santé et de la Recherche Médicale et Institut National de la Recherche Agronomique, Equipe 2: Régulation de la Masse Musculaire et Désordres Métaboliques, Faculté de Médecine LYON SUD, OULLINS, France) et Monsieur J. RIPPERGER, docteur (Département de biologie, Université de Fribourg, Suisse), autorise l'impression de la présente thèse, sans exprimer d'opinion sur les propositions qui y sont énoncées.

Genève, le 11 décembre 2017

Thèse - 5151 -

Le Doyen

N.B. - La thèse doit porter la déclaration précédente et remplir les conditions énumérées dans les "Informations relatives aux thèses de doctorat à l'Université de Genève".

AKNOWLEDGEMENTS

I sincerely thank **Dr. Charna Dibner**, **Pr. Jacques Philippe** and **Pr. Robbie Loewith** for giving me the opportunity to do my PhD under their supervision. Especially, **Dr. Charna Dibner** welcomed me in her lab already since my Bachelor thesis and proposed me to continue with a Master and then with a PhD. I'm very grateful for the support and the knowledge learnt near **Dr. Charna Dibner** along these years.

My research was possible thanks to **Dr. Etienne Lefai** who provided us the human primary myoblasts, his expertise in regard of the muscle metabolism and who accepted to be part of my thesis committee. I would also thank **Dr. Stéphanie Chanon** for her help with western blots and glucose uptake assays.

I am grateful for the essential contribution achieved by **André Liani** and **Georges Severi** to the perifusion system development and to **Pr. Ueli Schibler** for his advices and help. I would like to thank **Pr. Pascale Roux-Lombard** and **Christine Modoux** for the Luminex assay, **Pr. Emmanouil Dermitzakis**, **Cédric Howald**, **Dr. Nicolas Hulo** and **Laura Isenegger** for conducting the RNA sequencing and for the analyses. Thank you also to **Dr. Marie-Luce Bochaton-Piallat**, **Anita Hiltbrunner**, **Chiraz Chaabane** and **Luis Miguel Cardoso Dos Santos** for their great collaboration with the porcine smooth muscle project.

Thank you to **Dr. Jürgen Ripperger** who accepted to be part of my thesis committee.

All these years would not have been the same without **Dr. Anne-Marie Makhlouf** who shared with me studious lunches and her attitude always positive.

A special thank goes to **Svetlana**, **Ursula**, **Pamela**, **Flore**, **Marie-Claude, Tiphaine**, **Camille**, **Laurianne**, **Nicolette**, **Xénia**, **Sara, Sandra**, **Volodymyr**, **Miguel**, **Florian**, **Yvan**, **Rodolphe**, **Jonas**, and **Pr. Richard James** for their advices, help, support, enthusiasm and all the great moments we spent together.

Many thanks to my **family**, especially my parents **Ariane** and **Jean-Louis**, **Elodie** and my **friends**, particularly **Anna**, **Szabolcs**, **Daniel**, **Nicolas** and **Mathias** who always supported me during these years.

In memory of my beloved grandfather **Robert**, who left us too early.

ABBREVIATIONS

α-SMA	Alpha-smooth muscle actin
AMPK	5' adenosine monophosphate-activated protein kinase
ARNT	Aryl hydrocarbon receptor nuclear translocator protein
bHLH-PAS	Basic helix-loop-helix Per Arnt Sim domain
BMAL1	Brain-Muscle ARNT-Like 1
Bmal1-luc	Bmal1-luciferase
BMI	Body Mass Index
CCGs	Clock-controlled genes
CLOCK	Circadian locomotor output cycles kaput
CREB	C-AMP response element-binding
CRY	Cryptochrome
DBP	Albumin D-box binding protein
FGF	Fibroblasts growth factor
h	Hour
HFD	High fat diet
HPRT	Hypoxanthine guanine phosphoribosyl transferase
hSKM	Human skeletal myotubes
IS	Insulin sensitivity
KO	Knock-out
MOI	Multiplicity of infection
NAD	Nicotinamide adenine dinucleotide
NAMPT	Nicotinamide phosphoribosyltransferase
NPAS2	Neuronal PAS domain protein 2
O-GlcNAc	β-linked N-acetylglucosamine
PDGF-BB	Platelet-derived growth factor-BB
PDH	Pyruvate dehydrogenase
PER	Period
Per2-luc	Per2-luciferase
PGC1	Peroxisome proliferator-activated receptor gamma coactivator-1-alpha
PPIA	Peptidylprolyl Isomerase A
PVDF	Polyvinylidene difluoride
qRT-PCR	Quantitative real-time polymerase chain reaction
REV-ERB	Reverse-erb
RNA-seq	High throughput RNA sequencing
ROR	Retinoid-related orphan receptors
RPKM	Reads per kilobase per million mapped reads
SCN	Suprachiasmic nucleus
SD	Standard deviation
SDS-PAGE	Sodium dodecyl sulfate polyacrylamide gel electrophoresis
SEM	Standard error of the mean
siRNA	Small interference RNA
SIRT1	Sirtuin 1
SNP	Single-nucleotide-polymorphism

SM22-α	Smooth muscle protein 22-alpha
SMC	Smooth muscle cell
SMMHCs	Smooth muscle myosin heavy chains
SUMO	Small ubiquitin-like modifier
T2D	Type 2 Diabetes
TTFL	Transcriptional-translational feedback loop
VAMP3	Vesicle associated membrane protein 3
WT	Wild-type

CONTENT

1. ABSTRACT

Background: Circadian clocks are operative in all light-sensitive organisms, allowing an adaptation to the external world in anticipation of daily environmental changes. Over the last decades, substantial efforts in the field have been undertaken to unravel the tight connection between the circadian clock and most aspects of physiology. Majority of the studies have been conducted in rodent models, with molecular studies of the peripheral oscillators in humans lagging behind due to obvious difficulties in sample collection in human individuals in a repetitive manner. Since the skeletal muscle plays a central role in the regulation of whole-body metabolism, we aimed at characterizing circadian oscillators operative in primary human skeletal myotubes (hSKM) *in vitro,* and investigate their roles in regulating gene transcription, myokine secretion, insulin response and lipid metabolism. Moreover, the approaches established for the study of the circadian clockwork impact on the skeletal muscle cells have been extended to additional model of primary smooth muscle cells (SMCs) isolated from porcine arteries, allowing to assess the circadian rhythm in normal and pathological SMCs.

Methods: Human skeletal muscle biopsies for the *in vitro* part were obtained from *Gluteus maximus* and *Rectus abdominus* during planned surgery, whereas the *Vastus lateralis* was sampled for the *in vivo* part under standardized protocol, with the consent of donors. Human primary skeletal myoblasts differentiated from isolated satellite cells were cultured and differentiated into myotubes. We established experimental system for long-term bioluminescence recording in hSKM, employing delivery of the *Bmal1-luciferase* (*Bmal1-luc*) and *Per2-luciferase* (*Per2-luc*) circadian reporters by lentiviral transduction. Furthermore, we have developed settings allowing to disrupt the circadian clock in adult skeletal muscle cells by transfecting siRNA targeting *CLOCK*. Next, using an experimental approach combining long-term bioluminescence recording and outflow medium collection in cultured human primary cells, we assessed the basal secretion of a large panel of myokines in a circadian manner, in the presence or absence of a functional clock. RNA-seq was conducted on hSKM transfected either with siControl or siCLOCK, and harvested every 2 h during 48 h following *in vitro* synchronization, and on human skeletal muscle biopsies taken every 4 h during 24 h. Glucose uptake by hSKM was measured by the incorporation of 2-deoxy-[^{3}H]-D-glucose before and after insulin stimulation. Finally, using circadian lipidomics analyses, we investigated temporal lipid profiles over 24 h in human skeletal muscle *in vivo*, and in hSKM cultured *in vitro*. Furthermore, these experimental settings were applied to primary

porcine spindle and rhomboid SMCs. SMCs were cultured and subjected to transduction with *Bmal1-luc* or *Per2-luc* reporters for circadian bioluminescence recording. qRT-PCR for core clock and target genes were performed on samples synchronized by forskolin, and harvested every 4 h between 12 h and 36 h following *in vitro* synchronization. Treatment with PDGF-BB or FGF-2 of spindle SMCs was applied to induce the phenotypical switch toward rhomboid-like SMCs, with subsequent synchronization and monitoring of the circadian bioluminescence.

Results: Bioluminescence reporter assays revealed that hSKM, synchronized *in vitro* with forskolin pulse, exhibit a self-sustained circadian rhythm with a period length of 25.29 ± 0.13 h (*Bmal1-luc*) and 25.20 ± 0.19 h (*Per2-luc*). By transfecting primary hSKM with siRNA targeting *CLOCK*, efficient downregulation of *CLOCK* mRNA expression by at least 80% and protein by 74% has been observed, leading to significant dampening of the *Bmal1-luc* bioluminescent reporter circadian amplitude. Molecular oscillators operative in hSKM have been further characterized by measuring endogenous core clock transcript expression around-the-clock using quantitative real-time polymerase chain reaction (qRT-PCR). Moreover, we demonstrated that the basal secretion of IL-6, IL-8 and MCP-1 by synchronized hSKM exhibited a circadian profile. Importantly, the secretion of IL-6 and several additional myokines was strongly downregulated upon siCLOCK-mediated clock disruption. Of note, glucose uptake by hSKM was reduced in the absence of functional cellular clocks, upon basal conditions and in response to insulin, suggesting an essential role for the human skeletal muscle clock in regulating insulin sensitivity. Furthermore, we demonstrated that circadian clock has an impact on muscle lipid metabolism, with about 20% of lipid metabolites exhibiting rhythmic profiles in human muscle biopsies collected around-the-clock *in vivo*, and in cultured hSKM, synchronized *in vitro*. These oscillations were strongly attenuated upon siRNA-mediated clock disruption in the primary myotubes. Additionally, our study provides the first large-scale circadian transcriptome analysis in human skeletal muscle, conducted by high throughput RNA sequencing (RNA-seq) following similar design *in vivo* and *in vitro,* allowing to distinguish cell-autonomous and systemic effects of the circadian clock on the muscle transcription. Importantly, genes involved in myokine secretion, insulin response and lipid metabolism have been identified, providing candidates to explain our previous observations. Of note, mRNA expression of core clock genes was in coherence with peak levels of lipid accumulation both *in vivo* and *in vitro*, and temporal lipid profiles correlated with transcript profiles of genes implicated in their biosynthesis. Regarding the SMC part, significantly longer period length of *Per2-luc* reporter oscillations

has been observed in rhomboid SMCs, and PDGF-BB- and FGF-2-treated SMCs synchronized *in vitro* by forskolin pulse, as compared to the control counterparts. Endogenous gene expression revealed an upregulation of almost all core clock gene tested, along with a phase shift in rhomboid SMCs compared to spindle.

Conclusions: We provide for the first time an evidence that primary hSKM possess a high-amplitude cell-autonomous circadian clocks. Taken together, our data suggest an essential role for endogenous human skeletal muscle oscillators in regulating glucose uptake by the skeletal muscle, myokine secretion, and lipid metabolism. Our model for studying circadian rhythm in the primary human cells synchronized *in vitro* is of the particular importance, as it allows to dissect the cell-autonomous effects of the local clocks on transcript and lipid oscillations in hSKM, and to separate the cell-autonomous effects from the central ones, driven by diurnal cycles of rest/activity and food intake. Indeed, we demonstrated that the muscle circadian clock bears important functional outputs in the absence of external synchronizers. Moreover, the experimental approach established in this work has been implemented for studying circadian clocks operative in cultured human pancreatic islets and porcine SMCs, and it can be further adapted to various cells types, primary cells or cell lines. This would allow for examining the molecular makeup of peripheral oscillators, and their impact on the organ transcription and function under physiological or pathophysiological conditions.

2. RÉSUMÉ

Introduction: Les horloges circadiennes, opérantes dans tous les organismes photosensibles, permettent une adaptation au monde extérieur en anticipant les changements environnementaux journaliers. Au cours des dernières décennies, d'importants efforts ont été entrepris afin d'examiner le lien étroit entre l'horloge circadienne et la plupart des aspects physiologiques. Le plus souvent, les études ont été conduites en utilisant des modèles de rongeurs, les études moléculaires sur les oscillateurs périphériques chez l'humain étant minoritaires, dues aux évidentes difficultés que représente la collection de prélèvements répétitifs chez les individus. Puisque le muscle squelettique joue un rôle central dans la régulation du métabolisme corporel, nous avons cherché à caractériser les oscillateurs circadiens opérants dans des myotubes squelettique primaires humain (MSH) *in vitro*, et à investiguer leurs rôles dans la régulation de la transcription génique, dans la sécrétion de myokines en réponse à l'insuline et dans le métabolisme des lipides. De plus, les approches établies pour cette étude sur l'impact de la machinerie circadienne humaines dans les cellules musculaires squelettiques ont été combinées à un modèle de cellules primaires de muscle lisse (CMLs) isolées à partir d'artères de porc, permettant d'évaluer le rythme circadien dans les CMLs normales ou pathologiques.

Méthodes: Des biopsies de muscle squelettique humain ont été obtenues pour la partie *in vitro*, à partir du *Gluteus maximus* et du *Rectus abdominus* au cours de chirurgies planifiées, et à partir du *Vastus lateralis* pour la partie *in vivo* durant un protocole contrôlé, avec le consentement des donneurs. Les myoblastes squelettiques primaires humain différentiés à partir des cellules satellites isolées ont été cultivés et différentiés en myotubes. Nous avons établi un système expérimental pour enregistrer pendant une longue durée la bioluminescence dans les MSH, en introduisant les gènes rapporteurs circadiens de la luciférase *Bmal1-luciférase* (*Bmal1-luc*) et *Per2-luciférase* (*Per2-luc*) par transduction lentivirale. En outre, nous avons développé des outils permettant de dérégler l'horloge circadienne dans les cellules de muscle squelettique chez l'adulte par transfection d'ARN interférent ciblant l'ARN *CLOCK*. Ensuite, en utilisant une procédure expérimentale combinant enregistrement longue-durée de la bioluminescence et collection de milieu issu de la culture de cellules primaires humaines, nous avons évalué la sécrétion basale circadienne d'un large panel de myokines, en présence ou absence d'une horloge fonctionnelle. Un séquençage à très haut débit (RNA-seq) a été réalisé sur des MSH transfectés, soit avec siControl, soit avec siCLOCK, et collectés chaque 2 h durant 48 h après

synchronisation *in vitro*, et sur des biopsies de muscle squelettique humain prises chaque 4 h durant 24 h. L'absorption de glucose par les MSH a été mesurée par l'incorporation de 2-deoxy-[^{3}H]-D-glucose avant et après stimulation par l'insuline. Finalement, grâce à des analyses lipidomiques, nous avons investigué les profiles temporels des lipides pendant 24 h dans le muscle squelettique humain *in vivo*, et dans les MSH *in vitro*. De plus, ces paramètres expérimentaux ont été appliqués aux CMLs primaires de porc de forme allongées (fusiformes ou « spindle ») et en forme de parallélogramme (« rhomboid »). Les CMLs ont été cultivées et transduites avec les rapporteurs *Bmal1-luc* ou *Per2-luc* pour l'enregistrement circadien de la bioluminescence. L'analyse en temps réel, *via* la réaction en chaîne par polymérase quantitative (qRT-PCR), des gènes essentiels de l'horloge et des gènes cibles, a été effectuée sur des échantillons synchronisés par la forskoline, et collectés toutes les 4 h entre 12 h et 36 h après synchronisation *in vitro*. Finalement, un traitement avec du PDGF-BB ou du FGF-2 des CMLs fusiformes a été appliqué pour induire un changement phénotypique vers la forme parallélogramme de CMLs, avec synchronisation et enregistrement de la bioluminescence circadienne.

Résultats: L'analyse de l'expression des rapporteurs bioluminescents a révélé que les MSH synchronisés *in vitro* avec la forskoline arborent un rythme circadien soutenu avec une longueur de période de 25.29 ± 0.13 h (*Bmal1-luc*) et 25.20 ± 0.19 h (*Per2-luc*). En transfectant les MSH primaires avec un petit ARN interférent ciblant *CLOCK*, une réduction efficace de l'ordre de 80% du niveau de l'ARN messager (ARNm) et de 74% au niveau protéique a été observée, conduisant à une diminution significative de l'amplitude du rapporteur bioluminescent circadien *Bmal1-luc*. Les oscillateurs moléculaires opérants dans les MSH ont été par la suite caractérisés en mesurant l'expression endogène des transcrits essentiels de l'horloge au cours du cycle de 24h (« around-the-clock ») en utilisant la RT-PCR quantitative. De plus, nous avons démontré que la sécrétion basale d'IL-6, IL-8 et MCP-1 par les MSH synchronisés présentent un profile circadien. En outre, la sécrétion de l'IL-6 et de plusieurs autres myokines est fortement diminuée lorsque l'horloge est perturbée grâce au siCLOCK. Il est important de noter que la captation de glucose par les MSH est réduite en l'absence d'horloges cellulaires fonctionnelles, en condition basale et en réponse à l'insuline, suggérant un rôle essentiel de l'horloge du muscle squelettique humain dans la régulation de la sensibilité à l'insuline. Nous avons aussi démontré que l'horloge circadienne a un impact sur le métabolisme des lipides dans le muscle, avec environ 20% de métabolites lipidiques présentant un profile rythmique dans les biopsies de muscle humain collectées au cours du temps *in vivo*, et chez les MSH en culture et synchronisés *in vitro*. Ces

oscillations sont considérablement atténuées par la perturbation de l'horloge *via* ARN interférence dans les myotubes primaires. Par ailleurs, notre étude fournit la première analyse transcriptomique circadienne à grande échelle dans le muscle squelettique humain, conduite par séquençage d'ARN (RNA-seq) suivant un protocole similaire *in vivo* et *in vitro*, permettant de distinguer les effets de l'horloge circadienne propres à la cellule (« cell-autonomous ») de ceux systémiques sur la transcription dans le muscle. Les gènes impliqués dans la sécrétion de myokines, la réponse à l'insuline et le métabolisme des lipides ont été identifiés, confortant ainsi nos précédentes observations. Remarquablement, l'expression de l'ARNm des gènes essentiels à l'horloge est cohérente avec les pics d'accumulation des lipides *in vivo* et *in vitro* et les profiles temporels des lipides sont corrélés avec les profiles des gènes impliqués dans leur biosynthèse. Concernant la partie sur les CMLs, une durée de période significativement plus longue des oscillations du rapporteur *Per2-luc* a été observée dans les CMLs en forme de parallélogramme, les CMLs traitées avec PDGF-BB et FGF-2 synchronisées *in vitro* avec de la forskoline, comparé aux contrôles. L'expression endogène des transcrits a révélé une augmentation de la quasi-totalité des gènes essentiels de l'horloge testés ainsi qu'un décalage de phase dans les CMLs en forme de parallélogramme comparé au CMLs fusiformes.

Conclusions: Nous fournissons pour la première fois une preuve que les MSH primaires possèdent des horloges circadiennes autonomes dotées d'une grande amplitude. Collectivement, nos données suggèrent un rôle essentiel pour les oscillateurs endogènes du muscle squelettique humain en régulant la captation de glucose, la sécrétion de myokine et le métabolisme des lipides. Notre modèle pour l'étude du rythme circadien dans les cellules primaires humaines synchronisées *in vitro* est de la plus grande utilité car il permet de disséquer les effets autonomes des horloges locales sur les oscillations de transcrits et des lipides dans les MSH, et de les séparer des effets centraux induits par les cycles de repos/activité et de la prise alimentaire. En effet, nous démontrons que l'horloge circadienne du muscle possède d'importantes fonctionnalités en l'absence de synchronisateurs externes. De plus, l'approche expérimentale établie dans ce travail a été transposée à l'étude des horloges circadiennes opérantes dans les ilots pancréatiques humain en culture, et peut être adapté à d'autres types cellulaires, cellules primaires ou lignées, pour l'étude de la composition moléculaire des horloges périphériques humaines et de leurs rôles en conditions physiologiques ou pathophysiologiques.

3. INTRODUCTION

3.1. Circadian rhythm

3.1.1. Definition and concept

All photosensitive organisms from bacteria to humans are subjected to daily light/dark and temperature cycles due to the Earth rotation (**Figure 1**) (1). During evolution, an internal timekeeping mechanism called circadian clock, from the Latin "*circa diem*", meaning about a day (24 hours (h)), has been acquired for a better adaptation by anticipating these environmental changes. Numerous biological processes are regulated by the circadian clock allowing proper gene expression and chemical reactions to occur at the right timing (2).

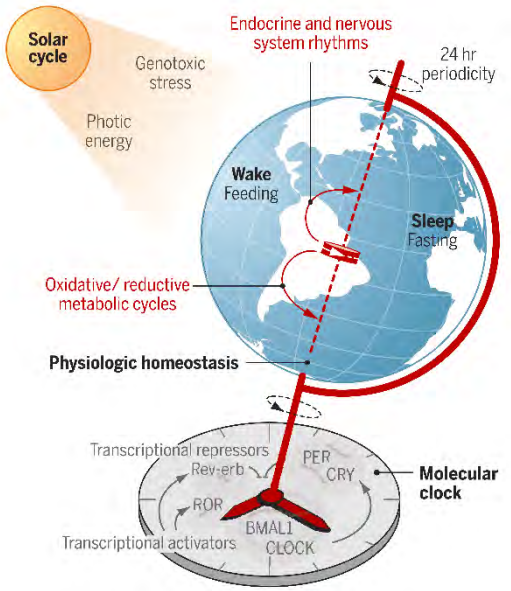

Figure 1. (Adopted from (2)). Geophysical time drives circadian maintenance of homeostasis.

Four parameters characterize a circadian oscillation (**Figure 2**). Firstly, the period, which is defined as the time when an identical phenomenon occurs again. In case of circadian rhythm, the period length is around 24 h. Secondly, the amplitude that represents the difference between two successive points where the slope of the oscillation is equal to zero. Thirdly, the magnitude, defined as the absolute value of the amplitude. Lastly, the phase is the state of an oscillation at a time *t*.

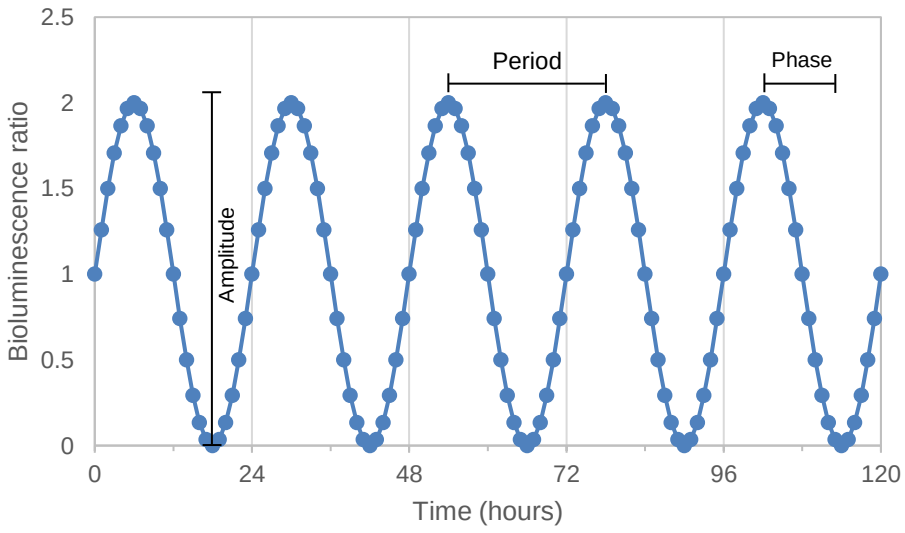

Figure 2. Characteristics of an oscillation curve. The amplitude, the period and the phase are commonly used to define circadian oscillatory profiles.

3.1.2. Hierarchical organization of the circadian time-keeping system

In mammals, circadian control of physiology and behavior is coordinated by a central clock, located in the paired suprachiasmatic nuclei (SCN) of the hypothalamus (3), which synchronizes on a daily basis peripheral, or slave, oscillators found in most of the organs including liver (4), kidney (5), heart (6), adipose tissue (7), endocrine pancreas (8, 9), and skeletal muscle (10-12). It has been demonstrated that the clock is ticking in almost all body cells in a self-sustained autonomous manner (13-15). Interestingly, it was recently discovered that inside the endocrine pancreas, the two main cell-types, i.e. α- and β-cells, exhibit distinct clock properties, suggesting a very precise cell-type specific regulation (16). Interestingly, the peripheral cellular oscillators were found to be resilient to large variations in general transcription and temperature (17).

3.1.3. Synchronization of the clock

3.1.3.1. The circadian synchronization of central and peripheral clocks *in vivo*

The master pacemaker in the SCN is entrained by external *Zeitgeber* cues (from German, meaning “time giver”), with the light intensity being the principal signal (18, 19), acting through the photosensitive retinal ganglion cells (ipRGCs) expressing the melanopsin photo pigment, and the optic nerve (20). This photo pigment is sensitive to the blue/green light spectrum, but less to the red light (21). SCN controls the synchrony of peripheral clocks directly, *via* sympathetic neural system and humoral signals, and indirectly by controlling rest-activity and temperature cycles (**Figure 3**) (18). Feeding/fasting cycle is an important *Zeitgeber* for peripheral oscillators, which was shown to be potent enough to entrain circadian peripheral clocks (22-29). Moreover, uncoupling between peripheral and SCN clocks has been demonstrated by inversion of feeding-fasting cycle (23, 30). In mouse liver with conditional clock disruption by hepatocyte-specific overexpression of *Rev-Erbα* in a doxycycline-dependent inducible manner, most of the transcripts became non-rhythmic (31). Importantly, 31 genes expressed in liver, including *Per2,* kept their circadian rhythmicity following liver clock disruption (31). Daytime-restricted feeding restored rhythmic gene expression in liver from *Cry1*$^{-/-}$; *Cry2*$^{-/-}$ double mutant mice (32). Taken together, these results indicate that rhythmicity in liver gene expression is entrained by systemic signals. Moreover, variations of body temperature (33-38) and exercise (39-42) represent additional physiological synchronizers for peripheral clocks. Mimicked body temperature cycles, but not a serum shock, induce expression of the cold-inducible RNA-binding protein (CIRP/CIRBP) in culture fibroblasts, which is required for high amplitude circadian gene expression (43). Of note, change of 1°C of the body

temperature was recently found to control rhythmic alternative splicing in mammals by regulating SR protein phosphorylation (44).

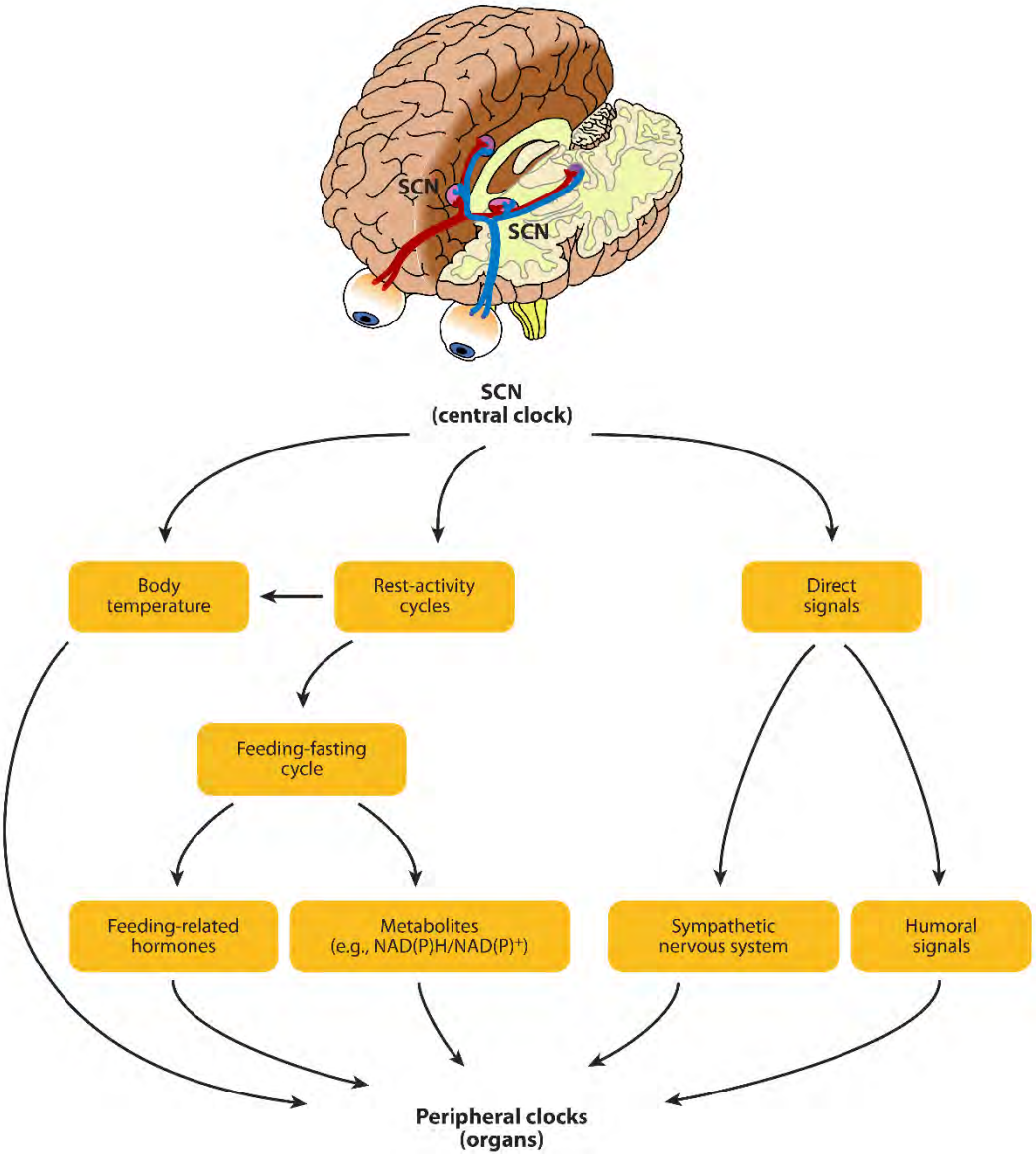

Figure 3. (Modified from (18)). **Entrainment of peripheral clocks by the SCN.** The central clock synchronizes the peripheral oscillators either directly, *via* nervous or humoral signals, or indirectly by changing behavior.

3.1.3.2. The *in vitro* synchronization

Field-breaking work by Ueli Schibler and colleagues demonstrated that a 50% horse serum pulse of 1 h is sufficient to synchronize the Rat1 fibroblast clock *in vitro* (13, 14), thus opening the new horizons for studying circadian oscillators in cells taken out of the body, cultured and synchronized *in vitro*. Later on, glucocorticoid hormone dexamethasone (25, 45-49), forskolin, and additional compounds (50, 51) were found to be potent *in vitro* synchronizers. Glucocorticoids bind the glucocorticoid receptor (GR), inducing its translocation to the nucleus, where it interacts with glucocorticoid response elements (GREs) to activate transcription of target genes (52-54). Forskolin acts by increasing cAMP levels using

protein kinase A (PKA) signaling pathway. This results in the phosphorylation and activation of calcium/cAMP responsive element binding protein (CREB) (51). Synchronization of the circadian clock induces high expression of *Per1*, phenomenon called the immediate early response, required to initiate the cycle in Rat1 fibroblasts *in vitro*. *Per2* was shown to be induced by certain synchronizers (horse serum), but its induction is not mandatory for cellular synchronization (50). Additional physiologically relevant stimuli including adrenaline, glucose or insulin are able to synchronize different cell types *in vitro* (16, 55). Employing cell cultures as model for studying circadian rhythm has been extensively developed since the pioneering work by Ueli Schibler. Moreover, application of this approach to the human primary cells, including primary human skin fibroblasts, which exhibited period length measured *in vitro* strongly correlating to the individual circadian phenotype *in vivo* (56, 57), offered a unique and powerful tool for studying human peripheral clocks in physiological condition and in diseases, which has been extensively utilized in this work.

3.2. Molecular clock

Circadian rhythms are generated by interaction of the core clock genes (**Figure 4**), forming the molecular core clock interconnecting feedback loops of transcription and translation, and activating in turn target genes dubbed clock-controlled genes (CCGs).

3.2.1. Transcriptional-translational feedback loop (TTFL) regulation

In mammals, the main TTFL entraining the circadian clock is driven by two transcriptional activators, the circadian locomotor output cycles kaput (*Clock*) and the brain and muscle ARNT-like1 genes (*Bmal1* also known as *Arntl*), forming the positive limb of the TTFL (**Figure 4**) (58, 59). BMAL1:CLOCK heterodimers are formed *via* their basic helix-loop-helix (bHLH)-PAS domains, allowing their translocation back to the nucleus, where they bind to the E-box (5'-CACGTC-3') sequence located in the promoter region of the negative limb members, the *Period* (*Per1, Per2* and *Per3*) and *Cryptochrome* (*Cry1 and Cry2*) genes. However, it has been demonstrated that CLOCK can also bind non-canonical E-boxes (60, 61). Once PERs and CRYs proteins enter the nucleus, they form one or more protein complexes (57, 62), composed by up to 30 different proteins (63, 64). PERs and CRYs inhibit *Bmal1* and *Clock* transcription, and thus indirectly induce their own repression (65-69). After a certain time, PERs and CRYs proteins are degraded (70-74), which leads to the reactivation of *Bmal1* and *Clock* expression, about 24 h after their previous expression peak (75, 76). Several studies have reported a

number of additional regulators which negatively control CLOCK and BMAL1 expression (43) or function (57, 77-79). An auxiliary TTFL comprises the nuclear receptors RORα-ɣ and REV-ERBα-β (also

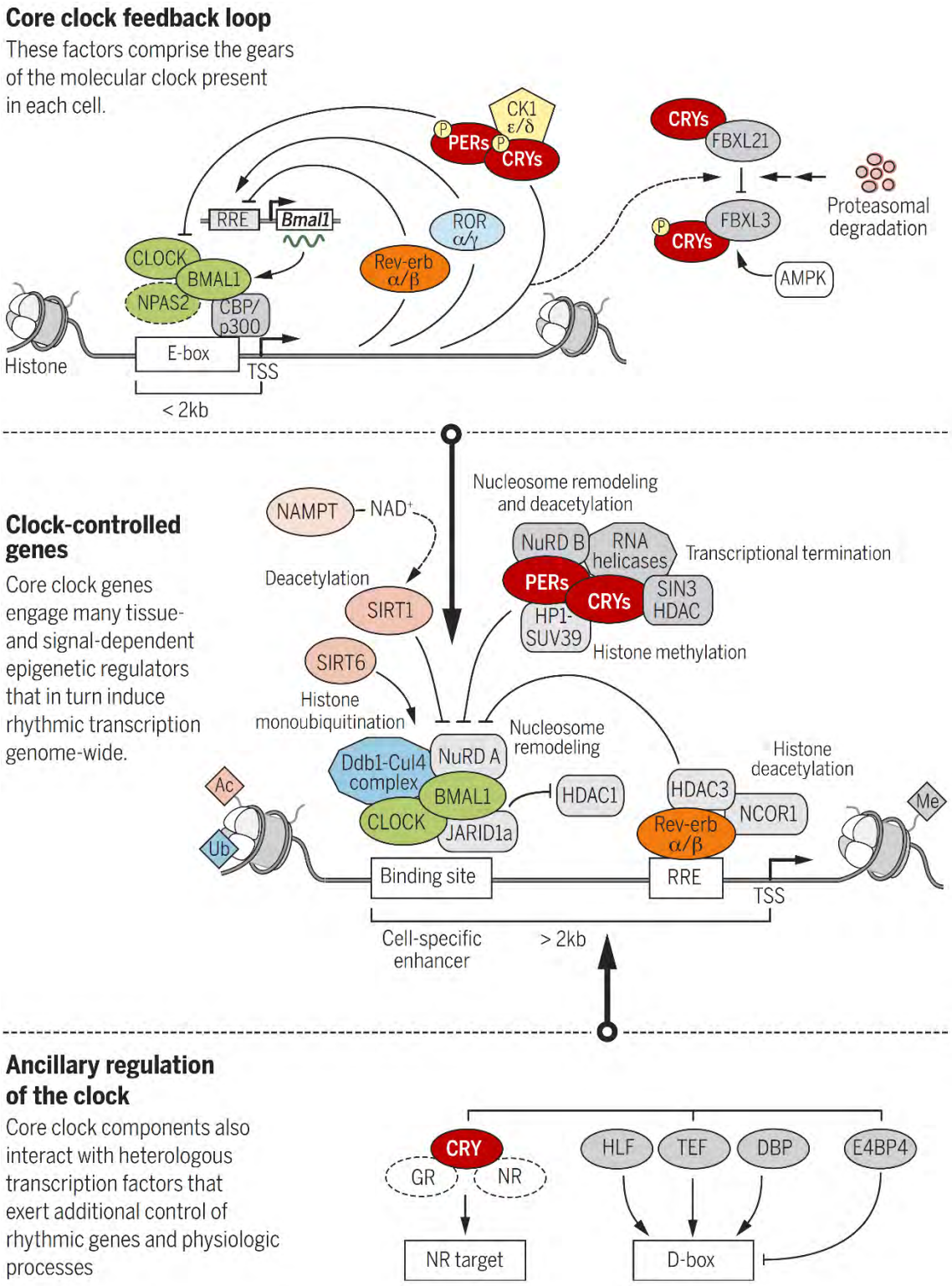

Figure 4. (Adopted from (2)). **Molecular makeup of the mammalian circadian clock.** The core clock system is based on interlocked transcriptional-translational negative feedback loops, with two activators, BMAL1 and CLOCK, and repressors constituted by the PERs and CRYs proteins. REV-ERBs and RORs form an auxiliary loop controlling *BMAL1* expression. Regulation of core clock genes and CCGs require several epigenetic modifiers which are in turn regulated by the clock. Additional transcription factors control rhythmic genes expression and physiological processes.

known as NR1D1 and NR1D2) which are positively and negatively controlling the expression of *Bmal1*, respectively, *via* the retinoic acid-related orphan receptor response elements (ROREs) (80). REV-ERBα uses heme as ligand to recruit the co-repressor N-CoR/histone deacetylase 3 to regulate *Bmal1* expression (81-86). The albumin D element-binding protein (*Dbp*) gene is activated by BMAL1:CLOCK heterodimer and inactivated by PERs and CRYs proteins (87, 88). DBP binds *Per1* on its D-box element regulating its transcription (89). Finally, CCGs are regulated *via* binding of the core clock proteins to E-box, RORE or D-box binding site in their promoter regions (**Figure 4**) (90).

The circadian clock appears to be an essential machinery, since nature rendered this system very conserved across the species at the molecular level, and redundant, possibly in order to minimize the detrimental effects in its components defects (91). Indeed, CLOCK protein can be replaced by the neuronal PAS domain protein 2 (NPAS2), which forms the heterodimer with BMAL1 allowing regulation of target gene expression (92, 93). Moreover, BMAL2 can replace BMAL1 (94), whereas REV-ERBβ (NR1D2) can substitute for the lack of REV-ERBα, to maintain the rhythmicity (95, 96).

3.2.2. Post-translational regulation of core clock genes

Beyond the TTFL, post-translational modifications including phosphorylation, acetylation, sumoylation, ubiquitination and glycosylation are required for daily oscillations in clock genes products (97).

Glycogen synthase kinase 3β (GSK3β) can modulate the period of the mammalian clockwork (98, 99). Circadian phosphorylation pattern of this enzyme regulates its activity, as it has been reported in SNC and in liver *in vivo,* as well as in NIH3T3 and COS1 cells *in vitro* (100, 101). By phosphorylating Ser-17 and Thr-21 of BMAL1 (102), Ser-427 of CLOCK (100, 103, 104) and Ser-553 of the mouse CRY2 protein in liver (101, 105), GSK3β promotes their degradation. Additionally, GSK3β stabilizes REV-ERBα (106) and triggers the nuclear translocation of PER2 (100).

Mitogen activated protein kinase (MAPK) decreases the transcriptional activity of the BMAL1:CLOCK complex by phosphorylating Ser-527, Thr-534, and Ser-599 of BMAL1 (107). It acts also on Ser-247 of mCRY1 and Ser-265 and Ser-557 of mCRY2 to reduce their affinity for BMAL1 (108).

Although casein kinase (CK) 1ε shows neither rhythmic oscillation at the protein level, nor at the levels of its activity *in vivo*, it was reported to critically regulate the time of the repressive state by

phosphorylating PERs and CRYs proteins and thus triggering their degradation (109-113). In turn, CRY1 negatively regulates the casein kinase 2 (CK2) which activates BMAL1 by phosphorylation on Ser-90 (114). In addition, CRY1 is phosphorylated by the nutrient-responsive adenosine monophosphate–activated protein kinase (AMPK) leading to its destabilization (115).

Sirtuin 1 (SIRT1) is a nicotinamide adenine dinucleotide (NAD+)–dependent histone deacetylase, involved in the regulation of the circadian clock. Not only levels of NAD+ oscillate in liver and adipose tissue due to the circadian regulation of the nicotinamide phosphoribosyl transferase NAMPT, but they are altered in mice models with a disrupted clock (116, 117). SIRT1 binding to BMAL1:CLOCK heterodimer occurs in a circadian manner, inducing the subsequent deacetylation and degradation of PER2 (118, 119). Inhibition of PER2 deacetylation results in the disruption of the circadian rhythm (120).

Protein sumoylation plays a role in various cellular processes, including regulation of protein stability (121). The small ubiquitin-like modifier 1 (SUMO-1), together with CLOCK protein, sumoylates BMAL1 on its Lys-259 in a circadian manner (122). Furthermore, SUMO2/3 triggers BMAL1 ubiquitination by ubiquitin ligases and proteasomal degradation (123). CRY proteins were shown to protect PER2 against ubiquitination and degradation (124), whereas BMAL1:CLOCK recruits ubiquitin ligases to PER1-2, CRY1-2 and others circadian proteins, to control the circadian feedback mechanism (73). Recently, REV-ERBα/β stability was shown to be regulated through the Seven in absentia 2 (Siah2) ubiquitin ligase. Overexpression of Siah2 destabilizes REV-ERBα/β while its downregulation lengthens the period length due to delayed degradation of REV-ERBα (125).

O-glycosylation is driven by the β-*N*-acetylglucosaminyl transferase (O-GlcNAc transferase or OGT) which adds a β-*N*-acetylglucosaminyl moiety (O-GlcNAc) on serine/threonine residues and by the β-*N*-acetylglucosaminidase (O-GlcNAcase or OGA). It was reported that total protein O-GlcNAc level exhibits a circadian rhythm in mouse cardiomyocytes (126), and that O-GlcNAcylation regulates protein stability and localization of several core clock genes, including *BMAL1*, *CLOCK*, *PER1* and *PER2* (127-130).

3.2.3. Circadian clock outputs: transcriptional, translational and functional regulation

Circadian regulation occurs at different levels in mammals (131). Transcription and translation are highly controlled by the clock, as levels of pre-mRNA and mRNA, nucleosome composition, ribosome biogenesis and assembly are all subjected to daily oscillations (132-134). Because of the ribosome assembly rhythm, the mouse liver mass changes over 24 h period (135). Furthermore, each organ

exhibits its specific subset and number of oscillating controlled genes (136), as it was demonstrated for instance in liver (12, 132, 137), pancreatic islets (138, 139), skeletal muscle (11, 12, 140) and adipose tissue (7, 141).

Circadian transcriptomic studies have been performed in all mouse organs, especially liver and skeletal muscle. Of note, a circadian gene atlas has been elaborated in mouse, concluding organ specific gene expression with little overlap among different organs (136). Liver is the most rhythmic organ with 14% to 54% of oscillating mRNA according to different studies (132, 142-144), whereas skeletal muscle is the organ with the lowest rhythmic gene number (4%) and amplitude (136). Importantly, these transcriptomic studies have linked the circadian clockwork to regulation of glucose and lipid metabolism in mouse skeletal muscle (145, 146).

Proteomic analyses conducted around-the-clock have demonstrated that 195 proteins (~3.3% of the mouse liver proteome) exhibit rhythmic accumulation pattern. Of note, only 102 of them were translated from the rhythmically expressed mRNA molecules, whereas the rest of circadian proteins were encoded by mRNAs bearing flat temporal profiles (147, 148).

Lipidomic studies have shown that lipid metabolites accumulation occurs in a circadian manner in mouse liver cells, and even in separated mitochondria and nuclei (137, 149), as well as in human blood (150). Recent metabolomic studies reported about 15% of all identified metabolites exhibiting circadian oscillations in human plasma and saliva (151). However, Krishnaiah S. Y. and colleagues argued against previous study designs with low temporal resolution, typically 4 h for 24 h, done in light/dark conditions, claiming that these settings were not robust enough to detect circadian rhythms in metabolism (152). Therefore, they investigated the circadian oscillation of various metabolites in mouse liver *in vivo*, in primary mouse hepatocytes, and in the human osteosarcoma U2OS cell line, a well-accepted cell-autonomous model *in vitro*, using an experimental design with 1 or 2 h temporal resolution across 48 h. The authors have found that 50% of detected metabolites were oscillating in mouse liver *in vivo*, 29% in primary mouse hepatocytes, and 28% in U2OS cells. Among cycling metabolites, 18 were commonly oscillating between tissues and cell types across human and mice, suggesting that these 18 metabolites are regulated by primary clock outputs (152). The authors have also reanalyzed previous transcriptomic data from Hughes M. E. *et al.* (153) using JTK_Cycle, and have reported about 37% of transcripts oscillating in mouse liver *in vivo,* but strikingly only 1.5% in U2OS *in vitro*.

Inducible skeletal muscle *Bmal1*$^{-/-}$ mice present glucose intolerance and higher non-fasted blood levels of insulin and glucose. This might be explained by the decrease of both mRNA and protein levels of GLUT4 (or SLC2A4), as well as mRNA levels of two key rate-limiting enzymes of glycolysis, hexokinase II (*Hk2*) and phosphofructokinase 1 (*Pfk1*). Metabolomic analyses indicated a reduced glycolytic flux, a decrease of some intermediates of the tricarboxylic acid (TCA) cycle, such as citrate/isocitrate, and an increase of amino acid levels. Taken together, these results suggest an energy switch from glucose toward fat utilization upon clock disruption (154).

The important roles of peripheral clocks in regulating gene expression and organ function have been established in liver (155, 156), in pancreatic islets (9, 16, 157, 158), in skeletal muscle (145, 146, 154, 159) and in adipose tissue (160). Many metabolic functions are regulated by the clock including xenobiotic detoxification by liver, kidney and the small intestine (161), glucose and lipid metabolism (131), as well as immunity (162). Core clock genes, including *REV-ERBα* and *BMAL1,* mediate the expression of specific genes for innate lymphoid lineage cells and pro-inflammatory cytokines, such as IL-6 (163, 164). Moreover, nutrient sensors like NAD+, NAMPT, or SIRT1 show strong association with the circadian clock system (116, 118, 165). Secretion of the hormones, such as glucocorticoid (165), melatonin (38), insulin and glucagon (16, 158), are also under the tight control of the circadian system in mice and in humans.

3.2.4. Circadian clock and diseases

Growing evidences have pointed out the connection between the circadian clockwork perturbations and disease development in mice and humans (**Figure 5**). On one hand, circadian rhythms can be dysregulated through environmental perturbations. Modern life style with intensive use of computer and smartphone/tablet emitting blue light during the night has been demonstrated to strongly perturb the circadian rhythm (166-168), leading to increased incidence of metabolic and cardiovascular problems (169), as well as cancer (170, 171). Of note, most of the genetic mouse models with clock ablation exhibit hyperglycemia, compromised glucose tolerance, hypoinsulinemia, and increased insulin sensitivity (131) (for more details see **chapter 3.2.4.2.**). In addition, chronic shifted work schedules increase the risk to develop metabolic diseases and several types of cancer, including breast cancer, leukemia and lymphoma (172, 173). Additionally, genetic variants of almost all core clock genes were linked to increased risk of cancer and metabolic diseases (131, 174). PER2 has been reported to play

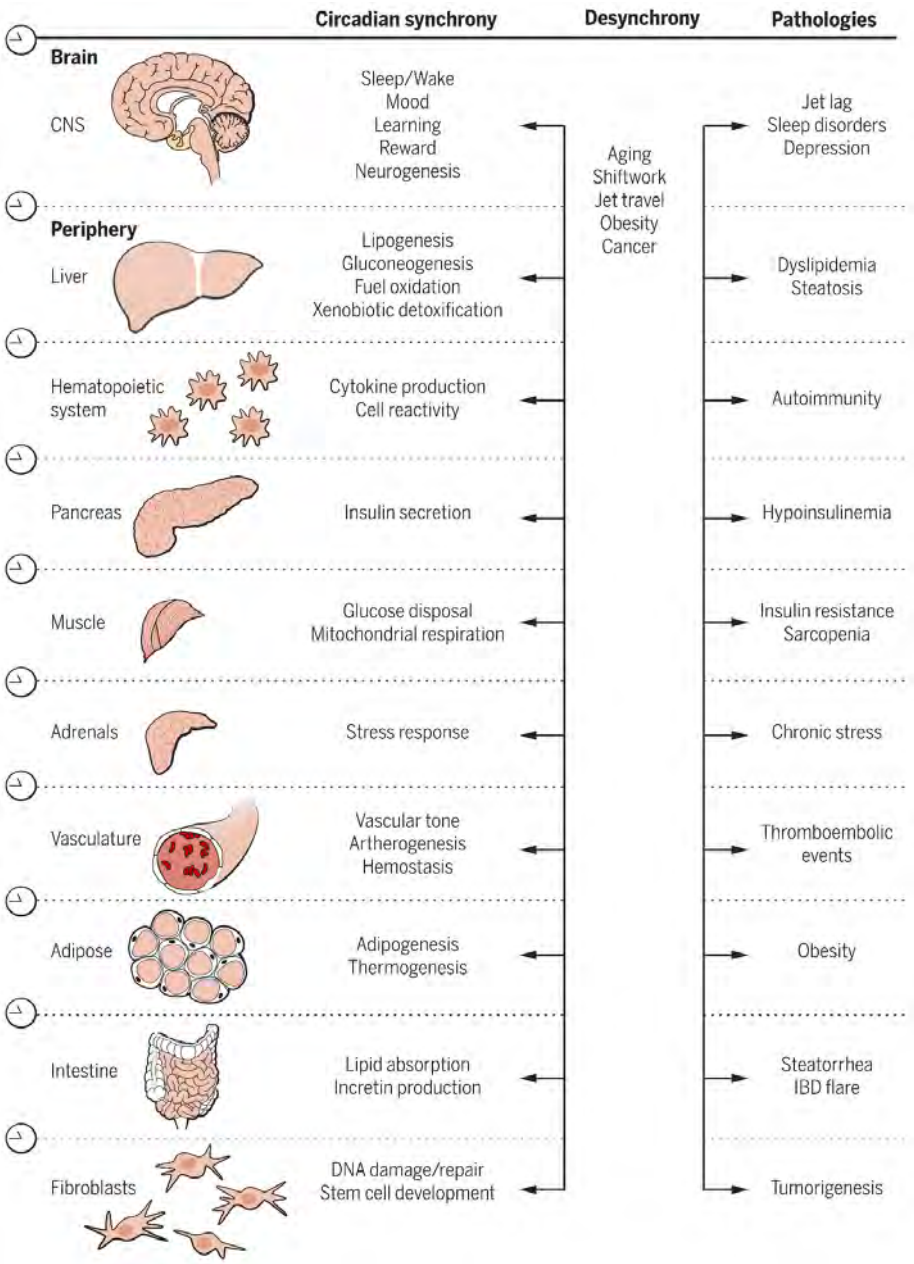

Figure 5. (Adopted from (2)). **Perturbations of the circadian system leads to pathologies.** Circadian disruption in a specific organ can lead to severe diseases including cancer, metabolic syndrome or cardiovascular complications.

a role in tumor suppression by inducing apoptotic cell death (175, 176). Moreover, our laboratory has demonstrated that the circadian rhythm is altered with the thyroid cancer progression in humans, with an upregulation of BMAL1 and a downregulation of CRY2 and PER2 (177-179). The Familial Advanced Sleep Phase Syndrome, or FASPS, is related to a mutation of the phosphorylation site for CK1ε in the PER2 protein which causes about a 4 h phase advance in sleep-wake cycle (180). In FASPS patients, sleep time occurs at around 8:00 pm and wakefulness occurs at around 3:00 am, with progressive impairment of the sleep quality by an increase of night-time awakenings (181). Delayed sleep phase syndrome (DSPS) causes delayed sleep and wake time, with sleep time occurring between 2:00 am

and 6:00 am in some cases. However, this disease does not affect either sleep architecture or the maintenance of sleep, but rather triggers chronic sleep-onset insomnia, which, combined with forced early awakening, frequently results in marked daytime sleepiness (181). Abnormal peak of melatonin during the day and human *PER3* polymorphisms for 4 and 5 repeat amino acid sequences were linked to DSPS (181, 182).

3.2.4.1. Obesity and the clock

Obesity is a worldwide health problem affecting more than 600 million people in 2014 (183). A person is categorized as obese if his/her body mass index (BMI) is higher than 30 kg/m^2. This multifactorial disease is often associated with the metabolic syndrome, characterized by intra-abdominal fat depot, dyslipidemia, insulin resistance, hyperglycemia and hypertension.

Since the circadian system controls various aspects of metabolism, it is not surprising that recent animal studies provided a compelling evidence for the tight reciprocal link between obesity and circadian perturbations (184, 185). For instance, homozygous *Clock* mutant mice fed with a high fat diet (HFD) become obese and develop hyperleptinemia, hyperlipidemia, hepatic steatosis, hyperglycemia, and hypoinsulinemia (186). Furthermore, it has been shown that BMAL1 regulates adipogenesis (187). Interestingly, adipocyte-specific *Bmal1* knockout (KO) and whole-body *Bmal1* KO result in different phenotypes, leading to obesity development (188), or to a reduction of body weight despites a higher fat accumulation, respectively (94, 189). One plausible explanation for these different phenotypes recently came out with the finding that altered feeding behavior of the *Bmal1* KO mice modifies transcription, translation and post-translational events in liver (132).

HFD diet alone has an impact on the clock. Indeed, it was reported that after one-two weeks, wild-type (WT) mice exhibited a longer period length with altered expression of core clock genes and genes involved in lipid metabolism in fat and liver, including sterol regulatory element-binding proteins (*Srebp*)-*1c*, *Fabp1* and *Fabp4*, compared to mice fed with a regular chow. However, no difference in body weight was observed between these two groups of mice (190). Numerous studies in mice have shown that inversed feeding restricted to daytime either with regular chow or obesogenic diets, including HFD or high-fructose and high-sucrose diet, leads to developing obesity and to circadian rhythm disruption in peripheral organs. On the contrary, when HFD access is restricted to the activity phase (night feeding in mice), obesity development is prevented (reviewed in (185)).

Obesity was reported to be associated with a chronic light-dark schedule changes, due to frequent time zone changes associated with acute jet-lag, or with long term shifted work schedules (191). It has been demonstrated that under phase-advanced light:dark (LD) cycle, mice developed obesity when fed *ad libitum* (185). Of note, leptin, a major regulator of satiety, is rhythmic at mRNA and protein levels in mouse adipose tissue, due to the direct control by BMAL1:CLOCK. The adipose clock and leptin rhythms are disrupted under chronic jet lag, causing leptin resistance development in mice (192). Therefore, both food availability and feeding schedule mediate the repertoire, phase, and amplitude of the circadian transcriptome in WT mouse liver (32), as well as in other peripheral tissues, including skin (193), heart (194), and skeletal muscle (195, 196). Shift workers, for instance nurses or policemen, are more prone to developing a metabolic syndrome and having a higher risk of cardiovascular diseases (197-199). Gender related differences have been identified among shift workers, with men exhibiting more frequently higher body mass index (BMI) and waist circumference, whereas women exhibiting a more significant elevation of blood glycaemia and glycated hemoglobin (HbA1c) levels (200, 201).

In humans, dietary changes in healthy subjects from high carbohydrates-low fat diet to low carbohydrates-high fat diet for a period of 6 weeks each, altered oscillations profiles of *PER1-3* and *TEF* genes in monocytes, as well as those of transcripts involved in inflammation and lipid metabolism (202). Analyses on subcutaneous adipose tissue (SAT) samples, collected before and after 8 weeks of hypocaloric diet aimed to induce weight loss in 50 obese men, resulted in a restored *PER2* and *REV-ERBα* expression, and correlated with the expression levels of genes involved in fat and energy metabolism, autophagy and inflammatory response (203). Importantly, improved fasting glucose, insulin sensitivity, and lipid profile, as well as greater weight loss, were observed in subjects consuming high caloric dietary intake at earlier time of the day (185).

Moreover, a single-nucleotide polymorphism (SNP) on the human *CLOCK* gene (3111T/C) triggers alteration of circadian rhythm, sleep and eating behavior, along with reduced weight loss ability and higher plasma levels of ghrelin (204, 205). Additional SNPs in the *CLOCK* gene were associated in obesity development in the human population (206), whereas one haplotype was identified as protective against weight gain (207). Two SNPs in REV-ERBα were associated with obesity risk in both Mediterranean and North American human populations (208, 209).

3.2.4.2. Type 2 diabetes (T2D) and the clock

Nutrient ingestion acutely raises blood glucose concentration (hyperglycemia), that induces insulin secretion by the pancreatic β-cells, further stimulated by the insulinotropic polypeptide (GIP) and glucagon-like peptide-1 (GLP-1), released from the intestine in a nutrient-dependent manner, whereas glucagon is used to promote releasing of glucose into the blood stream under hypoglycemia (**Figure 6**). Glucose is absorbed mostly by the liver, the adipose tissue and skeletal muscle, with simultaneous inhibition of hepatic glucose production (210). The type 2 diabetes (T2D) is characterized by an incapacity to regulate blood glucose concentration, especially after food intake, due to insulin resistance in target organs, and impaired insulin secretion caused by pancreatic β-cell dysfunction (211). Insulin normally induces increase in glucose transporters recruited to the membrane in peripheral metabolic organs, mostly skeletal muscle and adipose tissue, *via* the AKT-phosphatidylinositol-4,5-bisphosphate 3-kinase (PI3K) signaling pathway, allowing to absorb blood glucose to the organs, and thus to decrease systemic glucose levels (212). Despite enormous long-standing effort undertaken in the field, etiology of T2D stays not entirely understood now days. It is believed to comprise genetic predisposition along with environmental factors, such as alimentation, stress, or physical inactivity. T2D is the most spread form of diabetes worldwide, with 422 million of people affected in 2014 (213), and up to 642 million predicted for 2040 (211). Moreover, the age of the affected population is constantly decreasing, as reported in the United Kingdom (UK), where 5% of the T2D population were <30 years in 2003, increasing to 12% by 2006 (214), and reaching 24% of the T2D subjects younger than 40 years old in 2008 (215).

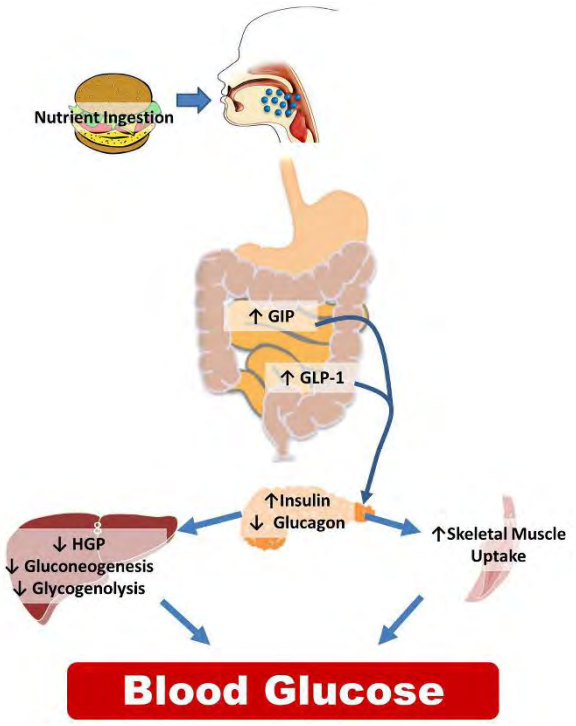

Figure 6. (Adopted from (210)). **Peripheral regulation of glucose homeostasis.** See text for detailed explanations.

We, and others, have demonstrated that peripheral clocks operative in metabolic organs are regulating glucose homeostasis (**Figure 7**) (131). Of note, cell-autonomous clocks are ticking in the endocrine pancreas of mammals (8, 9, 138), and our group has published several papers describing the role of the circadian clock in human islet cells (8, 16, 158). Moreover, we have recently found that mouse and human islet cells secrete basal insulin in a circadian manner *in vitro* (16, 158). Strikingly, this secretion profile was disrupted, and absolute levels of both acute and chronic glucose-induced insulin secretion were decreased upon siCLOCK-mediated clock disruption in adult human islet cells. Using high throughput RNA sequencing (RNA-seq) analysis, alteration of gene expression involved in vesicle trafficking and secretion mechanisms have been identified, providing a plausible hypothesis for a mechanism of the observed phenomenon (158). Furthermore, upon T2D in humans, mRNA levels of *PER2*, *PER3*, and *CRY2* were significantly lower, and correlated with insulin content and HbA1c levels in the same human donors (216). In line with these findings, mRNA levels of *BMAL1*, *PER1* and *PER3* appeared to be reduced also in leucocytes from T2D human subjects (217).

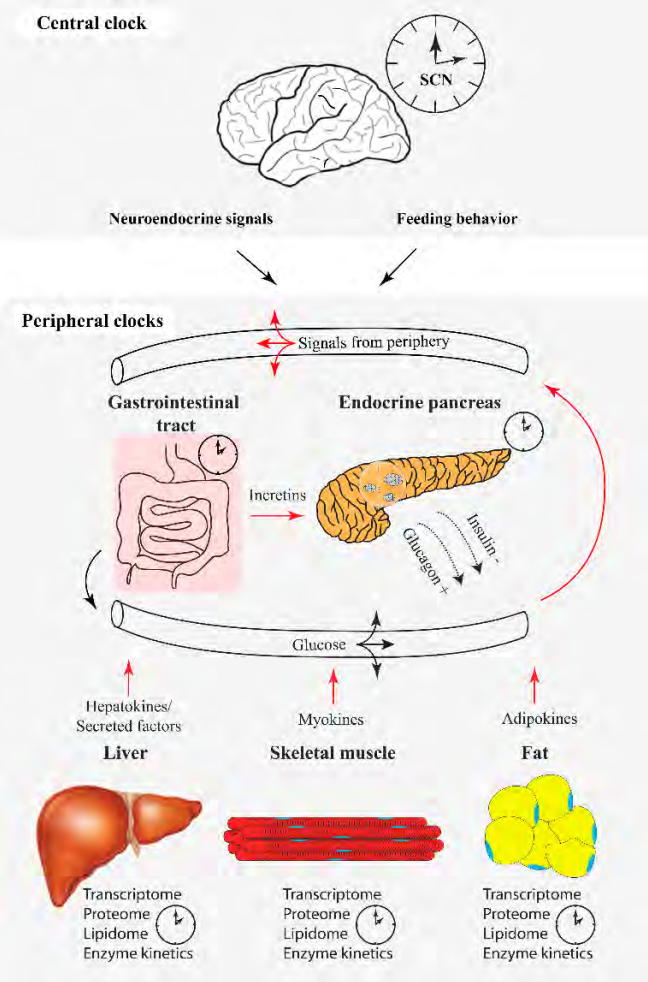

Figure 7. (Adopted from (131)). **Circadian system regulates glucose homeostasis.** Local clocks are required for proper organ function and inter-organ crosstalk.

Several studies reported that disruption of the circadian rhythm leads to T2D and insulin resistance development in both rodents (9, 139, 157) and humans (158). First demonstration of a such an important direct link came out with the finding that *Clock*$^{\Delta 19}$ mutant and *Bmal1* KO mice exhibited smaller islet size, together with an altered function, which resulted in hyperglycemia and hypoinsulinemia. Reduced levels of insulin secretion might be linked to defect of insulin exocytosis, as several genes coding for SNAREs and transporters have a modified expression (139, 157). Even stronger phenotype was reported in the

islets-specific *Bmal1* KO mice (157), resulting in the development of overt T2D already at the age of two months (9). Moreover, the *Rev-Erbα* agonists were shown to increase energy expenditure, improve glucose concentration in blood, decrease body weight and fat mass in WT mice fed with both regular chow or HFD (218) and regulate adipogenesis (219). Collectively, these data suggest that the intact molecular clock is required for proper endocrine pancreas functions.

Liver is an important regulator of the glucose homeostasis, as it produces glucose during the starvation and stores its excess as glycogen and lipids in the fed state (212). Reports arguing that functional liver clock is necessary for regulation of glucose homeostasis have been recently published. Hepatic glucose export follows daily oscillations, with liver-specific *Bmal1* KO mice displaying hypoglycemia during the fasting phase, a tendency for a hypoinsulinemia with no difference in body weight and fat percentage, which was similar to the *Per1*$^{-/-}$ *Per2*$^{-/-}$ mice phenotype (220). The same study has shown that total *Bmal1* KO leads to weight gain with more fat accumulation, a clear reduction of the insulin plasma level, and hyperglycemia (220). In line with these results, another study has demonstrated that *Bmal1* KO mice do not exhibit rhythmic insulin action profile as compared to WT mice. Moreover, rescue experiment with overexpressing *Bmal2* successfully restored insulin action and activity patterns in these mice (221). HFD causes hyperinsulinemia, and alters the expression of core clock genes and lipogenic genes in mouse liver (222). In addition, CRY1 and CRY2 proteins inhibit cAMP accumulation and CREB activity, thus resulting in the arrest of the glucagon-induced gluconeogenesis and regulation of the fasting glucose concentration by the liver. Overexpression of *Cry1* in liver leads to lower blood glucose levels and insulin resistance in the *db/db* mouse model (223).

In humans, the link between disturbed circadian rhythm in peripheral organs and T2D development has emerged but it is far to be totally understood. Diurnal variations in glucose tolerance have been described (224), however the underlying molecular mechanism remains unknown. Moreover, genetic linkage analyses in the human population have shown that *BMAL1* (225), *CRY2* (226), *NPAS2* and *PER2* (227) genetic variants might be related to high fasting plasma glucose levels.

Metformin is a common anti-diabetic drug used for T2D treatment, mediating its effect *via* activation of AMPK, leading to the reduction of hepatic glucose production (228, 229). Since AMPK plays a role in the regulation of the circadian clock, it is most likely that metformin might have an impact on peripheral oscillators. Indeed, metformin blocks the mitochondrial Complex I which triggers elevation

of NADH and AMP levels. The decrease of the NAD^+/NADH ratio increases CLOCK:BMAL1-mediated transcription resulting in a high amplitude rhythms. The increased AMP/ATP ratio promotes AMPK phosphorylation, which activates SIRT1 and NAMPT in order to restore NAD+ levels. This reduces CLOCK:BMAL1 DNA binding activity and promotes a phase delay (230, 231). Interestingly, in white adipose tissue (WAT) of *db/db* mice, and in WAT from WT mice fed with HFD, mRNA expression and/or protein levels of *Nampt*, *Sirt1*, *Clock* and *Bmal1* are decreased. Treatment with metformin restored mRNA/protein levels of these four genes (232). In addition, AMPK phosphorylates CKIα (liver), and CKIε on Ser-389 (muscle), causing the degradation of PERs protein and release of CLOCK:BMAL1 inhibition, leading to a phase advance in expression of clock and metabolic genes or protein, such as *Pgc1α* and *Pparα* (230, 233). Taken together, these results indicate that balance between NAMPT and AMPK activities determines the clock phase shift in a tissue-specific manner (230), and that the phase shifting effects of metformin on peripheral clocks observed in rodent models should be studied in humans, in view of its utmost clinical importance for T2D treatment.

3.3. Skeletal muscle

3.3.1. Characterization, origin and basic functions of skeletal muscle

The human body comprises three types of muscle tissue: the smooth muscle, the cardiac muscle tissue, and the skeletal muscle, each having a specific architecture, function and localization. With more than 600 different muscles, human skeletal muscle represents the largest tissue in the total body mass, acting to maintain body posture, voluntary movements, breathing and heat release (234).

The skeletal muscle is derived from transient embryonic structures, called somites, originating from the paraxial mesoderm (234). Myogenesis is divided into two phases, with the first one starting by the expression of the myogenic factor *Myf5* in $Pax3^+$ mouse and $Pax3^+$/$Pax7^+$ chicken embryonic progenitors (or myoblasts). After the first mitosis, skeletal muscle cells are called myocytes, and they express specific genes including myosin light chain 1 (or *MyLC1*, *Myl1*) and the slow myosin heavy chain (MyHC) *Myh7*. During the second phase in mouse embryos, *Pax3* is downregulated and *Pax7* is activated. This Pax7+ myoblast pool fuses together and gives rise to secondary fibers expressing *Myl3*, *Myh3*, α-actin cardiac form (*Actc1*), skeletal form (*Acta1*), and desmin genes. Others transcription factors are then activated in the trunk and limbs, comprising *Pax3*, *Myf5*, *MyoD* (or *Myod1*), *MRF4* (or *Myf6*),

and myogenin (or *Myog*). Muscle growth is promoted mostly by fusion Pax7+ progenitor cells until birth, then addition of myofibrils causes individual fiber hypertrophy.

In humans, specific isoforms of MyHCs, along with metabolic and electrophysiological properties, characterize the myofiber type (234). Despite the human skeletal muscle is the principal energy consumer in the body, low ATP levels are commonly found inside the muscle cell. Energy is obtained through either dephosphorylation of creatine by the creatine kinase, that triggers formation of ATP from ADP, or *via* the aerobic respiration, also called oxidative phosphorylation, consisting of the degradation of either pyruvic acid, or fatty acid or amino acid to produce ATP, CO_2 and H_2O, or finally by the anaerobic glycolysis, where glucose coming from blood or glycogen storage is degraded (235). Slow twitch fibers use oxidation to produce energy, and they express slow MyHC including *Myh7*. By contrast, the fast twitch fibers use glycolysis as main energy source, and are composed of three sub-groups with specific fast MyHC genes expression: *Myh2* in type IIa, *Myh4* in type IIb and *Myh1* in type IIx (234, 236).

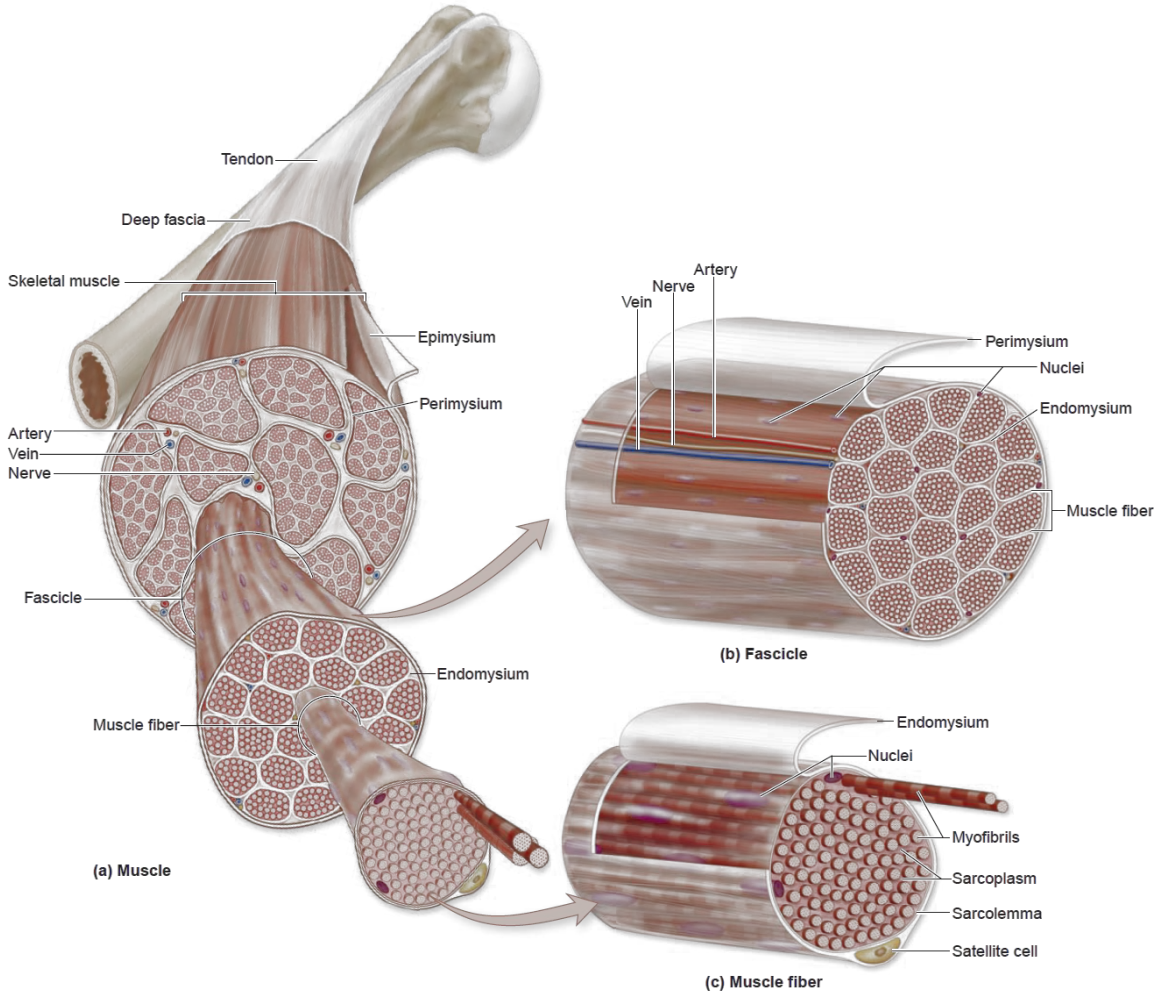

Figure 8. (Modified from (237)). **Anatomy of the skeletal muscle.** See text for detailed explanations.

The architecture of the mature myofiber is complex, comprising aligned myofibrils with sarcomeres, allowing contraction and forming the cytoskeleton. Myofibrils are in turn composed of myotubes (a plurinucleated syncytium), which are resulting from the myoblast fusion (**Figure 8**). Individual myofiber is surrounded by an endomysium (a basal lamina) with a sarcolemma (a specialized plasma membrane) (234, 238). Muscle fibers are attached to bones *via* tendon and myotendinous junctions, and can measure in human from 100 µm to 30 cm length, with a diameter ranging from 10 to 100 µm (237). The satellite cells are found close to the endomysium, and are arising from the $Pax7^+$ myoblast pool (234).

Conditions for establishing primary mouse and human skeletal myoblasts and their culture *in vitro*, followed by differentiation to human skeletal myotubes (hSKM), have been developed (239). This approach has an extensive implication for studies of the muscle physiology and pathophysiology, as will be exemplified later on in our work. In humans, satellite cells are isolated from muscle biopsies, with subsequent FACS sorting which increases the purity. These cells differentiate into myoblasts when plated, and can be amplified during a limited number of passages (5 to 6 passages) prior to induction of their differentiation into myotubes. Importantly, myotubes keep their metabolic characteristics *in vitro*, thus representing the closest physiological state to *in vivo* situation, allowing genetic, metabolic and physiologic studies of insulin sensitive and insulin-resistant muscle (see below) (239).

3.3.2. Role of skeletal muscle in type 2 diabetes

Skeletal muscle is responsible for 70-80% of insulin-stimulated glucose uptake in the postprandial state, therefore representing the largest insulin sensitive organ in the body, and the most important site of insulin resistance in T2D patients (240).

In vitro studies on hSKM established from T2D subject biopsies have revealed several defects in the insulin signaling pathway (241-244), in an agreement to previous works on the skeletal muscle *in vivo* (245, 246). Impaired muscle glycogen synthase activity, reduced phosphatidylinositol (PI) 3-kinase activity, and its association with insulin receptor substrate (IRS)-1 bearing increased phosphorylation on Ser-636 were observed (247-254). Moreover, the signal transducer and activator of transcription 3 (STAT3) has been shown to be constitutively phosphorylated and activated in T2D hSKM (255). Physical exercise, oxidative stress or glucose restriction are all leading to an increase in the AMP:ATP ratio in hSKM, which in turn stimulates ATP-producing pathways to restore energy status of the cell, including glucose uptake, fatty acid oxidation and mitochondrial biogenesis. At the same time, ATP-consuming

pathways, such as fatty acid, glycogen and protein synthesis, are inhibited (256, 257). Alteration of the AMPK pathway triggers higher intramuscular lipid content in hSKM established from T2D patient biopsies (257).

The glucose transporter GLUT4 plays a critical role in regulating blood glucose homeostasis by the skeletal muscle. GLUT4 translocation following insulin stimulation is regulated by two Rab GTPase-activating proteins (GAPs), TBC1D1 and AS160 (TBC1D4) (258). AS160 has been shown to be downstream of the AKT signaling (259), regulating insulin- and contraction-stimulated glucose uptake in mouse SKM (260). AS160 exhibits a decreased phosphorylation after insulin stimulation in hSKM from T2D patients (261). Not only the glucose regulation is impaired in hSKM from T2D, but also free fatty acid metabolism, in particular the mitochondrial β-oxidation, is reduced upon the disease (262). Moreover, it has been shown that T2D hSKM expresses more the fat mass and obesity-associated gene (*FTO*) then hSKM from nondiabetic and type 1 diabetic subjects. *FTO* overexpression *in vitro* increased basal AKT phosphorylation, enhanced lipogenesis and oxidative stress, and reduced mitochondrial oxidative function (263).

Importantly, the muscle fiber composition impacts on insulin response and glucose uptake. A recent study has determined that type I fibers express lower protein levels of AKT2, TBC1D1 and AS160, and higher protein levels for insulin receptor (IR), GLUT4, hexokinase II (HK2), glycogen synthase (GYS1), and pyruvate dehydrogenase-E1a (PDH-E1a), as compared to type II fibers. Thus, type I fiber appears to have a greater capacity for glucose-handling compared to type II fiber (264).

Among the hundred variants and related traits in genome-wide association studies (GWAS), more than 90% occur in non-coding regions. A recent study using skeletal muscle biopsies from 271 human subjects grouped into four categories: 1) normoglycemic, 2) impaired fasting glucose, 3) impaired glucose tolerance and 4) T2D, has linked T2D status, metabolic traits, and genetic variation to gene expression (265). Moreover, a recent transcriptome study using RNA-seq data from primary differentiated myotubes from 24 human subjects (healthy/T2D and non-obese/obese) has shown that myocytes derived from human T2D non-obese and from obese non-T2D subject biopsies keep their inherent characteristics even in the absence of obesogenic or diabetogenic environment. Obesity alone exhibits a similar genetic program as T2D, possibly mediated by the epigenetic histone mark H3K27me3 commonly identified in obese and T2D subjects. In addition, GO-term analysis has highlighted that

myogenesis and epithelial-mesenchymal transition processes were respectively down- and upregulated in myotubes from T2D, obese or T2D-obese *in vitro* compared to controls. Taken together, the presence of the H3K27me3 mark and the downregulation of key myogenic transcription factors and genes involved muscle contraction, including *MYOD1*, *MYOG*, *TNNI1*, *MYH2* and *MEF2C*, in T2D, suggest a decrease in muscle development program activity (266).

3.3.3 Skeletal muscle as a secretory organ

Since almost two decades, along with its structural importance and function as major site of glucose absorption, hSKM has been identified as the largest secretory organ in the body, producing and releasing cytokines called myokines. Myostatin, preventing myoblast hyperplasia, was the first identified myokine (267), followed by interleukins IL-6, IL-7, IL-8, IL-15, IL-18, fibroblasts growth factor (FGF) 21, brain-derived neurotrophic factor (BDNF), and many others (268). Myokines exert autocrine effect on muscle (269, 270), regulating muscle fiber development (271, 272), muscle growth (273, 274), angiogenesis (274, 275), and the control of reactive oxygen species (ROS) (276), as well as endocrine effects on distant organs, including adipose tissue and liver (268). Basal myokine expression levels were related to the fiber type composition in humans, rather than to daily muscle activity. TNF-α and IL-18 are more expressed in type II fibers, whereas IL-6 expression levels are higher in type I fibers (277). Studies addressing the IL-6 fiber-specific protein expression following the physical exercise have reported conflicting results depending on the type, intensity and duration of the exercise. One study shows no difference between type I and type II fibers after 3 h of bicycling at 60% of V_{O_2max} (278). Another study reports more IL-6 protein level in type II fibers following 2 h of bicycling at 55% of V_{O_2max} (279), and a third one finds more IL-6 protein expression in type I fibers in response to 3 h of dynamic knee-extensor exercise (280). Altogether these results indicate that IL-6 is preliminary expressed in type I fiber, as and when the exercise becomes more intense and/or lasts longer, IL-6 is getting expressed also in type II fiber (280). IL-15 mRNA was also found to be more expressed in type II fibers, with the protein content being comparable between type I and II fibers (273).

IL-6, which has been well-characterized as an inflammatory cytokine, currently also represents the most studied myokine. The human *Il6* gene located on the chromosome 7p21, codes for the IL-6 protein comprising 184 amino acids. Post-translational modifications (phosphorylation and glycosylation) confer a molecular weight between 21 to 28 kDa (281). Systemic IL-6 levels are mostly attributed to secretion

by monocytes/macrophages, microglial cell lines, and B and T lymphocytes, nevertheless adipose tissue and skeletal muscle secrete IL-6 as well (272, 282, 283). It has been shown that in resting muscle the mRNA levels of *Il6* are low, however, after prolonged exercise, such as marathon race, local concentration increased up to 100-fold is observed (283, 284). Importantly, this upregulation is not stemming from inflammatory response caused by muscle damages (285-287).

IL-6 acts as an energy sensor in SKM, enhancing energy consumption and increasing basal glucose uptake *via* an increased GLUT4 translocation from the intracellular compartment to the plasma membrane (272), and fat oxidation *via* AMPK and/or PI3K (268, 284, 285, 288). IL-6 production is increased when muscle glycogen levels are low (289). IL-6 negatively regulates the pyruvate dehydrogenase (PDH) activity during prolonged exercise in order to reduce carbohydrate oxidation (290). Ingestion of carbohydrates during exercise has no effect on the *Il6* mRNA expression in contracting muscle, nevertheless it prevents the increase of plasma IL-6 (274, 291, 292). Taken together, these results indicate that IL-6 could participate in the energy source switch required for muscle function during exercise.

It has been demonstrated that *Il6* knockout mice develop obesity and insulin resistance (293). From the other hand, constantly elevated IL-6 levels have been shown to induce hyperinsulinemia, reduction in body mass, and defects in insulin-stimulated glucose uptake by the mouse skeletal muscle (294). In humans, elevated circulating IL-6 and IL-1β levels increase the risk to develop T2D (295). An acute IL-6 infusion improves glucose metabolism in hSKM derived from normoglycemic subjects (296), which however was neither the case for hSKM isolated from T2D and cultured *in vitro* (297), nor *in vivo* in human muscle biopsies (298). Additionally, in hSKM from both normoglycemic and T2D subjects, IL-6 promotes fatty acid oxidation (297). It has been determined that the duration of the exposure to high IL-6 levels is critical for metabolic outcomes. Of note, short term IL-6 application on mouse myotubes *in vitro* combined with insulin stimulation, triggers the improvement of glucose uptake, mimicking the physiological response to IL-6 after exercise. However, chronically elevated IL-6 levels induce insulin resistance with impaired GLUT4 translocation, and insulin signaling defect at the level of insulin receptor substrate (IRS)-1 (299). IL-6 and other myokines, including IL-8 and monocyte chemotactic protein (MCP)-1, are secreted in excess by hSKM from T2D *in vitro* (273, 300-302).

3.3.4. Circadian clocks operative in mouse skeletal muscle and its roles in transcriptional and metabolic regulation

In rodents, it has been well established that skeletal muscle possesses a circadian clock essential for proper metabolic function (256, 303). At the transcriptional level, numerous *in vivo* studies in mice have shown rhythmic expression ranging from 3.4% to 16% of the SKM transcriptome (11, 12, 136, 145, 146). Mouse models of the circadian clock disruption have been generated to allow for deeper understanding of the relationship between circadian rhythm and muscle metabolism and physiology. In addition to their loss of circadian locomotor activity (58, 304), *Clock*$^{\Delta 19}$ mutant and whole-body *Bmal1* KO mice present equivalent functional and structural defects in SKM, similarly to those observed in *MyoD* KO mice, in the human Duchenne muscular dystrophy, and in aging (159). Furthermore, whole-body *Bmal1* KO mice exhibit reduction in satellite cell number, growth and proliferation *ex vivo* (305). These effects could be explained as the BMAL1:CLOCK heterodimer represses transcription of *MyoD* by directly binding to its core enhancer sequence, suggesting a direct control of the myogenesis by the clock (11, 306). Moreover, glucose restriction and *SIRT1* overexpression in SKM *in vitro* lead to the deacetylation of MYOD, and the arrest of myoblast proliferation and differentiation into myocytes (307, 308).

The use of muscle-specific *Bmal1* (MS-*Bmal1*) KO mice and inducible skeletal muscle-specific *Bmal1*$^{-/-}$ (iMS-*Bmal1*$^{-/-}$) allowed to explore more precisely the role of the muscle clock in regulating muscle metabolism and physiology. It is of importance to note that in contrast to whole-body *Bmal1* KO mice, these two genetic models exhibit normal whole-body circadian rhythm in locomotor activity, normal life span and growth curve, with muscle structure equivalent to WT mice despite the muscle force of the MS-*Bmal1* KO mice was reduced *in vivo* (145). Using these two muscle-specific *Bmal1* KO mouse models, it was found that a functional muscle clock is required for proper glucose homeostasis and lipid metabolism in rodents (145, 146, 154). Significant reduction at both mRNA and protein levels of GLUT4, TBC1D1 and HK2, and PDH activity have been identified in MS-*Bmal1* KO and in iMS-*Bmal1*$^{-/-}$ models, leading to defect in insulin-stimulated glucose uptake (145, 146, 154).

Differential rhythmic gene expression pattern between different skeletal muscle types has been observed, suggesting a fiber-specific regulation by the muscle clock (140). In line with these results, it has been shown that the *Extensor digitorum longus* (EDL) muscles isolated from iMS-*Bmal1*$^{-/-}$ mice do

not respond to insulin *ex vivo,* due to significant decrease of *Glut4* mRNA and protein levels. Furthermore, metabolomics analyses have provided evidences of an energy source switch occurring in iMS-*Bmal1*$^{-/-}$ SKM toward fat utilization, with augmentation of protein breakdown to support the tricarboxylic acid (TCA) cycle (154) and microarray analysis has identified a gene signature favoring a fast-to-slow fiber-type transition (146). Collectively, the rodent studies point out that circadian clock operative in skeletal muscle is essential for the muscle fiber metabolism and phenotype specificity.

Peroxisome proliferator-activated receptor-gamma coactivator (PGC) 1 family regroups two specific muscle genes (*Pgc1-α* and *Pgc1-β*) involved in nutrients sensing and exercise, and regulating several enzymes such as alpha ketoglutarate dehydrogenase (αKGDH) and PDH. PGC1α improves glucose uptake by increasing GLUT4 receptor, and together with PGC1β stimulates mitochondrial biogenesis, and regulates fatty acid metabolism (256, 309). *Pgc1-β* mRNA and protein levels are circadian in mouse skeletal muscle, and seem to be under the direct control of *Clock* and *Bmal1*, with loss of its circadian pattern in *Clock*$^{\Delta 19}$ arrhythmic mutant mice. However, *Pgc1-α* circadian expression in SKM is still debated, although it triggers *Bmal1* and *Rev-Erbα* expression through interaction with RORα and RORγ, and its mRNA levels are downregulated in skeletal muscle of *Clock*$^{\Delta 19}$ and *Bmal1*$^{-/-}$ mice compared with WT mice (11, 159, 310, 311).

Although substantial progress in understanding of the inputs and outputs of the molecular clocks in skeletal muscle in rodents has been achieved over the last decade, the molecular studies in humans have been substantially lagging behind. It is therefore of scientific and clinical importance to provide further insight into the emerging connection between circadian oscillator function, metabolic regulation and T2D in human beings, with a specific focus on the human skeletal muscle circadian oscillator molecular makeup.

3.4. Aims of the project

Overall goal of this project is to characterize the clock machinery operative in primary hSKM isolated from healthy subjects, and to address its impact on gene transcription and skeletal myotube function.

Specifically, we aimed at:

1. Providing molecular characterization of the circadian clocks operative in human skeletal muscle. For this purpose, primary hSKM isolated from muscle biopsies of healthy subjects were used as an *in vitro* model.
2. Assessing the impact of a disrupted muscle clock on gene expression and metabolic function. To this end, small interference RNA (siRNA) transfection technology was employed to alter the adult human myotube oscillator *in vitro*. Transduction with circadian bioluminescence lentiviral reporters (*Bmal1-luciferase* and *Per2-luciferase*) has been performed to monitor continuous circadian oscillation profile in living cells harboring functional or disrupted clock.
3. Evaluating the temporal profile of secretory capability of hSKM *in vitro,* and its relation to the circadian clock. To do so, basal myokines secretion by hSKM bearing functional or disrupted circadian clock was monitored using a home-made perifusion machine, followed by human cytokine array multiplex assay.
4. Assessing glucose uptake by hSKM bearing functional or disrupted oscillator.
5. Studying clock regulation of the lipid homeostasis in human skeletal muscle by circadian lipidomics.
6. RNA-seq was used for large-scale hSKM circadian transcriptome analysis in control versus siCLOCK-transfected myotubes.
7. In collaboration with the group of Dr. Bochaton-Piallat, we applied our methodology to another system, primary porcine smooth muscle cells (SMCs), in order to characterize circadian oscillators operative in smooth muscle cells, and their role in regulating cellular gene transcription and function in physiological conditions, and during the development of atherosclerosis.

4. RESULTS

4.1. Human skeletal myotubes display a cell-autonomous circadian clock implicated in basal myokine secretion

This work led to a first scientific paper in first author entitled "*Human skeletal myotubes display a cell-autonomous circadian clock implicated in basal myokine secretion*" that has been published in Molecular Metabolism in July 2015 (10). I led this project, conducted the experiments, analyzed the data, prepared all figures and tables, and wrote the first draft of the manuscript.

Original article

MOLECULAR METABOLISM

Human skeletal myotubes display a cell-autonomous circadian clock implicated in basal myokine secretion

Laurent Perrin [1], Ursula Loizides-Mangold [1,6], Svetlana Skarupelova [1,6], Pamela Pulimeno [1], Stephanie Chanon [2], Maud Robert [3], Karim Bouzakri [4], Christine Modoux [5], Pascale Roux-Lombard [5], Hubert Vidal [2], Etienne Lefai [2], Charna Dibner [1,*]

ABSTRACT

Objective: Circadian clocks are functional in all light-sensitive organisms, allowing an adaptation to the external world in anticipation of daily environmental changes. In view of the potential role of the skeletal muscle clock in the regulation of glucose metabolism, we aimed to characterize circadian rhythms in primary human skeletal myotubes and investigate their roles in myokine secretion.

Methods: We established a system for long-term bioluminescence recording in differentiated human myotubes, employing lentivector gene delivery of the *Bmal1-luciferase* and *Per2-luciferase* core clock reporters. Furthermore, we disrupted the circadian clock in skeletal muscle cells by transfecting siRNA targeting *CLOCK*. Next, we assessed the basal secretion of a large panel of myokines in a circadian manner in the presence or absence of a functional clock.

Results: Bioluminescence reporter assays revealed that human skeletal myotubes, synchronized *in vitro,* exhibit a self-sustained circadian rhythm, which was further confirmed by endogenous core clock transcript expression. Moreover, we demonstrate that the basal secretion of IL-6, IL-8 and MCP-1 by synchronized skeletal myotubes has a circadian profile. Importantly, the secretion of IL-6 and several additional myokines was strongly downregulated upon *siClock*-mediated clock disruption.

Conclusions: Our study provides for the first time evidence that primary human skeletal myotubes possess a high-amplitude cell-autonomous circadian clock, which could be attenuated. Furthermore, this oscillator plays an important role in the regulation of basal myokine secretion by skeletal myotubes.

Keywords Circadian clock; Human skeletal myotube; Myokine; Interleukin-6; Circadian bioluminescence recording

1. INTRODUCTION

Circadian oscillations are daily cycles in behavior and physiology that have been described from photosynthetic bacteria to vertebrates. They are reflected by the existence of underlying intrinsic biological clocks with near 24 h periods that generate self-sustained rhythms, influenced by environmental stimuli, such as light and feeding [1]. Under homeostatic conditions, the clock acts as a driver of metabolic processes with remarkable tissue specificity that reflects the unique demand of each tissue [2]. In peripheral organs, a large number of key metabolic functions are subject to daily oscillations, such as carbohydrate and lipid metabolism by the liver, and xenobiotic detoxification by the liver, kidney and small intestine [2,3]. In rodents, the presence of peripheral circadian oscillators and their impact on gene expression and organ function has been demonstrated in liver, whole pancreas, pancreatic islets, and in adipose tissue (reviewed in [4]). Of note, feeding rhythms represent a potent synchronizing cue for peripheral oscillators. Elegant studies involving inverted or restricted feeding schedules convincingly demonstrate that feeding rhythms are powerful enough to uncouple liver and other organ clocks from the SCN [5]. Moreover, rhythmicity in a number of clock-deficient mouse models could be restored by feeding rhythms [6–8].

There is growing evidence for a tight reciprocal link between a number of metabolic diseases, including obesity and type 2 diabetes mellitus (T2D), and the circadian clockwork [3,4]. Mice with circadian clock ablation develop hyperphagia, obesity, hyperglycemia and hypoinsulinemia [9]. The adipocyte-specific *Bmal1* knockout leads to obesity development [10], while the islet-specific *Bmal1* ablation

[1]Division of Endocrinology, Diabetes and Nutrition, Department of Clinical Medicine, Faculty of Medicine, University of Geneva, Geneva, Switzerland [2]CarMeN Laboratory, INSERM U1060, INRA 1397, University Lyon 1, Oullins, France [3]Department of Digestive and Bariatric Surgery, Edouard Herriot Hospital, Lyon, France [4]Department of Genetic Medicine and Development, Faculty of Medicine, University of Geneva, Geneva, Switzerland [5]Division of Immunology and Allergy, Department of Medical Specialties, University Hospital and Faculty of Medicine, University of Geneva, Geneva, Switzerland

[6] U. Loizides-Mangold and S. Skarupelova contributed equally to this study.

*Corresponding author. Division of Endocrinology, Diabetes, Hypertension and Nutrition, Department of Clinical Medicine, Faculty of Medicine, University of Geneva, Aile Jura 4-774, Rue Gabrielle-Perret-Gentil 4, CH-1211 Geneva, Switzerland. Tel.: +41 22 372 93 18; fax: +41 22 372 93 26. E-mail: Charna.Dibner@hcuge.ch (C. Dibner).

Received July 15, 2015 • Revision received July 27, 2015 • Accepted July 30, 2015 • Available online 6 August 2015

http://dx.doi.org/10.1016/j.molmet.2015.07.009

Abbreviations

BMAL1	brain and muscle ARNT-like 1
CLOCK	circadian locomotor output cycles kaput
CRY	cryptochrome
DBP	D-albumin binding protein
GLP-1	glucagon-like peptide 1
HPRT	hypoxanthine-guanine phosphoribosyltransferase
IL-6	interleukin-6
IL-8	interleukin-8
Luc	luciferase
MOI	multiplicity of infection
MCP-1	monocyte chemotactic protein 1
M-CSF	macrophage colony-stimulating factor
PER	period
RORα	retinoid-related orphan receptor alpha
REV-ERBα	reverse-erb alpha
SCN	suprachiasmatic nucleus
T2D	type 2 diabetes mellitus
VEGF	vascular endothelial growth factor
ZT	zeitgeber time

directly triggers the onset of T2D in mice [11]. In humans, genetic analyses have shown a close association between glucose levels and variants of the *CRY2* and melatonin receptor 1B (*MTNR1B*) genes [2]. Skeletal muscle is the largest insulin sensitive organ in the body, playing an essential role in whole body glucose homeostasis. It is responsible for 70–80% of insulin-stimulated glucose uptake and therefore representing the most important site of insulin resistance in T2D patients [12]. The primary and best-described function of skeletal muscles is their mechanical activity. During the last decade, however, skeletal muscle has been characterized also as a secretory organ, producing and releasing myokines that act on the muscle itself and display endocrine effects on distant organs [13,14]. Recently, it has been proposed that fully differentiated primary human skeletal muscle cells secrete over 300 potential myokines [15]. Interleukin-6 (IL-6) is one of the first identified myokines, which is produced by the contracting skeletal muscle [16]. Acute high plasma levels of IL-6 are associated with exercise, while chronically elevated IL-6 is observed upon obesity and T2D. Moreover, IL-6 promotes pancreatic alpha cell mass expansion [17] and stimulates GLP-1 production and secretion by alpha and L-cells upon metabolic syndrome, thus exerting beneficial effects in T2D mouse models [18]. Besides IL-6, skeletal muscle produces a number of additional myokines, such as MCP-1 and IL-8, which play a role in skeletal muscle inflammation, recruitment of macrophages and insulin sensitivity [19,20].

In rodents, about 7% of the skeletal muscle transcriptome is expressed in a circadian manner [21]. Moreover, clock ablation (*Bmal1*$^{-/-}$) leads to skeletal muscle pathologies [22]. *MyoD*, a master regulator of myogenesis, exhibits a robust circadian rhythm and was identified as a direct target of CLOCK and BMAL1. In addition, disruption of myofilament organization was detected in *Bmal1*$^{-/-}$, *Clock*$^{\Delta 19}$, and in *MyoD*$^{-/-}$ mice, suggesting a direct link between the circadian clock and skeletal muscle function in rodents [22]. Furthermore, a recent study suggests that in mice muscle insulin sensitivity might be clock-dependent [23].

In view of the accumulating evidence in rodent models, it has been accepted that the skeletal muscle clock plays an essential role in maintaining proper metabolic functioning (reviewed in [24]), although the mechanism of this important regulation is not entirely clear, particularly in human subjects. Given that, the circadian clock in human skeletal muscle has remained largely unexplored, we aimed to characterize the circadian oscillator in primary human myotubes and explore its impact on the regulation of human skeletal muscle myokine secretion.

2. MATERIAL AND METHODS

2.1. Study participants, skeletal muscle tissue sampling and primary cell culture

Muscle biopsies were derived from non-obese or obese donors with the informed consent obtained from all participants (see Table 1 for the

Table 1 — Characteristics of donors for skeletal muscle biopsies.

Donor	Sex	Age (years)	BMI (kg/m^2)	Biopsy source
Non-obese	**M = 14, F = 5**	**58 ± 18**	**24.88 ± 3.20**	
1[a]	M	48	21.7	*Rectus abdominus*
2[a,f]	M	45	21	*Rectus abdominus*
3[a,f]	F	58	20.5	*Rectus abdominus*
4[a,f]	F	42	19.5	*Rectus abdominus*
5[b,d,k]	M	23	29.34	*Gluteus maximus*
6[a,b,d,e,g,h,i,j]	M	62	24.3	*Gluteus maximus*
7[a,b,f]	F	77	25.6	*Gluteus maximus*
8[b,d,g,i,j]	M	57	26	*Gluteus maximus*
9[b,d,g,h]	M	60	24	*Gluteus maximus*
10[b]	F	88	29.64	*Gluteus maximus*
11[a,b,c,d]	F	65	25.8	*Gluteus maximus*
12[b,d,k]	M	25	19.27	*Gluteus maximus*
13[b,d,g,h]	M	64	28	*Gluteus maximus*
14[b,d]	M	87	25.51	*Gluteus maximus*
15[b,d]	M	85	25.54	*Gluteus maximus*
16[b,d]	M	72	26.5	*Gluteus maximus*
17[b,e,f,h]	M	48	24.3	*Gluteus maximus*
18[b,d,h]	M	45	28.1	*Gluteus maximus*
19[a,b,c,d,g,i,j]	M	57	28.1	*Gluteus maximus*
Obese	**M = 1, F = 4**	**53 ± 15**	**39.21 ± 7.16**	
20[b]	M	70	30.1	*Gluteus maximus*
21[e]	F	70	32.9	*Gluteus maximus*
22[b,e,g,h,i]	F	43	43	*Gluteus maximus*
23[b,d,g,i]	F	39	45.48	*Rectus abdominus*
24[b,d,g,i]	F	45	44.58	*Rectus abdominus*
All donors	**M = 15, F = 9**	**57 ± 17**	**27.87 ± 7.23**	

M, male; F, female.
Non-obese, data are mean ± SD, $n = 19$.
Obese, data are mean ± SD, $n = 5$.
All donors, data are mean ± SD, $n = 24$.
[a] donor cells used for the recording of *Bmal1-luc* bioluminescence of dexamethasone-synchronized samples.
[b] donor cells used for the recording of *Bmal1-luc* bioluminescence of forskolin-synchronized samples.
[c] donor cells used for the recording of *Bmal1-luc* bioluminescence of dexamethasone vs. forskolin-synchronized samples.
[d] donor cells used for the recording of *Per2-luc* bioluminescence of forskolin-synchronized samples.
[e] donor cells used for the around-the-clock experiment with dexamethasone synchronization.
[f] donor cells used to quantify the silencing of *CLOCK* in *siControl* / *siClock* samples synchronized with dexamethasone.
[g] donor cells used to quantify the silencing of *CLOCK* in *siControl* / *siClock* samples synchronized with forskolin.
[h] donor cells used for the around-the-clock experiment in forskolin-synchronized *siControl* / *siClock* samples.
[i] donor cells used for the IL-6 perifusion experiments with forskolin synchronization.
[j] donor cells used for the multiplex assay analysis of perifusion samples synchronized with forskolin.
[k] donor cells used for the IL-6 perifusion experiments with forskolin vs. dexamethasone synchronization.

MOLECULAR METABOLISM 4 (2015) 834–845

donor characteristics). The experimental protocol ('DIOMEDE') was approved by the Ethical Committee SUD EST IV (Agreement 12/111) and performed according to the French legislation (Huriet's law). All donors had HbAc1 levels inferior to 6.0% and fasting glycemia inferior to 7 mmol/L, were not diagnosed for T2D, neoplasia or chronic inflammatory diseases, and not doing shift work. Biopsies were taken from the *Gluteus maximus* ($n = 18$) or the *Rectus abdominus* ($n = 6$) muscles during the planned surgeries. Primary skeletal myoblasts were purified and differentiated into myotubes according to the previously described procedure [25]. Briefly, after removal of apparent connective and fat tissue contaminants, the muscle biopsy was minced with scissors and incubated successively at least 4 times for 20 min in Trypsin-EDTA (Invitrogen, Thermo Fisher Scientific, Waltham, MA, USA) at 37 °C under agitation. Trypsin-EDTA digested extracts were pooled, and centrifuged (150 *g*). The pellet was rinsed several times with PBS and cells were filtered on a 70-μm filter before being plated in a Primaria flask (Falcon; Becton Dickinson, Bedford, MA) containing growth medium composed of HAM F-10 supplemented with 2% Ultroser G (BioSepra SA, Cergy-Saint-Christophe, France), 2% fetal bovine serum (FBS, Invitrogen), and 1% antibiotics (Invitrogen). After 4 days, the myoblasts were immuno-selected using a monoclonal human CD56 antibody combined with paramagnetic beads (CD56 MicroBeads, Miltenyi Biotec, Germany), according to the manufacturer's instructions. The selected cells were plated on Primaria plastic ware at 4500 cells/cm^2 and cultured in growth medium at 37 °C. After reaching confluence, myoblasts were differentiated into myotubes during 7–10 days in DMEM supplemented with 2% FBS. Muscle differentiation was characterized by the fusion of myoblasts into polynucleated myotubes (Supplementary Figure 1).

2.2. siRNA transfection and lentiviral transduction

Human primary myoblasts were differentiated into myotubes as described above. Cells were transfected with 20 nM siRNA targeting *CLOCK* (*siClock*), or with non-targeting *siControl* (Dharmacon, GE Healthcare, Little Chalfont, UK), using HiPerFect transfection reagent (Qiagen, Hombrechtikon, Switzerland) following the manufacturer's protocol, 24 h prior to synchronization. To produce lentiviral particles, *Bmal1-luc* [26] or *Per2-luc* [27] lentivectors were transfected into 293T cells using the polyethylenimine method (for detailed procedure see [28]). Myoblasts were transduced with the indicated lentiviral particles with a multiplicity of infection (MOI) = 3 for each, grown to confluence, and subsequently differentiated into myotubes.

2.3. *In vitro* skeletal myotube synchronization and real-time bioluminescence recording

To synchronize primary myotubes, 10 μM forskolin (Sigma, Saint-Louis, MO, USA) or 100 nM dexamethasone (Alfa Aesar, Johnson Matthey, London, UK) were added to the culture medium, respectively. Following 60 min (forskolin) or 30 min (dexamethasone) incubation at 37 °C in a cell culture incubator, the medium was changed to a phenol red-free recording medium containing 100 μM luciferin and cells were transferred to a 37 °C light-tight incubator (Prolume LTD, Pinetop, AZ, USA), as previously described by us [28]. Bioluminescence from each dish was continuously monitored using a Hamamatsu photomultiplier tube (PMT) detector assembly. Photon counts were integrated over 1 min intervals. Luminescence traces are either shown as raw or detrended data. For detrended time series, luminescence signals were smoothened by a moving average with a window of 144 data points and detrended by an additional moving average with a window of 24 h [29]. For quantification of the circadian amplitude and period the first cycle was not taken into consideration.

2.4. mRNA extraction and quantitative PCR analysis

Differentiated myotubes were synchronized by forskolin or dexamethasone, collected every 4 h during 48 h (0 h–48 h), or during 24 h (12 h–36 h), deep-frozen in liquid nitrogen and kept at −80 °C. Total RNA was prepared using RNeasy Plus Micro kit (Qiagen). 0.5 μg of total RNA was reverse-transcribed using Superscript III reverse transcriptase (Invitrogen) and random hexamers and PCR-amplified on a LightCycler 480 (Roche Diagnostics AG, Rotkreuz, Switzerland). Mean values for each sample were calculated from the technical duplicates of each qRT-PCR analysis, and normalized to the mean of two housekeeping genes (*HPRT* and *9S* or *GAPDH* and *9S),* which served as internal controls. Primers used for this study are listed in Supplementary Table 1.

2.5. Circadian analysis of basal myokine secretion by ELISA and multiplex assay

In vitro synchronized differentiated myotubes, transduced with *Bmal1-luc* reporter, were placed into an in-house developed two-well horizontal perifusion chamber, connected to the LumiCycle. Cells were continuously perifused for 48 h with culture medium containing 100 μM luciferin. Bioluminescence recordings were performed in parallel to the automated collection of outflow medium in 4 h intervals. Basal IL-6 levels were quantified in the outflow medium using the Human IL-6 Instant ELISA kit (eBioscience, Affymetrix, Santa Clara, CA, USA) following the manufacturer's instructions. Data were normalized to the genomic DNA content, extracted using the QIAamp DNA Blood Mini Kit (Qiagen). Perifusion medium samples were further concentrated using Amicon Ultra 2 ml centrifugal filters (Ultracel-3K, Merck Millipore, Darmstadt, Germany). The evaluation of myokine release from human primary skeletal muscle cells was carried out using a multiplex bead array assay system (R&D Systems, Minneapolis, MN, USA). Custom-made luminex screening plates (CD44, CHI3L1, FABP3, galectin-3, GRO-alpha, IGFBP-3, IL-7, IL-13, IL-17A, M-CSF, MCP-1, MMP-2, Serpin C1, Serpin E1, TIMP-1) and high sensitivity performance plates (IL-1 beta, IL-2, IL-4, IL-6, IL-8, IL-10, IL-12 p70, IFN-gamma, TNF-alpha and VEGF) were analyzed according to the manufacturer's instructions. Plate analysis was performed on a Bio-Plex 200 array reader (Bio-Rad Laboratories, Hercules, CA, USA), with the Bio-Plex software (Bio-Rad) used for data analysis.

2.6. Data analysis

Actimetrics LumiCycle analysis software (Actimetrics LTD) and the JTK_CYCLE algorithm [30] were used for bioluminescence and myokine secretion profile data analyses, respectively. For the ELISA and multiplex data analysis, 2 technical duplicates from 3 biological samples were analyzed for each myokine. From these values the average ± the SEM was calculated for each time point. For JTK_CYCLE analysis the period width was set at 20–24 h. Statistical analyses were performed using a paired Student's *t*-test. Differences were considered significant for $p < 0.05$ (*), $p < 0.01$ (**) and $p < 0.001$ (***).

3. RESULTS

3.1. High-amplitude self-sustained clocks are functional in primary human skeletal myotubes

Circadian bioluminescence recordings in living cells allow for the study of molecular clocks in human peripheral tissues, as previously demonstrated by us [28,31] and others [32]. We applied this powerful methodology to assess clock properties in human primary skeletal myotubes established from human donor biopsies and differentiated *in vitro* (see Supplementary Figure 1 and Table 1 for donor

characteristics). Multiple *in vitro* stimuli have previously been demonstrated to efficiently synchronize cultured cells, among them forskolin and dexamethasone [28,33]. As shown in Supplementary Figure 2, short pulses of dexamethasone or forskolin were able to strongly synchronize human myotubes bearing the *Bmal1-luc* lenti-vector. Both forskolin and dexamethasone induced oscillations with comparable period length: 25.29 ± 0.13 h, $n = 19$ for forskolin (Table 2), and 24.48 ± 0.24 h, $n = 8$ for dexamethasone (data not shown). However, the forskolin pulse induced more sustained cycles with higher circadian amplitude compared to dexamethasone-synchronized cells (Supplementary Figure 2) and was therefore mainly used in this study as the *in vitro* synchronization stimulus. The here established experimental settings allowed for continuous recording of oscillation profiles in human primary myotubes for several days with high resolution (Figure 1A, B). As expected, the profiles of the *Bmal1-luc* and *Per2-luc* reporters were antiphasic (Figure 1A, B; [3]). High-amplitude self-sustained oscillations were reproducibly recorded from human primary myotubes for *Bmal1-luc* and *Per2-luc* reporters with an average period length of 25.29 ± 0.13 h and 25.20 ± 0.19 h, respectively (Figure 1C). Of note, no significant difference in period length of the *Bmal1-luc* or *Per2-luc* reporter was observed between myotubes established from non-obese and obese donors (Table 2), which might reflect the resistance of the core clock to metabolic changes.

To further validate the results obtained by circadian bioluminescence reporter studies, we examined endogenous core clock gene expression profiles in forskolin-synchronized myotubes (Figure 2C, closed circles). mRNA accumulation patterns from synchronized skeletal myotubes were monitored every 4 h during 48 h by quantitative RT-PCR, using amplicons for *BMAL1*, *REV-ERBα, PER3* and *DBP.* The values obtained were normalized to the mean of the housekeeping genes *HPRT* and *9S*. In agreement with our *Bmal1-luc* reporter experiments, endogenous *BMAL1* transcript levels exhibited circadian oscillations over 48 h in synchronized myotubes (compare Figure 2C *BMAL1* panel to Figure 1A), clearly antiphasic to the profiles of the endogenous *REV-ERBα, PER3,* and *DBP* transcripts (Figure 2C). Similar experiments were conducted in dexamethasone-synchronized myotubes (Supplementary Figure 3). *BMAL1* and *CRY1* mRNAs exhibited oscillatory profiles antiphasic to those of *REV-ERBα* and *PER2-3,* consistent with the dexamethasone-induced oscillations of the *Bmal1-luc* reporter (Supplementary Figure 2).

3.2. Human myotube clock disruption by siRNA-mediated *CLOCK* knockdown

In order to disrupt the circadian clock in cultured human myotubes, we set up an efficient *siClock* transfection protocol, resulting in more than 80% knockdown of *CLOCK* transcript levels (Figure 2A, Supplementary Figure 4A). Circadian expression of the *Bmal1-luc* reporter was blunted in *siClock*-transfected myotubes upon forskolin or dexamethasone synchronization, if compared to cells transfected with non-targeting sequences (*siControl*) or to non-transfected counterparts (Figure 2B, Supplementary Figure 4B), thus validating circadian clock disruption. Moreover, the amplitudes of endogenous *REV-ERBα*, *PER3* and *DBP* transcript profiles were strongly blunted in *siClock*-transfected cells, in comparison to *siControl* cells (Figure 2C, Supplementary Table 2). By contrast, *BMAL1* transcript levels were slightly upregulated (Figure 2C, Supplementary Table 2).

Table 2 — Circadian period length of forskolin-synchronized human myotubes assessed by circadian bioluminescent reporters.

	Bmal1-luc period (h)		*Per2-luc* period (h)		Mean period (h)	
	n	Mean ± SEM	*n*	Mean ± SEM	*n**	Mean ± SEM
Non-obese	15	25.35 ± 0.14	12	25.25 ± 0.22	27	25.31 ± 0.12
Obese	4	25.04 ± 0.35	2	24.85 ± 0.30	6	24.98 ± 0.24
All donors	19	25.29 ± 0.13	14	25.20 ± 0.19	33	25.25 ± 0.11

**n* represents the number of experimental repetitions.

3.3. Regulation of basal IL-6 secretion by the circadian clock in human primary myotubes

Given the accumulating evidence on the essential role of IL-6 secretion by skeletal muscle under physiological conditions and upon metabolic diseases [14,17,18], we next monitored basal circadian IL-6 secretion by human primary myotubes established from non-obese and obese donors. To this end, we developed an in-house perifusion system connected to the LumiCycle chamber that allows for parallel cell perifusion and bioluminescence profile recordings. Basal IL-6 secretion from *in vitro* synchronized skeletal myotubes was monitored in "around-the-clock" experimental settings, with a continuous flow of culture medium (see Material and methods for details). The perifusion experiments suggested that forskolin-synchronized myotubes exhibited a circadian profile of basal IL-6 secretion over 48 h, with a *Zenith* around 8 h—12 h and 32 h—36 h and a *Nadir* of 20 h—24 h (Figure 3A). JTK_CYCLE analysis [30] revealed that average profile of basal IL-6 secretion did not reach significance to be qualified as circadian over the entire time span of 48 h. However it was significantly circadian over the first 36 h of perifusion following *in vitro* synchronization (**$p < 0.01$, $n = 6$). Similar basal IL-6 secretion profiles were observed from dexamethasone-synchronized myotubes (Supplementary Figure 5).

We next tested the effect of *CLOCK* depletion on IL-6 secretion. Similar to previous experiments (Figure 2), *CLOCK* transcript expression was at least 80% downregulated in *siClock*-transfected myotubes (***$p < 0.001$, paired *t*-test, Table 3) compared to *siControl*-transfected cells. The achieved clock disruption was also confirmed by parallel *Bmal1-luc* bioluminescence recording in perifused cells (Figure 3B). Importantly, IL-6 secretion decreased on average 64% in *siClock*-transfected myotubes compared to *siControl*-transfected counterparts (*$p < 0.05$, Table 3). Furthermore, the profile of basal IL-6 secretion became flat upon clock disruption if compared to the *siControl*-transfected profile (see red line vs. black line, Figure 3A). Of note, overall basal IL-6 secretion was on average higher in obese *siControl*-transfected subjects ($n = 3$) compared to non-obese *siControl*-expressing counterparts ($n = 3$), although values did not reach statistical significance (Table 3).

To get an insight into the regulation of basal IL-6 secretion by the circadian clock, we assessed *IL6* transcript levels following *in vitro* synchronization with forskolin. No clear circadian pattern was observed (Figure 3C). The strong immediate early peak of *IL6* transcription induced by the forskolin pulse might be attributed to the presence of a cAMP response element previously identified in IL-6 promoter region [34]. Moreover, *CLOCK* depletion by *siClock* had no effect on basal *IL6* transcription (Figure 3C).

3.4. Multiplex screen identifies additional clock-regulated myokines

Since we obtained convincing evidence on the requirement of a functional circadian clock for basal IL-6 secretion by skeletal myotubes (Figure 3A,B), we selected an additional panel of myokines for analysis by multiplex assay. The around-the-clock secretory profiles of IL-6 and 24 other myokines were assessed in perifusion samples obtained from

MOLECULAR METABOLISM 4 (2015) 834–845

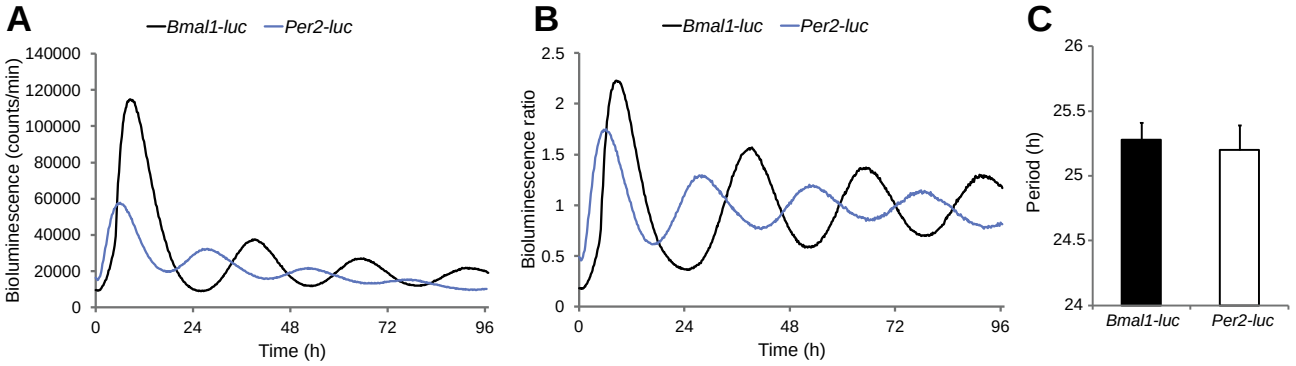

Figure 1: High-amplitude cell autonomous oscillators are functional in differentiated human primary myotubes. Human primary myoblasts were transduced with lentiviral particles expressing *Bmal1-luc* (black line) or *Per2-luc* (blue line). Cells were differentiated into myotubes, synchronized with forskolin, and transferred to the Actimetrics LumiCycle for bioluminescence recording. Raw (A) and detrended (B) oscillation profiles are representative of 19 and 14 independent experiments, respectively (one donor per experiment). (C) The period length of *Bmal1-luc* or *Per2-luc* was on average 25.29 ± 0.13 h, ($n = 19$) or 25.20 ± 0.19 h, ($n = 14$), respectively. Data represent the mean ± SEM.

primary human myotubes as described in Figure 3, and further concentrated to allow for the detection of basal myokine secretion in *siControl* and *siClock*-transfected myotubes. Selected myokines were chosen based on their presence in the secretome of differentiated primary skeletal muscle cells [15], their function and implication in metabolic diseases, and their availability and compatibility for multiplex array analysis. Out of the selected panel of 25 myokines, 15 myokines were detected in the concentrated perifusion samples, while 10 myokines remained undetectable, due to their low levels of basal secretion (Table 4).

Importantly, the profile and concentration levels of around-the-clock IL-6 secretion measured by multiplex analysis were very similar to those obtained by ELISA (compare Figure 3D—A). JTK_CYCLE analysis [30] confirmed that the average profile of secreted IL-6 measured by multiplex analysis was significantly circadian within 48 h (Figure 3D, Table 4). In addition to IL-6, MCP-1 and IL-8 were secreted in a circadian manner according to JTK_CYCLE analysis (Figure 4A, Table 4). M-CSF and GRO-alpha exhibited a secretion profile that might be clock-controlled; however, the adjusted minimal *p*-value did not reach significance according to JTK_CYCLE analysis (Figure 4B, Table 4). Furthermore, although the temporal secretion patterns of VEGF, CD44, FABP3, Galectin-3 and TIMP-1 were not identified as circadian, the overall secretion levels of these myokines were significantly reduced upon *CLOCK* depletion (Figure 4C, Table 4).

4. DISCUSSION

4.1. Molecular makeup of the circadian oscillator operative in human skeletal muscle

Our study provides for the first time evidence for cell-autonomous self-sustained circadian oscillators, operative in human primary skeletal myotubes. Molecular characteristics of the human myotube clock were assessed by two complementary approaches. Pronounced circadian oscillations were recorded with high temporal resolution for at least 4—5 consecutive days from *in vitro* synchronized primary skeletal myotubes, transduced with *Bmal1-luciferase* or *Per2-luciferase* lentivectors (Figure 1A,B). The circadian characteristics of human skeletal myotubes were in accordance with those reported for human primary thyrocytes, pancreatic islets, skin fibroblasts [28,31,35], and for mouse skeletal muscle assessed *in vivo* [21,22]. Sustained circadian oscillations were efficiently induced in our system by both forskolin (Figure 1) and dexamethasone (Supplementary Figure 2) pulses, suggesting that these oscillators are functional irrespective of the synchronization stimulus or entrainment pathway. It might be of interest to further explore whether other physiologically relevant stimuli like glucose, insulin, or myokine-induced signaling pathways play a role in human myotube synchronization.

In line with the outcome of our reporter experiments, endogenous around-the-clock gene expression analyses suggested that the core clock genes *BMAL1*, *REV-ERBα*, and *PER3*, as well as the clock output gene *DBP*, exhibit circadian oscillatory patterns in forskolin and dexamethasone-synchronized myotubes (Figure 2C closed circles, Supplementary Figure 3). Of note, the circadian amplitude of oscillations induced *in vitro* is typically lower if compared to *in vivo* oscillations from the same tissue, as demonstrated, for instance, for mouse islets synchronized *in vitro* or collected *in vivo* [11]. Thus, identifying clock-controlled genes *in vitro* by RT-qPCR represents a significant challenge due to rather low amplitudes [21,28]. More accurate methods like RNA sequencing of samples collected with higher temporal resolution might represent a solution to this problem.

4.2. Experimental model for circadian clock disruption in human primary myotubes

Here, we have established experimental settings for a highly reproducible siRNA-mediated *CLOCK* transcript knockdown of more than 80% in human primary muscle cells (Figure 2A, Supplementary Figure 4A). Upon such *CLOCK* silencing, significant flattening of the circadian amplitude was observed for the *Bmal1-luc* reporter (Figure 2B, Figure 3B, Supplementary Figure 4B) and for endogenous *REV-ERBα, PER3* and *DBP* transcripts (Figure 2C), confirming circadian core clock disruption. The discrepancy between *Bmal1-luc* reporter data and endogenous *BMAL1* expression upon *siClock* might be related to the fact that the knockdown effect of *CLOCK* on the *Bmal1-luc* reporter is evident primarily after 48 h, and that the promoter length of the *Bmal1* reporter is different from the endogenous gene. While *REV-ERBα, PER3* and *DBP* transcript profiles only exhibited residual circadian oscillations, which might be explained by incomplete clock ablation, the amplitude of the endogenous *BMAL1* oscillatory profile was not reduced and even slightly increased (Figure 2C). Similarly, siRNA-mediated depletion of *CLOCK* in U2OS cells was reported to increase *BMAL1* expression levels [36]. Moreover, *Clock*-deficient mice continue to exhibit circadian patterns of behavioral and molecular

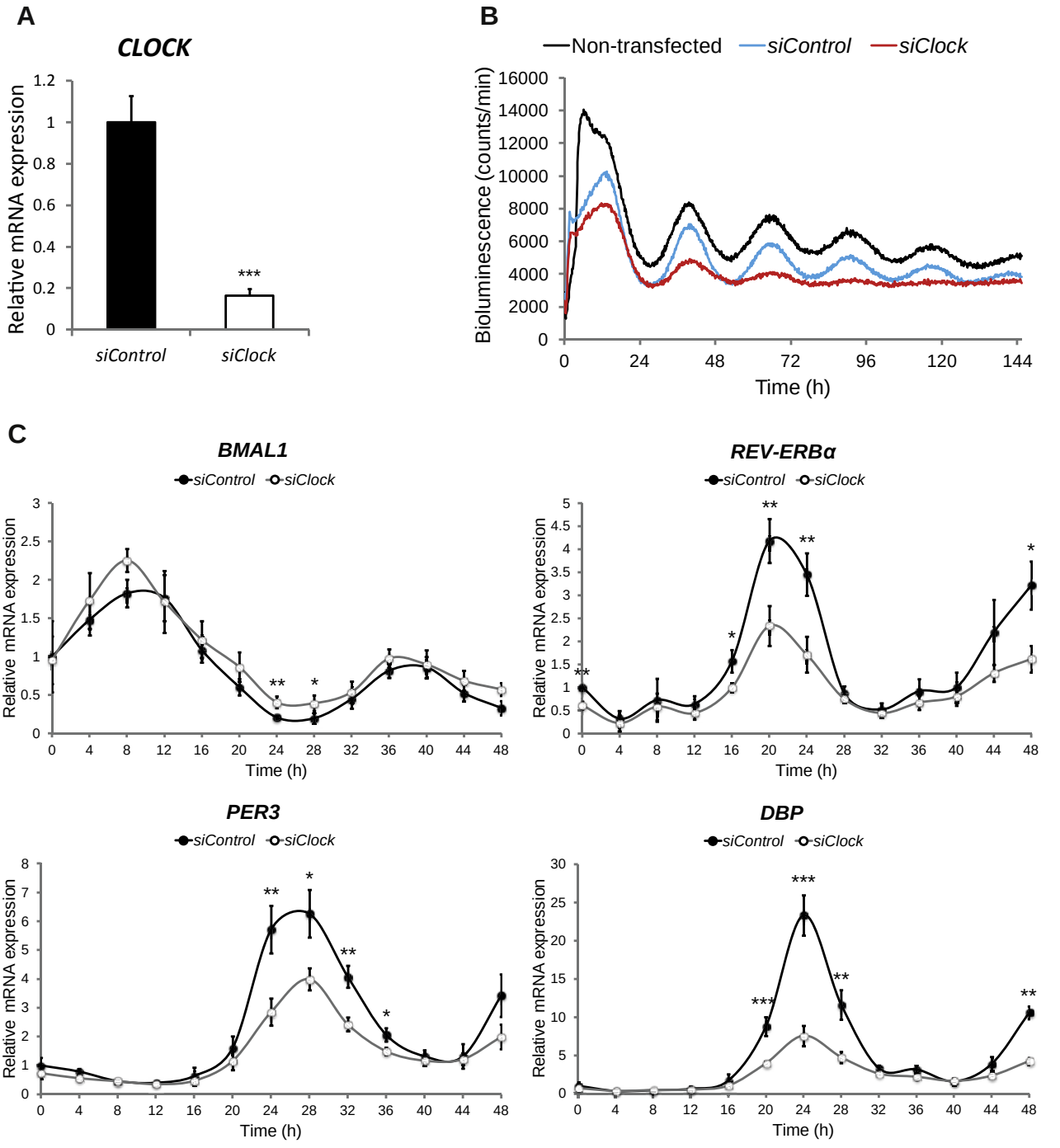

Figure 2: Silencing of *CLOCK* expression attenuates circadian oscillations in human skeletal myotubes. (A) *CLOCK* mRNA was measured in human myotubes transfected with *siControl* or *siClock* by RT-qPCR and normalized to the mean of *9S* and *HPRT*. *CLOCK* expression was reduced by 83.5 ± 3.4% (mean ± SEM, $n = 8$; ***$p < 0.001$) in *siClock*-transfected cells. (B) Amplitude of the *Bmal1-luc* reporter is strongly reduced in *siClock*-transfected myotubes. Representative *Bmal1-luc* oscillation profiles are shown for non-transfected (black line), *siControl* (blue line), and *siClock* (red line) transfected myotubes. *Bmal1-luc* oscillation profiles were recorded in duplicates (3 experiments, one donor per experiment). (C) RT-qPCR was performed for *BMAL1*, *REV-ERBα*, *PER3* and *DBP* on RNA samples extracted from forskolin-synchronized human myotubes, transfected with *siClock* (open circles) or *siControl* (closed circles). Samples were collected every 4 h and normalized to the mean of *9S*/*HPRT*. Profiles (mean ± SEM) are representative of 3 experiments (2 donors for time points 0 h–48 h and 3 donors for time points 12 h–36 h) with duplicates per time point.

rhythms. In the SCN and liver of *Clock*-deficient mice, *Bmal1* mRNA was elevated, as well as in pancreatic islets of *Clock*-mutant mice, which was attributed to reduced REV-ERBα expression and a compensatory effect of NPAS2 [11,37].

Clockwork perturbations may develop in humans with ageing and upon a number of disorders [3,4]. In this respect, our experimental model, which allows for reproducible clock disruption mediated by *CLOCK* depletion in differentiated skeletal myotubes, represents a valuable

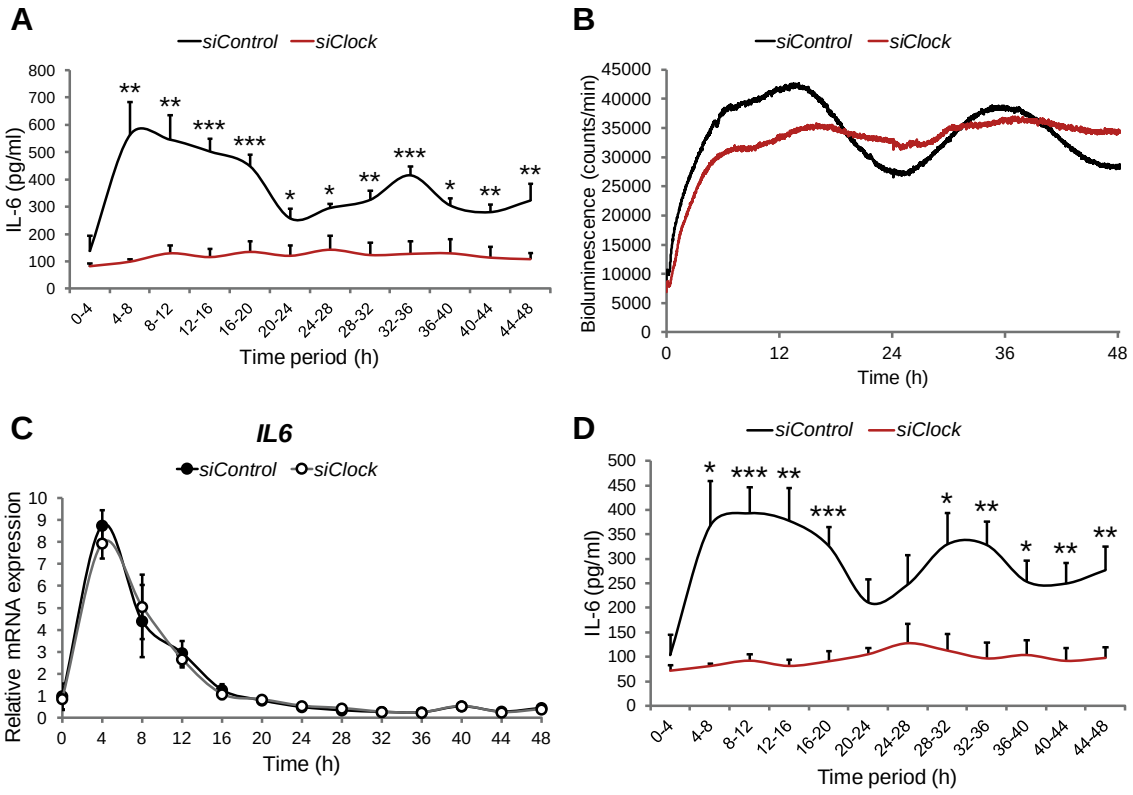

Figure 3: Basal IL-6 secretion by human skeletal myotubes is strongly inhibited in the absence of a functional circadian clock. Myoblasts were transduced with the *Bmal1-luc* lentivector, differentiated into myotubes and transfected with either *siControl* or *siClock* siRNA. 24 h following transfection, myotubes were synchronized with forskolin and subjected to continuous perifusion with parallel bioluminescence recording. (A) Basal IL-6 secretion profile (mean + SEM) in the presence or absence of a functional clock. The perifusion outflow medium was collected continuously in an automated manner in 4 h intervals until 48 h (0–4 corresponds to the accumulation of IL-6 between 0 h and 4 h). IL-6 levels in the perifusion outflow medium were assessed by ELISA. The results represent basal IL-6 levels normalized to the total DNA content. 2 technical duplicates from 3 independent experiments (3 non-obese donors, see Table 3) were analyzed for each time point. (B) *Bmal1-luc* bioluminescence profiles of *siControl*-transfected myotubes (black line) and *siClock*-transfected myotubes (red line), representative of 3 experiments, with one donor cell line used per experiment. (C) RT-qPCR was performed for *IL6* on RNA samples extracted from forskolin-synchronized human myotubes, transfected with *siClock* (open circles) or *siControl* (closed circles). Samples were collected every 4 h and normalized to the mean of *9S*/*HPRT*. Profiles (mean ± SEM) are representative of 3 experiments (2 donors for time points 0 h–48 h and 3 donors for time points 12 h–36 h) with duplicates per time point. (D) Basal IL-6 secretion profiles in the presence or absence of a functional clock obtained from concentrated perifusion samples, assessed by multiplex analysis. Data shown as mean + SEM of 2 technical duplicates from 3 biological samples for each time point, normalized to the total DNA content.

tool for getting significant insights into the roles of clock perturbations in different aspects of human skeletal muscle function. In order to detect oscillatory alterations caused by metabolic changes it might be necessary to develop further readouts involving clock output genes, as the here assessed *Bmal1-luc* and *Per2-luc* reporter profiles, although definitely informative regarding the core clock, might be of limited value as readout for metabolic perturbations.

4.3. Basal IL-6 secretion by human skeletal muscle is regulated by the circadian clock

Importantly, our study demonstrates that human skeletal myotubes, synchronized *in vitro* by forskolin or dexamethasone, secrete basal IL-6 in a circadian manner (Figure 3A,D, Supplementary Figure 5). Furthermore, this circadian pattern is flattened under *siClock*-mediated clockwork disruption, with overall basal IL-6 secretion being strongly downregulated by oscillator perturbation (Figure 3A,D, Table 3). The experimental settings we have developed, combining continuous perifusion and bioluminescence recording, allow for the direct assessment of IL-6 secretion by cultured human myotubes. Studies in healthy adults have suggested that IL-6 levels in the cerebrospinal fluid exhibit a 24 h oscillatory profile, and plasma levels of IL-6 have a biphasic 12 h component [38,39]. However, it has to be taken into account that plasma levels are originating from different sources of IL-6 and are also influenced by absorption in effector organs.

Our finding that basal IL-6 secretion is regulated locally by the skeletal muscle clock is in line with accumulating evidence that endocrine body rhythms are tightly regulated in humans by the circadian system at several levels (reviewed in [40]). Insulin secretion by beta cells in rodents was suggested to be a subject for clock regulation [11]. Moreover, a number of proinflammatory cytokines exhibit pronounced circadian alterations in the magnitude of their response to an endotoxin challenge at different times of the day [41], among them IL-6. Such circadian gating of the inflammatory response was lost for IL-6 in *REV-ERBα* knockout mice. Moreover, attenuation of REV-ERBα levels in human macrophages implied a direct link between REV-ERBα and IL-6 secretion [41].

Given a general controversy around the roles of IL-6 level alterations in the etiology of metabolic diseases [42], such downregulation might have a positive or negative impact on skeletal muscle function and body metabolism. A recent *in vivo* study in humans suggested that injection of IL-6 to T2D patients did not affect insulin-stimulated glucose uptake [43], while it was reported to have beneficiary effects on the glucose uptake in young, healthy subjects [44]. Indeed,

Table 3 — Overall basal IL-6 secretion after forskolin synchronization in human myotubes.

	Non-obese ($n = 3$)	Obese ($n = 3$)	All donors ($n = 6$)
	Mean ± SEM	Mean ± SEM	Mean ± SEM
IL-6/48h in *siControl* samples (pg)	4386.54 ± 411.71	5888.25 ± 1547.86	5137.40 ± 796.43
IL-6/48h in *siClock* samples (pg)	1424.12 ± 408.83	2395.52 ± 625.60	1909.82 ± 385.20
Inhibition of secretion (%)	69.30 ± 10.61	59.66 ± 7.04	64.48 ± 6.09
Clock mRNA silencing (%)	91.32 ± 2.67	78.57 ± 8.15	84.94 ± 4.57

acute high levels of IL-6 found after exercise improve insulin sensitivity, glucose metabolism [18,45], and fat metabolism [46], whereas chronic exposure to IL-6 causes insulin resistance in mice [47]. At the same time, *IL6* knockout mice develop mature-onset obesity and glucose intolerance [48]. We speculate that similar to cortisol, thyroid hormones, insulin, and other key hormones, which exhibit circadian rhythmicity of their levels [40,49], the oscillatory pattern of IL-6 secretion by the skeletal muscle might give an advantage for the temporal coordination of this myokine with the rest—activity cycle, thus ensuring optimal IL-6 response to external cues.

Our results presented in Figure 3C suggest that the circadian regulation of basal IL-6 secretion may not occur at the transcriptional level. As it has been reported, the clock is quite insensitive to large fluctuations of transcription rate [50]. Moreover, in mouse livers almost 50% of the cycling proteins do not have rhythmic steady-state mRNA levels [51,52]. Similarly, the *IL6* transcriptional profile was not circadian in cultured mHypoE-37 neurons [53], while a low amplitude oscillatory profile of *IL6* transcription was detected in human monocyte-derived macrophages [41] and in mouse astrocytes, where *Il6* transcription was suggested to be directly regulated by RORα [41,54]. Application of more sensitive transcription analysis approaches (RNA sequencing in samples with a higher temporal resolution), as well as addressing the potential regulation of *IL6* transcription in human skeletal muscle in particular by REV-ERBα and RORα, might shed additional light on this conjunction. As IL-6 is extensively modified at the post-translational level, one plausible hypothesis beyond transcription could be that the circadian profile of IL-6 secretion is controlled by post-translational modification [55]. Visualizing IL-6 secretion at the single cell level in synchronized human myotubes would be necessary to provide an insight into the mechanism of this phenomenon.

4.4. Functional circadian oscillator in human skeletal myotubes is required for proper basal secretion of a broader range of myokines

Of note, our screening for additional clock-controlled myokines, employing a human cytokine array, suggests that the regulatory role of the skeletal muscle clock is not restricted solely to basal IL-6 secretion but might represent a more general mechanism involved in the fine-tuning of a panel of myokines (Figure 4, Table 4). Specifically, the temporal profiles and/or overall levels of basal secretion of IL-8, MCP-1, M-CSF, GRO-alpha, VEGF, CD44, Galectin-3, FABP3 and TIMP-1 by human skeletal myotubes imply that these myokines might be regulated by the circadian clock (Figure 4, Table 4).

The following limitations of this part of the study should be taken into account: the low number of around-the-clock perifusion experiments analyzed by multiplex, due to the high experimental complexity of the automated perifusion system, and the low basal concentration levels of many myokines. Therefore, although the technical reproducibility for the duplicates in each around-the-clock experiment was high, in view of the large variability among the human donors with respect to their myokine secretion levels, these experiments must be interpreted with caution. More experimental repetitions will therefore be required to claim the circadian regulation of the myokines identified in our screen. Furthermore, in order to allow for the detection and quantification of myokines with low concentration levels in a circadian manner, more sensitive tools need to be developed.

Table 4 — Myokines with clock-regulated basal secretion.

	Circadian analysis (*p*-values calculated by JTK_CYCLE, $n = 3$)		Fold change of secretion (mean ± SEM, $n = 3$)		
	siControl	*siClock*	*siControl*	*siClock*	Paired t-test
CD44[a]	0.777	0.692	1.00	0.67 ± 0.13	0.025*
CHI3L1/YKL40[a]	1.000	1.000	1.00	2.12 ± 1.22	0.378
FABP3/H-FABP[a]	1.000	0.231	1.00	0.53 ± 0.11	0.002**
Galectin-3[a]	1.000	0.096	1.00	0.41 ± 0.07	5.19E-6***
GRO-alpha/CXCL1[a]	0.096	1.000	1.00	0.55 ± 0.23	0.083
IGFBP-3[a]	1.000	1.000	1.00	0.70 ± 0.23	0.226
IL-6[b]	0.01*	1.000	1.00	0.44 ± 0.16	0.006**
IL-8[b]	0.020*	1.000	1.00	0.47 ± 0.20	0.036*
MCP-1/CCL2[a]	0.020*	0.096	1.00	0.59 ± 0.27	0.157
M-CSF/CSF1[a]	0.059	0.777	1.00	0.64 ± 0.16	0.053
MMP-2[a]	1.000	1.000	1.00	0.78 ± 0.19	0.268
Serpin E1/PAI-1[a]	1.000	1.000	1.00	0.69 ± 0.16	0.070
Serpin C1[a]	0.492	1.000	1.00	0.64 ± 0.19	0.123
TIMP-1[a]	1.000	1.000	1.00	0.68 ± 0.14	0.043*
VEGF[b]	0.949	0.231	1.00	0.60 ± 0.10	0.002**

IFN-gamma[b], IL-1 beta[b], IL-2[b], IL-4[b], IL-7[a], IL-10[b], IL-12p70[b], IL-13[a], IL-17A[a], TNF alpha[b] were below detection level.
*$p < 0.05$,**$p < 0.01$,***$p < 0.001$.
[a] custom-made luminex screening plate.
[b] high sensitivity luminex performance plate.

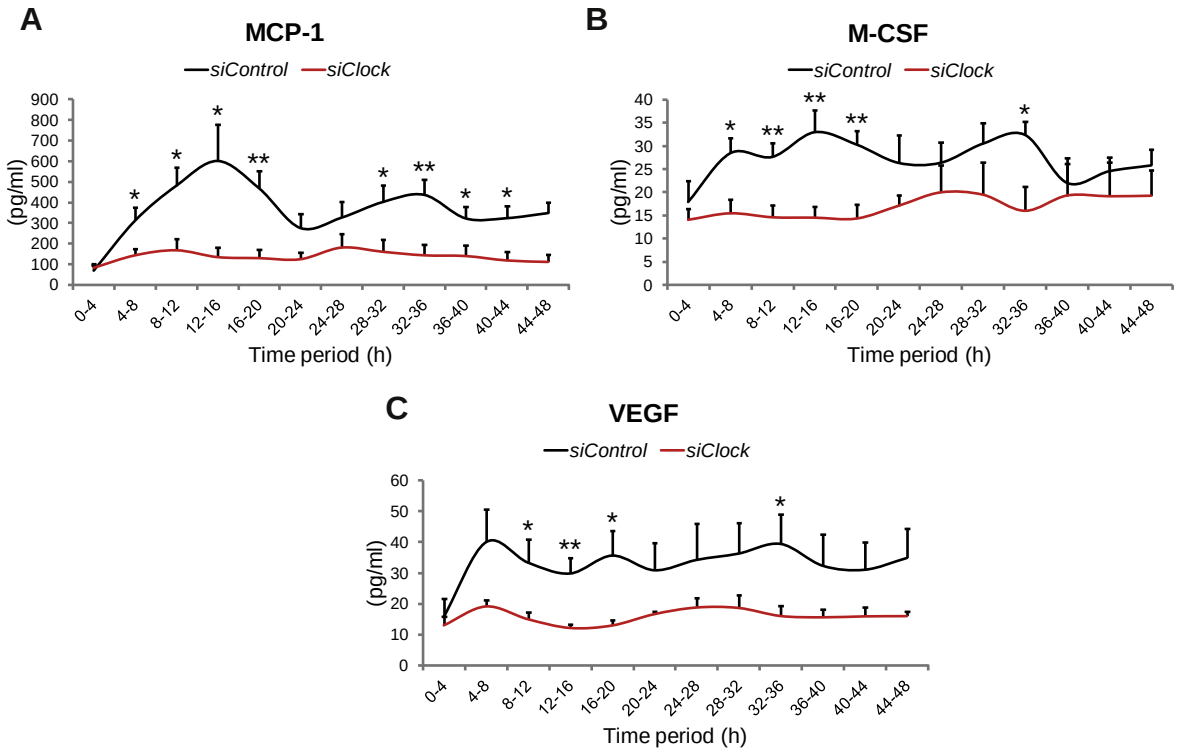

Figure 4: Basal myokine secretion by human skeletal myotubes is affected by circadian clock disruption. Myoblasts were transduced with the *Bmal1-luc* lentivector, differentiated into myotubes, transfected with either *siControl* or *siClock* siRNA, and subjected to continuous perifusion with parallel bioluminescence recording. Concentrated perifusion samples were assessed by multiplex analysis. 2 technical duplicates from 3 biological samples were analyzed for each time point, and normalized to the total DNA content. Basal secretion profiles (mean + SEM) in the presence or absence of a functional clock are shown for (A) MCP-1, (B) M-CSF, and (C) VEGF.

Of note, myokines identified in our multiplex screen as potentially clock-regulated for their basal secretion (Table 4, Figure 4) have been previously linked to obesity or T2D. For instance, serum IL-8 levels are increased in T2D patients, with a significant diurnal variation observed for IL-8 in blood upon LPS-stimulation [56,57]. Furthermore, insulin-resistant human myotubes secrete higher levels of IL-8 [19]. MCP-1, which mediates skeletal muscle macrophage recruitment, was also suggested to play a role in the etiology of T2D [20]. Interestingly, this proinflammatory cytokine has been previously shown to exhibit pronounced circadian alterations in the magnitude of its response to endotoxin challenge at different times of the day [41]. M-CSF has been shown to play an important role in inflammatory diseases including obesity [58]. VEGF, known for its angiogenic properties, is transcriptionally regulated by the circadian clock [59], and has also been implicated in T2D and insulin resistance [60,61]. Plasma levels of CD44 were positively correlated with insulin resistance in humans [62,63]. Furthermore, genetic association studies have linked CD44 with T2D [62,64]. Taken together, our data suggest that disruption of the circadian clock might affect the level and temporal profile of basal secretion for a number of myokines that play a role in the etiology of T2D and obesity. Inevitably, our findings raise the question on the physiological relevance of basal myokine secretion. One plausible argument is that while induced myokine secretion is regulated acutely (for instance by exercise), circadian regulation of basal myokine secretion might represent a fine-tuning mechanism, allowing adaptation of the skeletal muscle function to the rest—activity cycle. Given the major role of the circadian clock in allowing organisms to anticipate daily environmental changes rather than react to them, circadian regulation of basal myokine secretion might represent such an anticipatory mechanism that coordinates skeletal muscle "availability". Furthermore, this newly discovered link between the functional skeletal muscle clock and basal secretion of a number of myokines might bear potential consequences for the development of chronic diseases, such as obesity and T2D.

5. CONCLUSION

Skeletal muscle represents the most important site of insulin resistance in T2D patients [12]. Moreover, the emerging critical role of inflammation in the etiology of T2D makes inflammatory cytokines plausible candidates for developing new therapeutic approaches for the treatment of this disease [65]. It is therefore of highest scientific and clinical importance to provide further insight into the emerging connection between circadian oscillator function, metabolic regulation, and T2D. Given that human primary myotubes, established from T2D patient biopsies and cultured *in vitro,* have been demonstrated to maintain their *in vivo* phenotypes of inflammation and insulin resistance [66], our model of synchronized cultured primary myotubes represents a valuable experimental tool that allows for studying the role of the circadian oscillator in human skeletal muscle function upon metabolic diseases. This work is the first detailed characterization of the human skeletal myotube circadian oscillator and its critical impact on basal myokine secretion. It opens the way for future studies that may link defects in these pathways with insulin resistance, obesity, and T2D. Given obvious obstacles for studying the human circadian

oscillator *in vivo*, our experimental approach, using human primary cell cultures established from biopsies that express a luciferase reporter driven from a circadian promoter, constitutes a powerful model system for human skeletal muscle clock studies.

FUNDING

This work was funded by the Swiss National Science Foundation Grant No. 31003A_146475/1, Fondation Romande pour la Recherche sur Diabète, Fondation Ernst et Lucie Schmidheiny, Société Académique de Genève (CD), and the Sinergia Swiss National Science Foundation Grant No. CRSII3-154405 (CD, EL).

ACKNOWLEDGMENTS

We are grateful to our colleagues from University Hospital of Geneva: Jacques Philippe for constructive comments on this work and Thierry Berney for generously providing human samples; and to our colleagues from the University of Geneva: Ueli Schibler for invaluable help with the perifusion system development and for scientific inspiration; Andre Liani and George Severi for assistance with the perifusion experiments; Anne-Marie Makhlouf and Camille Saini for lentivirus preparations; Christelle Barraclough and Mylene Docquier (iGE3 Genomics Platform) for assistance in performing qPCR experiments; Nicolas Hulo (iGE3 BioSC) for assistance with the statistical analysis.

CONFLICT OF INTEREST

The authors have no conflict of interest to declare.

APPENDIX A. SUPPLEMENTARY DATA

Supplementary data related to this article can be found at http://dx.doi.org/10.1016/j.molmet.2015.07.009.

REFERENCES

[1] Albrecht, U., 2012. Timing to perfection: the biology of central and peripheral circadian clocks. Neuron 74:246–260.
[2] Bass, J., 2012. Circadian topology of metabolism. Nature 491:348–356.
[3] Dibner, C., Schibler, U., 2015 May. Circadian timing of metabolism in animal models and humans. Journal of Internal Medicine 277(5):513–527. http://dx.doi.org/10.1111/joim.12347.
[4] Marcheva, B., Ramsey, K.M., Peek, C.B., Affinati, A., Maury, E., Bass, J., 2013. Circadian clocks and metabolism. Handbook of Experimental Pharmacology, 127–155.
[5] Damiola, F., Le Minh, N., Preitner, N., Kornmann, B., Fleury-Olela, F., Schibler, U., 2000. Restricted feeding uncouples circadian oscillators in peripheral tissues from the central pacemaker in the suprachiasmatic nucleus. Genes & Development 14:2950–2961.
[6] Adamovich, Y., Rousso-Noori, L., Zwighaft, Z., Neufeld-Cohen, A., Golik, M., Kraut-Cohen, J., et al., 2014. Circadian clocks and feeding time regulate the oscillations and levels of hepatic triglycerides. Cell Metabolism 19:319–330.
[7] Feillet, C.A., Albrecht, U., Challet, E., 2006. "Feeding time" for the brain: a matter of clocks. Journal of Physiology Paris 100:252–260.
[8] Iijima, M., Yamaguchi, S., van der Horst, G.T., Bonnefont, X., Okamura, H., Shibata, S., 2005. Altered food-anticipatory activity rhythm in Cryptochrome-deficient mice. Neuroscience Research 52:166–173.
[9] Turek, F.W., Joshu, C., Kohsaka, A., Lin, E., Ivanova, G., McDearmon, E., et al., 2005. Obesity and metabolic syndrome in circadian Clock mutant mice. Science 308:1043–1045.
[10] Paschos, G.K., Ibrahim, S., Song, W.L., Kunieda, T., Grant, G., Reyes, T.M., et al., 2012. Obesity in mice with adipocyte-specific deletion of clock component Arntl. Nature Medicine 18:1768–1777.
[11] Marcheva, B., Ramsey, K.M., Buhr, E.D., Kobayashi, Y., Su, H., Ko, C.H., et al., 2010. Disruption of the clock components CLOCK and BMAL1 leads to hypoinsulinaemia and diabetes. Nature 466:627–631.
[12] DeFronzo, R.A., Tripathy, D., 2009. Skeletal muscle insulin resistance is the primary defect in type 2 diabetes. Diabetes Care 32(Suppl. 2):S157–S163.
[13] Bostrom, P., Wu, J., Jedrychowski, M.P., Korde, A., Ye, L., Lo, J.C., et al., 2012. A PGC1-alpha-dependent myokine that drives brown-fat-like development of white fat and thermogenesis. Nature 481:463–468.
[14] Pedersen, B.K., Febbraio, M.A., 2012. Muscles, exercise and obesity: skeletal muscle as a secretory organ. Nature Reviews. Endocrinology 8:457–465.
[15] Hartwig, S., Raschke, S., Knebel, B., Scheler, M., Irmler, M., Passlack, W., et al., 2014. Secretome profiling of primary human skeletal muscle cells. Biochimica et Biophysica Acta 1844:1011–1017.
[16] Ostrowski, K., Rohde, T., Zacho, M., Asp, S., Pedersen, B.K., 1998. Evidence that interleukin-6 is produced in human skeletal muscle during prolonged running. Journal of Physiology 508(Pt 3):949–953.
[17] Ellingsgaard, H., Ehses, J.A., Hammar, E.B., Van Lommel, L., Quintens, R., Martens, G., et al., 2008. Interleukin-6 regulates pancreatic alpha-cell mass expansion. Proceedings of the National Academy of Sciences of the United States of America 105:13163–13168.
[18] Ellingsgaard, H., Hauselmann, I., Schuler, B., Habib, A.M., Baggio, L.L., Meier, D.T., et al., 2011. Interleukin-6 enhances insulin secretion by increasing glucagon-like peptide-1 secretion from L cells and alpha cells. Nature Medicine 17:1481–1489.
[19] Bouzakri, K., Plomgaard, P., Berney, T., Donath, M.Y., Pedersen, B.K., Halban, P.A., 2011. Bimodal effect on pancreatic beta-cells of secretory products from normal or insulin-resistant human skeletal muscle. Diabetes 60:1111–1121.
[20] Patsouris, D., Cao, J.J., Vial, G., Bravard, A., Lefai, E., Durand, A., et al., 2014. Insulin resistance is associated with MCP1-mediated macrophage accumulation in skeletal muscle in mice and humans. PLoS One 9:e110653.
[21] McCarthy, J.J., Andrews, J.L., McDearmon, E.L., Campbell, K.S., Barber, B.K., Miller, B.H., et al., 2007. Identification of the circadian transcriptome in adult mouse skeletal muscle. Physiological Genomics 31:86–95.
[22] Andrews, J.L., Zhang, X., McCarthy, J.J., McDearmon, E.L., Hornberger, T.A., Russell, B., et al., 2010. CLOCK and BMAL1 regulate MyoD and are necessary for maintenance of skeletal muscle phenotype and function. Proceedings of the National Academy of Sciences of the United States of America 107:19090–19095.
[23] Dyar, K.A., Ciciliot, S., Wright, L.E., Bienso, R.S., Tagliazucchi, G.M., Patel, V.R., et al., 2014. Muscle insulin sensitivity and glucose metabolism are controlled by the intrinsic muscle clock. Molecular Metabolism 3:29–41.
[24] Harfmann, B.D., Schroder, E.A., Esser, K.A., 2014. Circadian rhythms, the molecular clock, and skeletal muscle. Journal of Biological Rhythms.
[25] Agley, C.C., Rowlerson, A.M., Velloso, C.P., Lazarus, N.L., Harridge, S.D., 2015 Jan 12. Isolation and quantitative immunocytochemical characterization of primary myogenic cells and fibroblasts from human skeletal muscle. Journal of Visualized Experiments (95):52049. http://dx.doi.org/10.3791/52049.
[26] Liu, A.C., Tran, H.G., Zhang, E.E., Priest, A.A., Welsh, D.K., Kay, S.A., 2008. Redundant function of REV-ERBalpha and beta and non-essential role for Bmal1 cycling in transcriptional regulation of intracellular circadian rhythms. PLoS Genetics 4:e1000023.
[27] Fujioka, A., Takashima, N., Shigeyoshi, Y., 2006. Circadian rhythm generation in a glioma cell line. Biochemical and Biophysical Research Communications 346:169–174.
[28] Pulimeno, P., Mannic, T., Sage, D., Giovannoni, L., Salmon, P., Lemeille, S., et al., 2013. Autonomous and self-sustained circadian oscillators displayed in human islet cells. Diabetologia 56:497–507.

[29] Saini, C., Morf, J., Stratmann, M., Gos, P., Schibler, U., 2012. Simulated body temperature rhythms reveal the phase-shifting behavior and plasticity of mammalian circadian oscillators. Genes & Development 26:567—580.
[30] Hughes, M.E., Hogenesch, J.B., Kornacker, K., 2010. JTK_CYCLE: an efficient nonparametric algorithm for detecting rhythmic components in genome-scale data sets. Journal of Biological Rhythms 25:372—380.
[31] Mannic, T., Meyer, P., Triponez, F., Pusztaszeri, M., Le Martelot, G., Mariani, O., et al., 2013. Circadian clock characteristics are altered in human thyroid malignant nodules. The Journal of Clinical Endocrinology and Metabolism 98:4446—4456.
[32] Gaspar, L., van de Werken, M., Johansson, A.S., Moriggi, E., Owe-Larsson, B., Kocks, J.W., et al., 2014. Human cellular differences in cAMP—CREB signaling correlate with light-dependent melatonin suppression and bipolar disorder. European Journal of Neuroscience 40:2206—2215.
[33] Balsalobre, A., Brown, S.A., Marcacci, L., Tronche, F., Kellendonk, C., Reichardt, H.M., et al., 2000. Resetting of circadian time in peripheral tissues by glucocorticoid signaling. Science 289:2344—2347.
[34] Dendorfer, U., Oettgen, P., Libermann, T.A., 1994. Multiple regulatory elements in the interleukin-6 gene mediate induction by prostaglandins, cyclic AMP, and lipopolysaccharide. Molecular and Cellular Biology 14:4443—4454.
[35] Brown, S.A., Fleury-Olela, F., Nagoshi, E., Hauser, C., Juge, C., Meier, C.A., et al., 2005. The period length of fibroblast circadian gene expression varies widely among human individuals. PLoS Biology 3:e338.
[36] Baggs, J.E., Price, T.S., DiTacchio, L., Panda, S., Fitzgerald, G.A., Hogenesch, J.B., 2009. Network features of the mammalian circadian clock. PLoS Biology 7:e52.
[37] Debruyne, J.P., Noton, E., Lambert, C.M., Maywood, E.S., Weaver, D.R., Reppert, S.M., 2006. A clock shock: mouse CLOCK is not required for circadian oscillator function. Neuron 50:465—477.
[38] Agorastos, A., Hauger, R.L., Barkauskas, D.A., Moeller-Bertram, T., Clopton, P.L., Haji, U., et al., 2014. Circadian rhythmicity, variability and correlation of interleukin-6 levels in plasma and cerebrospinal fluid of healthy men. Psychoneuroendocrinology 44:71—82.
[39] Vgontzas, A.N., Bixler, E.O., Lin, H.M., Prolo, P., Trakada, G., Chrousos, G.P., 2005. IL-6 and its circadian secretion in humans. Neuroimmunomodulation 12:131—140.
[40] Philippe, J., Dibner, C., 2014. Thyroid circadian timing: roles in physiology and thyroid malignancies. Journal of Biological Rhythms.
[41] Gibbs, J.E., Blaikley, J., Beesley, S., Matthews, L., Simpson, K.D., Boyce, S.H., et al., 2012. The nuclear receptor REV-ERBalpha mediates circadian regulation of innate immunity through selective regulation of inflammatory cytokines. Proceedings of the National Academy of Sciences of the United States of America 109:582—587.
[42] Pedersen, B.K., Febbraio, M.A., 2008. Muscle as an endocrine organ: focus on muscle-derived interleukin-6. Physiological Reviews 88:1379—1406.
[43] Harder-Lauridsen, N.M.N., Krogh-Madsen, R., Holst, J.J., Plomgaard, P., Leick, L., Pedersen, B.K.B., et al., 2014 Apr 1. The effect of IL-6 on the insulin sensitivity in patients with type 2 diabetes. American Journal of Physiology Endocrinology and Metabolism 306(7):E769—E778. http://dx.doi.org/10.1152/ajpendo.00571.2013.
[44] Carey, A.L., Steinberg, G.R., Macaulay, S.L., Thomas, W.G., Holmes, A.G., Ramm, G., et al., 2006. Interleukin-6 increases insulin-stimulated glucose disposal in humans and glucose uptake and fatty acid oxidation in vitro via AMP-activated protein kinase. Diabetes 55:2688—2697.
[45] Weigert, C., Hennige, A.M., Lehmann, R., Brodbeck, K., Baumgartner, F., Schauble, M., et al., 2006. Direct cross-talk of interleukin-6 and insulin signal transduction via insulin receptor substrate-1 in skeletal muscle cells. Journal of Biological Chemistry 281:7060—7067.
[46] Wueest, S., Item, F., Boyle, C.N., Jirkof, P., Cesarovic, N., Ellingsgaard, H., et al., 2014. Interleukin-6 contributes to early fasting-induced free fatty acid mobilization in mice. American Journal of Physiology. Regulatory, Integrative and Comparative Physiology 306:R861—R867.
[47] Nieto-Vazquez, I., Fernandez-Veledo, S., de Alvaro, C., Lorenzo, M., 2008. Dual role of interleukin-6 in regulating insulin sensitivity in murine skeletal muscle. Diabetes 57:3211—3221.
[48] Wallenius, V., Wallenius, K., Ahren, B., Rudling, M., Carlsten, H., Dickson, S.L., et al., 2002. Interleukin-6-deficient mice develop mature-onset obesity. Nature Medicine 8:75—79.
[49] Kalsbeek, A., Fliers, E., 2013. Daily regulation of hormone profiles. Handbook of Experimental Pharmacology, 185—226.
[50] Dibner, C., Sage, D., Unser, M., Bauer, C., d'Eysmond, T., Naef, F., et al., 2009. Circadian gene expression is resilient to large fluctuations in overall transcription rates. The EMBO Journal 28:123—134.
[51] Mauvoisin, D., Wang, J., Jouffe, C., Martin, E., Atger, F., Waridel, P., et al., 2014. Circadian clock-dependent and -independent rhythmic proteomes implement distinct diurnal functions in mouse liver. Proceedings of the National Academy of Sciences of the United States of America 111:167—172.
[52] Reddy, A.B., Karp, N.A., Maywood, E.S., Sage, E.A., Deery, M., O'Neill, J.S., et al., 2006. Circadian orchestration of the hepatic proteome. Current Biology 16:1107—1115.
[53] Greco, J.A., Oosterman, J.E., Belsham, D.D., 2014. Differential effects of omega-3 fatty acid docosahexaenoic acid and palmitate on the circadian transcriptional profile of clock genes in immortalized hypothalamic neurons. American Journal of Physiology. Regulatory, Integrative and Comparative Physiology 307:R1049—R1060.
[54] Journiac, N., Jolly, S., Jarvis, C., Gautheron, V., Rogard, M., Trembleau, A., et al., 2009. The nuclear receptor ROR(alpha) exerts a bi-directional regulation of IL-6 in resting and reactive astrocytes. Proceedings of the National Academy of Sciences of the United States of America 106:21365—21370.
[55] Simpson, R.J., Hammacher, A., Smith, D.K., Matthews, J.M., Ward, L.D., 1997. Interleukin-6: structure-function relationships. Protein Science 6:929—955.
[56] Zozulinska, D., Majchrzak, A., Sobieska, M., Wiktorowicz, K., Wierusz-Wysocka, B., 1999. Serum interleukin-8 level is increased in diabetic patients. Diabetologia 42:117—118.
[57] Hermann, C., von Aulock, S., Dehus, O., Keller, M., Okigami, H., Gantner, F., et al., 2006. Endogenous cortisol determines the circadian rhythm of lipopolysaccharide—but not lipoteichoic acid—inducible cytokine release. European Journal of Immunology 36:371—379.
[58] Chitu, V., Stanley, E.R., 2006. Colony-stimulating factor-1 in immunity and inflammation. Current Opinion in Immunology 18:39—48.
[59] Jensen, L.D., Cao, Y., 2013. Clock controls angiogenesis. Cell Cycle (Georgetown, Tex) 12:405—408.
[60] Elias, I., Franckhauser, S., Ferre, T., Vila, L., Tafuro, S., Munoz, S., et al., 2012. Adipose tissue overexpression of vascular endothelial growth factor protects against diet-induced obesity and insulin resistance. Diabetes 61:1801—1813.
[61] Hagberg, C.E., Mehlem, A., Falkevall, A., Muhl, L., Fam, B.C., Ortsater, H., et al., 2012. Targeting VEGF-B as a novel treatment for insulin resistance and type 2 diabetes. Nature 490:426—430.
[62] Kodama, K., Horikoshi, M., Toda, K., Yamada, S., Hara, K., Irie, J., et al., 2012. Expression-based genome-wide association study links the receptor CD44 in adipose tissue with type 2 diabetes. Proceedings of the National Academy of Sciences of the United States of America 109:7049—7054.
[63] Liu, L.F., Kodama, K., Wei, K., Tolentino, L.L., Choi, O., Engleman, E.G., et al., 2015. The receptor CD44 is associated with systemic insulin resistance and proinflammatory macrophages in human adipose tissue. Diabetologia 58:1579—1586.
[64] Kodama, K., Toda, K., Morinaga, S., Yamada, S., Butte, A.J., 2015. Anti-CD44 antibody treatment lowers hyperglycemia and improves insulin resistance,

adipose inflammation, and hepatic steatosis in diet-induced obese mice. Diabetes 64:867–875.

[65] Donath, M.Y., 2014. Targeting inflammation in the treatment of type 2 diabetes: time to start. Nature Reviews Drug Discovery 13:465–476.

[66] Green, C.J., Pedersen, M., Pedersen, B.K., Scheele, C., 2011. Elevated NF-kappaB activation is conserved in human myocytes cultured from obese type 2 diabetic patients and attenuated by AMP-activated protein kinase. Diabetes 60:2810–2819.

Supplementary data to :

Human skeletal myotubes display a cell-autonomous circadian clock implicated in basal myokine secretion

Laurent Perrin[1], Ursula Loizides-Mangold[1,6], Svetlana Skarupelova[1,6], Pamela Pulimeno[1], Stephanie Chanon[2], Maud Robert[3], Karim Bouzakri[4], Christine Modoux[5], Pascale Roux-Lombard[5], Hubert Vidal[2], Etienne Lefai[2], Charna Dibner[1,*]

[1]Division of Endocrinology, Diabetes and Nutrition, Department of Clinical Medicine, Faculty of Medicine, University of Geneva, Geneva, Switzerland

[2]CarMeN Laboratory, INSERM U1060, INRA 1397, University Lyon 1, Oullins, France

[3]Department of Digestive and Bariatric Surgery, Edouard Herriot Hospital, Lyon, France

[4]Department of Genetic Medicine and Development, Faculty of Medicine, University of Geneva, Geneva, Switzerland

[5]Division of Immunology and Allergy, Department of Medical Specialties, University Hospital and Faculty of Medicine, University of Geneva, Geneva, Switzerland

[6]U. Loizides-Mangold and S. Skarupelova contributed equally to this study

***Corresponding author.** Charna Dibner; Division of Endocrinology, Diabetes, Hypertension and Nutrition, Department of Clinical Medicine, Faculty of Medicine, University of Geneva, Aile Jura 4-774, Rue Gabrielle-Perret-Gentil 4, CH-1211 Geneva, Switzerland

email: Charna.Dibner@hcuge.ch

Phone: +41 22 372 93 18; Fax: +41 22 372 93 26

Table of Contents

Supplementary Tables

Supplementary Table 1

Sequences of human qPCR primers		
Gene name	Primer sequence	
BMAL1	Forward	5'-CCCTTGGACCAAGGAAGTAGAA-3'
	Reverse	5'-CTTCCAGGACGTTGGCTAAAAC-3'
CRY1	Forward	5'-GAGAACAGATCCCAATGGAGACTATAT-3'
	Reverse	5'-CCTCTTAGGACAGGCAAATAACG-3'
REV-ERBα	Forward	5'-GATCGTGAGTCGCGGGGTCC-3'
	Reverse	5'-TGTAGGTGATGACGCCACCTGTGT-3'
PER2	Forward	5'-CGCAGGGTGCGCTCGTTTGAA-3'
	Reverse	5'-GCTGGGCTCTGGAACGAAGCTTTCG-3'
PER3	Forward	5'-CCTGGACCCTGAACATGCA-3'
	Reverse	5'-TGTGAGCCCCACGTGTTTAA-3'
DBP	Forward	5'-TAGAAGGAGCGCCTTGAGTC-3'
	Reverse	5'-GCAACCCTCCAGTATCCAGA-3'
CLOCK	Forward	5'-CAAGCCACCGCAACAATT-3'
	Reverse	5'-GGATTCCCATGGAGCAACCTA-3'
IL6	Forward	5'-GGTACATCCTCGACGGCATCT-3'
	Reverse	5'-GTGCCTCTTTGCTGCTTTCAC-3'
9S	Forward	5'-CTCCGGAACAAACGTGAGGT-3'
	Reverse	5'-TCCAGCTTCATCTTGCCCTC-3'
GAPDH	Forward	5'-GAAGGTGAAGGTCGGAGTC-3'
	Reverse	5'-GAAGATGGTGATGGGATTTC-3'
HPRT	Forward	5'-GATTTTATCAGACTGAGGAGC-3'
	Reverse	5'-TCCAGTTAAAGTTGAGAGATC-3'

Supplementary Table 2

Amplitude of *siControl* and *siClock*-transfected samples determined by JTK_CYCLE				
	BMAL1	***REV-ERBα***	***PER3***	***DBP***
	Normalized mean amplitude (fold change)			
siControl	0.62	0.77	2.6	5.91
siClock	0.8	0.51	1.46	2.99

Supplementary Figures

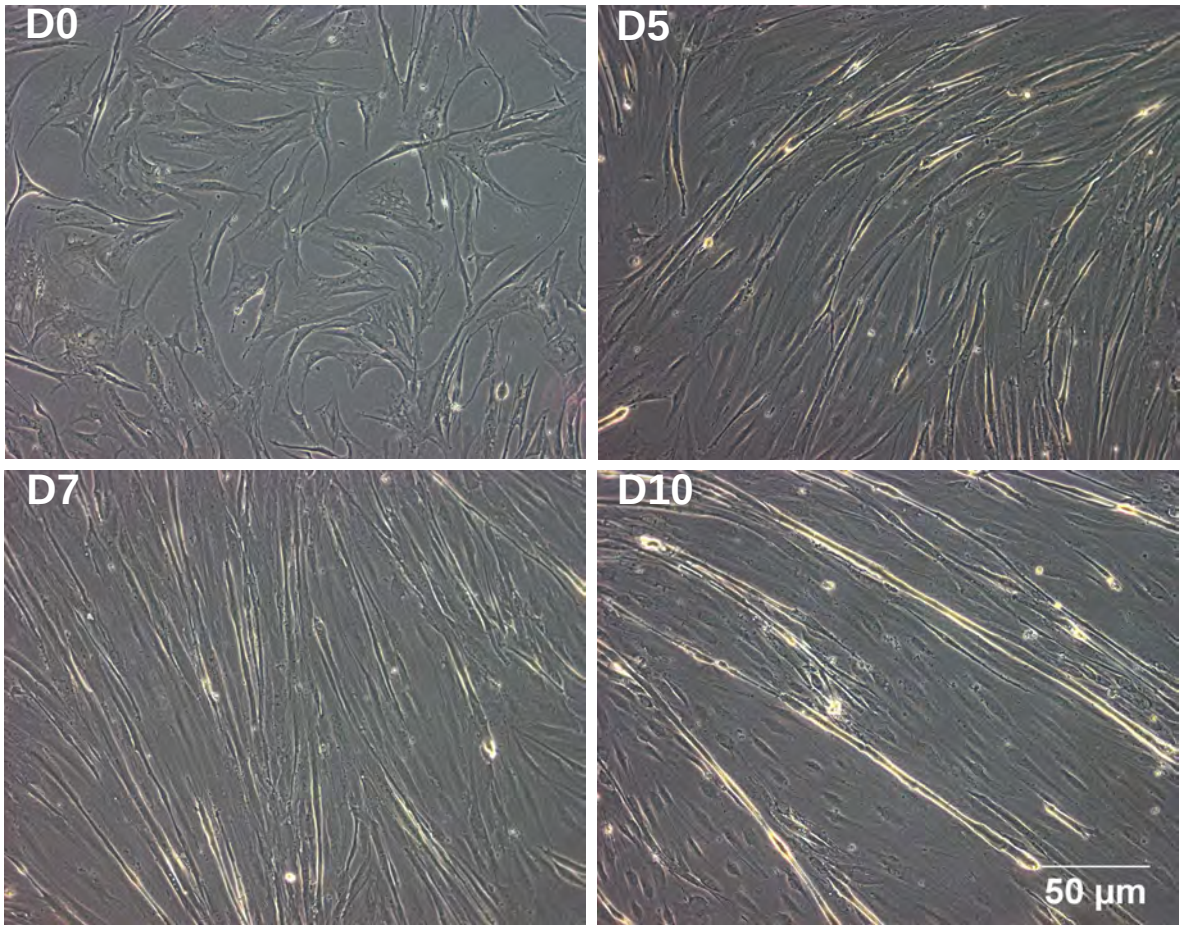

Supplementary Figure 1: Differentiation of *in vitro* cultured human skeletal myoblasts to myotubes.
Representative photos were taken with a Zeiss Axiovert 200 microscope at day 0 (D0), D5, D7, and D10 following start of the differentiation process (switch from 20% to 2% FBS-containing medium, see Material and Methods for details). D0: start of the differentiation process; D5: cells are oriented in the same direction and fusion has already begun; D7: differentiation is complete; D10: myotubes keep the differentiated status for several days.

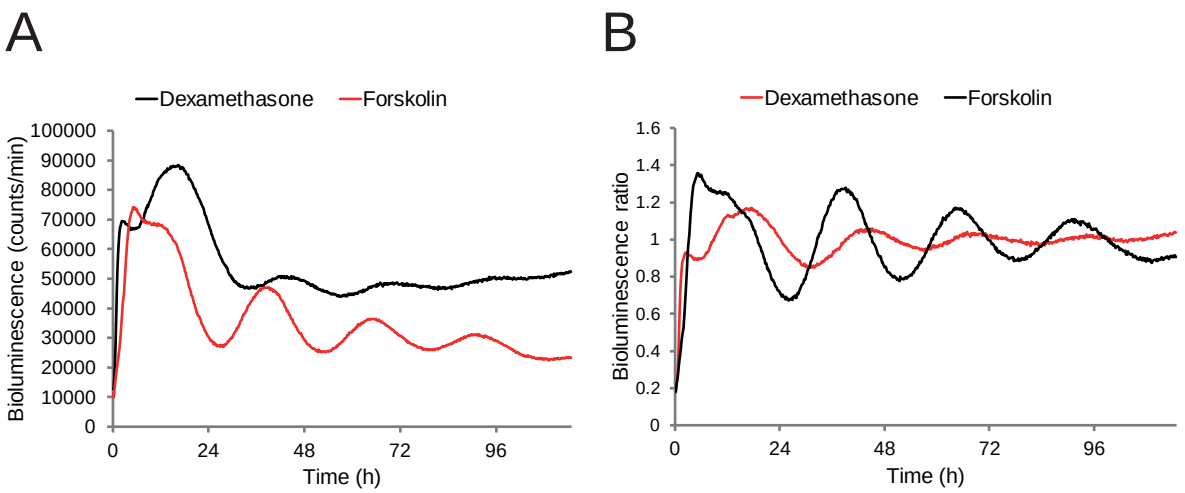

Supplementary Figure 2: *In vitro* synchronization by forskolin or dexamethasone induces pronounced circadian oscillations in human skeletal myotubes.
Bmal1-luc bioluminescence profiles were recorded from human myotubes, synchronized with a 30 min pulse of 100 nM dexamethasone (black line) or with a 1 h pulse of 10 μM forskolin (red line). Raw (A) and detrended (B) oscillation profiles are representative of 2 independent experiments (one donor each) performed in duplicates.

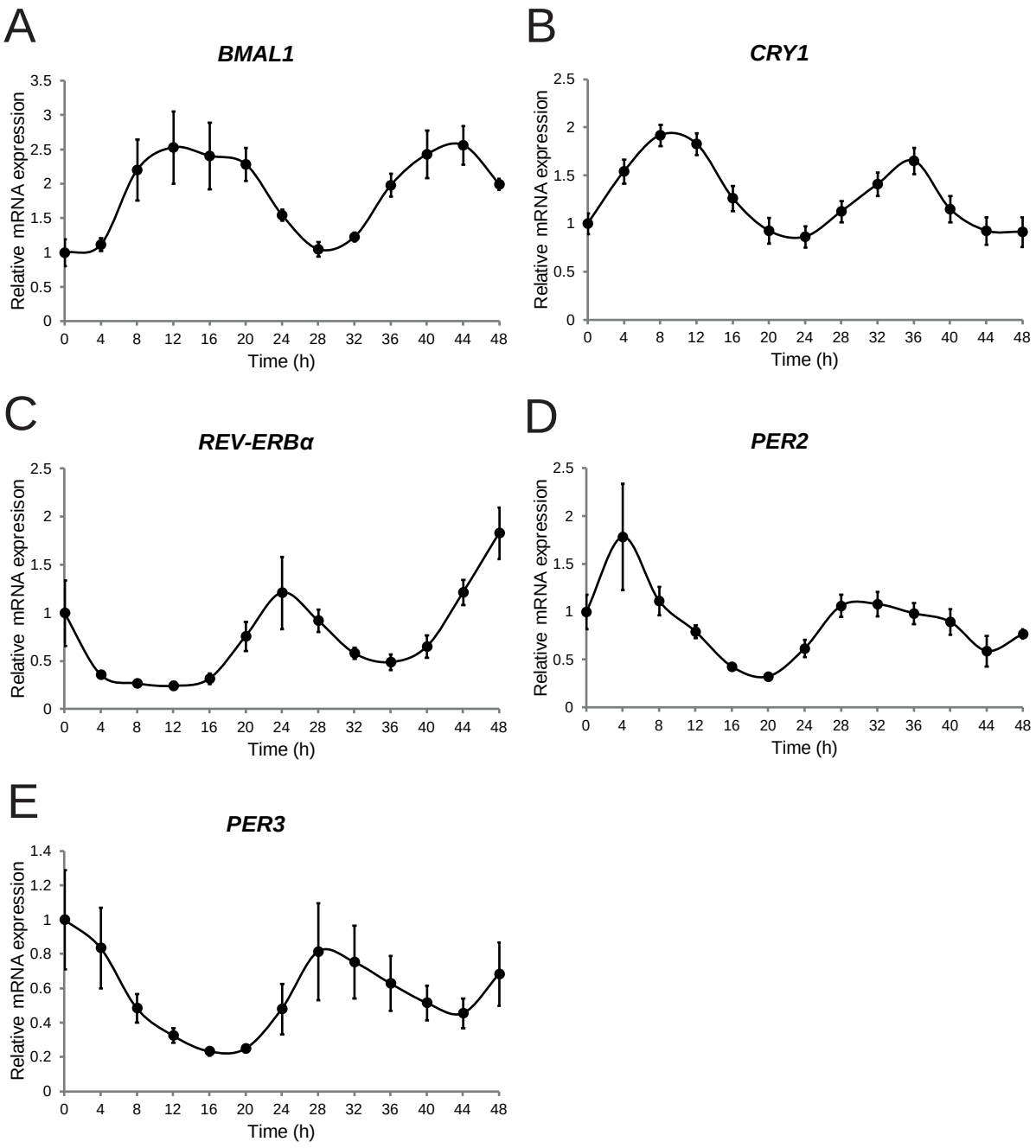

Supplementary Figure 3: Oscillation profiles of core clock transcripts in dexamethasone-synchronized human myotubes.

Endogenous expression of core clock transcripts was assessed in dexamethasone-synchronized myotubes, collected every 4 h during 48 h following synchronization. RT-qPCRs were performed in RNA samples extracted from human myotubes to assess (A) *BMAL1*, (B) *CRY1*, (C) *REV-ERBα*, (D) *PER2*, (E) *PER3*, and normalized to the mean of *9S-GAPDH*. Profiles are representative of $n = 4$ experiments (mean ± SEM), each performed with myotubes from one donor in duplicates for every condition.

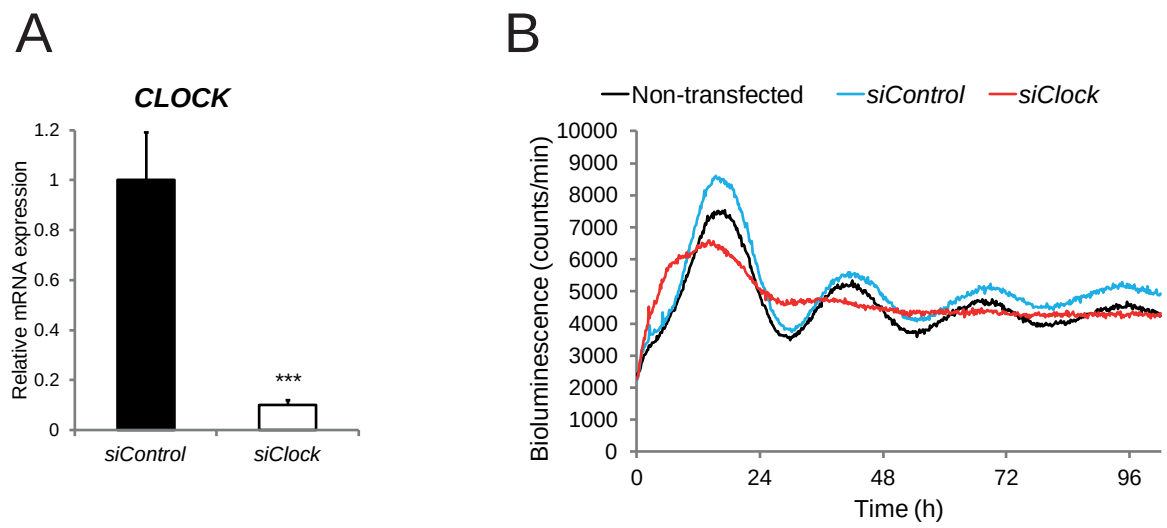

Supplementary Figure 4: Impact of CLOCK knockdown on the oscillatory profile of dexamethasone-synchronized human myotubes.
Myoblasts were transfected with *siClock* or *siControl* and differentiated into myotubes. (A) *CLOCK* transcript expression, as assessed by RT-qPCR and normalized to the mean of *9S-GAPDH*, was reduced 90 ± 2.2% (mean ± SEM, n = 5) in *siClock* transfected samples compared to *siControl* counterparts (*** $p < 0.001$). (B) Representative *Bmal1-luc* oscillation profiles in *siControl*-transfected (blue line), *siClock*-transfected (red line), or non-transfected (black line) human myotubes, synchronized with dexamethasone. *Bmal1-luc* oscillation profiles were recorded in duplicates in n = 8 experiments (one donor per experiment).

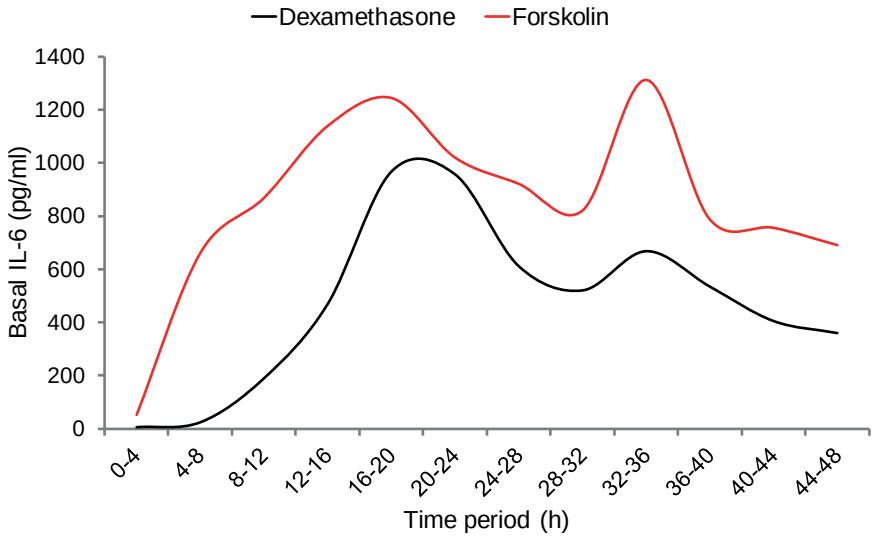

Supplementary Figure 5: Basal IL-6 protein secretion profile after dexamethasone or forskolin synchronization.
Human myotubes, transduced with the *Bmal1-luc* lentivector, were synchronized with dexamethasone (black line) or with forskolin (red line), and perifused for 48 h with culture medium; *n* = 2 experiments with one donor each. The perifusion outflow medium was collected in 4 h intervals and basal IL-6 levels in the medium were assessed by ELISA (0-4 corresponds to the accumulation of IL-6 between 0 and 4 h), normalized to the total DNA content.

4.2. Parallel measurement of circadian clock gene expression and hormone secretion in human primary cell cultures

This work led to a second scientific paper in co-first author with Dr. V. Petrenko and Dr. C. Saini entitled "*Parallel measurement of circadian clock gene expression and hormone secretion in human primary cell cultures*" that has been published in the Journal of Visualized Experiments (JoVE) in November 2016 (312). I developed the methodology underlying all parts related to human skeletal muscle culture, conducted the experiments, prepared the figures, and wrote this part of the manuscript. Moreover, I prepared most parts of the Video, guided by JoVE professionals.

Video Article

Parallel Measurement of Circadian Clock Gene Expression and Hormone Secretion in Human Primary Cell Cultures

Volodymyr Petrenko*[1], Camille Saini*[2], Laurent Perrin*[1], Charna Dibner[1]

[1]Department of Medical Specialties, Division of Endocrinology, Diabetes, Hypertension and Nutrition, Diabetes Center, University of Geneva Medical School, Institute of Genetics and Genomics in Geneva (iGE3)

[2]Population Epidemiology Unit (UEP), Community Medicine, Geneva University Hospital

*These authors contributed equally

Correspondence to: Charna Dibner at Charna.Dibner@hcuge.ch

URL: http://www.jove.com/video/54673
DOI: doi:10.3791/54673

Keywords: Genetics, Issue 117, Human pancreatic islet cells, human primary skeletal myotubes, circadian bioluminescence, lentiviral transduction, *in vitro* synchronization, continuous perifusion

Date Published: 11/11/2016

Citation: Petrenko, V., Saini, C., Perrin, L., Dibner, C. Parallel Measurement of Circadian Clock Gene Expression and Hormone Secretion in Human Primary Cell Cultures. *J. Vis. Exp.* (117), e54673, doi:10.3791/54673 (2016).

Abstract

Circadian clocks are functional in all light-sensitive organisms, allowing for an adaptation to the external world by anticipating daily environmental changes. Considerable progress in our understanding of the tight connection between the circadian clock and most aspects of physiology has been made in the field over the last decade. However, unraveling the molecular basis that underlies the function of the circadian oscillator in humans stays of highest technical challenge. Here, we provide a detailed description of an experimental approach for long-term (2-5 days) bioluminescence recording and outflow medium collection in cultured human primary cells. For this purpose, we have transduced primary cells with a lentiviral luciferase reporter that is under control of a core clock gene promoter, which allows for the parallel assessment of hormone secretion and circadian bioluminescence. Furthermore, we describe the conditions for disrupting the circadian clock in primary human cells by transfecting siRNA targeting *CLOCK*. Our results on the circadian regulation of insulin secretion by human pancreatic islets, and myokine secretion by human skeletal muscle cells, are presented here to illustrate the application of this methodology. These settings can be used to study the molecular makeup of human peripheral clocks and to analyze their functional impact on primary cells under physiological or pathophysiological conditions.

Video Link

The video component of this article can be found at http://www.jove.com/video/54673/

Introduction

The circadian timing system (from *Latin "Circa diem")* has emerged in all light-sensitive organisms, as an adaptive mechanism to the rotation of the Earth. In mammals, it is organized in a hierarchical manner, encompassing the central clock, which is situated in the suprachiasmatic nucleus of the ventral hypothalamus, and peripheral (or slave) oscillators that are operative in different organs. Moreover, these cell autonomous self-sustained oscillators are functional in nearly every cell of the body [1]. Photic signals represent a dominant synchronizing cue (*Zeitgeber*) for the SCN neurons, whereas neural and humoral signals emanating from the SCN reset the peripheral clocks. In addition rest-activity rhythms, that drive in turn feeding-fasting cycles, are further synchronizers for peripheral clocks [2]. According to our current understanding, the molecular makeup of the core clock is based on transcriptional and translational feedback loops, which are conserved between organisms. This comprises the transcriptional activators BMAL1 and CLOCK, which together activate transcription of the negative core clock *PER* and *CRY* genes. High levels of PER and CRY proteins will inhibit their own transcription through inhibition of the BMAL1/CLOCK complex. An auxiliary loop consists of the nuclear receptors REV-ERBs and RORs, which also regulate the transcription of *BMAL1* and *CLOCK*. Furthermore, posttranslational events including phosphorylation, sumoylation, acetylation, O-GlcNAcylation, degradation and nuclear entry of the core clock proteins represent an additional important regulatory layer in establishing the 24 hr oscillation cycle [3].

Accumulating evidence stems from studies in rodent models and highlights the critical role of the circadian system in the coordination of metabolic and endocrine functions [4-5]. A number of large-scale transcriptome analysis suggest that feeding – fasting cycles play a central role in the synchronization of peripheral oscillators [6-8]. In an agreement with these studies, metabolomic and lipidomic analysis in rodents and humans have revealed that a large number of metabolites oscillate in tissue, plasma, and saliva in a circadian manner [9-11]. Importantly, most hormones exhibit circadian rhythms in blood [5,12-13]. Moreover, circadian clocks of the corresponding hormone producing peripheral tissue might regulate hormone secretion locally. Cell-autonomous circadian oscillators have been described in rodent and human pancreatic islet cells [14-16]. These oscillators play an essential role in regulating the pancreatic islet transcriptome and function [15,17-18]. Furthermore, myokine secretion by human skeletal myotubes has been recently demonstrated to exhibit a circadian pattern, which is regulated by cell-autonomous oscillators operative in these cells [19].

Several approaches for studying circadian rhythms in humans *in vivo* have been widely used. For instance, plasma melatonin or cortisol levels as well as thoracic skin surface temperature (reviewed in references [3,20]) have been studied to assess endogenous circadian clocks. Although these methods allow studying systemic circadian oscillations *in vivo*, they are far from providing a reliable assessment of free-running autonomous circadian rhythms in different organs and tissues. Nevertheless, such dissection from the systemic regulation would be an indispensable tool for understanding the specific effect of intracellular molecular clocks on the function of these cells. Therefore, a substantial effort has been undertaken to develop reliable approaches for studying human clocks in immortalized or primary cultured cells synchronized *in vitro*. Importantly, it has been demonstrated that clock characteristics measured in cultured primary skin fibroblast cells closely reflect the individual clock properties of the whole organism [21]. The development of fluorescent and bioluminescent circadian reporters has greatly advanced this approach [22-27]. Furthermore, studying primary cell clocks that are derived from different peripheral organs allows for the investigation of the molecular properties of human tissue-specific clocks [3,5,16,19-20,28]. Thus, assessment of circadian clocks in *in vitro* synchronized primary explants or cells, by using bioluminescent reporters, represents a highly useful method to study the molecular makeup of human peripheral clocks and their impact on organ function.

In this article, we will present detailed protocols for assessing circadian gene expression in human primary islet and skeletal muscle cells synchronized *in vitro* as well as the impact of autonomous cellular clock disruption on the secretory function of these cells.

Protocol

Ethics statement: Manipulations included in this protocol were approved by the Ethics Committee of the Geneva University Hospital and by the Ethical Committee SUD EST IV (Agreement 12/111) [19]. Human islets were isolated from pancreases of brain-dead multi-organ donors in the Islet Transplantation Centre at the University Hospital of Geneva (Switzerland) as described by us in references [16,18], or obtained from a commercial source.

1. Preparation of Primary Cell Culture

1. Human Pancreatic Islet Isolation, Dissociation and Culture
   NOTE: Coat every tube, plastic tip or pipette with Connaught Medical Research Laboratories (CMRL) medium in order to prevent islets or islet cells from sticking to the plastic surface, which can lead to a significant loss of cell material.
   1. One day prior to islet cell dissociation add 1 ml of laminin-5-rich extracellular matrix (derived from 804G cells as described in reference [29]) per 3.5 cm dish. Before plating cells, aspirate the matrix and wash the dish 3 times with sterile bi-distillated water. Allow the dish to dry under the laminar flow cabinet for 5 min.
   2. Inside the laminar flow cabinet, distribute the obtained islets with CMRL medium into 15 ml tube(s). Centrifuge at 272 x g for 5 min.
   3. Aspirate the supernatant, and then resuspend the pellet in 1 ml of sterile Dulbecco's phosphate-buffered saline (DPBS) pre-warmed to 37 °C without calcium and magnesium. Centrifuge at 272 x g for 5 min.
   4. Aspirate the supernatant and resuspend the cell pellet in 1 ml of DPBS.
   5. To count the total number of islets, pipet 10 µl from the 1 ml islet suspension into a new 3.5 cm dish. Count the number of islets in the 10 µl drop under the microscope and from this calculate the total number of islets in the 1 ml islet suspension. Add 14 ml of DPBS and centrifuge the cell suspension one more time at 272 x g for 5 min.
   6. For islet cell dissociation, aspirate the supernatant and add 1 ml of cell detachment solution for a maximum of 1,000 islet equivalents (IEQ). Place the tube in a water bath at 37 °C and gently mix the islets by pipetting up and down several times every minute, during 6-10 min.
      NOTE: To check the digestion quality, pipet a 2 µl drop of suspension on a glass slide and check under the microscope that all cells are well separated, and that no doublets or cell clumps have remained.
   7. Stop the reaction by adding 14 ml of cold CMRL with supplements (10% fetal bovine serum (FBS), 1% of L-alanyl-L-glutamine dipeptide, 1% penicillin-streptomycin (P/S), 1% gentamycin, 1% sodium pyruvate). Centrifuge at 425 x g for 5 min. Aspirate the supernatant and add 15 ml of CMRL medium to the cell pellet.
   8. Resuspend the pellet in a small volume of CMRL with supplements. Count the number of cells under the microscope using a hemocytometer, adjust the CMRL volume in order to obtain a cell concentration of ~650, 000 cells/ml.
   9. Pipet 3 separated drops of 100 µl each from the dispersed cell suspension obtained in step 1.1.8 in a 3.5 cm dish pre-coated with laminin.
      NOTE: Cells attach to the dish in about 24 hr.
   10. Incubate cells (**Figure 1A**) in a tissue culture incubator at 37 °C in a humid chamber. Change the medium of the cell drops every 2-3 days by aspirating 100 µl from each drop and replacing it with the same volume of fresh medium.

2. Human Primary Myoblast Culture and Differentiation into Myotubes
   1. Tissue biopsy, satellite cell isolation and myoblast culture
      Note: Muscle biopsies were obtained from the group of Etienne Lefai (INSERM, Lyon, France) [19].
      1. Purify primary skeletal myoblasts according to the previously described procedure [30].

   2. Differentiating primary human myoblasts into myotubes
      1. Take one vial (1 x 10^6 cells) of human myoblasts stored in liquid nitrogen and thaw cells quickly by putting the vial for 30 sec to 1 min in a water bath at 37 °C with agitation.
      2. Pipet cells (1 ml) into 24 ml of growth medium composed of HAM F-10 supplemented with 20% FBS, 1% P/S, 0.5% gentamycin and 0.2% amphotericin B.
      3. Centrifuge 5 min at 150 x g.
      4. Remove the supernatant and resuspend cells with 15 ml of fresh growth medium per 2.5 x 10^5 cells.
      5. Plate at least 2.5 x 10^5 cells per F75 adherent flask. Keep the myoblasts in a cell incubator at 37 °C and 5% CO_2.
      6. Once cells reach 60-80% confluency, dissociate cells with trypsin-EDTA 0.05% for 1-2 min and plate them in 2 ml of growth medium on adherent 3.5 cm petri dishes.

7. After reaching confluence, remove the growth medium.
8. Start the differentiation protocol of human myoblasts into myotubes by culturing them in 2 ml of Dulbecco's Modified Eagle Medium (DMEM) containing 1 g/L of glucose, 2% FBS, 1% P/S, 0.5% gentamycin and 0.2% amphotericin B (differentiation medium) in a cell incubator at 37 °C and 5% CO_2. Change the medium every 2 to 3 days.
   NOTE: Myotubes are usually formed within 7-10 days.
9. Check muscle cell differentiation under the microscope (**Figure 2A**) by observing the fusion of myoblasts into polynucleated myotubes [19].

2. Small Interfering RNA (siRNA) Transfection

1. siRNA Transfection of Human Islet Cells
   NOTE: The transfection protocol is performed in drops of 100 µl on the next day after cell dissociation (steps 1.1.1-1.1.10).
   1. Aspirate 100 µl of CMRL medium from each drop and replace it with the same volume of serum-free Minimal Essential Medium (MEM) 2 hr before transfection by pipetting.
   2. Prepare a MEM-based mix of transfection reagent and 50 nM of target *siRNA (siClock*) or 50 nM of non-targeting *siControl* according to the manufacturer's instructions.
      1. For one dish with 3 drops prepare two 1.5 ml tubes with 200 µl of MEM each.
      2. Add to one of these tubes 4 µl of transfection reagent.
      3. Add to the second tube 1 µl of the of appropriate siRNA stock solution (20 µM).
      4. Agitate these two tubes slowly on the orbital shaker for 5 min and then mix the content of the tubes together and agitate for 20 more min.
   3. Aspirate 100 µl of MEM from each drop and replace it with the same volume of transfection mix obtained in the previous step by pipetting.
   4. Replace the transfection solution with CMRL medium after 4 hr of incubation at 37 °C. Repeat steps 2.1.1-2.1.3 the following day for cell re-transfection.

2. siRNA Transfection of Human Myotubes
   1. Before transfection, replace the medium (see step 1.2.2.8) with 2 ml of fresh differentiation medium per 3.5 cm petri dish.
   2. In a sterile 1.5 ml tube, prepare a mix of 20 nM siRNA (*siControl* or *siClock*), which corresponds to 2.4 µl of a 20 µM siRNA solution, and 12 µl of transfection reagent diluted in 100 µl of differentiation medium. Incubate the solution at room temperature for 15 min with gentle agitation.
   3. Transfect cells with 114.4 µl of the siRNA mix per 3.5 cm petri dish and place cells into a tissue culture incubator at 37 °C and 5% CO_2 for 24 hr.

3. Continuous Long-term Circadian Bioluminescence Recording Performed in Parallel with the Assessment of Hormone Secretion in Living Human Primary Cells

1. Introducing Circadian Bioluminescence Reporters into Human Primary Cells by Lentiviral Transduction
   NOTE: All procedures with lentiviral particles must be performed in a biosafety level 2 facility to take additional precautions for work with agents that pose a moderate potential hazard to personnel and the environment.
   1. Prepare reporter lentiviral particles by co-transfecting the vector of interest pLenti6.4/R4R2/V5-DEST/Bmal1-luc or pLV156-Per2-dLuc (called *Bmal1-luc* and *Per2-luc*, respectively,) plasmid [31] with lentiviral vectors pMD2G and psPAX into 293T cells using the polyethylenimine method (for detailed procedure see reference [16]).
   2. Titrate the obtained lentiviral particles (details on the titration can be obtained at http://lentilab.unige.ch/). For further experiments, use lentiviruses with titers ranging 10^4 to 10^5 transducing units [TU/µl].
   3. Place dishes with human islet cells or human myoblasts (at 30-50% confluency) inside the laminar flow cabinet and replace the medium with 2 ml of fresh supplemented CMRL medium (see step 1.1.7) or growth medium (see step 1.2.2.2), respectively.
   4. Calculate the multiplicity of infection (MOI) (*i.e.* infectious particles (transducing units)/number of cells).
   5. Transduce the primary cell culture by pipetting lentivirus solution to the dish in order to obtain a MOI = 3 (for example, for 65,000 attached cells add 3 µl of the virus solution with the titer of 6.5 x 10^4 to 100 µl medium drop).
   6. Incubate overnight in a tissue culture incubator. Change medium the next day.
      NOTE: Transduce human islet cells at least 4 days prior to bioluminescence recording in order to achieve sufficient expression of the reporter construct. Myoblasts are transduced during the expansion phase, then grown to confluence, and subsequently differentiated into myotubes.

2. *In Vitro* Synchronization of Human Primary cells
   1. Add 10 µM of adenylyl cyclase activator in 2 ml of medium per 3.5 cm petri dish containing the primary cells previously transduced in step 3.1.5.
   2. Incubate for 60 min at 37 °C in a cell culture incubator.
   3. Change the medium containing the adenylyl cyclase activator with 2.5 ml of the recording medium containing 100 µM luciferin.
      NOTE: For human islet cells use CMRL supplemented with 10% FBS, 1% L-alanyl-L-glutamine dipeptide, 1% P/S, 1% gentamycin; for human myotubes use phenol red - free DMEM with 1 g/L glucose supplemented with 2% FBS, 2% L-alanyl-L-glutamine dipeptide, 1% P/S, 0.5% gentamycin and 0.2% amphotericin B.

4. Parallel Assessment of Circadian Bioluminescence Recording and Hormone Secretion Profiles in Synchronized Human Secretory Primary Cells

1. Setting Up Long-term Constant Perifusion and Bioluminescence Recording for Human Primary Cells.
   NOTE: When working outside the laminar flow cabinet, clean all contact surfaces and limit exposure of cultures or medium to the air to avoid contamination.
   1. To prepare the perifusion medium, add 100 µM of luciferin to the medium.
      NOTE: For human islet cells use CMRL supplemented with 10% FBS, 1% L-alanyl-L-glutamine dipeptide, 1% P/S, 1% gentamycin; for human myotubes use phenol red – free DMEM with 1 g/L glucose supplemented with 2% FBS, 2% L-alanyl-L-glutamine dipeptide, 1% P/S, 0.5% gentamycin and 0.2% amphotericin B.
   2. Inside the laminar flow cabinet, open the 3.5 cm dishes containing the transduced, transfected and synchronized primary cell cultures (islet cells or myotubes) as described above. Insert sterile metallic caps (developed in house) (**Figure 1B2**) into the 3.5 cm dishes that are equipped with silicone influx/efflux connecting tubes (**Figure 1B1/B5**).
   3. Place the dishes on the measurement platform in the 37 °C light-tight incubator. Fix the dishes to the platform by using a screwable adaptor (**Figure 1B3**). Insert the influx/efflux tubes of the perifusion system into the appropriate silicone tubes of the cap (**Figure 1B1/B5**) and set the speed of the pump at a flow rate of ~0.5 ml of medium per 1 hr.
   4. Open the in-house developed Drip-biolumicorder software that records the signals from the photomultiplier tube (PMT) detector. Chose the directory where the data will be stored and start continuous bioluminescence recording from each dish by clicking the "start" icon.
      NOTE: Alternatively to the Drip-biolumicorder software, other programs (*e.g.* LumiCycle), can be used to record signals from PMT detector.
   5. Place sterile 6-well tissue culture plates in the collection box on ice.
   6. Open the control software that controls the timing of the automated switch among the collection wells. Set up the time window of medium collection (sec). Start collection of the outflow medium every 4 hr (14,400 sec; ~2 ml per time-point) by clicking the "run" icon.
   7. Transfer and measure the outflow medium from each collection well into sterile 2 ml tubes by pipetting. Keep tubes in a -20 °C freezer before starting the next step. Repeat steps 4.1.5-4.1.6 every 24 hr.
   8. Stop the bioluminescence recording and the medium flow by clicking the "stop" icon on the corresponding software. Remove the metallic caps and aspirate the residual medium from the dishes.
   9. In order to normalize the secreted protein values obtained in different experiments, either extract DNA (normalization by genomic DNA content for myotubes [19]), or add 1 ml of lysis acid-ethanol buffer (normalization by total hormone content for islet cells [18]) to the dishes.

5. Measuring Islet Hormone and Myokine Levels in the Outflow Medium Obtained by Continuous Perifusion of Human Primary Endocrine Cells

1. Insulin
   1. Quantify basal insulin levels in the outflow medium from collected time-points by using a human insulin enzyme-linked immunosorbent assay (ELISA) kit following the manufacturer's instructions.
   2. Normalize data to the absolute volume of collected medium in each well and to the total insulin content, extracted from acid-ethanol treated cells at the end of the experiment (step 4.1.9) [18].

2. Interleukin-6 (IL-6)
   1. Quantify basal IL-6 levels in the outflow medium from collected time-points by using a human IL-6 ELISA kit following the manufacturer's instructions.
   2. Normalize data to the absolute volume of collected medium in each well and to genomic DNA content at the end of the experiment (step 4.1.9).

6. Circadian Dataset Analyses for Bioluminescence and Hormone Secretion Profiles

1. Bioluminescence Analysis
   1. Analyze bioluminescence profile using the provided software [19].

2. JTK-cycle Analysis
   1. Analyze hormone secretion profiles and bioluminescence recording results by using the JTK_CYCLE algorithm [32].
   2. Set the circadian period width at 20-24 hr.
      NOTE: In case the experimental conditions were recorded in parallel, a paired statistical analysis can be performed to compare the experiments.

3. CosinorJ Analysis
   1. Alternatively, analyze hormone secretion and circadian bioluminescence profiles using the CosinorJ software [28].

Representative Results

Assessment of Islet Hormone Secretion with Parallel Circadian Bioluminescence Recording from Perifused Human Islet Cells

After providing a first molecular characterization of the circadian clock, operative in human islet cells [16], we aimed at studying the impact of clock disruption on islet function and transcription [18]. We set up an efficient *siClock* transfection protocol in dispersed human islet cells (see **Protocol** for details), which resulted in more than 80% knockdown of *CLOCK* mRNA, and in efficient clock ablation as measured by circadian bioluminescence profiling [18]. Glucose induced insulin secretion (GSIS) analysis revealed significantly reduced basal and stimulated insulin secretion upon such clock disruption (not shown). To assess hormone secretion by human islet cells around-the-clock, a continuous perifusion system was connected to a luminometer (depicted in **Figure 1B**). Human islet cells, bearing a functional (*siControl*) or dysfunctional (*siClock*) oscillator were transduced with *Bmal1-luc* lentiviral particles. Cells were subsequently synchronized with a pulse of adenylyl cyclase activator followed by parallel analysis of circadian bioluminescence and insulin secretion into the outflow medium during 48 hr (**Figure 1C, D** [18]). These experiments suggest that under constant physiological glucose concentration (5.6 mM glucose), insulin secretion by *in vitro* synchronized human islet cells exhibits a circadian profile, which is disrupted in *siClock* bearing samples (**Figure 1D**).

Studying Myokine Secretion by Human Skeletal Myotubes Synchronized *in vitro* in the Presence or Absence of Functional Clock

In view of the potential role of the skeletal muscle clock in the regulation of glucose metabolism in rodents [33], we aimed at characterizing circadian rhythms in primary human skeletal myotubes and at investigating their role in myotube function [19]. To this end, disruption of the circadian clock in skeletal myotubes was achieved by transfecting siRNA targeting *CLOCK*. Circadian bioluminescence reporter assays with *Bmal1-luc* and *Per2-luc* reporters revealed that human skeletal myotubes, synchronized *in vitro*, exhibit a self-sustained circadian rhythm, which was further confirmed by endogenous core clock transcript expression (**Figure 2B;** [19]). This endogenous clock was efficiently disrupted in the presence of siRNA targeting *CLOCK* (**Figure 2B**). Moreover, the basal secretion of IL-6 (**Figure 2C**), interleukin-8 (IL-8) and Monocyte Chemotactic Protein 1 (MCP-1) (not shown) by synchronized skeletal myotubes, assessed by the here described perifusion system (**Figure 1B**) and subsequent large-scale myokine multiplex analysis (not shown), exhibits a circadian profile, which is strongly dysregulated upon clock disruption (**Figure 2C** [19]).

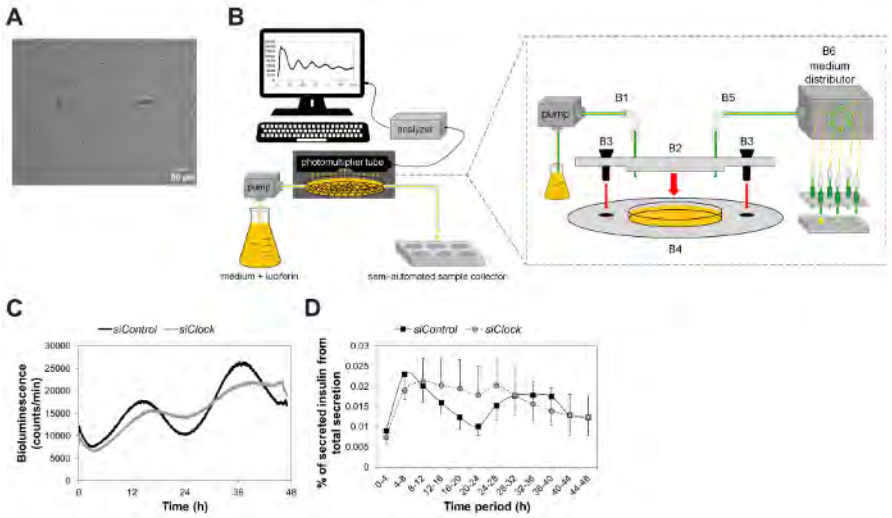

Figure 1: Assessment of Hormone Secretion with Parallel Circadian Bioluminescence Recording from Perifused Human Islet Cells. (**A**) Representative picture of attached human islet cells one day after islet dissociation. (**B**) Schematic presentation of the home-made perifusion system that includes a bottle with the perifusion medium, a pump, a measurement platform equipped with a photomultiplier tube (PMT) within the light-tight incubator, a luminometer device, controlled by the recording software, and a semiautomatic sample collector. Insert: (**B1**) Influx connecting tube; (**B2**) metallic cap for the 3.5 cm Petri dish; (**B3**) screwable adaptor that attaches the cap to the measurement platform (**B4**); (B5) efflux connecting tube; (**B6**) automatically controlled medium distributor. (**C**) Human islet cells were transfected with either scrambled siRNA (*siControl*) or siRNA targeting CLOCK (*siClock*) and transduced with the *Bmal1-luc* reporter. Cells were constantly perifused with culture medium containing 5.6 mM glucose. Circadian bioluminescence was recorded following synchronization by an adenylyl cyclase activator pulse. (**D**) Insulin levels were assessed by ELISA in the outflow samples collected every 4 hr during 48 hr. Application of JTK_CYCLE algorithm [32] confirmed that in the presence of a functional clock (*siControl*), the average profile of secreted insulin was circadian within 48 hr, with a period length of 24.19 ± 0.89 hr (***p* = 0.009; *n* = 7 donors). This circadian profile was lost upon clock disruption (*siClock*). Data are presented as % of secreted hormone from the total hormone content (mean ± SEM) for *n* = 7 donors (one replicate for each donor).This figure has been modified from reference [18]. Please click here to view a larger version of this figure.

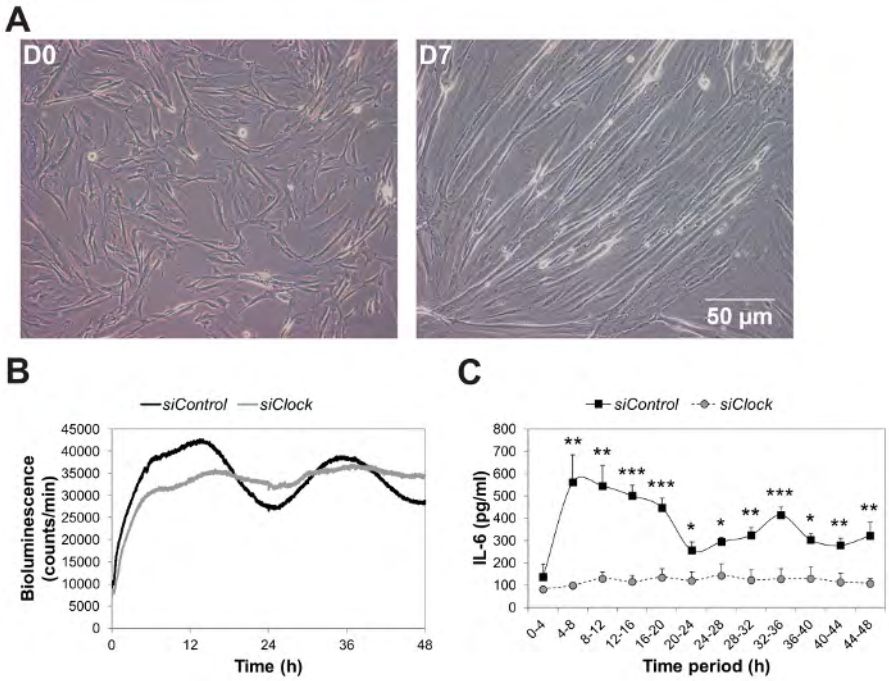

Figure 2: Basal IL-6 Secretion by Human Skeletal Myotubes is Strongly Inhibited in the Absence of a Functional Circadian Clock. Myoblasts were transduced with lentiviral particles containing the *Bmal1-luc* transgene, differentiated into myotubes, and transfected with either *siControl* or *siClock* siRNA. 24 hr following transfection, myotubes were synchronized with an adenylyl cyclase activator pulse and subjected to continuous perifusion with parallel bioluminescence recording. (**A**) Representative pictures were taken at day 0 (D0) and D7 following the switch from 20% to 2% FBS containing medium to induce myotubes differentiation. During the differentiation process, human myoblasts are reoriented, become elongated and fuse together to form a plurinuclated syncytium. (**B**) *Bmal1-luc* bioluminescence profiles of *siControl*-transfected myotubes (black line) and *siClock*-transfected myotubes (grey line). *Bmal1-luc* oscillation profiles were recorded in three independent experiments (one donor per experiment). (**C**) Representative basal IL-6 secretion profile in the presence or absence of a functional clock. The perifusion outflow medium was collected in 4 hr intervals during 48 hr (0-4 corresponds to the accumulation of IL-6 between 0 hr and 4 hr). IL-6 levels in the medium were assessed by ELISA in two technical duplicates from three independent experiments. The results represent basal IL-6 levels normalized to the total DNA content. IL-6 secretion was reduced on average of 69.30 ± 10.61% upon circadian clock disruption (mean ± SEM, $n = 3$; $*p < 0.05$, paired t test). This figure has been modified from reference [19]. Please click here to view a larger version of this figure.

Discussion

The experimental settings described here are composed of lentiviral delivery of circadian bioluminescence reporters into cultured human primary cells, followed by subsequent *in vitro* synchronization and continuous recording of bioluminescence for several days, and parallel analysis of hormone secretion by the same cells. They represent an efficient approach for exploring molecular mechanisms and functional aspects of circadian clocks in human primary cells.

The quality of the donor material is an important issue for the preparation of viable primary tissue cultures. The quality of human islets should be evaluated each time before starting the experiment. Islets with estimated purity or/and viability inferior to 70% are not recommended for these experiments. Islet cells tend to re-establish contacts in dissociated cultures, which plays an important role in their survival and function. Since islet cells do not proliferate in culture, they must be plated at a high density, which allows cells to establish contacts with neighboring cells. This is achieved by plating cells in droplets of a small volume. Importantly, cell death is higher in low-density islet cell cultures. Note that medium replacement should be performed promptly in order to avoid cell drying.

Myoblasts should be passaged preferably at 60% confluence, since a higher density may induce myoblast differentiation. After trypsinization, myoblasts should be carefully resuspended and dispersed to avoid cell clusters.

Bacterial or fungal contamination of primary cells should be excluded microscopically before starting the perifusion assay. Culture medium might be supplemented with antifungal substances. Additionally, the perifusion tubing should be rinsed by alcohol iodine disinfection/sterile water and the metallic caps should be sterilized by autoclaving. These steps are recommended between each experiment.

For efficient bioluminescence recording, the quality of the reporter lentivirus preparation should be determined by the intensity of the bioluminescent signal. The details of lentivirus production including troubleshooting can be found at http://lentilab.unige.ch/. Prior to plasmid transfection for lentivirus production, 293T cells should be plated at 30-50% confluence. It is highly recommended to perform a control of the transfection efficiency in a parallel dish, for instance by using CMV-GFP or an alternative fluorescent lentivector. For each virus preparation the virus titer should be established.

As the described experiments are typically long-lasting (48 hr or more), it is crucial to have stable silencing during this time span. The concentration of siRNA should be optimized as well as the cell confluency according to the siRNA reagent protocol. Efficiency of gene silencing must be tested at the end of the experiment by RT-qPCR or by Western blotting.

During perifusion, the flow rate determines the time necessary to completely exchange the medium in the dish but also has a mechanical impact on the primary cell culture. Indeed, setting up the flow at a rate, which is too low, will not allow for a complete exchange of medium in the dish, and will decrease the sensitivity of the method. On the contrary, a high-speed flow rate may damage the cells. In our hands, the optimal speed for both cell types did allow to collect 0.5 ml of the outflow medium per 1 hr.

Importantly, to obtain a measurable concentration of substances in the outflow medium, a sufficient number of secreting cells should be present in the perifused dish. The follow up method for the detection of the secreted substance (ELISA or other) should be sensitive enough, especially for substances secreted in very low concentrations. Higher cell density might be recommended to overcome this problem when possible. Alternatively, the outflow medium can be concentrated by dialysis or with centrifugal filters, as described by us in details in reference [19].

Taken together our experiments in human pancreatic islet cells and in primary myotubes provide for the first time compelling evidence that these human cells possess high-amplitude cell-autonomous circadian clocks [18-19]. Employing the here described perifusion system combined with a luminometer device (**Figure 1B**) we have demonstrated that these clocks play an important role in the circadian regulation of basal insulin secretion by pancreatic islet cells (**Figure 1D**), and of basal IL6 secretion by skeletal myotubes (**Figure 2C**). Moreover, by knocking down the core clock gene *CLOCK* in both experimental systems, we show that a functional circadian oscillator is required for proper rhythmic insulin and IL-6 secretion by human islet and skeletal muscle cells, respectively (**Figures 1C, D** and **2B, C**). Our results indicate a critical role of the human islet clock for proper insulin secretion, and are in good agreement with works performed in rodent genetic models [15,17]. Given the major role of the circadian clock in allowing organisms to anticipate daily environmental changes rather than to react to them, circadian regulation of basal insulin and myokine secretion might represent such an anticipatory mechanism that coordinates pancreatic islet and skeletal muscle secretory activities to the rest-activity cycle of the whole body.

The here proposed methodology can be easily modified in order to study additional hormone secretion from the same tissues. We have already analyzed an additional large panel of myokines secreted by skeletal muscle cells, using multiplex human myokine arrays [19], and we are in the process of assessing glucagon secretion by human islet cells using the Glucagon ELISA kit (data not shown). Moreover, these experimental conditions can be optimized for other cell types, for instance primary adipocytes, for studying adipokine secretion, primary thyrocytes for studying thyroid hormone secretion, primary enterocytes for studying incretins secretion, *etc.* An additional important application of this system could be to explore the impact of physiological and/or pharmacological compounds on cellular circadian clock function and secretion. The compound of interest might be applied continuously throughout the entire experiment (for instance studying insulin secretion by human islet cells in the presence of high glucose or different levels of free fatty acids), or the compound might be added at a chosen phase of the circadian cycle.

This technique has the limitations of an *in vitro* study and does not represent the complexity of circadian rhythm regulation on a whole body level. At the same time, it helps to distinguish the role of an autonomous clock on cellular metabolism under controlled conditions. Currently available methods are based on snapshot measurements of secretion activity in the cells or explants following *in vitro* synchronization [17]. The protocol described here represents a unique method allowing a concordant and continuous analysis of circadian rhythm and secretory activity within the same cell culture. Alternatively, this methodology could be applied to study the kinetics of non-circadian bioluminescent reporters, in conjunction with cell secretion, as well as for detecting the effects of different substances added to the perifusion medium on cell function. The critical steps in the protocol are: 1) efficient lentivirus preparation, 2) efficient cell transfection with siRNA and reporter vectors transduction; 3) constant medium outflow collection and 4) making sure that a sufficient number of cells is used in order to obtain measurable levels of hormones or cytokines in the collected outflow medium (see the troubleshooting above).

In view of recent evidences on the link between circadian clock perturbations and metabolic diseases and cancer in humans [3-4,28,34-35], studying human peripheral clock properties in primary cultures may represent an important and unique approach for understanding the potential clock connection to these diseases. Thus, our discovery of the existence of links between functional human pancreatic islet and skeletal muscle clock and basal secretion of insulin and myokines, might bear potential consequences for the understanding of the development of chronic diseases, such as obesity and type 2 diabetes [18-19] and will bring new avenues in the treatment of these diseases. Importantly, due to the established correlation between the *in vitro* assessed oscillator characteristics and the *in vivo* circadian phenotype [36], implication of human circadian clock properties as a hallmark of diseases, is of highest and immediate clinical relevance [20].

Disclosures

The authors have nothing to disclose.

Acknowledgements

We are grateful to our colleagues from the University of Geneva: Jacques Philippe for constructive comments on this work, Ueli Schibler for invaluable help with the development of the perifusion system and for scientific inspiration, André Liani for the having conceived design, manufacturing and commissioning of the perfusion system, Lesa-Technology LTD company for the assistance in the perifusion system and Drip-biolumicorder software development, George Severi for assistance with the perifusion experiments, Ursula Loizides-Mangold for critically reading the manuscript, and Anne-Marie Makhlouf for lentivirus preparations; to Etienne Lefai, Stéphanie Chanon and Hubert Vidal (INSERM, Lyon) for preparing human primary myoblasts; and to Domenico Bosco and Thierry Berney (Human Islet Transplantation Center, Geneva University Hospital) for providing human islets. This work was funded by the Swiss National Science Foundation Grant No. 31003A_146475/1, the Sinergia Swiss National Science Foundation Grant No. CRSII3-154405, Fondation Romande pour la Recherche sur Diabète, Bo Hjelt Foundation, Fondation Ernst et Lucie Schmidheiny, and Société Académique de Genève (CD).

References

1. Albrecht, U. Timing to perfection: the biology of central and peripheral circadian clocks. *Neuron.* **74** (2), 246-260 (2012).
2. Dibner, C., Schibler, U., & Albrecht, U. The mammalian circadian timing system: organization and coordination of central and peripheral clocks. *Annu Rev Physiol.* **72** 517-549 (2010).
3. Dibner, C., & Schibler, U. Circadian timing of metabolism in animal models and humans. *J Intern Med.* (2015).
4. Marcheva, B. *et al.* Circadian clocks and metabolism. *Handb Exp Pharmacol.* (217), 127-155 (2013).
5. Philippe, J., & Dibner, C. Thyroid circadian timing: roles in physiology and thyroid malignancies. *J Biol Rhythms.* **30** (2), 76-83 (2015).
6. Andrews, J. L. *et al.* CLOCK and BMAL1 regulate MyoD and are necessary for maintenance of skeletal muscle phenotype and function. *Proc Natl Acad Sci U S A.* **107** (44), 19090-19095 (2010).
7. McCarthy, J. J. *et al.* Identification of the circadian transcriptome in adult mouse skeletal muscle. *Physiol Genomics.* **31** (1), 86-95 (2007).
8. Shostak, A., Husse, J., & Oster, H. Circadian regulation of adipose function. *Adipocyte.* **2** (4), 201-206 (2013).
9. Dallmann, R., Viola, A. U., Tarokh, L., Cajochen, C., & Brown, S. A. The human circadian metabolome. *Proc Natl Acad Sci U S A.* **109** (7), 2625-2629 (2012).
10. Adamovich, Y. *et al.* Circadian clocks and feeding time regulate the oscillations and levels of hepatic triglycerides. *Cell Metab.* **19** (2), 319-330 (2014).
11. Chua, E. C. *et al.* Extensive diversity in circadian regulation of plasma lipids and evidence for different circadian metabolic phenotypes in humans. *Proc Natl Acad Sci U S A.* **110** (35), 14468-14473 (2013).
12. Kalsbeek, A., & Fliers, E. Daily regulation of hormone profiles. *Handb Exp Pharmacol.* (217), 185-226 (2013).
13. Hastings, M., O'Neill, J. S., & Maywood, E. S. Circadian clocks: regulators of endocrine and metabolic rhythms. *J Endocrinol.* **195** (2), 187-198 (2007).
14. Muhlbauer, E., Wolgast, S., Finckh, U., Peschke, D., & Peschke, E. Indication of circadian oscillations in the rat pancreas. *FEBS Lett.* **564** (1-2), 91-96 (2004).
15. Marcheva, B. *et al.* Disruption of the clock components CLOCK and BMAL1 leads to hypoinsulinaemia and diabetes. *Nature.* **466** (7306), 627-631 (2010).
16. Pulimeno, P. *et al.* Autonomous and self-sustained circadian oscillators displayed in human islet cells. *Diabetologia.* **56** (3), 497-507 (2013).
17. Perelis, M. *et al.* Pancreatic beta cell enhancers regulate rhythmic transcription of genes controlling insulin secretion. *Science.* **350** (6261), aac4250 (2015).
18. Saini, C. *et al.* A functional circadian clock is required for proper insulin secretion by human pancreatic islet cells. *Diabetes Obes Metab.* (2015).
19. Perrin, L. *et al.* Human skeletal myotubes display a cell-autonomous circadian clock implicated in basal myokine secretion. *Mol Metab.* **4** (11), 834-845 (2015).
20. Saini, C., Brown, S. A., & Dibner, C. Human peripheral clocks: applications for studying circadian phenotypes in physiology and pathophysiology. *Front Neurol.* **6** 95 (2015).
21. Brown, S. A. *et al.* Molecular insights into human daily behavior. *Proc Natl Acad Sci U S A.* **105** (5), 1602-1607 (2008).
22. Asher, G. *et al.* SIRT1 regulates circadian clock gene expression through PER2 deacetylation. *Cell.* **134** (2), 317-328 (2008).
23. Dibner, C. On the robustness of mammalian circadian oscillators. *Cell Cycle.* **8** (5), 681-682 (2009).
24. Dibner, C. *et al.* Circadian gene expression is resilient to large fluctuations in overall transcription rates. *EMBO J.* **28** (2), 123-134 (2009).
25. Nagoshi, E. *et al.* Circadian gene expression in individual fibroblasts: cell-autonomous and self-sustained oscillators pass time to daughter cells. *Cell.* **119** (5), 693-705 (2004).
26. Sage, D., Unser, M., Salmon, P., & Dibner, C. A software solution for recording circadian oscillator features in time-lapse live cell microscopy. *Cell Div.* **5** 17 (2010).
27. Kowalska, E., Moriggi, E., Bauer, C., Dibner, C., & Brown, S. A. The circadian clock starts ticking at a developmentally early stage. *J Biol Rhythms.* **25** (6), 442-449 (2010).
28. Mannic, T. *et al.* Circadian clock characteristics are altered in human thyroid malignant nodules. *J Clin Endocrinol Metab.* **98** (11), 4446-4456 (2013).
29. Parnaud, G. *et al.* Proliferation of sorted human and rat beta cells. *Diabetologia.* **51** (1), 91-100 (2008).
30. Agley, C. C., Rowlerson, A. M., Velloso, C. P., Lazarus, N. L., & Harridge, S. D. Isolation and quantitative immunocytochemical characterization of primary myogenic cells and fibroblasts from human skeletal muscle. *J Vis Exp.* (95), e52049 (2015).
31. Liu, A. C. *et al.* Redundant function of REV-ERBalpha and beta and non-essential role for Bmal1 cycling in transcriptional regulation of intracellular circadian rhythms. *PLoS Genet.* **4** (2), e1000023 (2008).
32. Hughes, M. E., Hogenesch, J. B., & Kornacker, K. JTK_CYCLE: an efficient nonparametric algorithm for detecting rhythmic components in genome-scale data sets. *J Biol Rhythms.* **25** (5), 372-380 (2010).
33. Dyar, K. A. *et al.* Muscle insulin sensitivity and glucose metabolism are controlled by the intrinsic muscle clock. *Mol Metab.* **3** (1), 29-41 (2014).
34. Innominato, P. F. *et al.* The circadian timing system in clinical oncology. *Ann Med.* **46** (4), 191-207 (2014).
35. Chitikova, Z. *et al.* Identification of new biomarkers for human papillary thyroid carcinoma employing NanoString analysis. *Oncotarget.* **6** (13), 10978-10993 (2015).
36. Pagani, L. *et al.* The physiological period length of the human circadian clock in vivo is directly proportional to period in human fibroblasts. *PLoS One.* **5** (10), e13376 (2010).

4.3. Transcriptomic analyses reveal rhythmic and CLOCK-driven pathways in human skeletal muscle

This work led to a third scientific paper in first author entitled "*Transcriptomic analyses reveal rhythmic and CLOCK-driven pathways in human skeletal muscle*" that was recently submitted to eLife (December 2017). I led the project related to the *in vitro* part, conducted most of the experiments for this part, analyzed the data for the *in vitro* part including active participation in bioinformatics analyses, prepared all figures and tables, and wrote the first draft of the manuscript for the *in vitro* part.

Transcriptomic analyses reveal rhythmic and CLOCK-driven pathways in human skeletal muscle

Laurent Perrin [1,2,3,4], Ursula Loizides-Mangold [1,2,3,4,†], Stéphanie Chanon [5,†], Cédric Gobet [6,7,†], Nicolas Hulo [4,8], Laura Isenegger [8], Benjamin D. Weger [6], Eugenia Migliavacca [6], Aline Charpagne [6], James A. Betts [9], Jean-Philippe Walhin [9], Iain Templeman [9], Keith Stokes [9], Dylan Thompson [9], Kostas Tsintzas [10], Maud Robert [11], Cédric Howald [4,12], Howard Riezman [13], Jerome N Feige [6,7], Leonidas G. Karagounis [14,15], Jonathan D. Johnston [16], Emmanouil Dermitzakis [4,12], Frédéric Gachon [6,7,ç], Etienne Lefai [5,ç], Charna Dibner [1,2,3,4,*]

[1]Division of Endocrinology, Diabetes, Hypertension and Nutrition, Department of Internal Medicine Specialties, University Hospital of Geneva, Geneva, Switzerland;

[2]Department of Cell Physiology and Metabolism, Faculty of Medicine, University of Geneva;

[3]Diabetes Center, Faculty of Medicine, University of Geneva;

[4]Institute of Genetics and Genomics in Geneva (iGE3), Geneva, Switzerland;

[5]CarMeN Laboratory, INSERM U1060, INRA 1397, University Lyon 1, Oullins, France;

[6]Nestlé Institute of Health Sciences, Lausanne, Switzerland;

[7]School of Life Sciences, Ecole Polytechnique Fédérale de Lausanne, Lausanne, Switzerland;

[8]Service for Biomathematical and Biostatistical Analyses; Section of Biology, University of Geneva, Geneva, Switzerland;

[9]Department for Health, University of Bath, Bath, United Kingdom;

[10]MRC/ARUK Centre for Musculoskeletal Ageing, School of Life Sciences, University of Nottingham, NG7 2UH, United Kingdom;

[11]Department of Digestive and Bariatric Surgery, Edouard Herriot University Hospital, Lyon 1 University, France;

[12]Department of Genetic Medicine and Development, Faculty of Medicine, University of Geneva, Geneva, Switzerland;

[13]Department of Biochemistry, NCCR Chemical Biology, University of Geneva, Geneva, Switzerland;

[14]Experimental Myology and Integrative Biology Research Cluster, Faculty of Sport and Health Sciences, University of St Mark and St John, Plymouth, United Kingdom;

[15]Institute of Nutritional Science, Nestlé Research Centre, Lausanne, Switzerland;

[16]Faculty of Health and Medical Sciences, University of Surrey, Guildford, United Kingdom.

[†]These authors contributed equally to this work

[ç]These authors contributed equally to this work

***CORRESPONDING AUTHOR**

Charna Dibner

Faculty of Medicine, University of Geneva

D05.2147c Rue Michel-Servet, 1

CH-1211 Geneva 4, Switzerland

Phone: +41 22 3795934

ABSTRACT

Circadian regulation of transcriptional processes has a broad impact on cell metabolism. Here, we compared the diurnal transcriptome of human skeletal muscle conducted on serial muscle biopsies *in vivo* with profiles of human skeletal myotubes synchronized *in vitro*. More extensive rhythmic transcription was observed in human skeletal muscle compared to *in vitro* cell culture as a large part of the *in vivo* mRNA rhythmicity was lost *in vitro*. siRNA-mediated clock disruption in primary myotubes significantly affected the expression of ~8% of all genes, with impact on glucose homeostasis and lipid metabolism. Genes involved in GLUT4 expression, translocation and recycling were negatively affected, whereas lipid metabolic genes were altered to promote activation of lipid utilization. Moreover, basal and insulin stimulated glucose uptake were significantly reduced upon *CLOCK* depletion. Our findings suggest an essential role for cell-autonomous circadian clocks in coordinating muscle glucose homeostasis and lipid metabolism in humans.

INTRODUCTION

Circadian rhythms are daily cycles of most bodily processes driven by a system of intrinsic biological clocks organized in a complex hierarchical manner. This mechanism ensures a temporal coordination of physiology and behaviour with a near 24 h period of rest-activity and feeding-fasting cycles, thus providing the organism with an evolutionary conserved advantage (Albrecht 2012; Spoelstra et al. 2016). In mammals, the circadian system is driven by a central pacemaker, situated in the paired suprachiasmatic nuclei (SCN) of the hypothalamus, and by secondary oscillators located in peripheral organs. The SCN clock is readjusted on a daily basis, mainly by light inputs coming from the retina. In turn, the central pacemaker orchestrates peripheral clocks through a combination of neuronal, endocrine, and metabolic signaling pathways (Saini et al. 2015). As a result, metabolic processes in the liver, skeletal muscle, and other organs are subject to daily oscillations (Asher and Sassone-Corsi 2015) with the SCN keeping these rhythms in appropriate synchrony with each other.

Skeletal muscle is responsible for ~70% of glucose uptake resulting from ingested carbohydrates (DeFronzo et al. 1981; Gachon et al. 2017), and perturbations in glucose sensing and metabolism in this organ are strongly associated with insulin resistance in type 2 diabetes (T2D) (Muoio and Newgard 2008). In rodents, it has been established that the skeletal muscle clock plays an essential role in maintaining proper metabolic homeostasis, with skeletal muscle pathologies stemming from clock disruption via deletion of the core clock component *Bmal1* (Andrews et al. 2010; Harfmann et al. 2015). Disruption of muscle insulin sensitivity by modulating glucose uptake, with a reduction in *Glut4* mRNA and protein levels, has been reported in two muscle-specific *Bmal1* knockout models (Dyar et al. 2014; Harfmann et al. 2016). In humans, diurnal variations in glucose tolerance have been described (Kalsbeek et al. 2014), although the molecular mechanism responsible for such variations remains largely unexplored. Feeding-fasting cycles accompanying rest-activity rhythms represent major timing cues in the synchronization of peripheral clocks, including skeletal muscle oscillators (Dibner and Schibler 2015; Wehrens et al. 2017). Although several studies have reported that in murine

models 3.4% to 16% of the skeletal muscle transcriptome is expressed in a circadian manner (McCarthy et al. 2007; Miller et al. 2007; Dyar et al. 2014; Zhang et al. 2014; Hodge et al. 2015), it is unclear to what extent the muscle circadian transcriptome is regulated by feeding-fasting rhythms and additional central synchronizers, and how local muscle clocks contribute in generating these transcript oscillations. Cell-autonomous circadian clocks operating in human primary skeletal myotubes (hSKM) established from muscle biopsies have been recently characterized (Perrin et al. 2015; Hansen et al. 2016; Loizides-Mangold et al. 2016). Importantly, proper function of these cellular oscillators is indispensable for the normal secretion of interleukin 6 (IL-6), interleukin-8 (IL-8), the monocyte chemotactic protein 1 (MCP-1), and additional myokines, regulating skeletal muscle insulin sensitivity and inflammation (Perrin et al. 2015).

In order to dissect the impact of the endogenous circadian clock on skeletal muscle gene transcription from external factors and their reciprocal influence, we performed a genome-wide transcriptome analysis by high-throughput RNA sequencing (RNA-seq) in skeletal muscle biopsies collected from human subjects placed under a controlled laboratory routine, as well as in cultured hSKM synchronized *in vitro* in the presence of a functional or compromised clock. Important overlap between the genes exhibiting rhythmic patterns in tissue biopsies and in synchronized hSKM was observed. Expression patterns of the genes related to insulin response, myokine secretion, and lipid metabolism were strongly altered in the absence of a fully functional clock *in vitro*. These transcriptional changes had important functional outputs, with basal glucose uptake as well as glucose uptake in response to insulin, and lipid metabolism being altered by perturbation of the oscillators operative in hSKM. Altogether, these results strongly suggest that cell-autonomous skeletal muscle clocks drive rhythmic gene expression, and are indispensable for proper insulin response, lipid homeostasis, and myokine secretion by the skeletal muscle.

RESULTS

Diurnal rhythms of gene expression in human skeletal muscle under controlled laboratory routine

To assess rhythms of gene expression in human skeletal muscle, RNA samples derived from *vastus lateralis* biopsies taken every 4 h across 24 h from 10 healthy volunteers were analyzed by total RNA-seq (see Table S1 for *in vivo* donor characteristics, n=10). Sample collection was performed under controlled laboratory routine by implementing a protocol designed to minimize the effect of confounding factors (see Methods and Loizides-Mangold et al. 2017). In total 13'377 genes were quantified at the exonic level (Supplemental Dataset 1), of which 9'211 genes were quantified at the intronic level as well. To identify genes with coordinated rhythmic expression, we used a mixed linear model with harmonic terms across the 10 individuals at the pre-mRNA (intronic signal) and mRNA (exonic signal) levels. This method allowed for the identification of 5’748 rhythmic genes that were rhythmic at the pre-mRNA or/and mRNA level with a False Discovery Rate (FDR) of 5% (Figure 1A). When rhythmicity levels were further analyzed, it became apparent that 4'792 genes showed rhythmic transcription at the intronic pre-mRNA level (Figure 1A, upper and middle left panels). However, from these rhythmic pre-mRNA transcripts, only 57% were also rhythmic at the mRNA level (R-I.R-E, upper panels Figure 1A), likely because of the long half-life of their mRNA. Indeed, approximation of mRNA half-life by the exon/intron ratio showed that among these rhythmic pre-mRNA transcripts, those that are only rhythmic at the pre-mRNAs level (R-I) have a longer half-life compared to those that are rhythmic at the mRNA level (R-E and R-I.R-E, Figure 1B). In parallel, around 10% of the global transcriptome (956 genes) were only rhythmic at the mRNA level (R-E, Figure 1A, lower panels), likely through post-transcriptional regulation and in particular mRNA degradation (Luck et al. 2014). Amplitude distribution suggested that among the genes that were rhythmic at the pre-mRNA level those with higher amplitude of transcription had a greater probability to be rhythmic at the mRNA accumulation level (R-I.R-E, Figure 1C). Taken together, our results highlight the high rhythmicity of gene expression in human skeletal

muscle, even under controlled laboratory routine. However, the number of genes being qualified as significantly rhythmic at the pre-mRNA and/or mRNA level was strongly dependent on the threshold level that was applied (Figure 1D).

Strikingly, rhythmic transcription was distributed into two sharp phases of transcript accumulation (04:00 and 16:00, Figure 1E). The afternoon peak (16:00) was enriched in genes related to muscle contraction and mitochondrial activity as previously reported for the corresponding active phase in mice (McCarthy et al. 2007; Miller et al. 2007; Hodge et al. 2015) (Supplemental Dataset 2). In contrast, among the genes highly activated in the middle of the night (04:00), many were associated with inflammation and immune response (Figure 1F).

Among the rhythmic genes, we observed high amplitude oscillations for the core clock genes *ARNTL* (*BMAL1*), *NPAS2*, *CLOCK*, *PER2*, *PER3*, *CRY2*, *NR1D1* (*REV-ERB*α), and *RORA,* which were well synchronized among the 10 individuals (Figure 1G). In addition, several transcription factors associated with muscle metabolism and physiology like *TFEB*, a key regulator of lysosomal biogenesis and autophagy that also regulates glucose homeostasis and oxidative phosphorylation (Mansueto et al. 2017), *KLF13*, which plays a role in cardiac muscle cell development (Lavallee et al. 2006), and *KLF15*, an important transcriptional regulator of muscle lipid metabolism (Haldar et al. 2012), showed an oscillatory profile. Moreover, also *PPARD*, the most abundant PPAR isoform in skeletal muscle and master regulator of muscle mitochondrial function (Jordan et al. 2017), and *MYOD1*, the key regulator of myogenesis were under control of the circadian clock (Andrews et al. 2010), likely orchestrating the muscle rhythmic transcriptome (Figure 1H). In addition to these transcription factors, genes involved in the secretion of myokines, glucose homeostasis and lipid metabolism displayed rhythmic transcription (Figure S1A, B and C, respectively, Supplemental Dataset 2).

Cell-autonomous circadian clocks regulate functional gene expression in hSKM

To assess the impact of cell-autonomous circadian clocks operative in hSKM on skeletal muscle gene transcription and function, we used our previously developed model of efficient

siCLOCK-mediated clock disruption (Perrin et al. 2015). RNA-seq was conducted on siCLOCK-transfected hSKM obtained from two male donors matched for age and BMI (Table S1, donors 1 and 2, *in vitro* part). Human primary myoblasts were cultured and differentiated *in vitro* into myotubes, transfected with siRNA, synchronized *in vitro* with a forskolin pulse, with subsequent sample collection every 2 h during 48 h for RNA-seq analysis (Figure S2 and Methods). *CLOCK* expression was reduced by at least 80% upon siCLOCK depletion, as assessed by RNA-seq and quantitative real-time PCR (Figures 2A and S3A). In parallel, bioluminescence profiles derived from hSKM transduced with a lentiviral *Bmal1*-luciferase vector were monitored as described previously (Perrin et al. 2015). As expected, the circadian amplitude of *Bmal1*-luciferase bioluminescence reporter profile became dampened upon siCLOCK compared to siControl and non-transfected counterparts (Figure S3B).

We first performed a differential analysis of the global gene expression profile across all 25 time points, starting from 0 h and until 48 h following synchronization. Out of the 16’776 mapped genes, the median values for all the time points, reflecting the overall expression levels of 1'330 genes (8%), were significantly altered in siCLOCK-transfected hSKM compared to their control counterparts, with 742 being downregulated and 588 being upregulated (Figure 2B; Supplemental Dataset 3). As expected, core clock gene expression was affected, with *NR1D1 (REVERBα*), *NR1D2* (*REVERBβ*), *PER3*, *TEF*, *BHLHE41* (*DEC2*), and *DBP* being significantly downregulated, and *CRY1* being upregulated upon *CLOCK* depletion (Figure 2A).

Functional clocks operative in hSKM are required for proper lipid metabolism and response to insulin

Remarkably, genes encoding for proteins essential for vesicle formation including SNAREs, solute transporters, and Rab GTPases exhibited significantly altered expression levels upon *CLOCK* depletion (Table S2). Additional genes involved in secretion pathways and exhibiting altered mRNA expression levels upon *CLOCK* depletion are listed in Table S3. Using the Panther classification system (Mi et al. 2017) for gene ontology (GO) term analysis, overrepresentation of genes associated with the regulation of nucleotide metabolism,

transcription and RNA processing, as well as muscle contraction were identified within the significantly down- and/or up-regulated genes (Table S4, and Supplemental Dataset 4). Furthermore, enrichment analysis using the Reactome pathway database was performed on the down- and/or upregulated genes. Of note, overrepresentation of genes related to muscle contraction, regulation of gene transcription, and cellular responses to stress and membrane trafficking were also identified (Table S5, Supplemental Dataset 5).

In addition, 42 transcripts involved in lipid metabolism were affected by *CLOCK* disruption. These comprised genes related to glycerophospholipid and triglyceride metabolism as well as lipid storage and transport (Figure 2C), in addition to those regulating inositol phosphate (Figure 2D) and sphingolipid metabolic pathways (Figure 2E). Importantly, the observed modifications in gene expression level were in an accord with significant alterations in absolute lipid metabolite levels, resulting in total phosphatidylcholine levels being downregulated, and glycosylceramide levels being upregulated in the absence of a functional myotube clock (Figure 2F, Table S1, donors 7-10 for *in vitro* part). The first matching a reduction in lysophosphatidylcholine symporter 1 (*MFSD2A*) and phosphatase *LPIN1* levels (Figures 2C and 2F), and the latter matching the transcriptome outcome for UDP-glucose ceramide glucosyltransferase (*UGCG*) the key enzyme of *de novo* glucosylceramide biosynthesis (Figures 2E and 2F).

Our differential analysis in human muscle cells demonstrates that genes involved in insulin-stimulated and contraction-induced glucose uptake, comprising *TBC1D13*, T*BC1D4* (*AS160*), *14-3-3θ* (*YWHAQ*), *RAB35*, *STX6,* and *PDPK1* (*PDK1*), were significantly downregulated upon siCLOCK (Table S2), highlighting the pleiotropic effect of the skeletal muscle CLOCK gene/protein in regulating glucose uptake in response to insulin and/or to contraction.

To determine the protein levels of candidate genes identified by RNA-seq, hSKM cells established from five additional donor biopsies (for donor characteristics see Table S1) were transfected by siRNA targeting *CLOCK*. Matching the changes observed by RNA-seq, *CLOCK* mRNA was reduced by siCLOCK as determined by RT-qPCR (Figure 3A), leading to a

reduction in CLOCK protein expression by 74% (Figure 3B). Moreover, the expression of the 14-3-3θ protein, a key regulator of GLUT4 translocation (Sakamoto and Holman 2008; Kleppe et al. 2011), was decreased by about 28% under these conditions (Figure 3C), matching the decrease in its gene expression (Table S2). In contrast, AS160 protein levels did not change significantly (Figure S4) despite a reduction at the mRNA expression level (Table S2).

Finally, we analyzed the impact of clock disruption on the ability of hSKM to take up glucose in response to insulin. The assessment of glucose uptake, using a radioactive glucose analogue, demonstrated an increase in glucose uptake upon insulin stimulation in non-synchronized siControl and siCLOCK-transfected myotubes (siControl: basal *vs.* insulin p-value = 0.019; siCLOCK: basal *vs.* insulin p-value = 0.017). Importantly, we observed a significant decrease in both basal (30%), and insulin-stimulated (27%) glucose uptake in siCLOCK-transfected myotubes, as compared to their siControl counterparts (Figure 3D left and right panels, respectively).

RNA-seq reveals rhythmically expressed genes in cultured hSKM synchronized *in vitro*

We next aimed at identifying genes that exhibited rhythmic profiles in hSKM synchronized *in vitro*. The existing algorithms JTK_CYCLE (Hughes et al. 2010) and CosinorJ (Mannic et al. 2013) do not allow for a satisfactory analysis of datasets containing large differences in amplitude, observed among the two cycles in our datasets. We therefore developed a novel algorithm, adapted for the analysis of our RNA-seq datasets, comprising high resolution analysis of two full cycles (25 time points over 48 h) following *in vitro* synchronization (see Methods for details). Briefly, after conversion of the raw data to $\log_2$ RPKM values and filtering for $\log_2$ RPKM>0, temporal patterns of the resulting 12’985 genes were grouped into 16 models (Figure 4A, Supplemental Datasets 6 and 7), with models 1 to 15 comprising 994 rhythmic genes (7.65%), and model 16 comprising 11’991 non-rhythmic genes (92.35%).

Because the number of rhythmic genes exhibited larger variations between the two analyzed cell cultures, established from two different human individuals, than between siControl and siCLOCK (Figure S5A), we proceeded with a deeper analysis of models 1 to 4,

which group together genes that are rhythmic in the siControl situation for both donor cell cultures. According to our analysis, model 1 comprises 73 genes, classified as rhythmic in both donors upon siControl and siCLOCK, models 2 and 3 include 39 and 34 genes, respectively, that are rhythmic in both siControl donors and in one siCLOCK donor respectively, and model 4 comprises 44 genes that are rhythmic in siControl, but not in siCLOCK (Figure 4B). Circadian core clock genes clustered to model 1, as they exhibited a rhythmic mRNA profile in siControl and a flattened, but still rhythmic, profile upon siCLOCK (Figure 4C and Figure S6), indicating a presence of partially functional circadian oscillator. Of note, classification of a temporal gene profile as rhythmic by our algorithm did not take into consideration amplitude alterations, like those generated by siCLOCK-treatment, as long as the temporal profile was qualified as circadian. As amplitude values were indeed often blunted upon siCLOCK treatment, to quantify such amplitude changes a $\log_{10}$ transformation was applied, providing approximation to a normal distribution using a paired *t*-test. In agreement with our previous publication (Perrin et al. 2015), the amplitude of mRNA accumulation was significantly decreased in siCLOCK samples (Table S6, Figure S5B).

In summary, 190 genes were qualified as rhythmic in the two analyzed cell cultures, and were clustered into models 1-4 (Supplemental Datasets 6 and 7), as exemplified in Figure 4D (upper panels) and in Figure S5C. Importantly, similarly to core clock genes, also these functional genes exhibited a blunted circadian amplitude upon clock disruption (Figure 4D, lower panels, Figure S5B). For instance, *CAMKK1,* classified as rhythmic in both siControl and siCLOCK conditions (model 1), exhibited a significant circadian amplitude reduction upon siCLOCK (Figure 4D, Table S6). In addition, *SERPINE1*, a myokine whose secretion by myotube cells was reduced upon clock disruption (Perrin et al. 2015), presented lower amplitude in siCLOCK-transfected cells (Table S6). Panther database analysis for genes assigned to models 1-4 suggested enrichment for a number of GO term and Reactome pathways, comprising cell cycle and mitotic regulation (Figure S7, Tables S4-5, Supplemental Datasets 8 and 9).

Comparative analysis of diurnal rhythms of gene expression in human skeletal muscle tissue and cultured hSKM

Consequently, we compared rhythmic gene expression between muscle biopsy and cultured hSKM cells (Figure 5A). Among the 190 transcripts that were identified as rhythmic in hSKM cells (Figure 4A, models 1-4, Supplemental Dataset 10), 14 transcripts were excluded as they were representing non-protein coding sequences or pseudogenes. Additional 26 genes, associated with mitotic cell cycle functions, and further 17 genes related to cell proliferation, adhesion and differentiation, were only found in hSKM and are likely a consequence of incomplete myotube differentiation in cell culture, as opposed to fully differentiated muscle tissue. Cultured muscle cells lack the *in vivo* environment and the chemical communication that exists within the tissue. Notably, the absence of neuronal connections further limits the final differentiation of cultured myotubes (for review see (Aas et al. 2013)).

Among the remaining 133 genes, 99 were expressed in human muscle biopsies. Within this group of overlapping genes, 35 were also qualified as rhythmic at the mRNA level (q-val < 0.05) in muscle tissue (Supplemental Dataset 10). The genes rhythmic in both *in vivo* and *in vitro* datasets included the core clock components (Figure 5A), as well as functional genes that were enriched at the 04:00 time point (Figure 5B). Interestingly, genes implicated in glucose homeostasis (*KLF11*, *GFPT2*, *NAMPT*) and in muscle regeneration (*PLAU, PLD1, PIM1*), were rhythmic both *in vivo* and *in vitro,* suggesting an important role for the circadian clock in regulating muscle physiology (Figure 5C).

DISCUSSION

This study presents the first large-scale circadian transcriptome RNA-seq analysis in muscle biopsies from multiple volunteers and in hSKM cells synchronized *in vitro* with 2-hour resolution over 48 hours, in the presence of a functional or disrupted cell-autonomous clock, with subsequent analysis of its impact on gene expression. Moreover, physiological consequences

of the circadian regulation of gene transcription were studied, suggesting a critical role for the cellular clock in the regulation of basal and insulin-stimulated glucose uptake, lipid homeostasis, and myokine secretion, as summarized in Figure 6. These results provide new insights into the targets of the molecular clock in human skeletal muscle, previously only studied in rodents (McCarthy et al. 2007; Miller et al. 2007; Dyar et al. 2014; Zhang et al. 2014; Dyar et al. 2015). Finally, to dissect the effects of the cell-autonomous endogenous clock from SCN signals and entrainment cues, this dataset was compared to the diurnal transcriptome of human skeletal muscle collected in form of serial muscle biopsies across 24 h (Figures 1, 5).

Comparison between the circadian transcriptome of synchronized myotube cells in vitro, and human muscle tissue collected in vivo

Our *in vitro* myotube system allows us to explore the transcriptional regulation of muscle target genes without confounding effects of the SCN, rest-activity and feeding-fasting cycles (Harfmann et al. 2015). Regarding the rhythmic analysis of *in vitro* RNA-seq data, larger variations were observed between the two donors than between siControl and siCLOCK conditions (Figure S5), likely due to the genetic heterogeneity among human individuals. The low number of subjects therefore represents a limitation of our study, despite high time-resolution of 2 h for sample collection conducted over 48 h, that resulted in as many as 25 time points per myotube donor. We therefore concentrated on genes, which were rhythmic in both donors in siControl condition, irrespectively of rhythmicity disruption by siCLOCK treatment. In total, 994 circadian genes (7.65% of the global transcriptome) were rhythmic in at least one of the four models (models 1-4, Figure 4A-B), exceeding the value found for U2OS cells, exhibiting 1.5% of oscillating gene transcripts (Krishnaiah et al. 2017). When compared with the diurnal transcriptome of human skeletal muscle biopsies, the percentage of rhythmic genes was considerably lower, likely due to the cell culture situation where the circadian amplitude is gradually lost (Figure S3B) in the absence of entrainment (Hughes et al. 2009), or due to effects driven by the SCN or behavioral rhythms rather than by the local peripheral clock. Additional differences with respect to gene rhythmicity among the two datasets may stem from

potential differences due to fiber type composition or the different algorithms employed for the data analyses.

Among the 35 genes classified as rhythmic in cell culture and in skeletal muscle tissue, were genes involved in glucose metabolism and in muscle regeneration, including *PLAU* (Lluis et al. 2001) and *PIM1* kinase (Fischer et al. 2009), along with core clock components such as *NR1D1* and *NR1D2* (Figure 5A), previously identified as the most rhythmic transcripts across all human and mouse datasets (Laing et al. 2015). Phospholipase *PLD1* (Teng et al. 2015), involved in intracellular membrane trafficking and maintenance of glucose homeostasis in human skeletal muscle (Huang et al. 2005) was rhythmically expressed *in vivo* and *in vitro*. Moreover, oscillatory genes in both datasets included *NAMPT*, *KLF11,* and *GFPT2*, the latter controlling the flux of glucose into the hexosamine pathway, tightly linked to hyperglycemia and insulin resistance (Coomer and Essop 2014).The expression of *NAMPT*, a key regulator of NAD^+ synthesis and muscle maintenance (Frederick et al. 2016), was previously shown to be regulated by CLOCK and BMAL1 in complex with SIRT1 (Ramsey et al. 2009; Garten et al. 2015). Importantly, the diurnal rhythm of secreted NAMPT is disturbed by sleep loss, and positively associates with impairment of postprandial glucose metabolism (Benedict et al. 2012). The transcription factor *KLF11*, a glucose-inducible regulator of insulin transcription and secretion, that is a member of the Krüppel-like family of transcription factors proposed as circadian (Yoshitane et al. 2014), was found to be regulated by the circadian clock in mouse kidney and epididymal fat tissue (Guillaumond et al. 2010), and is possibly involved in postprandial glucose metabolism in skeletal muscle (Neve et al. 2005).

An important observation was the strong induction of genes associated with inflammation and immune response in human muscle in the early morning hours (04:00) (Figure 1F), 16 hours after sampling of the first biopsy. We cannot fully rule out that repeated muscle sampling contributed to this signature, as previously reported for repeated biopsy sampling of a single muscle via the same skin incision site over 25 hours (Friedmann-Bette et al. 2012). However, clinical sampling was optimized to minimize this effect, as serial *vastus lateralis* biopsies were sampled across alternating limbs and from separate skin incision sites,

each proximal to the previous (Van Thienen et al. 2014), not excluding the possibility that circulating molecules may diffuse an inflammatory signal between limbs (Catoire et al. 2012). Importantly, this immune signature was restricted to a single time point in the early morning hours, and thus likely does not exclusively result from responses to muscle injury which would have further increased at the last time point (08:00). Given that inflammatory cytokines have been described as myokines and important regulators of muscle physiology, this could thus represent a true signature with relevant outcomes for muscle physiology.

One limitation of the comparison between RNA-seq datasets obtained for *in vivo* and *in vitro* skeletal muscle and hSKM samples in the present study stems from different analyses methods applied for the two datasets. The algorithms applied here for these two datasets were chosen to optimally fit each dataset differing in the number of time points and the time span of samples collection. Indeed, cellular samples were collected every 2 h over 48 h resulting in 25 time points, whereas muscle tissue biopsies were collected every 4 h over 24 h, resulting in 6 time points only, due to obvious practical limitations of repetitive muscle tissue biopsies from the same individuals.

Effect of CLOCK depletion on myotube gene transcription and core clock gene regulation

Efficient clock disruption in adult hSKM cells via siRNA-mediated *CLOCK* knockdown by our previously validated protocol led to significant changes in gene expression (Figure 2A and 2B) (Perrin et al. 2015; Petrenko et al. 2016; Loizides-Mangold et al. 2017). Most of core clock genes were downregulated upon siCLOCK transfection, in addition to a flattening of the *Bmal1*-luciferase profile (Figure S3B), consistent with our previous data for hSKM and human pancreatic islets (Perrin et al. 2015; Saini et al. 2016). However, despite the observed amplitude blunting, core clock components still presented remnant circadian expression profiles that can likely be attributed to the partial downregulation of *CLOCK,* and to compensatory mechanisms that occur to maintain the circadian machinery (DeBruyne et al. 2007) (Figure 2A, Figure S3A), leading to the observation that the effect on absolute gene expression was more pronounced than the effect on mRNA rhythmicity (Figure 4C and 4D).

Muscle fiber type parameters are affected in response to siCLOCK

Gluteus maximus is a slow muscle characterized by high levels of *MYH7* expression, fatigue resistance, and slow speed contraction as well as an oxidative metabolic type (Talbot and Maves 2016). Although the levels of key transcription factors regulating fiber type specific genes, including *MYOD1*, *NFATC1*, *SIRT1* and *PPARGC1A* were not significantly altered upon siCLOCK, we identified multiple genes promoting the type I slow fiber phenotype, as well as a downregulation of genes associated with type II fast fibers (Table S7). We also observed an upregulation of myosin light chain kinase *MLCK* (*MYLK*) that contributes to force generation by myofilaments. Taken together these observations reinforce the hypothesis that clock disruption induces a global switch in the genetic program towards slow type I muscle fibers, as it was previously suggested in muscle-specific *Bmal1* KO mice (Hodge et al. 2015).

Muscle clock alteration impairs glucose uptake in response to insulin

Skeletal muscle is responsible for 70-80% of insulin-stimulated glucose uptake (DeFronzo and Tripathy 2009). Importantly, we observed a 30% decrease in glucose uptake for both basal and insulin stimulated conditions in siCLOCK-transfected hSKM (Figure 3C). Previous studies have reported similar observations in either *Bmal1*-specific muscle KO, or in *Clock∆19* mutant mice (Kennaway et al. 2007; Dyar et al. 2014; Harfmann et al. 2016). Recently, it was shown that cardiomyocyte-specific *Bmal1* KO and *Clock∆19* mutant mice exhibit defects in insulin-regulated processes, including over-activation of AKT and mTOR signaling (McGinnis et al. 2017). Though we did not see significant changes in *GLUT1* or *GLUT4* gene expression levels, our differential analysis highlighted many genes involved in the regulation of the GLUT4 translocation pathway (Table S2 and Supplemental Dataset 3).

Upon closer analysis of the GLUT4 translocation and recycling pathways, we observed changes upon siCLOCK treatment at each step, with several genes being differentially expressed. Specifically, the enzyme PI4K2A, catalyzing the phosphorylation of phosphatidylinositol (PI) to phosphatidylinositol 4-phosphate (PI4P), was downregulated at the

mRNA level, which may result in decreased PIP2 and PIP3 levels (Pullen et al. 1998; Sakamoto and Holman 2008). Additionally, siCLOCK depleted cells overexpressed *MAPKAP1* (*mSIN1*), one component of the mTORC2 complex required for AKT phosphorylation (Frias et al. 2006), and *CAV-3*, essential for PI3K and AKT activity as well as GLUT4 translocation in muscle (Fecchi et al. 2006; Tan et al. 2012). Moreover, the observed reduction of *14-3-3θ* (*YWAHQ*) upon siCLOCK at both the mRNA and protein level may lead to an attenuated inhibition of TBC1D1 and TBC1D4 (AS160), and thus block GLUT4 translocation to the plasma membrane (Ramm et al. 2006; Roach et al. 2007; An et al. 2010; Kleppe et al. 2011; Szekeres et al. 2012). Consistent with this theory, we observed a modest upregulation of the Rab-GTPase-activator *TBC1D1*, in addition to a downregulation of *RGC2* and an upregulation of *TPM3* at the mRNA level. In summary, regulation of GLUT4 translocation and recycling pathways may be affected upon clock disruption with important consequences on glucose uptake and insulin sensitivity as summarized in Figure 6.

Muscle clock disruption influences the expression of genes involved in vesicle trafficking

GLUT4 located at the plasma membrane, is endocytosed in clathrin-coated vesicles and further recycled (Leto and Saltiel 2012; Jaldin-Fincati et al. 2017). We observed that several factors of the clathrin-mediated endocytosis machinery were altered upon *CLOCK* depletion (Table S2), among them *FNBP1* (*FBP17*), *EPN2, HIP1, and SYT1*. Furthermore, our results suggest that *CLOCK* depletion impacts on calcium levels in the cytoplasm as SYT1 acts as a calcium sensor, and in the presence of elevated Ca^{2+} levels promotes the fusion of close membranes (Martin 2015).

Once GLUT4 is endocytosed, it is transported to early endosomes using RAB5 (Stenmark et al. 1994; Leto and Saltiel 2012). As *RAB5B* was upregulated upon siCLOCK, it is suggesting that this recycling step might be increased. Moreover, we found downregulation of *TBC1D16*, which was shown to regulate RAB4 activity, suggesting a possible increase in the fast remobilization of GLUT4 at the plasma membrane (Goueli et al. 2012).

We have previously demonstrated that the basal secretion of myokines, such as IL-6, IL-8, and MCP-1, exhibits a circadian pattern, which was strongly disrupted in hSKM after *CLOCK* silencing *in vitro* (Perrin et al. 2015). Here, our transcriptional analysis showed that key regulators of the exocytosis machinery were altered upon clock disruption (Table S2 and Table S3). Both *VAMP3* and *STX6*, which are involved in IL-6 secretion in mouse macrophages (Manderson et al. 2007), were downregulated at the mRNA level (Table S2 and Table S6), confirming previous results that clock disruption impacts on vesicle trafficking and secretion (Marcheva et al. 2010; Saini et al. 2016). Importantly, when compared with results from clock disrupted human islets (Saini et al. 2016) we found that numerous genes involved in hormone secretion by pancreatic islets were affected in a similar manner in hSKM (Table S8).

Further downstream, GLUT4 is sent to the late endosome for degradation by the lysosome or targeted to the endosomal recycling compartment (ERC), through its interaction with VAMP3 (Dugani et al. 2008; Rose et al. 2009). PI4K2A, which was downregulated upon clock depletion (Table S2), might be involved here as it regulates VAMP3 trafficking to perinuclear membranes (Volchuk et al. 1995; Jovic et al. 2014). In addition, *CAMSAP2*, involved in microtubule stabilization (Hendershott and Vale 2014), and *KIF13A*, associated with recycling endosome tubules (Delevoye et al. 2014), were also downregulated upon *CLOCK* disruption (Table S2 and Table S3). Taken together these results, as summarized in Figure 6, suggest that the muscle clock may play an important regulatory function in the control of the secretion machinery via transcriptional regulation.

Cell-autonomous clock disruption in hSKM might impact energy substrate utilization

The circadian clock has been associated with the control of muscle development and regeneration, as clock mutant mice exhibit defects in muscle metabolism, architecture and composition (for review see (Chatterjee and Ma 2016; Schiaffino et al. 2016)). Here, we found alterations in the expression of several genes involved in lipid metabolism, calcium handling, electron transport chain, and glucose metabolism (Figure 2C-E, Table S7), suggesting a shift in energy substrate utilization upon clock disruption, as has been proposed previously in

rodents upon loss of *Bmal1* (Hodge et al. 2015; Harfmann et al. 2016). AMP-activated protein kinase, a potent regulator of skeletal muscle fat metabolism (Thomson and Winder 2009) might be dysregulated upon clock disruption as we observed upregulation of its regulatory subunit PRKAG2 and downregulation of subunit PRKAG3. Previous work reported downregulation of both subunits in *Bmal1*-specific muscle KO mice (Hodge et al. 2015), suggesting that this gene could be directly controlled by BMAL1.

Clock disruption causes changes in lipid levels as has been described previously for the liver of *Per1/2* KO mice (Adamovich et al. 2014). In hSKM, siCLOCK treatment affected several genes involved in lipid metabolic processes, lipid storage and transport (Figure 2C-E), which resulted in total phosphatidylcholine and glycosylceramide level alterations (Figure 2F). Specifically, we found an increase in the long chain fatty acid transporter *CD36* and in *FABP3,* consistent with previous results obtained in mouse skeletal muscle upon clock disruption (Hodge et al. 2015; Schiaffino et al. 2016). In addition, we observed an upregulation of *MSTN* upon siCLOCK, which could further promote the increase in *CD36* and *FABP3,* leading to impaired glucose uptake (Figure 3D). Interestingly, muscle-specific *myostatin* (*Mstn*) KO mice exhibit a reduction of lipid transporters, including FABP3 and CD36, a diminution of lipid oxidation, higher levels of saturated and unsaturated fatty acids, and a decrease of cardiolipin and triglycerides (Baati et al. 2017). Furthermore, downregulation of *Mstn* in skeletal muscle from type 1 diabetic mice leads to an increase of *Glut1* mRNA and GLUT4 protein levels, promoting insulin-stimulated glucose uptake (Coleman et al. 2016). Altogether, these results confirm previous rodents studies and indicate a shift in substrate utilization in skeletal muscle from carbohydrates to lipids with impact on muscle metabolism and glucose homeostasis (Dyar et al. 2014; Dyar et al. 2015; Hodge et al. 2015; Harfmann et al. 2016).

Conclusions

In summary, our study provides 1) a comparison between rhythmic transcriptome databases obtained from human muscle tissue and cultured primary cells derived from muscle biopsies, and 2) the identification of pathways regulated by *CLOCK* in skeletal muscle, involved in

glucose uptake, myokine secretion, and lipid metabolism (Figure 6). Human primary cells cultured *in vitro* have been used as a model to study human disease and metabolism (Aas et al. 2013; Saini et al. 2015). In combination with tissue analysis as presented here, primary cell culture constitutes a powerful model to study human metabolism, and warrants further analyses in additional metabolically active tissues in physiological conditions, and in the context of metabolic diseases.

MATERIALS AND METHODS

Human skeletal muscle biopsies

10 healthy volunteers were recruited for the *in vivo* study (see Table S1 for donor characteristics). One week prior to the scheduled laboratory visit, participants had to adhere to a consistent daily feeding and sleeping routine. Participants arrived in the laboratory at 19:00 h on the day prior to the testing day and ingested one standardized meal that first evening. Participants remained for the duration of their stay in a semi-recumbent position. During the waking hours of the testing day they were given mixed-macronutrient meal-replacement solutions at hourly intervals (Resource, Nestlé, CH) to ensure energy balance. The laboratory was free from natural light and with artificial lighting standardized to 800 lux in the direction of gaze, ambient temperature maintained between 20-25°C and noise levels tightly regulated. Participants were not permitted to sleep during waking hours when lights were on (i.e. 07:00-22:00 h) and wore eye masks whilst trying to sleep during lights-out (i.e. 22:00-07:00 h). Anesthetic administration (1% lidocaine w/o epinephrine) and skin/fascia incisions for this procedure (Bergstrom 1962) were completed within the hour prior to sleep such that night-time samples could be acquired with minimal discomfort. Six 100 mg biopsy samples were acquired from the *vastus lateralis* muscle at 4-hour intervals (12:00, 16:00, 20:00, 24:00, 04:00 & 08:00 h) and immediately snap frozen under liquid nitrogen. Samples were taken from each leg in alternating and ascending order with skin incisions separated by 2-3 cm. The study was conducted in accordance with the Declaration of Helsinki and with the approval of the Health Research Authority (NRES Committee South West; 14/SW/0123) and the Commission cantonal (VD) d'éthique de la recherche (Cer-VD). For further details see (Loizides-Mangold et al. 2017).

Human muscle RNA-sequencing and data analysis

Total Stranded RNA-Seq (*in vivo* muscle samples): RNA was quantified with Ribogreen (Life Technologies) and quality was assessed on a Fragment Analyzer (Advances Analytical).

Sequencing libraries were prepared from 250 ng total RNA using the TruSeq Stranded Total LT Sample Prep Kit (Illumina) with the Ribo-Zero Gold depletion set. The procedure was automated on a Sciclone NGS Workstation (Perkin Elmer). The manufacturer's protocol was followed, except for the PCR amplification step. The latter was run for 13 cycles with the KAPA HiFi HotStart ReadyMix (Kapa BioSystems). This optimal PCR cycle number was evaluated using the Cycler Correction Factor method as described previously (Atger et al. 2015). Purified libraries were quantified with Picogreen (Life Technologies) and the size pattern was controlled with the DNA High Sensitivity Reagent kit on a LabChip GX (Perkin Elmer). Libraries were then pooled by 24, and each pool was clustered at a concentration of 8 pmol on 8 lanes of v4 paired-end sequencing flow cells (Illumina). Sequencing was performed for 2 x 125 cycles on a HiSeq 2500 strictly following Illumina's recommendations.

Paired-end reads were mapped to the *Homo sapiens* genome (GRCh38/hg38) using *STAR* (Dobin et al. 2013) with parameters "—alignIntronMin 20 –alignIntronMax 1000000 –GTF (option –sjdbGTFfile). Mapped reads were quantified in intronic and exonic regions. For each gene, we defined a gene body by merging all the respective transcripts using *BEDtools* (Quinlan and Hall 2010). A region was defined as exonic if it occurs in a least one of the transcripts while an intronic region had to be shared between all the transcripts. We assigned uniquely mapping paired-reads to exonic regions (exon/exon and complete exon reads) or intronic regions (intron-exon and complete intron reads) considering reads orientation. Genes with less than 2 intronic reads or 10 exonic reads on average were discarded. Intronic and exonic reads count were normalized using EdgeR (Robinson et al. 2010) by the library scaling factor from the exonic regions and the respective intronic and exonic length (*rpkm()*). Genes with less than -2 RPKM (log2) at the exonic level were discarded. Genes with less than -3 RPKM (log2) at the intronic level were reported as NA for the intronic quantification.

Rhythmicity was assessed with a linear mixed-effects model using *lmer()* function from the *lme4* R package applied on the log2 normalized reads count. A standard harmonic regression with a 24 h period was fitted with a donor dependent random effect:

$$y_{ID,t} \sim \cos\left(\frac{2\pi}{24}\ t\right) + \sin\left(\frac{2\pi}{24} t\right) + (1|ID)$$

where $y_{ID,t}$ is the log2 normalized reads count for patient *ID* at time *t*. This full model was compared to the null model (without the harmonic terms) using the likelihood ratio test function *lrtest*() from the lmtest R package. The p-values were computed from a chi-squared distribution and were adjusted using the Benjamini- Hochberg procedure.

Gene ontology analysis was performed using the TopGO R package (Alexa A. and Rahnenfuhrer J. (2016). Enrichment analysis for GO terms derived from "Biological Process" was performed for the genes rhythmic in the different phase bins. GO terms with p-value <0.05, a minimum number of 3 genes, and less than 200 annotated genes were considered.

Study participants, skeletal muscle tissue sampling and primary cell culture

Biopsies from the *Gluteus maximus* muscles were derived from donors with their informed consent (see Figure S2 and Table S1 for donor characteristics). The experimental protocol ('DIOMEDE') was approved by the Ethical Committee SUD EST IV (Agreement 12/111) and performed according to the French legislation (Huriet's law). All donors had HbA1c levels inferior to 6.0% and fasting glycaemia inferior to 7 mmol/L, were not diagnosed for type 2 diabetic (T2D), neoplasia or chronic inflammatory diseases, and not doing shift work. Primary skeletal myoblasts were purified and differentiated into myotubes according to the previously described procedure (Agley et al. 2015; Perrin et al. 2015). After reaching confluence, myoblasts were differentiated into myotubes during 7-10 days in DMEM supplemented with 2% FBS.

siRNA transfection and lentiviral transduction

Human primary myoblasts were differentiated into myotubes as described above. Cells were transfected 24 h (RNA-seq) or 72 h (western blot, glucose uptake) prior to experiment with 20 nM siRNA targeting *CLOCK* (siCLOCK), or with non-targeting siControl (Dharmacon), using HiPerFect transfection reagent (Qiagen) following the manufacturer's protocol. To produce

lentiviral particles, *Bmal1*-luciferase (Liu et al. 2008) lentivectors were transfected into 293T cells using the polyethylenimine method (for detailed procedure see (Pulimeno et al. 2012)). Myoblasts were transduced with the indicated lentiviral particles with a multiplicity of infection (MOI) = 3 for each, grown to confluence, and subsequently differentiated into myotubes.

***In vitro* skeletal myotube synchronization and real-time bioluminescence recording**

Primary myotubes were synchronized with 10 µM forskolin (Sigma) for 60 min at 37°C in a cell culture incubator, then the medium was changed to a phenol red-free recording medium containing 100 µM luciferin (Prolume LTD), and cells were transferred to a 37°C light-tight incubator as previously described by us (Pulimeno et al. 2012). Bioluminescence from each dish was continuously monitored using a Hamamatsu photomultiplier tube (PMT) detector assembly. Photon counts were integrated over 1 min intervals. Luminescence traces are shown as detrended data.

Glucose uptake measurement

Human myotubes treated with siControl or siCLOCK as described before were serum-starved for 3 hours then incubated with 2-deoxy-[^{3}H]-D-glucose for 15 min. Incubations were performed with or without insulin stimulation (1 hour, 100 nM). After incubation, the medium was removed prior to cell lysis in 0.05 M NaOH. Cell content radioactivity was determined by liquid scintillation counting (Perkin Elmer 2900 TR) and protein content was quantified by using the Bradford protein assay. Glucose transport is expressed in pmol/mg.min (Chanon et al. 2017).

Protein analysis

Human myotubes transfected with siControl or siCLOCK for 24 to 72 h, were lysed in RIPA buffer. Protein extracts (8 µg) were analyzed by SDS-PAGE and immunoblotted to 0.45 µm nitrocellulose membrane or 0.2 µm PVDF membrane using a wet system (Bio-Rad) according to the manufacturer's instructions. Membranes were blocked and incubated with primary and secondary antibodies in 5% BSA/TBS-T 0.5% or 5% BSA/TBS-T 0.1%. Primary and secondary

antibodies were used at the following dilutions: anti-TBC1D4/AS160 (1/1000, Cell Signaling, #2670S), anti-14-3-3θ (1/200, Cell Signaling, #9638S), anti-CLOCK (1/200, Santa Cruz, H-276) and anti-ACTIN (1/1000, Sigma, A2066), anti-rabbit-HRP (1:3000, Sigma A8275). Signals were visualized using SuperSignal West Pico Chemiluminescent Substrate (Thermo Scientific). For protein quantification, 5 donors were analyzed but only the representative western blot result of one donor is shown.

Lipidomics

The lipidomics analysis was performed as described in (Loizides-Mangold et al. 2017). Briefly, human primary myotubes were harvested from one confluent 10 cm dish (~1.5 x 10^6 cells) and lipid extracts were prepared using the MTBE protocol (Matyash et al. 2008). Total phosphorus was determined as described in (Loizides-Mangold et al. 2017). Phospho- and sphingolipid were analyzed by mass spectrometry using on a TSQ Vantage Triple Stage Quadrupole Mass Spectrometer (Thermo Fisher Scientific) equipped with a robotic nanoflow ion source (Nanomate HD, Advion Biosciences), using multiple reaction monitoring (MRM). Lipid concentrations were calculated relative to the relevant internal standards and then normalized to the total phosphate content of each total lipid extract. Triacylglyceride analysis was performed by mass spectrometry analysis on a hybrid ion trap LTQ-Orbitrap XL mass spectrometer (Thermo Fisher Scientific) equipped with a micro LC binary pump UFLC-XR (Shimadzu). Lipid identification was carried out with the Lipid Data Analyzer II (LDA v. 2.5.1, IGB-TUG Graz University) (Hartler et al. 2011).

hSKM mRNA extraction and quantitative PCR analysis

Differentiated myotubes were synchronized by 10 µM forskolin, collected every 2 h during 48 h (0 - 48 h), deep-frozen in liquid nitrogen and kept at -80°C. Total RNA was prepared using RNeasy® Mini kit (Qiagen). 0.5 µg of total RNA was reverse-transcribed using Superscript III reverse transcriptase (Invitrogen) and random hexamers, and PCR-amplified on a LightCycler 480 (Roche). Mean values for each sample were calculated from the technical duplicates of

each RT-qPCR analysis, and normalized to the mean of two housekeeping genes (*HPRT* and *9S*), which served as internal controls. Primers used for this study are listed in Supplementary Table S9.

hSKM RNA-sequencing and data analysis

Total RNA was prepared from primary human skeletal myotubes from 2 donors, transfected either with siControl or siCLOCK, synchronized with a forskolin pulse and collected every 2 h during 48 h in duplicates, using RNeasy® Mini Kit (Qiagen). Total RNA libraries were prepared from 300 ng of RNA following customary Illumina TruSeq v2 protocols for next generation sequencing. PolyA-selected mRNAs were purified, size-fractioned, and subsequently converted to single-stranded cDNA by random hexamer priming. Following second-strand synthesis, double-stranded cDNAs were blunt-end fragmented and indexed using adapter ligation, after which they were amplified and sequenced according to protocol. RNA libraries were sequenced with a HiSeq2000 sequencer producing 49pb paired-end reads. Standard quality checks for material degradation (Bioanalyzer and TapeStation, Agilent Technologies) and concentration (Qubit, Life Technologies) were done before and after library construction, ensuring that samples are suitable for sequencing.

Paired-end reads were mapped to the human genome (version GRCh37/hg19) with GEMTools (v1.7.1) using GENCODE v19 as gene annotation. RNA-seq reads were subsequently filtered for correct orientation of the two ends, a minimum mapping quality score of 150 and allowing a maximum of 5 mismatches in both ends. GENCODE annotation v19 was used to assign filtered reads to their corresponding exons and genes. For each gene, we processed the exons from all transcripts, which we quantified by considering only filtered reads as above, in which both ends map to exons of the same gene. The gene counts were incremented non-redundantly, i.e. reads overlapping two exons are counted once to the total count sum per gene.

The differential gene expression analysis was performed with the R package edgeR (Robinson et al. 2010). First, transcripts expressed lower than 3 counts per million (CPM) and

679 noninformative (e.g., non-aligned) were filtered. To minimize the log-fold changes between the
680 samples for most genes, a set of scaling factors for the library sizes were estimated with the
681 trimmed mean of M-values (TMM) method (Robinson and Oshlack 2010). The dispersion was
682 estimated with the quantile-adjusted conditional maximum likelihood (qCML) method. Once
683 the dispersion estimates are obtained, we performed the testing procedures for determining
684 differential expression using the exact test (Robinson and Smyth 2008).

685 Regarding the rhythmic analysis, homemade algorithm was developed to analyze these
686 RNA-seq data. In short, raw data were transformed to $\log_2$ reads per kilobase per million
687 mapped reads (RPKM) as described previously (Atger et al. 2015), then only transcripts with
688 $\log_2$ RPKM>0 for each of the fourth conditions (2 subjects, siControl or siCLOCK) were kept
689 avoiding big variability for weakly expressed transcripts. The 48 time points of each condition
690 were used to define a local regression function (loess). This step allows smoothing the curve
691 and reducing local variability. The function was then used to calculate 10 different measures
692 (maximum and minimum slopes, first and second extremum, minimum-maximum ratio,
693 autocorrelation, measure of scattering, residues on the loess function, residues on a linear
694 function and period). These features were used to classify gene expression patterns in 4
695 different groups: rhythmic genes (category “circadian”), genes that show only one peak at the
696 beginning of the time course (category “one peak”), linearly (category “linear”) and scattered
697 expressed genes (category “cloud”). The algorithm attributes a probability to each transcript
698 per condition. To be classified in one category, this probability must be the highest value and
699 superior to 0.5 in at least one category. If no probabilities are superior to 0.5 for the four
700 categories, transcripts are grouped into model 16 (non-rhythmic). The 11 major circadian
701 genes, including *ARNTL* (*BMAL1*), *NR1D1* (*REVERBα*), *NR1D2* (*REVERBβ*), *PER1*, *PER2*,
702 *PER3*, *CRY1*, *CRY2*, *NPAS2*, *TEF* and *BHLHE41*, were selected to train a random forest
703 model. The same numbers of genes for the 3 other groups were also integrated in the training
704 dataset. This dataset was then passed to the training algorithm for random forests and gene
705 conditions that were assigned to one of these categories with a high score (0.9) were integrated
706 in the training dataset. This procedure was repeated until 500 curves per group were identified.

The last model was kept to classify the whole dataset and identify 1'485 curves from 994 transcripts as rhythmic among 12’985 transcripts. Altogether, transcripts were grouped into 16 models.

Bioluminescence and statistical data analysis

Bioluminescence data were analyzed with the Actimetrics LumiCycle analysis software (Actimetrics LTD). RNA-seq data and qPCR data analysis were performed using RStudio, GraphPad Prism 5 and Excel 2016. Panther analyses were performed using the PANTHER version 12.0 released on 10.07.2017. Statistical analyses were performed using Student’s *t*-test. Differences were considered significant for (*) p-value <0.05, (**) p-value <0.01, and (***) p-value <0.001. Exact p-values and raw data for Figures 2 and 3 are listed in Supplemental Dataset 11.

ACKNOWLEDGEMENTS

The authors thank Jacques Philippe and Sylvain Sardy for constructive discussions; Pamela Pulimeno for help with conducting the *in vitro* around-the-clock sample collection, RNA extractions and RT-qPCR experiments; Svetlana Skarupelova and Camille Saini for help with RNA extractions and Anne-Marie Makhlouf for lentivirus preparation; Luciana Romano and Deborah Beilser for the help with *in vitro* RNA sequencing (University of Geneva); Marc Moniatte and Johnathan Paz (PCF, EPFL) for help with the lipid analyses; and Ondine Walter (NIHS) for the ethical and logistical management of human samples.

This work was funded by the Sinergia Swiss National Science Foundation (Grant No. CRSII3-154405 to HR, CD, EL), the Swiss National Science Foundation (Grant No. 31003A-166700, the Fondation Privée de HUG, Fondation Ernst et Lucie Schmidheiny, the Société Académique de Genève (CD) and by the United Kingdom Biotechnology and Biological Sciences Research Council Grant BB/I008470/1 (JDJ).

COMPETING INTERESTS

J.A.B. has been a consultant for PepsiCo (Quaker) and Kellogg's. C.G., B.D.W., E.M., A.C. and J.N.F. are full-time employees of the Nestlé Institute of Health Sciences SA. L.G.K. is an employee of Nestec Ltd. The other authors have no conflict of interest to declare.

REFERENCES

Aas V, Bakke SS, Feng YZ, Kase ET, Jensen J, Bajpeyi S, Thoresen GH and Rustan AC. 2013. Are cultured human myotubes far from home? *Cell Tissue Res* **354**(3): 671-82 doi:10.1007/s00441-013-1655-1.

Adamovich Y, Rousso-Noori L, Zwighaft Z, Neufeld-Cohen A, Golik M, Kraut-Cohen J, Wang M, Han X and Asher G. 2014. Circadian clocks and feeding time regulate the oscillations and levels of hepatic triglycerides. *Cell metabolism* **19**(2): 319-30 doi:10.1016/j.cmet.2013.12.016.

Agley CC, Rowlerson AM, Velloso CP, Lazarus NL and Harridge SD. 2015. Isolation and quantitative immunocytochemical characterization of primary myogenic cells and fibroblasts from human skeletal muscle. *J Vis Exp*(95): 52049 doi:10.3791/52049 [doi].

Albrecht U. 2012. Timing to perfection: the biology of central and peripheral circadian clocks. *Neuron* **74**(2): 246-60 doi:S0896-6273(12)00332-7 [pii] 10.1016/j.neuron.2012.04.006.

An D, Toyoda T, Taylor EB, Yu H, Fujii N, Hirshman MF and Goodyear LJ. 2010. TBC1D1 regulates insulin- and contraction-induced glucose transport in mouse skeletal muscle. *Diabetes* **59**(6): 1358-65 doi:db09-1266 [pii] 10.2337/db09-1266 [doi].

Andrews JL, Zhang X, McCarthy JJ, McDearmon EL, Hornberger TA, Russell B, Campbell KS, Arbogast S, Reid MB, Walker JR, Hogenesch JB, Takahashi JS and Esser KA. 2010. CLOCK and BMAL1 regulate MyoD and are necessary for maintenance of skeletal muscle phenotype and function. *Proceedings of the National Academy of Sciences of the United States of America* **107**(44): 19090-5 doi:1014523107 [pii] 10.1073/pnas.1014523107.

Asher G and Sassone-Corsi P. 2015. Time for food: the intimate interplay between nutrition, metabolism, and the circadian clock. *Cell* **161**(1): 84-92 doi:10.1016/j.cell.2015.03.015.

Atger F, Gobet C, Marquis J, Martin E, Wang J, Weger B, Lefebvre G, Descombes P, Naef F and Gachon F. 2015. Circadian and feeding rhythms differentially affect rhythmic mRNA transcription and translation in mouse liver. *Proceedings of the National Academy of Sciences of the United States of America* **112**(47): E6579-88 doi:10.1073/pnas.1515308112.

Baati N, Feillet-Coudray C, Fouret G, Vernus B, Goustard B, Coudray C, Lecomte J, Blanquet V, Magnol L, Bonnieu A and Koechlin-Ramonatxo C. 2017. Myostatin deficiency is associated with lipidomic abnormalities in skeletal muscles. *Biochim Biophys Acta* doi:10.1016/j.bbalip.2017.06.017.

Benedict C, Shostak A, Lange T, Brooks SJ, Schioth HB, Schultes B, Born J, Oster H and Hallschmid M. 2012. Diurnal rhythm of circulating nicotinamide phosphoribosyltransferase (Nampt/visfatin/PBEF): impact of sleep loss and relation to glucose metabolism. *The Journal of clinical endocrinology and metabolism* **97**(2): E218-22 doi:10.1210/jc.2011-2241.

Bergstrom J. 1962. Muscle Electrolytes in Man - Determined by Neutron Activation Analysis on Needle Biopsy Specimens - Study on Normal Subjects, Kidney Patients, and Patients with Chronic Diarrhoea. *Scand J Clin Lab Inv* **14**: 1-&.

Catoire M, Mensink M, Boekschoten MV, Hangelbroek R, Muller M, Schrauwen P and Kersten S. 2012. Pronounced effects of acute endurance exercise on gene expression in resting and exercising human skeletal muscle. *PloS one* **7**(11): e51066 doi:10.1371/journal.pone.0051066.

Chanon S, Durand C, Vieille-Marchiset A, Robert M, Dibner C, Simon C and Lefai E. 2017. Glucose Uptake Measurement and Response to Insulin Stimulation in In Vitro Cultured Human Primary Myotubes. *J Vis Exp*(124) doi:10.3791/55743.

Chatterjee S and Ma K. 2016. Circadian clock regulation of skeletal muscle growth and repair. *F1000Res* **5**: 1549 doi:10.12688/f1000research.9076.1 [doi].

Coleman SK, Rebalka IA, D'Souza DM, Deodhare N, Desjardins EM and Hawke TJ. 2016. Myostatin inhibition therapy for insulin-deficient type 1 diabetes. *Sci Rep* **6**: 32495 doi:10.1038/srep32495.

809 Coomer M and Essop MF. 2014. Differential hexosamine biosynthetic pathway gene
810 expression with type 2 diabetes. *Mol Genet Metab Rep* **1**: 158-69
811 doi:10.1016/j.ymgmr.2014.03.003.
812
813 DeBruyne JP, Weaver DR and Reppert SM. 2007. CLOCK and NPAS2 have overlapping
814 roles in the suprachiasmatic circadian clock. *Nat Neurosci* **10**(5): 543-5 doi:10.1038/nn1884.
815
816 DeFronzo RA, Jacot E, Jequier E, Maeder E, Wahren J and Felber JP. 1981. The effect of
817 insulin on the disposal of intravenous glucose. Results from indirect calorimetry and hepatic
818 and femoral venous catheterization. *Diabetes* **30**(12): 1000-7.
819
820 DeFronzo RA and Tripathy D. 2009. Skeletal muscle insulin resistance is the primary defect
821 in type 2 diabetes. *Diabetes Care* **32 Suppl 2**: S157-63 doi:32/suppl_2/S157 [pii]
822 10.2337/dc09-S302 [doi].
823
824 Delevoye C, Miserey-Lenkei S, Montagnac G, Gilles-Marsens F, Paul-Gilloteaux P, Giordano
825 F, Waharte F, Marks MS, Goud B and Raposo G. 2014. Recycling endosome tubule
826 morphogenesis from sorting endosomes requires the kinesin motor KIF13A. *Cell Rep* **6**(3):
827 445-54 doi:S2211-1247(14)00003-5 [pii]
828 10.1016/j.celrep.2014.01.002 [doi].
829
830 Dibner C and Schibler U. 2015. Circadian timing of metabolism in animal models and
831 humans. *Journal of internal medicine* doi:10.1111/joim.12347.
832
833 Dobin A, Davis CA, Schlesinger F, Drenkow J, Zaleski C, Jha S, Batut P, Chaisson M and
834 Gingeras TR. 2013. STAR: ultrafast universal RNA-seq aligner. *Bioinformatics* **29**(1): 15-21
835 doi:10.1093/bioinformatics/bts635.
836
837 Dugani CB, Randhawa VK, Cheng AW, Patel N and Klip A. 2008. Selective regulation of the
838 perinuclear distribution of glucose transporter 4 (GLUT4) by insulin signals in muscle cells.
839 *Eur J Cell Biol* **87**(6): 337-51 doi:S0171-9335(08)00044-7 [pii]
840 10.1016/j.ejcb.2008.02.009 [doi].
841
842 Dyar KA, Ciciliot S, Tagliazucchi GM, Pallafacchina G, Tothova J, Argentini C, Agatea L,
843 Abraham R, Ahdesmaki M, Forcato M, Bicciato S, Schiaffino S and Blaauw B. 2015. The
844 calcineurin-NFAT pathway controls activity-dependent circadian gene expression in slow
845 skeletal muscle. *Molecular metabolism* **4**(11): 823-33 doi:10.1016/j.molmet.2015.09.004.
846
847 Dyar KA, Ciciliot S, Wright LE, Bienso RS, Tagliazucchi GM, Patel VR, Forcato M, Paz MI,
848 Gudiksen A, Solagna F, Albiero M, Moretti I, Eckel-Mahan KL, Baldi P, Sassone-Corsi P,
849 Rizzuto R, Bicciato S, Pilegaard H, Blaauw B and Schiaffino S. 2014. Muscle insulin
850 sensitivity and glucose metabolism are controlled by the intrinsic muscle clock. *Molecular*
851 *metabolism* **3**(1): 29-41 doi:10.1016/j.molmet.2013.10.005.
852
853 Fecchi K, Volonte D, Hezel MP, Schmeck K and Galbiati F. 2006. Spatial and temporal
854 regulation of GLUT4 translocation by flotillin-1 and caveolin-3 in skeletal muscle cells.
855 *FASEB journal : official publication of the Federation of American Societies for Experimental*
856 *Biology* **20**(6): 705-07 doi:10.1096/fj.05-4661fje.
857
858 Fischer KM, Cottage CT, Wu W, Din S, Gude NA, Avitabile D, Quijada P, Collins BL,
859 Fransioli J and Sussman MA. 2009. Enhancement of myocardial regeneration through
860 genetic engineering of cardiac progenitor cells expressing Pim-1 kinase. *Circulation* **120**(21):
861 2077-87 doi:10.1161/circulationaha.109.884403.
862

Frederick DW, Loro E, Liu L, Davila A, Jr., Chellappa K, Silverman IM, Quinn WJ, 3rd, Gosai SJ, Tichy ED, Davis JG, Mourkioti F, Gregory BD, Dellinger RW, Redpath P, Migaud ME, Nakamaru-Ogiso E, Rabinowitz JD, Khurana TS and Baur JA. 2016. Loss of NAD Homeostasis Leads to Progressive and Reversible Degeneration of Skeletal Muscle. *Cell Metab* **24**(2): 269-82 doi:10.1016/j.cmet.2016.07.005.

Frias MA, Thoreen CC, Jaffe JD, Schroder W, Sculley T, Carr SA and Sabatini DM. 2006. mSin1 Is Necessary for Akt/PKB Phosphorylation, and Its Isoforms Define Three Distinct mTORC2s. *Current Biology* **16**(18): 1865-70 doi:http://dx.doi.org/10.1016/j.cub.2006.08.001.

Friedmann-Bette B, Schwartz FR, Eckhardt H, Billeter R, Bonaterra G and Kinscherf R. 2012. Similar changes of gene expression in human skeletal muscle after resistance exercise and multiple fine needle biopsies. *Journal of applied physiology (Bethesda, Md. : 1985)* **112**(2): 289-95 doi:10.1152/japplphysiol.00959.2011.

Gachon F, Loizides-Mangold U, Petrenko V and Dibner C. 2017. Glucose homeostasis: regulation by peripheral circadian clocks in rodents and humans. *Endocrinology* doi:10.1210/en.2017-00218.

Garten A, Schuster S, Penke M, Gorski T, de Giorgis T and Kiess W. 2015. Physiological and pathophysiological roles of NAMPT and NAD metabolism. *Nat Rev Endocrinol* **11**(9): 535-46 doi:10.1038/nrendo.2015.117.

Goueli BS, Powell MB, Finger EC and Pfeffer SR. 2012. TBC1D16 is a Rab4A GTPase activating protein that regulates receptor recycling and EGF receptor signaling. *Proc Natl Acad Sci U S A* **109**(39): 15787-92 doi:10.1073/pnas.1204540109.

Guillaumond F, Grechez-Cassiau A, Subramaniam M, Brangolo S, Peteri-Brunback B, Staels B, Fievet C, Spelsberg TC, Delaunay F and Teboul M. 2010. Kruppel-like factor KLF10 is a link between the circadian clock and metabolism in liver. *Mol Cell Biol* **30**(12): 3059-70 doi:10.1128/MCB.01141-09.

Haldar SM, Jeyaraj D, Anand P, Zhu H, Lu Y, Prosdocimo DA, Eapen B, Kawanami D, Okutsu M, Brotto L, Fujioka H, Kerner J, Rosca MG, McGuinness OP, Snow RJ, Russell AP, Gerber AN, Bai X, Yan Z, Nosek TM, Brotto M, Hoppel CL and Jain MK. 2012. Kruppel-like factor 15 regulates skeletal muscle lipid flux and exercise adaptation. *Proc Natl Acad Sci U S A* **109**(17): 6739-44 doi:10.1073/pnas.1121060109.

Hansen J, Timmers S, Moonen-Kornips E, Duez H, Staels B, Hesselink MK and Schrauwen P. 2016. Synchronized human skeletal myotubes of lean, obese and type 2 diabetic patients maintain circadian oscillation of clock genes. *Sci Rep* **6**: 35047 doi:10.1038/srep35047.

Harfmann BD, Schroder EA and Esser KA. 2015. Circadian rhythms, the molecular clock, and skeletal muscle. *Journal of biological rhythms* **30**(2): 84-94 doi:10.1177/0748730414561638.

Harfmann BD, Schroder EA, Kachman MT, Hodge BA, Zhang X and Esser KA. 2016. Muscle-specific loss of Bmal1 leads to disrupted tissue glucose metabolism and systemic glucose homeostasis. *Skelet Muscle* **6**: 12 doi:10.1186/s13395-016-0082-x.

Hartler J, Trotzmuller M, Chitraju C, Spener F, Kofeler HC and Thallinger GG. 2011. Lipid Data Analyzer: unattended identification and quantitation of lipids in LC-MS data. *Bioinformatics* **27**(4): 572-7 doi:10.1093/bioinformatics/btq699.

Hendershott MC and Vale RD. 2014. Regulation of microtubule minus-end dynamics by CAMSAPs and Patronin. *Proc Natl Acad Sci U S A* **111**(16): 5860-5 doi:1404133111 [pii] 10.1073/pnas.1404133111 [doi].

Hodge BA, Wen Y, Riley LA, Zhang X, England JH, Harfmann BD, Schroder EA and Esser KA. 2015. The endogenous molecular clock orchestrates the temporal separation of substrate metabolism in skeletal muscle. *Skelet Muscle* **5**: 17 doi:10.1186/s13395-015-0039-5.

Huang P, Altshuller YM, Hou JC, Pessin JE and Frohman MA. 2005. Insulin-stimulated plasma membrane fusion of Glut4 glucose transporter-containing vesicles is regulated by phospholipase D1. *Mol Biol Cell* **16**(6): 2614-23 doi:10.1091/mbc.E04-12-1124.

Hughes ME, DiTacchio L, Hayes KR, Vollmers C, Pulivarthy S, Baggs JE, Panda S and Hogenesch JB. 2009. Harmonics of circadian gene transcription in mammals. *PLoS genetics* **5**(4): e1000442.

Hughes ME, Hogenesch JB and Kornacker K. 2010. JTK_CYCLE: an efficient nonparametric algorithm for detecting rhythmic components in genome-scale data sets. *J Biol Rhythms* **25**(5): 372-80 doi:25/5/372 [pii] 10.1177/0748730410379711 [doi].

Jaldin-Fincati JR, Pavarotti M, Frendo-Cumbo S, Bilan PJ and Klip A. 2017. Update on GLUT4 Vesicle Traffic: A Cornerstone of Insulin Action. *Trends in endocrinology and metabolism: TEM* doi:10.1016/j.tem.2017.05.002.

Jordan SD, Kriebs A, Vaughan M, Duglan D, Fan W, Henriksson E, Huber AL, Papp SJ, Nguyen M, Afetian M, Downes M, Yu RT, Kralli A, Evans RM and Lamia KA. 2017. CRY1/2 Selectively Repress PPARdelta and Limit Exercise Capacity. *Cell metabolism* **26**(1): 243-55 e6 doi:10.1016/j.cmet.2017.06.002.

Jovic M, Kean MJ, Dubankova A, Boura E, Gingras AC, Brill JA and Balla T. 2014. Endosomal sorting of VAMP3 is regulated by PI4K2A. *J Cell Sci* **127**(Pt 17): 3745-56 doi:jcs.148809 [pii] 10.1242/jcs.148809 [doi].

Kalsbeek A, la Fleur S and Fliers E. 2014. Circadian control of glucose metabolism. *Molecular metabolism* **3**(4): 372-83 doi:10.1016/j.molmet.2014.03.002.

Kennaway DJ, Owens JA, Voultsios A, Boden MJ and Varcoe TJ. 2007. Metabolic homeostasis in mice with disrupted Clock gene expression in peripheral tissues. *American Journal of Physiology - Regulatory, Integrative and Comparative Physiology* **293**(4): R1528-R37 doi:10.1152/ajpregu.00018.2007.

Kleppe R, Martinez A, Doskeland SO and Haavik J. 2011. The 14-3-3 proteins in regulation of cellular metabolism. *Semin Cell Dev Biol* **22**(7): 713-9 doi:S1084-9521(11)00122-4 [pii] 10.1016/j.semcdb.2011.08.008 [doi].

Krishnaiah SY, Wu G, Altman BJ, Growe J, Rhoades SD, Coldren F, Venkataraman A, Olarerin-George AO, Francey LJ, Mukherjee S, Girish S, Selby CP, Cal S, Er U, Sianati B, Sengupta A, Anafi RC, Kavakli IH, Sancar A, Baur JA, Dang CV, Hogenesch JB and Weljie AM. 2017. Clock Regulation of Metabolites Reveals Coupling between Transcription and Metabolism. *Cell metabolism* **25**(4): 961-74 e4 doi:10.1016/j.cmet.2017.03.019.

971 Laing EE, Johnston JD, Moller-Levet CS, Bucca G, Smith CP, Dijk DJ and Archer SN. 2015.
972 Exploiting human and mouse transcriptomic data: Identification of circadian genes and
973 pathways influencing health. *Bioessays* **37**(5): 544-56 doi:10.1002/bies.201400193.
974
975 Lavallee G, Andelfinger G, Nadeau M, Lefebvre C, Nemer G, Horb ME and Nemer M. 2006.
976 The Kruppel-like transcription factor KLF13 is a novel regulator of heart development. *Embo j*
977 **25**(21): 5201-13 doi:10.1038/sj.emboj.7601379.
978
979 Leto D and Saltiel AR. 2012. Regulation of glucose transport by insulin: traffic control of
980 GLUT4. *Nat Rev Mol Cell Biol* **13**(6): 383-96 doi:nrm3351 [pii]
981 10.1038/nrm3351 [doi].
982
983 Liu AC, Tran HG, Zhang EE, Priest AA, Welsh DK and Kay SA. 2008. Redundant function of
984 REV-ERBalpha and beta and non-essential role for Bmal1 cycling in transcriptional
985 regulation of intracellular circadian rhythms. *PLoS genetics* **4**(2): e1000023
986 doi:10.1371/journal.pgen.1000023.
987
988 Lluis F, Roma J, Suelves M, Parra M, Aniorte G, Gallardo E, Illa I, Rodriguez L, Hughes SM,
989 Carmeliet P, Roig M and Munoz-Canoves P. 2001. Urokinase-dependent plasminogen
990 activation is required for efficient skeletal muscle regeneration in vivo. *Blood* **97**(6): 1703-11.
991
992 Loizides-Mangold U, Koren-Gluzer M, Skarupelova S, Makhlouf AM, Hayek T, Aviram M and
993 Dibner C. 2016. Paraoxonase 1 (PON1) and pomegranate influence circadian gene
994 expression and period length. *Chronobiology international* **33**(4): 453-61
995 doi:10.3109/07420528.2016.1154067.
996
997 Loizides-Mangold U, Perrin L, Vandereycken B, Betts JA, Walhin JP, Templeman I, Chanon
998 S, Weger BD, Durand C, Robert M, Paz Montoya J, Moniatte M, Karagounis LG, Johnston
999 JD, Gachon F, Lefai E, Riezman H and Dibner C. 2017. Lipidomics reveals diurnal lipid
1000 oscillations in human skeletal muscle persisting in cellular myotubes cultured in vitro.
1001 *Proceedings of the National Academy of Sciences of the United States of America*
1002 doi:10.1073/pnas.1705821114.
1003
1004 Luck S, Thurley K, Thaben PF and Westermark PO. 2014. Rhythmic degradation explains
1005 and unifies circadian transcriptome and proteome data. *Cell Rep* **9**(2): 741-51
1006 doi:10.1016/j.celrep.2014.09.021.
1007
1008 Manderson AP, Kay JG, Hammond LA, Brown DL and Stow JL. 2007. Subcompartments of
1009 the macrophage recycling endosome direct the differential secretion of IL-6 and TNFalpha. *J*
1010 *Cell Biol* **178**(1): 57-69 doi:jcb.200612131 [pii]
1011 10.1083/jcb.200612131 [doi].
1012
1013 Mannic T, Meyer P, Triponez F, Pusztaszeri M, Le Martelot G, Mariani O, Schmitter D, Sage
1014 D, Philippe J and Dibner C. 2013. Circadian clock characteristics are altered in human
1015 thyroid malignant nodules. *The Journal of clinical endocrinology and metabolism* **98**(11):
1016 4446-56 doi:10.1210/jc.2013-2568.
1017
1018 Mansueto G, Armani A, Viscomi C, D'Orsi L, De Cegli R, Polishchuk EV, Lamperti C, Di Meo
1019 I, Romanello V, Marchet S, Saha PK, Zong H, Blaauw B, Solagna F, Tezze C, Grumati P,
1020 Bonaldo P, Pessin JE, Zeviani M, Sandri M and Ballabio A. 2017. Transcription Factor EB
1021 Controls Metabolic Flexibility during Exercise. *Cell Metab* **25**(1): 182-96
1022 doi:10.1016/j.cmet.2016.11.003.
1023
1024 Marcheva B, Ramsey KM, Buhr ED, Kobayashi Y, Su H, Ko CH, Ivanova G, Omura C, Mo S,
1025 Vitaterna MH, Lopez JP, Philipson LH, Bradfield CA, Crosby SD, JeBailey L, Wang X,

Takahashi JS and Bass J. 2010. Disruption of the clock components CLOCK and BMAL1 leads to hypoinsulinaemia and diabetes. *Nature* **466**(7306): 627-31 doi:nature09253 [pii] 10.1038/nature09253.

Martin TF. 2015. PI(4,5)P(2)-binding effector proteins for vesicle exocytosis. *Biochim Biophys Acta* **1851**(6): 785-93 doi:10.1016/j.bbalip.2014.09.017.

Matyash V, Liebisch G, Kurzchalia TV, Shevchenko A and Schwudke D. 2008. Lipid extraction by methyl-tert-butyl ether for high-throughput lipidomics. *J Lipid Res* **49**(5): 1137-46 doi:10.1194/jlr.D700041-JLR200.

McCarthy JJ, Andrews JL, McDearmon EL, Campbell KS, Barber BK, Miller BH, Walker JR, Hogenesch JB, Takahashi JS and Esser KA. 2007. Identification of the circadian transcriptome in adult mouse skeletal muscle. *Physiological genomics* **31**(1): 86-95 doi:00066.2007 [pii] 10.1152/physiolgenomics.00066.2007.

McGinnis GR, Tang Y, Brewer RA, Brahma MK, Stanley HL, Shanmugam G, Rajasekaran NS, Rowe GC, Frank SJ, Wende AR, Dale Abel E, Taegtmeyer H, Litovsky S, Darley-Usmar V, Zhang J, Chatham JC and Young ME. 2017. Genetic disruption of the cardiomyocyte circadian clock differentially influences insulin-mediated processes in the heart. *Journal of molecular and cellular cardiology* doi:10.1016/j.yjmcc.2017.07.005.

Mi H, Huang X, Muruganujan A, Tang H, Mills C, Kang D and Thomas PD. 2017. PANTHER version 11: expanded annotation data from Gene Ontology and Reactome pathways, and data analysis tool enhancements. *Nucleic acids research* **45**(Database issue): D183-D89 doi:10.1093/nar/gkw1138.

Miller BH, McDearmon EL, Panda S, Hayes KR, Zhang J, Andrews JL, Antoch MP, Walker JR, Esser KA, Hogenesch JB and Takahashi JS. 2007. Circadian and CLOCK-controlled regulation of the mouse transcriptome and cell proliferation. *Proceedings of the National Academy of Sciences of the United States of America* **104**(9): 3342-7.

Muoio DM and Newgard CB. 2008. Mechanisms of disease:Molecular and metabolic mechanisms of insulin resistance and beta-cell failure in type 2 diabetes. *Nature reviews* **9**(3): 193-205 doi:10.1038/nrm2327.

Neve B, Fernandez-Zapico ME, Ashkenazi-Katalan V, Dina C, Hamid YH, Joly E, Vaillant E, Benmezroua Y, Durand E, Bakaher N, Delannoy V, Vaxillaire M, Cook T, Dallinga-Thie GM, Jansen H, Charles MA, Clement K, Galan P, Hercberg S, Helbecque N, Charpentier G, Prentki M, Hansen T, Pedersen O, Urrutia R, Melloul D and Froguel P. 2005. Role of transcription factor KLF11 and its diabetes-associated gene variants in pancreatic beta cell function. *Proceedings of the National Academy of Sciences of the United States of America* **102**(13): 4807-12 doi:10.1073/pnas.0409177102.

Perrin L, Loizides-Mangold U, Skarupelova S, Pulimeno P, Chanon S, Robert M, Bouzakri K, Modoux C, Roux-Lombard P, Vidal H, Lefai E and Dibner C. 2015. Human skeletal myotubes display a cell-autonomous circadian clock implicated in basal myokine secretion. *Molecular metabolism* **4**(11): 834-45 doi:10.1016/j.molmet.2015.07.009.

Petrenko V, Saini C, Perrin L and Dibner C. 2016. Parallel Measurement of Circadian Clock Gene Expression and Hormone Secretion in Human Primary Cell Cultures. *J Vis Exp*(117) doi:10.3791/54673.

Pulimeno P, Mannic T, Sage D, Giovannoni L, Salmon P, Lemeille S, Giry-Laterriere M, Unser M, Bosco D, Bauer C, Morf J, Halban P, Philippe J and Dibner C. 2012. Autonomous and self-sustained circadian oscillators displayed in human islet cells. *Diabetologia* doi:10.1007/s00125-012-2779-7 [doi].

Pullen N, Dennis PB, Andjelkovic M, Dufner A, Kozma SC, Hemmings BA and Thomas G. 1998. Phosphorylation and Activation of $p70^{s6k}$ by PDK1. *Science* **279**(5351): 707-10 doi:10.1126/science.279.5351.707.

Quinlan AR and Hall IM. 2010. BEDTools: a flexible suite of utilities for comparing genomic features. *Bioinformatics* **26**(6): 841-2 doi:10.1093/bioinformatics/btq033.

Ramm G, Larance M, Guilhaus M and James DE. 2006. A role for 14-3-3 in insulin-stimulated GLUT4 translocation through its interaction with the RabGAP AS160. *J Biol Chem* **281**(39): 29174-80 doi:M603274200 [pii]
10.1074/jbc.M603274200 [doi].

Ramsey KM, Yoshino J, Brace CS, Abrassart D, Kobayashi Y, Marcheva B, Hong HK, Chong JL, Buhr ED, Lee C, Takahashi JS, Imai S and Bass J. 2009. Circadian clock feedback cycle through NAMPT-mediated NAD+ biosynthesis. *Science* **324**(5927): 651-4 doi:1171641 [pii]
10.1126/science.1171641.

Roach WG, Chavez JA, Miinea CP and Lienhard GE. 2007. Substrate specificity and effect on GLUT4 translocation of the Rab GTPase-activating protein Tbc1d1. *Biochem J* **403**(2): 353-8 doi:10.1042/bj20061798.

Robinson MD, McCarthy DJ and Smyth GK. 2010. edgeR: a Bioconductor package for differential expression analysis of digital gene expression data. *Bioinformatics* **26**(1): 139-40 doi:10.1093/bioinformatics/btp616.

Robinson MD and Oshlack A. 2010. A scaling normalization method for differential expression analysis of RNA-seq data. *Genome biology* **11**(3): R25 doi:10.1186/gb-2010-11-3-r25.

Robinson MD and Smyth GK. 2008. Small-sample estimation of negative binomial dispersion, with applications to SAGE data. *Biostatistics (Oxford, England)* **9**(2): 321-32 doi:10.1093/biostatistics/kxm030.

Rose AJ, Jeppesen J, Kiens B and Richter EA. 2009. Effects of contraction on localization of GLUT4 and v-SNARE isoforms in rat skeletal muscle. *Am J Physiol Regul Integr Comp Physiol* **297**(5): R1228-37 doi:00258.2009 [pii]
10.1152/ajpregu.00258.2009 [doi].

Saini C, Brown SA and Dibner C. 2015. Human peripheral clocks: applications for studying circadian phenotypes in physiology and pathophysiology. *Front Neurol* **6**: 95 doi:10.3389/fneur.2015.00095.

Saini C, Petrenko V, Pulimeno P, Giovannoni L, Berney T, Hebrok M, Howald C, Dermitzakis ET and Dibner C. 2016. A functional circadian clock is required for proper insulin secretion by human pancreatic islet cells. *Diabetes Obes Metab* **18**(4): 355-65 doi:10.1111/dom.12616.

Sakamoto K and Holman GD. 2008. Emerging role for AS160/TBC1D4 and TBC1D1 in the regulation of GLUT4 traffic. *Am J Physiol Endocrinol Metab* **295**(1): E29-37 doi:90331.2008 [pii]

10.1152/ajpendo.90331.2008 [doi].

Schiaffino S, Blaauw B and Dyar KA. 2016. The functional significance of the skeletal muscle clock: lessons from Bmal1 knockout models. *Skelet Muscle* **6**: 33 doi:10.1186/s13395-016-0107-5.

Spoelstra K, Wikelski M, Daan S, Loudon AS and Hau M. 2016. Natural selection against a circadian clock gene mutation in mice. *Proceedings of the National Academy of Sciences of the United States of America* **113**(3): 686-91 doi:10.1073/pnas.1516442113.

Stenmark H, Parton RG, Steele-Mortimer O, Lütcke A, Gruenberg J and Zerial M. 1994. Inhibition of rab5 GTPase activity stimulates membrane fusion in endocytosis. *The EMBO Journal* **13**(6): 1287-96.

Szekeres F, Chadt A, Tom RZ, Deshmukh AS, Chibalin AV, Bjornholm M, Al-Hasani H and Zierath JR. 2012. The Rab-GTPase-activating protein TBC1D1 regulates skeletal muscle glucose metabolism. *Am J Physiol Endocrinol Metab* **303**(4): E524-33 doi:ajpendo.00605.2011 [pii]
10.1152/ajpendo.00605.2011 [doi].

Talbot J and Maves L. 2016. Skeletal muscle fiber type: using insights from muscle developmental biology to dissect targets for susceptibility and resistance to muscle disease. *Wiley interdisciplinary reviews. Developmental biology* **5**(4): 518-34 doi:10.1002/wdev.230.

Tan Z, Zhou LJ, Mu PW, Liu SP, Chen SJ, Fu XD and Wang TH. 2012. Caveolin-3 is involved in the protection of resveratrol against high-fat-diet-induced insulin resistance by promoting GLUT4 translocation to the plasma membrane in skeletal muscle of ovariectomized rats. *The Journal of nutritional biochemistry* **23**(12): 1716-24 doi:10.1016/j.jnutbio.2011.12.003.

Teng S, Stegner D, Chen Q, Hongu T, Hasegawa H, Chen L, Kanaho Y, Nieswandt B, Frohman MA and Huang P. 2015. Phospholipase D1 facilitates second-phase myoblast fusion and skeletal muscle regeneration. *Mol Biol Cell* **26**(3): 506-17 doi:10.1091/mbc.E14-03-0802.

Thomson DM and Winder WW. 2009. AMP-activated protein kinase control of fat metabolism in skeletal muscle. *Acta Physiol (Oxf)* **196**(1): 147-54 doi:10.1111/j.1748-1716.2009.01973.x.

Van Thienen R, D'Hulst G, Deldicque L and Hespel P. 2014. Biochemical artifacts in experiments involving repeated biopsies in the same muscle. *Physiol Rep* **2**(5): e00286 doi:10.14814/phy2.286.

Volchuk A, Sargeant R, Sumitani S, Liu Z, He L and Klip A. 1995. Cellubrevin is a resident protein of insulin-sensitive GLUT4 glucose transporter vesicles in 3T3-L1 adipocytes. *J Biol Chem* **270**(14): 8233-40.

Wehrens SMT, Christou S, Isherwood C, Middleton B, Gibbs MA, Archer SN, Skene DJ and Johnston JD. 2017. Meal Timing Regulates the Human Circadian System. *Curr Biol* **27**(12): 1768-75 e3 doi:10.1016/j.cub.2017.04.059.

Yoshitane H, Ozaki H, Terajima H, Du NH, Suzuki Y, Fujimori T, Kosaka N, Shimba S, Sugano S, Takagi T, Iwasaki W and Fukada Y. 2014. CLOCK-controlled polyphonic regulation of circadian rhythms through canonical and noncanonical E-boxes. *Mol Cell Biol* **34**(10): 1776-87 doi:10.1128/MCB.01465-13.

Zhang R, Lahens NF, Ballance HI, Hughes ME and Hogenesch JB. 2014. A circadian gene expression atlas in mammals: implications for biology and medicine. *Proceedings of the National Academy of Sciences of the United States of America* **111**(45): 16219-24 doi:10.1073/pnas.1408886111.

FIGURE LEGENDS

Figure 1. Rhythmic gene expression in human skeletal muscle

(A) Heat map showing genes rhythmic at the pre-mRNA and mRNA level (R-I.R-E: upper panel), at the pre-mRNA level only (R-I: middle panel), and at the mRNA level only (R-E: lower panel). Standardized relative gene expression is indicated in green (low) and red (high) and ordered by their respective phase. (B) mRNA half-life proxy by exon/intron ratio showing lower stability for genes with rhythmic mRNA (R-E) profiles. (C) Amplitude distribution of genes that are rhythmic only at the mRNA level (R-E, blue), the pre-mRNA level (R-I, red), or rhythmic for both (R-I.R-E). Genes with higher amplitude of transcription at the pre-mRNA level have a higher probability to be rhythmic at the mRNA level (R-I.R-E). (D) Number of genes in each group in relation to the $-\log_{10}$ BH corrected p-value; dashed line indicates threshold of 0.05. (E) Phase distribution at the pre-mRNA and mRNA level for the three groups described in (A). (F) Phase distribution for genes activated by acute muscle exercise (red), inflammation (blue), or both (green). (G) Temporal expression of core clock components, and (H) key muscle transcription factors. N=10 human muscle biopsy donors.

Figure 2. Disruption of the circadian oscillator impacts on functional gene expression hSKM

Differential gene expression analysis between hSKM bearing a disrupted (siCLOCK) or intact (siControl) circadian clock. Comparison of the median gene expression at all analysed circadian time points between the two groups. A total of 16’776 genes were detected by RNA-seq as expressed above the threshold of counts per million (CPM) >3. (A) Core clock genes; (B) A total of 15’446 genes remained unchanged (dark blue), and 1’330 genes exhibited significantly different expression levels upon siCLOCK-mediated clock disruption (light blue), with 588 being up-regulated (orange) and 742 down-regulated (grey) (FDR <0.05 and p-value <0.05). Altered genes comprised those related to glycerophospholipid and triglyceride metabolism, storage and transport (C) inositol phosphate metabolism (D) and sphingolipid

metabolism and storage (E). (F) Relative levels of PC, PE, PI, PS, Cer GlcCer, SM, CL and TAG, analyzed by mass spectrometry based lipidomics in hSKM cells transfected with either siControl (orange bar) or siCLOCK (blue bar). Total phosphatidylcholine (PC) and glycosylceramide (GlcCer) levels are significantly decreased or increased, respectively, upon siCLOCK transfection. Data are mean ± SEM, N=4 (# p-value <0.05). (*) for FDR <0.05, (**) for FDR <0.01, (***) for FDR <0.001.

Figure 3. Basal and insulin induced glucose uptake by hSKM is downregulated in the absence of a functional circadian clock

(A) *CLOCK* mRNA was measured in hSKM cells transfected with siControl or siCLOCK by RT-qPCR and normalized to the mean of *9S* and *HPRT*. *CLOCK* expression was reduced by 91 ± 2% (mean ± SEM, N=4; (***) p-value <0.001) in siCLOCK-transfected cells. Protein levels of CLOCK (B) and 14-3-3θ (C) were assessed by western blot. Left panel: representative western blot; right panel protein quantification over all monoplicates (mean ± SEM, N=5). CLOCK and 14-3-3θ protein levels were reduced by 75 ± 2%, and 28 ± 8%, respectively.

(D) Glucose uptake rates (in pmol/mg.min) measured in the absence (basal) or presence (insulin) of insulin (1 h, 100 nM) in siControl or siCLOCK transfected cells. Note significant reduction of basal (31 ± 3%) and insulin-stimulated glucose uptake (28 ± 3%). Data are mean ± SEM of four independent experiments using myotubes from four different donors (same as for A-C). (*) p-value <0.05, (**) p-value <0.01, (***) p-value <0.001.

Figure 4. Temporal gene expression analysis in human skeletal myotubes bearing a disrupted or functional circadian clock

(A) Total of 12’985 genes were identified by RNA-seq as expressed above $\log_2$ RPKM>0. Genes were subjected to the circadian analysis, adapted for high-resolution datasets over 48 h. 994 genes were categorized as rhythmic or non-rhythmic (NR) (left diagram) and grouped into 15 models (right panel). Genes that were not rhythmic in either one of the 15 models (11'991 genes) are represented in model 16.

(B) Heat maps for genes assigned to models 1 to 4. Relative expression is indicated in green (low) and red (high). (C) Individual temporal expression profiles of core clock genes *ARNTL*, *NR1D1*, *NR1D2*, *CRY1*, *CRY2*, *PER1*, *PER2* and *PER3* in siControl or siCLOCK transfected cells. (D) Upper panel: Representative examples for genes assigned to models 1-4. Lower panel: Circadian amplitude quantification of siControl and siCLOCK in models 1-4.

Figure 5. Comparison between the circadian transcriptome of human skeletal muscle and human primary myotubes

(A) Scatter plot, representing the amplitude of expression in relation to the corrected p-value for genes that were rhythmic *in vivo* (human muscle biopsies). Genes that were also rhythmic *in vitro* (hSKM, models 1-4) are coloured in red. Blue dots represent genes with a p-value <0.01 and $\log_2$ amp >0.5. (B) Phase distribution plot of genes rhythmic in muscle biopsies and primary myotubes shows enrichment at the 04:00 time point. (C) Examples of genes, involved in glucose homeostasis and muscle regeneration, that are rhythmic *in vivo* and *in vitro* (RNA-seq data, N=10).

Figure 6. Schema summarizing impact of clock disruption on muscle metabolic function

Clock disruption leads to impaired insulin sensitivity and decrease in glucose uptake (1), causes a dysregulation of genes involved in vesicle trafficking (2) and impacts lipid metabolism and lipid metabolite oscillations (3) as reported in (Loizides-Mangold et al. 2017).

Figure 1

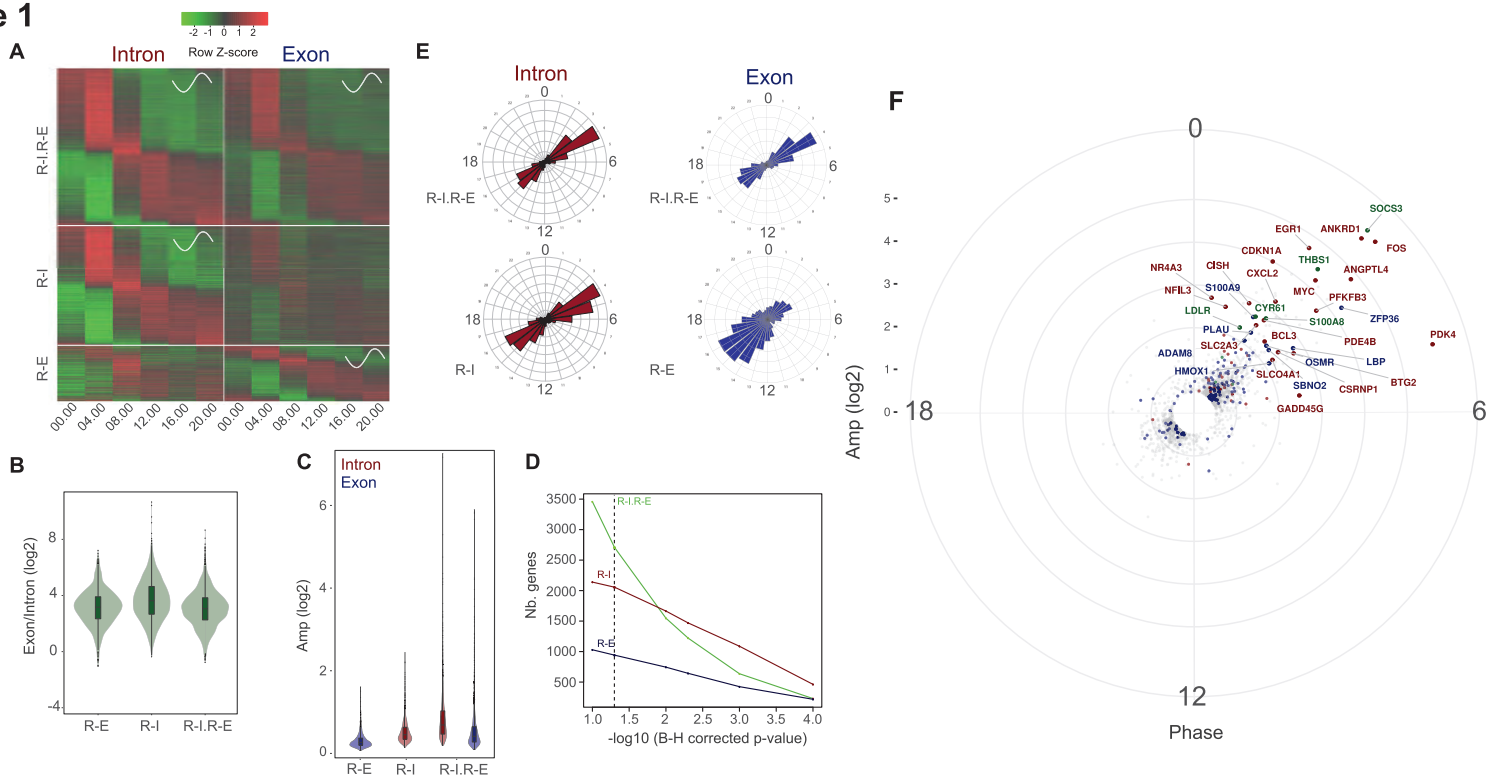
A
Intron
Exon
Row Z-score
-2 -1 0 1 2
R-I.R-E
R-I
R-E
00.00 04.00 08.00 12.00 16.00 20.00
E
Intron
Exon
R-I.R-E
R-I
R-E
F
Amp (log2)
Phase
SOCS3
EGR1
ANKRD1
FOS
CDKN1A
THBS1
NR4A3
CISH
CXCL2
ANGPTL4
NFIL3
S100A9
MYC
PFKFB3
LDLR
CYR61
S100A8
ZFP36
PLAU
BCL3
PDK4
SLC2A3
PDE4B
ADAM8
OSMR
LBP
HMOX1
SLCO4A1
BTG2
SBNO2
CSRNP1
GADD45G
B
Exon/Intron (log2)
R-E R-I R-I.R-E
C
Intron
Exon
Amp (log2)
R-E R-I R-I.R-E
D
Nb. genes
R-I.R-E
R-I
R-E
-log10 (B-H corrected p-value)

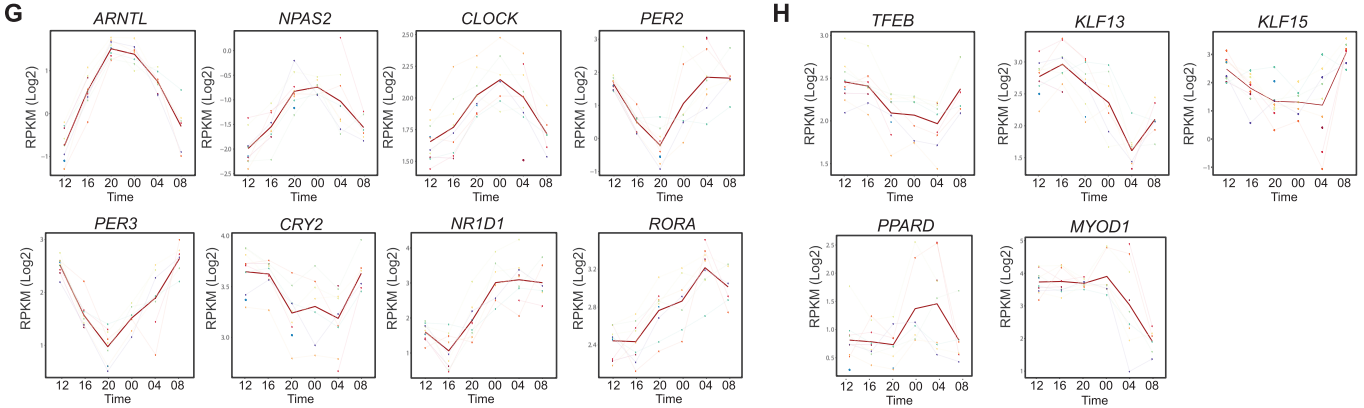
G
ARNTL
NPAS2
CLOCK
PER2
PER3
CRY2
NR1D1
RORA
RPKM (Log2)
Time
12 16 20 00 04 08

H
TFEB
KLF13
KLF15
PPARD
MYOD1
RPKM (Log2)
Time
12 16 20 00 04 08

Figure 2

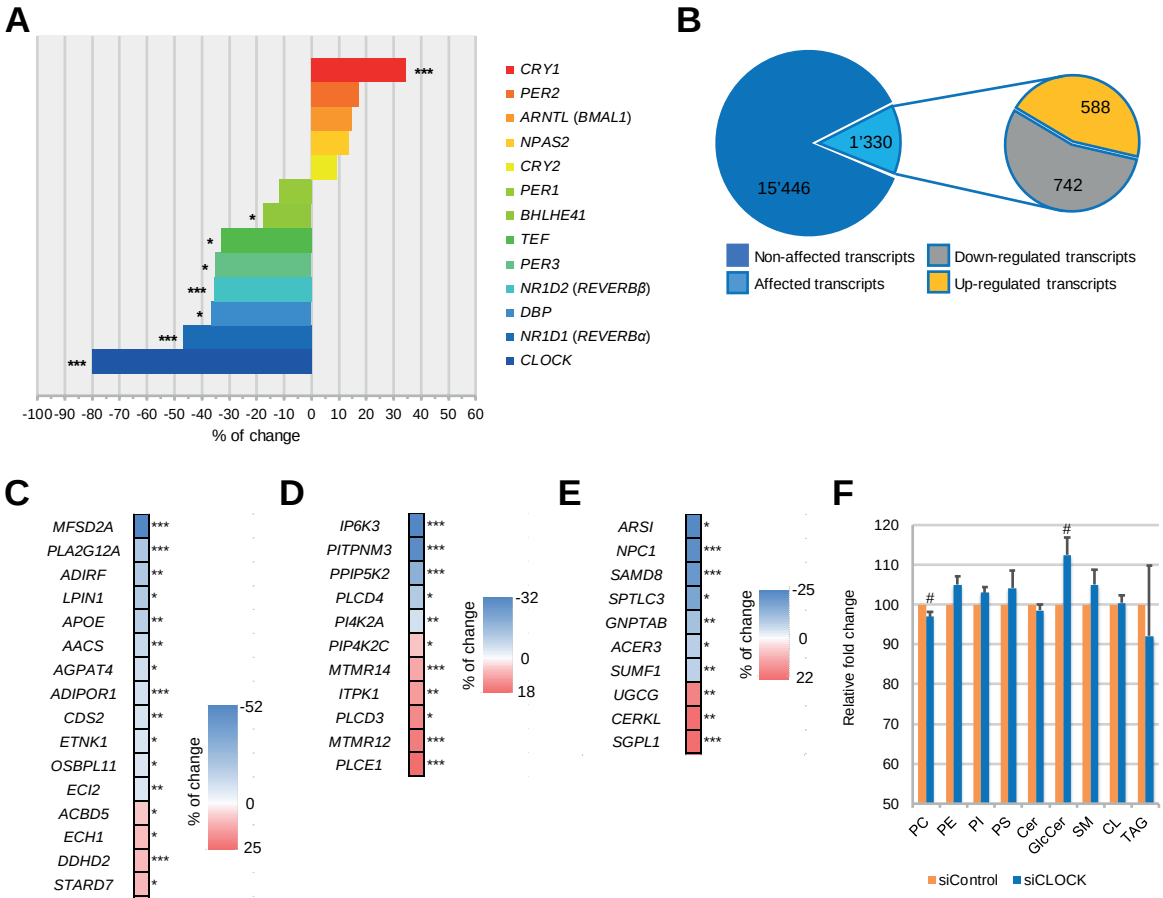
A
CRY1
PER2
ARNTL (BMAL1)
NPAS2
CRY2
PER1
BHLHE41
TEF
PER3
NR1D2 (REVERBβ)
DBP
NR1D1 (REVERBα)
CLOCK
% of change
B
15'446
1'330
588
742
Non-affected transcripts
Affected transcripts
Down-regulated transcripts
Up-regulated transcripts
C
MFSD2A
PLA2G12A
ADIRF
LPIN1
APOE
AACS
AGPAT4
ADIPOR1
CDS2
ETNK1
OSBPL11
ECI2
ACBD5
ECH1
DDHD2
STARD7
LRP4
OSBPL10
FABP3
PLD6
CD36
BAAT
% of change
D
IP6K3
PITPNM3
PPIP5K2
PLCD4
PI4K2A
PIP4K2C
MTMR14
ITPK1
PLCD3
MTMR12
PLCE1
% of change
E
ARSI
NPC1
SAMD8
SPTLC3
GNPTAB
ACER3
SUMF1
UGCG
CERKL
SGPL1
% of change
F
Relative fold change
PC
PE
PI
PS
Cer
GlcCer
SM
CL
TAG
siControl
siCLOCK

Figure 3

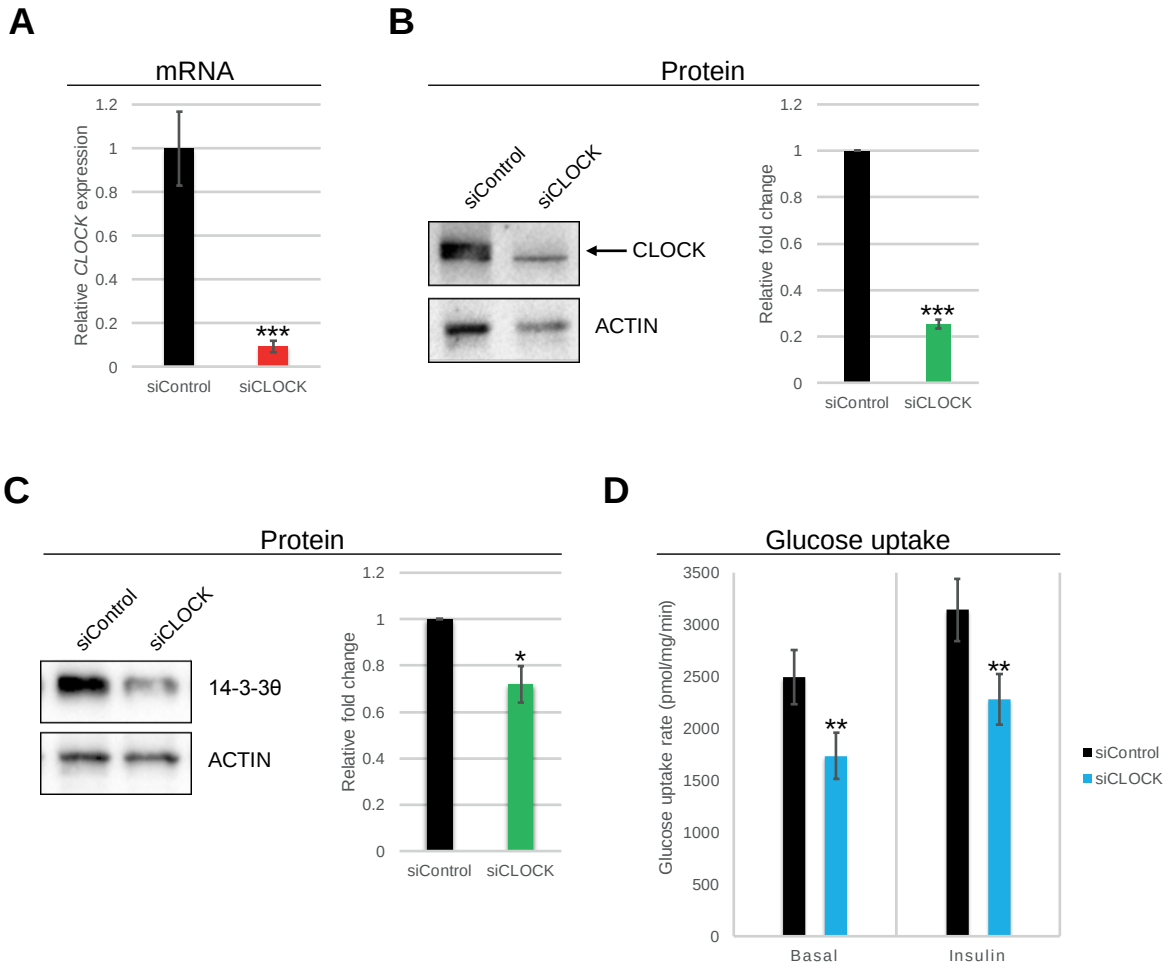
A
mRNA
Relative CLOCK expression
1.2
1
0.8
0.6
0.4
0.2
0
***
siControl
siCLOCK
B
Protein
siControl
siCLOCK
CLOCK
ACTIN
Relative fold change
1.2
1
0.8
0.6
0.4
0.2
0
***
siControl
siCLOCK
C
Protein
siControl
siCLOCK
14-3-3θ
ACTIN
Relative fold change
1.2
1
0.8
0.6
0.4
0.2
0
*
siControl
siCLOCK
D
Glucose uptake
Glucose uptake rate (pmol/mg/min)
3500
3000
2500
2000
1500
1000
500
0
**
**
Basal
Insulin
siControl
siCLOCK

Figure 4

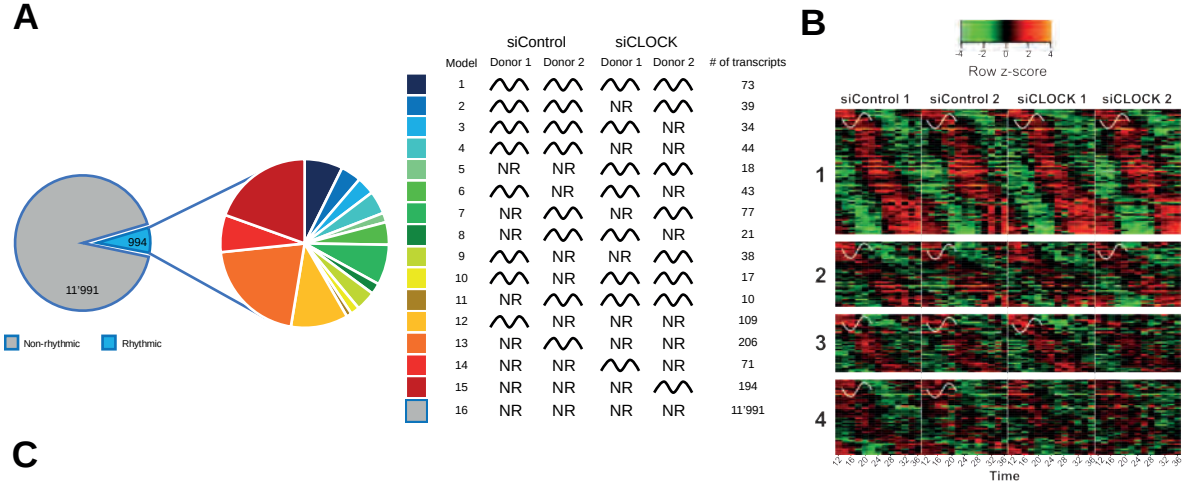
A
siControl
siCLOCK
Model
Donor 1
Donor 2
Donor 1
Donor 2
# of transcripts
1 73
2 39
3 34
4 44
5 18
6 43
7 77
8 21
9 38
10 17
11 10
12 109
13 206
14 71
15 194
16 11'991
994
11'991
Non-rhythmic
Rhythmic
B
Row z-score
siControl 1
siControl 2
siCLOCK 1
siCLOCK 2
1
2
3
4
Time

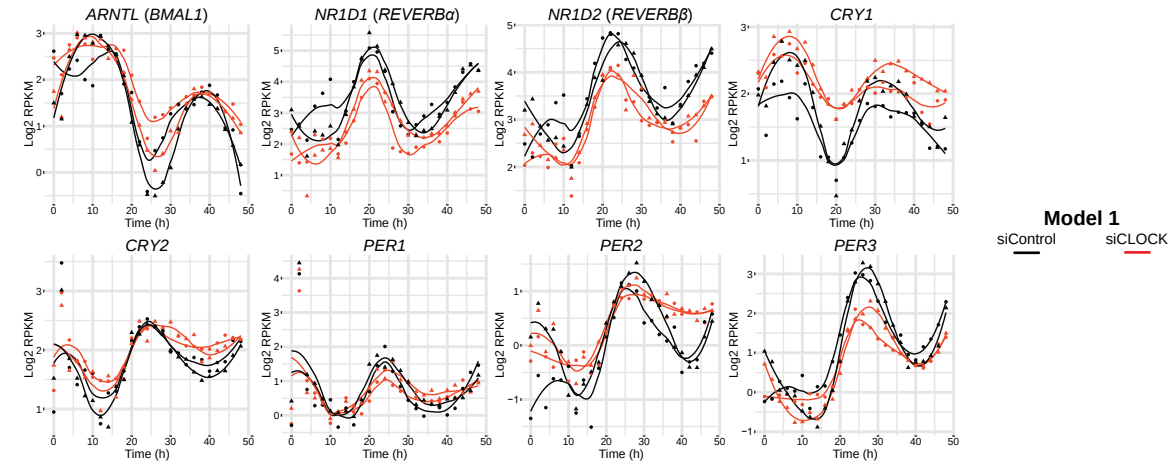
C
ARNTL (BMAL1)
NR1D1 (REVERBα)
NR1D2 (REVERBβ)
CRY1
CRY2
PER1
PER2
PER3
Log2 RPKM
Time (h)
Model 1
siControl
siCLOCK

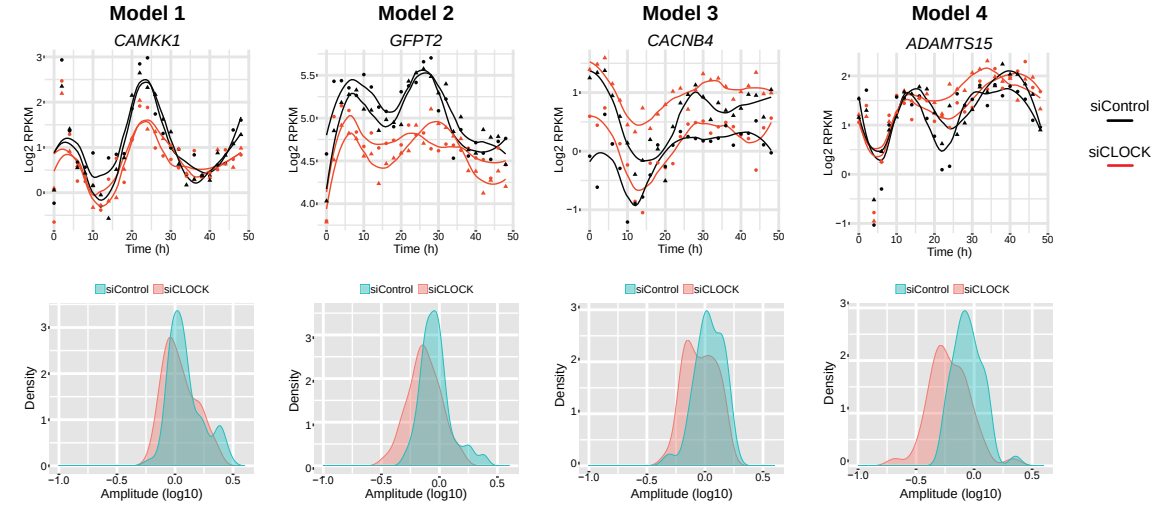
D
Model 1
Model 2
Model 3
Model 4
CAMKK1
GFPT2
CACNB4
ADAMTS15
Log2 RPKM
Time (h)
siControl
siCLOCK
Density
Amplitude (log10)

Figure 5

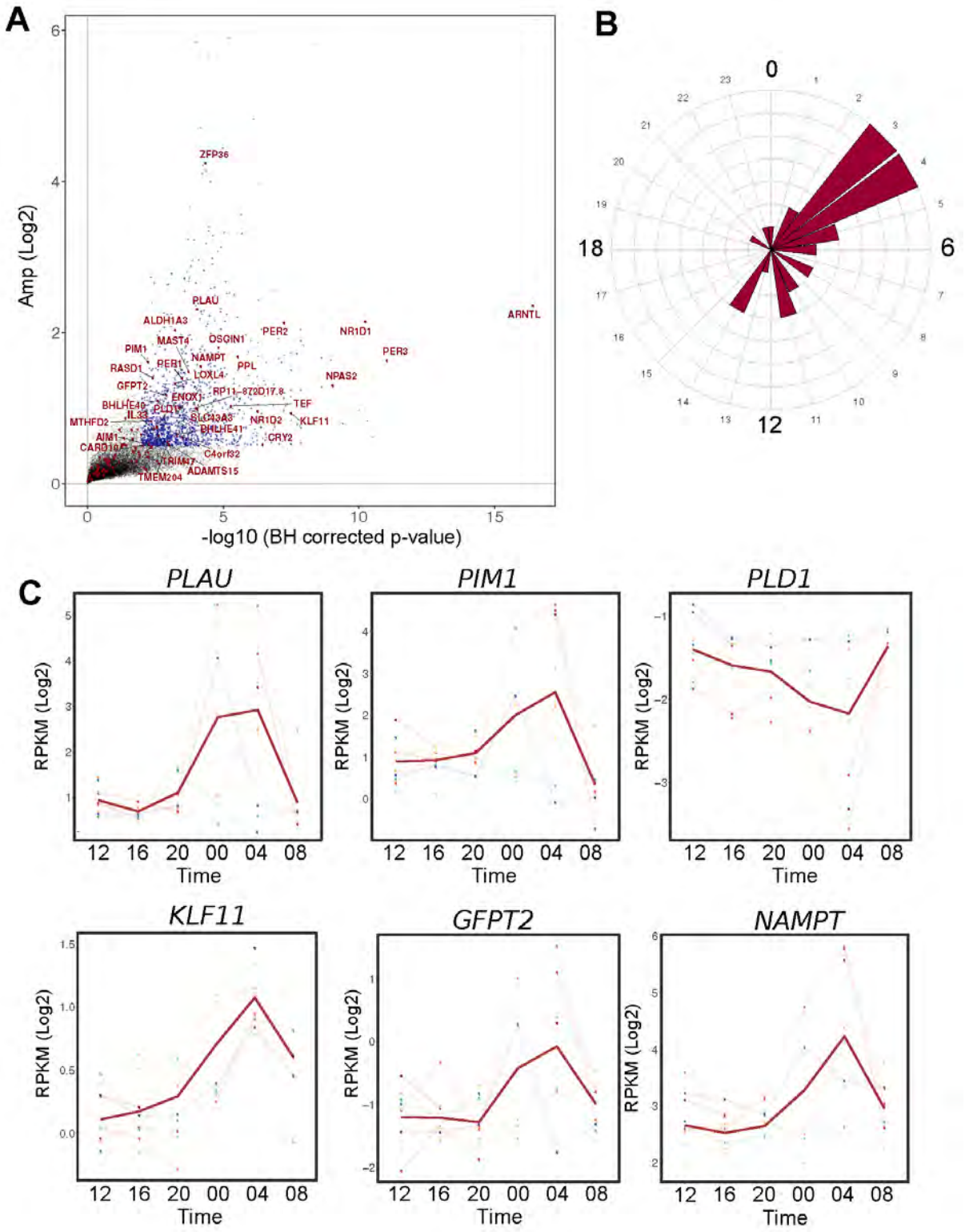
A
Amp (Log2)
-log10 (BH corrected p-value)
ZFP36
PLAU
ALDH1A3
MAST4
OSGIN1
PER2
NR1D1
ARNTL
PER3
PIM1
RASD1
PER1
NAMPT
PPL
NPAS2
LOXL4
GFPT2
ENOX1
RP11-872D17.8
BHLHE40
PLD1
TEF
IL33
MTHFD2
SLC43A3
NR1D2
KLF11
BHLHE41
AIM1
CRY2
CARD10
C4orf32
TRIM47
ADAMTS15
TMEM204
B
0
6
12
18
C
PLAU
PIM1
PLD1
KLF11
GFPT2
NAMPT
RPKM (Log2)
Time
12 16 20 00 04 08

Figure 6

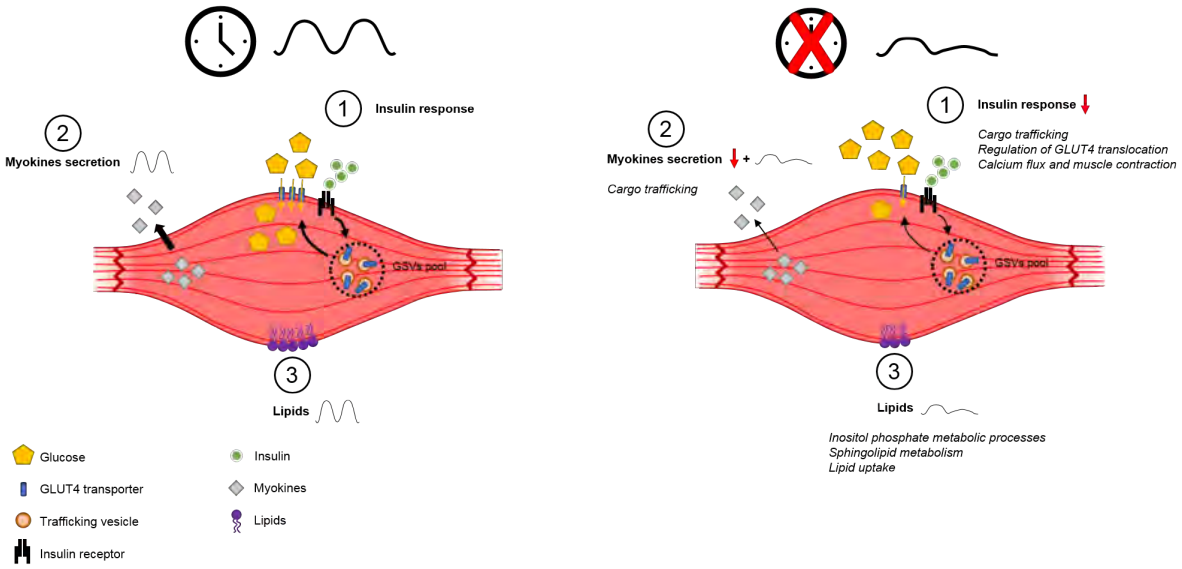
1
Insulin response
2
Myokines secretion
GSVs pool
3
Lipids
Glucose
GLUT4 transporter
Trafficking vesicle
Insulin receptor
Insulin
Myokines
Lipids
1
Insulin response
Cargo trafficking
Regulation of GLUT4 translocation
Calcium flux and muscle contraction
2
Myokines secretion
+
Cargo trafficking
GSVs pool
3
Lipids
Inositol phosphate metabolic processes
Sphingolipid metabolism
Lipid uptake

Supplementary data to:

Transcriptomic analyses reveal rhythmic and CLOCK-driven pathways in human skeletal muscle

Laurent Perrin [1,2,3,4], Ursula Loizides-Mangold [1,2,3,4,†], Stéphanie Chanon [5,†], Cédric Gobet [6,7,†], Nicolas Hulo [4,8], Laura Isenegger [8], Benjamin D. Weger [6], Eugenia Migliavacca [6], Aline Charpagne [6], James A. Betts [9], Jean-Philippe Walhin [9], Iain Templeman [9], Keith Stokes [9], Dylan Thompson [9], Kostas Tsintzas [10], Maud Robert [11], Cédric Howald [4,12], Howard Riezman [13], Jerome N Feige [6,7], Leonidas G. Karagounis [14,15], Jonathan D. Johnston [16], Emmanouil Dermitzakis [4,12], Frédéric Gachon [6,7,ç], Etienne Lefai [5,ç], Charna Dibner [1,2,3,4,*]

[1]Division of Endocrinology, Diabetes, Hypertension and Nutrition, Department of Internal Medicine Specialties, University Hospital of Geneva, Geneva, Switzerland;

[2]Department of Cell Physiology and Metabolism, Faculty of Medicine, University of Geneva;

[3]Diabetes Center, Faculty of Medicine, University of Geneva;

[4]Institute of Genetics and Genomics in Geneva (iGE3), Geneva, Switzerland;

[5]CarMeN Laboratory, INSERM U1060, INRA 1397, University Lyon 1, Oullins, France;

[6]Nestlé Institute of Health Sciences, Lausanne, Switzerland;

[7]School of Life Sciences, Ecole Polytechnique Fédérale de Lausanne, Lausanne, Switzerland;

[8]Service for Biomathematical and Biostatistical Analyses; Section of Biology, University of Geneva, Geneva, Switzerland;

[9]Department for Health, University of Bath, Bath, United Kingdom;

[10]MRC/ARUK Centre for Musculoskeletal Ageing, School of Life Sciences, University of Nottingham, NG7 2UH, United Kingdom;

[11]Department of Digestive and Bariatric Surgery, Edouard Herriot University Hospital, Lyon 1 University, France;

[12]Department of Genetic Medicine and Development, Faculty of Medicine, University of Geneva, Geneva, Switzerland;

[13]Department of Biochemistry, NCCR Chemical Biology, University of Geneva, Geneva, Switzerland;

[14]Experimental Myology and Integrative Biology Research Cluster, Faculty of Sport and Health Sciences, University of St Mark and St John, Plymouth, United Kingdom;

[15]Institute of Nutritional Science, Nestlé Research Centre, Lausanne, Switzerland;

[16]Faculty of Health and Medical Sciences, University of Surrey, Guildford, United Kingdom.

[†]These authors contributed equally to this work

[ç]These authors contributed equally to this work

***CORRESPONDING AUTHOR**

Charna Dibner

Faculty of Medicine, University of Geneva

D05.2147c Rue Michel-Servet, 1

CH-1211 Geneva 4, Switzerland

Phone: +41 22 3795934

SUPPLEMENTARY TABLES

Table S1. Characteristics of donors for skeletal muscle biopsies

Donor n°	Sex	Age (years)	BMI (kg/m2)	Muscle	Used for	
I	M	22	28.3	*Vastus lateralis*	RNA-seq	*In vivo*
II	F	37	28.3	*Vastus lateralis*		
III	M	27	20.4	*Vastus lateralis*		
IV	M	33	23.6	*Vastus lateralis*		
V	M	54	25.6	*Vastus lateralis*		
VI	M	24	24.6	*Vastus lateralis*		
VII	M	25	23.8	*Vastus lateralis*		
VIII	M	30	20.3	*Vastus lateralis*		
IX	M	22	23.2	*Vastus lateralis*		
X	M	25	23.4	*Vastus lateralis*		
Mean	M=9, F=1	30 ± 10	24.1 ± 2.7			
1	M	62	24.3	*Gluteus maximus*	RNA-seq	*In vitro*
2	M	60	24	*Gluteus maximus*		
Mean	M=2	61 ± 1	24.15 ± 0.21			
3	F	66	24	*Gluteus maximus*	Glucose uptake & Western blot	*In vitro*
4	F	65	22	*Gluteus maximus*		
5	M	70	30.1	*Gluteus maximus*		
6	M	72	26.5	*Gluteus maximus*		
7	F	77	25.6	*Gluteus maximus*		
Mean	M=2, F=3	70 ± 4	25.64 ± 3.02			
7	F	77	25.6	*Gluteus maximus*	Lipidomics	*In vitro*
8	M	57	26.3	*Gluteus maximus*		
9	F	65	22.77	*Gluteus maximus*		
10	F	53	22.41	*Gluteus maximus*		
Mean	M=1, F=3	63 ± 10	24.27 ± 1.97			

M, male; F, female.
Donors I-X, data are mean ± SD, N=10.
Donors 1-2, data are mean ± SD, N=2.
Donors 3-7, data are mean ± SD, N=5.
Donors 7-10, data are mean ± SD, N=4.

Table S2. Selected genes involved in cargo trafficking and GLUT4 regulation that have altered expression upon siCLOCK

Function	Name	% of change	p-value	FDR
Cargo trafficking	*ARFGAP2*	8.60	9.73E-06	4.11E-04
	CAMSAP2	-8.30	1.52E-04	4.03E-03
	EPN2	-10.05	3.49E-04	7.98E-03
	FNBP1 (*FNBP17*)	-10.20	7.18E-04	1.42E-02
	GBF1	-7.85	3.15E-04	7.35E-03
	HIP1	11.55	2.41E-04	5.96E-03
	KIF13A	-23.56	1.22E-27	1.14E-24
	PACSIN3	18.17	7.65E-07	4.47E-05
	PAFAH1B1 (*LYS1*)	-6.31	3.82E-04	8.58E-03
	STX6	-13.17	1.71E-10	2.24E-08
	SYT1	21.45	1.20E-03	2.11E-02
	VAMP3	-26.89	1.38E-27	1.22E-24
	VAMP4	-16.92	2.17E-09	2.22E-07
	VAMP8	15.77	1.21E-03	2.12E-02
	VPS36 (*VSP36*)	-15.48	9.14E-11	1.28E-08
Regulation of GLUT4 translocation	*14-3-3θ* (*YWHAQ*)	-14.70	1.70E-07	1.22E-05
	CALM1 [1+3]	-14.20	3.72E-06	1.80E-04
	CAV3 [1]	18.72	6.26E-10	7.35E-08
	EXOC3L4	-22.87	3.54E-04	8.08E-03
	MAPKAP1 (*mSIN1*)	8.90	3.07E-08	2.53E-06
	MEF2A	-28.09	3.25E-13	7.00E-11
	NAPB	-9.99	1.17E-04	3.24E-03
	NAPG	10.01	2.70E-03	3.81E-02
	NSF	13.26	1.94E-08	1.67E-06
	PDPK1 (*PDK1*)	-9.01	3.81E-08	3.10E-06
	RAB11FIP4	-17.90	6.95E-05	2.13E-03
	RAB35	-22.93	3.63E-23	2.18E-20
	RAB5B	6.46	1.33E-04	3.63E-03
	RALGAPA2 (*RGC2*)	-14.26	2.29E-04	5.72E-03
	TBC1D4 (*AS160*)	-8.38	1.99E-03	3.05E-02
	TBC1D13	-5.94	1.78E-03	2.82E-02
	TBC1D16	-14.91	3.80E-05	1.29E-03
	TPM3 [1]	10.01	1.29E-03	2.23E-02
	VPS45 (*VSP45*)	-7.26	1.41E-04	3.81E-03

Bold: gene classified as circadian (models 1 to 4).
Underscore: genes also found in regulation of GLUT4 translocation.
[n]: number corresponding to the functional group listed in Table S7.
*: gene with a FDR>0.05.

Table S3. Selected genes involved in secretion that have altered mRNA expression upon siCLOCK

Name	% of change	p-value	FDR
ABCB6	-13.21	1.37E-06	7.37E-05
ABCC5	-16.48	1.32E-05	5.29E-04
ATP1B4	8.85	9.91E-04	1.84E-02
ATP5G2	-32.87	1.99E-42	4.17E-39
ATP5G2P4	-37.85	9.18E-11	1.28E-08
ATP7B	28.54	1.98E-12	3.74E-10
CACNA1E	28.83	7.57E-11	1.09E-08
DNAH10OS	17.35	3.08E-03	4.18E-02
DYNLL2	9.72	4.32E-05	1.45E-03
ESYT2	-9.91	7.04E-05	2.15E-03
KCNB1	27.57	6.79E-15	1.93E-12
KIF1A	17.72	2.94E-03	4.05E-02
PCSK1	-18.24	3.54E-03	4.62E-02
RAB11FIP1	19.46	2.53E-04	6.20E-03
RAB15	23.31	1.57E-06	8.39E-05
RABGAP1	-10.20	2.06E-06	1.07E-04
SEC61A1	-15.71	3.08E-07	2.02E-05
SLC1A3	-16.10	1.97E-04	5.05E-03
SLC22A17	-13.13	8.05E-06	3.45E-04
SLC22A31	-29.20	4.80E-07	3.02E-05
SLC24A2	-12.60	5.19E-04	1.10E-02
SLC25A12	-8.48	5.97E-04	1.23E-02
SLC25A3	4.83	3.42E-03	4.50E-02
SLC25A44	-18.83	3.00E-09	2.96E-07
SLC26A7	36.77	3.84E-04	8.60E-03
SLC28A3	24.73	1.37E-03	2.35E-02
SLC2A3P1	11.18	4.86E-05	1.60E-03
SLC30A6	-17.80	1.74E-09	1.82E-07
SLC39A14	-8.51	1.77E-03	2.80E-02
SLC46A1	-11.64	1.49E-03	2.48E-02
SLC47A2	-24.49	3.40E-03	4.48E-02
SLC4A4	-11.39	3.81E-03	4.87E-02
SLC6A6	12.05	1.11E-03	1.99E-02
SLC7A7	11.21	1.62E-03	2.63E-02
SLC7A8	-22.71	1.76E-03	2.80E-02
SLC9A6	-12.59	1.23E-09	1.35E-07
SLC9B2	-10.72	1.53E-05	5.91E-04
SLCO5A1	-25.08	2.85E-13	6.30E-11
SYT6	-28.27	6.20E-07	3.73E-05
TBC1D12	10.80	2.44E-03	3.53E-02
TBC1D19	-8.62	2.99E-03	4.09E-02

Table S4. Enrichment of biological processes based on gene ontology (GO) term analysis

Category	PANTHER GO-Slim Biological Process	Fold enrichment	p-value
Downregulated	transcription, DNA-dependent (GO:0006351)	2.48	3.07E-05
Downregulated	⌞ RNA metabolic process (GO:0016070)	2.03	7.60E-06
Downregulated	⌞ nucleobase-containing compound metabolic process (GO:0006139)	1.46	8.72E-04
Downregulated	⌞ primary metabolic process (GO:0044238)	1.31	7.33E-04
Downregulated	⌞ **metabolic process (GO:0008152)**	1.26	4.09E-03
Downregulated	**regulation of nucleobase-containing compound metabolic process (GO:0019219)**	1.83	2.85E-05
Downregulated	**biosynthetic process (GO:0009058)**	1.7	4.51E-04
Downregulated	**nitrogen compound metabolic process (GO:0006807)**	1.61	1.90E-04
Downregulated	**cellular process (GO:0009987)**	1.21	8.15E-03
Upregulated	**muscle contraction (GO:0006936)**	4.97	5.06E-06
Down- & upregulated	**transcription, DNA-dependent (GO:0006351)**	1.76	1.61E-02
Down- & upregulated	**regulation of nucleobase-containing compound metabolic process (GO:0019219)**	1.47	5.41E-03
Down- & upregulated	**cellular process (GO:0009987)**	1.18	3.22E-04
Model 1	chromosome segregation (GO:0007059)	14.43	6.60E-03
Model 1	⌞ **cellular process (GO:0009987)**	1.79	2.38E-04
Model 1	**DNA metabolic process (GO:0006259)**	5.97	4.21E-02
Model 1	**cell cycle (GO:0007049)**	5.05	1.29E-04

Bold: main GO terms listed in Supplemental Datasets 4 and 8.

Table S5. Reactome pathway enrichment analysis

Category	Reactome pathways	Fold enrichment	p-value
Downregulated	Generic Transcription Pathway (R-HSA-212436)	2.91	6.19E-13
Downregulated	⌞**Gene Expression (R-HSA-74160)**	2.09	4.42E-10
Downregulated	Smooth Muscle Contraction (R-HSA-445355)	8.75	3.56E-02
Upregulated	⌞**Muscle contraction (R-HSA-397014)**	3.78	2.23E-03
Down- & upregulated	Generic Transcription Pathway (R-HSA-212436)	2.1	1.90E-08
Down- & upregulated	⌞**Gene Expression (R-HSA-74160)**	1.57	8.26E-05
Down- & upregulated	**Cellular responses to stress (R-HSA-2262752)**	2.1	2.28E-02
Down- & upregulated	**Membrane Trafficking (R-HSA-199991)**	1.83	4.80E-02
Model 1	Phosphorylation of Emi1 (R-HSA-176417)	> 100	9.48E-06
Model 1	⌞APC/C-mediated degradation of cell cycle proteins (R-HSA-174143)	17.96	1.72E-02
Model 1	⌞Regulation of mitotic cell cycle (R-HSA-453276)	17.96	1.72E-02
Model 1	⌞Cell Cycle, Mitotic (R-HSA-69278)	11.32	1.94E-10
Model 1	⌞**Cell Cycle (R-HSA-1640170)**	9.24	4.74E-09
Model 1	Activation of NIMA Kinases NEK9, NEK6, NEK7 (R-HSA-2980767)	> 100	3.24E-03
Model 1	⌞**M Phase (R-HSA-68886)**	10.14	4.78E-04
Model 1	BMAL1:CLOCK,NPAS2 activates circadian gene expression (R-HSA-1368108)	73.54	4.75E-13
Model 1	⌞**Circadian Clock (R-HSA-400253)**	49.81	2.22E-11
Model 1	**Golgi Cisternae Pericentriolar Stack Reorganization (R-HSA-162658)**	71.27	2.05E-02
Model 1	TP53 Regulates Transcription of Genes Involved in G2 Cell Cycle Arrest (R-HSA-6804114)	68.63	7.46E-04
Model 1	⌞**TP53 Regulates Transcription of Cell Cycle Genes (R-HSA-6791312)**	32.17	1.02E-03
Model 1	Polo-like kinase mediated events (R-HSA-156711)	57.91	3.79E-02
Model 1	⌞G2/M Transition (R-HSA-69275)	11.75	4.27E-03
Model 1	⌞**Mitotic G2-G2/M phases (R-HSA-453274)**	11.62	4.58E-03
Model 1	G0 and Early G1 (R-HSA-1538133)	49.42	2.73E-03
Model 1	⌞**Mitotic G1-G1/S phases (R-HSA-453279)**	17.78	3.39E-05
Model 1	Activation of the pre-replicative complex (R-HSA-68962)	38.61	7.20E-03
Model 1	⌞**G1/S Transition (R-HSA-69206)**	16.11	3.91E-03
Model 1	Activation of ATR in response to replication stress (R-HSA-176187)	33.39	1.27E-02
Model 1	⌞G2/M Checkpoints (R-HSA-69481)	12.44	1.70E-02
Model 1	⌞**Cell Cycle Checkpoints (R-HSA-69620)**	11.94	3.83E-03
Model 1	Resolution of Sister Chromatid Cohesion (R-HSA-2500257)	21.87	6.91E-06
Model 1	⌞**Mitotic Prometaphase (R-HSA-68877)**	20.42	1.17E-05
Model 1	RHO GTPases Activate Formins (R-HSA-5663220)	14.71	6.58E-03
Model 1	⌞**RHO GTPase Effectors (R-HSA-195258)**	8.28	4.06E-02
Model 1	**Separation of Sister Chromatids (R-HSA-2467813)**	10.47	4.45E-02

Bold: main pathways listed in Supplemental Datasets 3 and 7.

Table S6. Effect of siCLOCK on the amplitude of selected circadian genes from models 1-4

Name	siControl[a]	siCLOCK[a]	Amplitude	p-value[b]	Significance	Model
ALDH1A3	-0.018	-0.175	Reduced	4.26E-02	*	1
CAMKK1	0.370	0.229	Reduced	1.35E-02	*	
CRY1	0.092	-0.069	Reduced	1.41E-02	*	
KIF2C	**-0.053**	**0.058**	**Increased**	**1.54E-03**	**	
LPPR4	0.055	-0.106	Reduced	3.87E-02	*	
PER1	0.267	0.072	Reduced	3.55E-02	*	
PER2	0.211	-0.005	Reduced	3.48E-02	*	
PER3	0.398	0.211	Reduced	9.75E-03	**	
SERPINE1	0.079	-0.045	Reduced	4.89E-03	**	
TEF	0.414	0.293	Reduced	4.62E-02	*	
TLR3	-0.022	-0.055	Reduced	2.88E-02	*	
BHLHE40	-0.115	-0.280	Reduced	2.64E-02	*	2
LINC00857	-0.066	-0.273	Reduced	2.54E-02	*	
NPR3	**-0.216**	**-0.144**	**Increased**	**1.59E-03**	**	
H2AFX	**-0.309**	**-0.191**	**Increased**	**3.63E-03**	**	3
NUDT6	0.127	0.068	Reduced	4.32E-02	*	
RMI1	-0.022	-0.102	Reduced	7.60E-04	***	
EFNA5	0.053	-0.258	Reduced	4.87E-02	*	4
FOXC1	-0.097	-0.283	Reduced	3.23E-03	**	
PDGFC	-0.126	-0.284	Reduced	6.72E-03	**	
RP11-61A14.2	0.076	-0.135	Reduced	1.17E-02	*	
ZFP36	-0.234	-0.464	Reduced	2.64E-02	*	

[a]: Data represent the mean amplitude (in $\log_{10}$) of the two cell lines per condition.
[b]: Paired T-test, N=2 per condition, p-value (*)<0.05, (**)<0.01, (***)<0.001.

Table S7. Selected genes with modified expression involved in muscle function, metabolism, cell cycle and apoptosis

Function	Name	% of change
1. Calcium flux and muscle contraction	*ATP1B1*	-13.99
	ATP2A1 (*SERCA1*) [3]	-32.55
	CACNA2D1	7.02
	CACNG1	12.17
	CALD1	10.63
	CAMK2A	-13.57
	CAMK2G	-11.04
	CASQ2 [2]	11.71
	KAT2B	-33.67
	KCND3	26.98
	KCNE1L (*KCNE5*)	27.34
	MYH3 [2]	22.78
	MYL12A	15.68
	MYL2 [2]	33.51
	MYL3 [2]	51.93
	MYL9	14.07
	MYLK	22.36
	MYLPF [3]	11.45
	PVALB	23.06
	SCN1B	-14.84
	SCN5A	12.51
	SLC8A3	-22.17
	SRL	16.75
	TNNC1 [2]	21.46
	TNNC2 [3]	10.96
	TNNI1 [2]	10.40
	VCL [3]	-12.71
2. Slow twitch gene expression	*CSRP2*	24.53
	CSRP3	37.59
	FHL1	13.04
	MYOZ2	23.32
	XIRP1	20.97
3. Fast twitch gene expression	*FHL3*	-11.04
	MYH2	12.40
	MYOG	21.04
	PBX2	-9.41
	PDLIM1	10.51
4. Muscle energy provision	*CKM*	13.97
	EGLN1 [5]	-10.82
	*FABP3**	17.08
	GYS1	-10.74
	PYGL	11.59
5. HIF1α signaling	*VEGFA*	-18.04
	VHL	-13.82
6. Metabolic gene expression	*ACOT12*	68.74
	*AGPAT4**	-10.67
	AKT3	-8.20
	*CD36**	25.20
	COX6A2	10.14
	NDUFA7	-34.98
	NDUFS2	6.40
	PGM5	24.34
	PHKA1	-11.92

	PRKAG2	12.96
	PRKAG3	-13.85
	SDHC	5.95
	UQCR11	-10.62
7. Protein glycosylation	*AGER*	-19.43
	BCAN	39.64
	C1GALT1	-16.91
	CD34	38.98
	DPAGT1	-8.37
	DPH3	9.37
	EXTL3	8.89
	FAM20B	8.26
	GALNT12	-9.70
	GALNT15	-33.29
	GALNT7	-24.63
	GFPT2	**-26.59**
	*GNPTAB**	-11.12
	GPC1	-29.71
	IMPG2	16.72
	LYSMD2	-11.71
	MPI	11.97
	PRG4	-25.46
	SGCD	-13.47
	VCAN	-14.93
	VCAN-AS1	-14.74
8. Polyamine metabolism	*ADC*	-10.38
	OAZ2	6.89
	SAT1	-16.06
9. GPI anchor/Lipid glycosylation	*ART1*	126.17
	B3GAT2	-9.50
	B3GNT4	-11.36
	PIGG	-5.72
	PIGS	6.51
10. Muscle atrophy	*MSTN*	43.11
	TRIM63	19.58
11. Cell cycle	*CDK6*	16.47
	CLASP1	-11.03
	NONO	6.96
	RB1	8.63
	TEAD1 (*TEA1*)	-11.18
	TEAD2 (*TEA2*)	8.60
	WEE1	19.23
12. Apoptosis	*APAF1*	-16.07
	DAPK1	-27.96
	MYCL [10]	-30.67

Bold: circadian genes according to our models 1-4.
[n]: function number where a gene could also belong.
*: Genes presented in Figure 2 C and E.

Table S8. List of common significantly affected genes upon *CLOCK* silencing between human islets and hSKM (Saini et al. 2016)

Name	% of change	Name	% of change	Name	% of change
AACS	-12.68	*NR3C1*	-10.98	***CRY1***	**34.52**
ADAM10	-21.79	*NRP1*	-12.99	*EZR*	16.55
ADAR	-8.93	*NUDT21*	-18.05	*MMP15*	20.97
AIDA	-11.19	*OIP5-AS1*	-28.90	*NIPA1*	21.51
AKAP2	-12.17	*OSMR*	-12.46	*PEG10*	19.92
ANAPC15	-22.58	*PAFAH1B2*	-9.07	*PODXL2*	17.22
ANTXR2	-23.90	*PALM2-AKAP2*	-11.99	*PSEN2*	10.36
ARCN1	-24.40	*PCCB*	-14.84	*PSKH1*	27.86
ARHGEF17	-14.28	***PER3***	**-34.92**	*SGPL1*	15.94
ATP5G2	-32.87	*PHLDB1*	-11.10	*VAT1*	10.35
BCAT1	-11.46	*PPIP5K2*	-19.38		
BEX4	-16.92	*PPP2R3A*	-10.37		
BHLHE41	**-17.66**	*PRDX3*	-13.52		
BTG2	-16.62	*RP11-334E6.12*	-14.25		
BVES	-24.35	*RYBP*	-17.62		
C1GALT1	-16.91	*SAMD8*	-20.95		
C1orf51	-45.82	*SLC25A44*	-18.83		
CCDC6	-15.44	*SLC30A6*	-17.80		
CD46	-14.05	*SSR1*	-16.79		
CLOCK	-80.04	*TEAD1*	-11.18		
COL3A1	-7.96	***TEF***	**-32.96**		
CTDSPL	-37.50	*TFDP1*	-20.28		
DBP	-36.42	*THY1*	-15.10		
EIF4EBP2	-39.43	*TNPO1*	-7.12		
FAM126B	-18.87	*TNS1*	-8.67		
FAM160B1	-13.19	*TXN2*	-22.32		
FAM172A	-11.94	*UBA1*	-8.94		
FAM189B	-13.88	*UBE4A*	-12.66		
FAM210B	-12.29	*UBE4B*	-8.42		
FICD	-25.80	*USP22*	-8.44		
FURIN	-17.52	*VCAN-AS1*	-14.74		
GALNT7	-24.63	*VCL*	-12.71		
GNAQ	-9.93	*VDAC1*	-13.82		
GPC1	-29.71	*WDR83OS*	-15.73		
GPR124	-11.64	*ZNF252P*	-27.82		
KIF13A	-23.56	*ZNF268*	-31.67		
LUM	-10.08	*ZNF468*	-38.36		
MAGED2	-15.95	*ZNF664*	-10.01		
MAP3K11	-22.32	*VAMP3*	-26.89		
MAPK6	-18.23				
MAPKAPK2	-15.72				
MDFIC	-14.52				
MEF2A	-28.09				
MEX3C	-16.20				
NPC1	-23.35				
NR1D1 (REVERBα)	**-46.90**				
NR1D2 (REVERBβ)	**-35.56**				

Bold: circadian genes according to our models 1-4.
Underscore: genes also found in Table S4.

Supplemental Table S9. Sequences of human RT-qPCR primers

Gene name		Primer sequence
ARNTL/BMAL1	Forward	5'-CCCTTGGACCAAGGAAGTAGAA-3'
	Reverse	5'-CTTCCAGGACGTTGGCTAAAAC-3'
NR1D1/REVERBα	Forward	5'-GATCGTGAGTCGCGGGGTCC-3'
	Reverse	5'-TGTAGGTGATGACGCCACCTGTGT-3'
PER3	Forward	5'-CCTGGACCCTGAACATGCA-3'
	Reverse	5'-TGTGAGCCCCACGTGTTTAA-3'
CLOCK	Forward	5'-CAAGCCACCGCAACAATT-3'
	Reverse	5'-GGATTCCCATGGAGCAACCTA-3'
9S	Forward	5'-CTCCGGAACAAACGTGAGGT-3'
	Reverse	5'-TCCAGCTTCATCTTGCCCTC-3'
HPRT	Forward	5'-GATTTTATCAGACTGAGGAGC-3'
	Reverse	5'-TCCAGTTAAAGTTGAGAGATC-3'

SUPPLEMENTARY FIGURES

Figure S1. Temporal gene expression in human skeletal muscle

(A) Temporal expression of genes involved in vesicular trafficking; (B) Temporal expression of genes involved in glucose uptake; (C) Temporal expression of genes involved in lipid metabolism analyzed by RNA-seq. N=10 human muscle biopsy donors

Figure S2. Study design

Primary human myotubes were transfected with 20 nM of non-targeting siRNA (siControl) or with same amount of siCLOCK at day 6 of differentiation. 24 h following siRNA transfection, *in vitro* synchronization by 10 µM forskolin pulse during 1 h was conducted for all the dishes, except for those collected at time point 0 h. Cells were harvested in duplicate dishes for each time point and for each donor, every 2 h during 48 h. Extracted RNA samples were subjected to RNA sequencing analysis or to real time quantitative PCR (RT-qPCR).

Figure S3. siRNA-mediated *CLOCK* knockdown leads to a flattening of the *Bmal1-luc* circadian oscillation amplitude in hSKM

Human primary myoblasts were transduced with lentiviral particles expressing *Bmal1-luc* and differentiated into myotubes. siControl or siCLOCK transfection was performed 24 h prior synchronization with forskolin.

(A) *CLOCK* mRNA was measured by RT-qPCR in samples used for RNA-seq and collected at time points 0 h (before synchronization), 24 h and 48 h. Data were normalized to the mean of *9S* and *HPRT. CLOCK* expression was reduced by 82 ± 4% (mean of the 3 time ± SEM, N=2, done in duplicates; (***) p-value <0.001) in siCLOCK-transfected cells.

(B) *Bmal1-luc* bioluminescence profile shows an important reduction of amplitude in siCLOCK-transfected myotubes compared to controls. Representative *Bmal1-luc* oscillation profiles are shown for non-transfected (light blue line), siControl (black line), and siCLOCK (red line) transfected myotubes. *Bmal1-luc* oscillation profiles were recorded in duplicates (2 experiments, one donor per experiment).

Figure S4. TBC1D4/AS160 protein levels are not affected by siCLOCK

Representative western blot for TBC1D4/AS160 in hSKM cells transfected with either siControl or siCLOCK for 72 h. Quantification of TBC1D4/AS160 protein levels shows no statistically significant difference of upon *CLOCK* disruption. Data are mean ± SEM (N=5, monoplicates).

Figure S5. Comparison of rhythmic transcript profiles between the two donors

(A) More rhythmic transcripts are found in donor 2 compared to donor 1 in both siControl and siCLOCK condition due to the genetic differences between both donors or due to a better response to the forskolin pulse used for synchronization. (B) Circadian amplitude quantification for the summary of models 1-4 in siControl and siCLOCK.

Figure S6. Temporal profiles of core clock transcript expression

(A) Expression profile of *NPAS2*, *TEF* and *BHLHE41* assessed by RNA-seq. (B) *ARNTL* (*BMAL1*), *NR1D1* (*REVERBα*) and *PER3* measured by RT-qPCR. mRNA levels were analyzed every 4 h over 48 h for each donor to confirm the RNA-seq results. Data were normalized to the mean of *9S* and *HPRT*. For donor 1 data represent monoplicates, whereas for donor 2 data were done in duplicates. Donor 1: circle; donor 2: triangle; siControl: black line; siCLOCK: red line.

Figure S7. Genes involved in cell cycle regulation exhibit circadian expression profile in hSKM

CCNB1, *CDC6*, *CDC7*, *CDC20*, *CDK1*, *E2F1*, *E2F7*, *MCM2*, *MCM5*, *MCM7*, *PLK1*, *PRC1*, *RBL1/p107* and *TPX2* expression profiles obtained by RNA-seq. All genes shown were classified in model 1 except for *E2F1* and *MCM5* (model 3).

SUPPLEMENTARY DATASETS

Supplemental Dataset 1

List of 9'211 genes identified by RNA-seq analysis in human skeletal muscle. Rhythmic transcripts (5’748) were grouped into genes rhythmic at the pre-mRNA and mRNA level (R-I, R-E), at the pre-mRNA level only (R-I), and at the mRNA level only (R-E). Related to Figure 1.

Supplemental Dataset 2

GO term enrichment analysis for transcripts identified as rhythmic in human skeletal muscle. Related to Figure 1.

Supplemental Dataset 3

List of 16’776 genes identified in hSKM by RNA-seq and used for the differential analysis. Related to Figure 2 and Tables S2-8.

Supplemental Dataset 4

GO term enrichment analysis, using the Panther classification system, for transcripts that were down- and/or upregulated upon clock disruption. Related to Figure 2, Table S4.

Supplemental Dataset 5

Reactome pathway analysis, using the Panther classification system for transcripts that were down- and/or upregulated upon clock disruption. Related to Figure 2, Table S5.

Supplemental Dataset 6

List of genes found in each of the 16 models identified by rhythmic analysis of the RNA-seq data. A gene was classified into one category if the probability was >0.5. If the probability was <0.5, transcripts were grouped into model 16 (non-rhythmic). Related to Figures 4-5, Figure S5, Tables S4-S6.

Supplemental Dataset 7

This dataset contains the $\log_2$ RPKM values for all the 25 time points (0 to 48 h) and the mean of all time points per donor and per condition (siControl/siCLOCK) as well as the model where each gene is grouped.

Supplemental Dataset 8

GO term enrichment analysis, using the Panther classification system, for transcripts that were grouped into model 1. Related to Figures 4-5, Figures S4-7 and Table S4.

Supplemental Dataset 9

Reactome enrichment analysis, using the Panther classification system, for genes that were grouped into model 1. Related to Figures 4-5, Figures S4-7 and Table S5.

Supplemental Dataset 10

List of 190 genes, rhythmic in hSKMs. Transcripts representing non-protein coding sequences, pseudogenes or retired loci are colored in red, transcripts associated with cell cycle are colored in blue, transcripts related to cell differentiation, adhesion and proliferation are colored in green. Related to Figure 5.

Figure S1

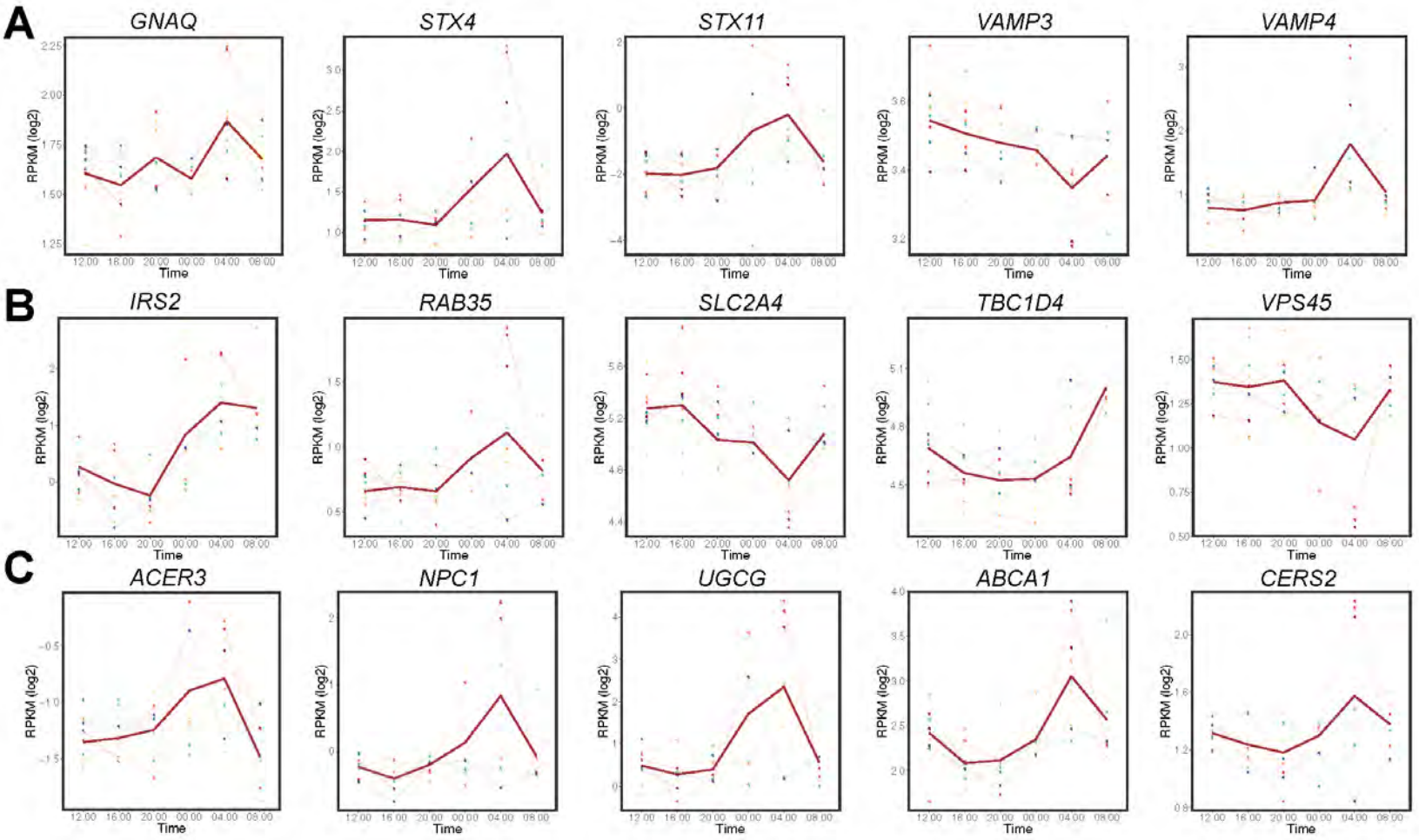
A
GNAQ
STX4
STX11
VAMP3
VAMP4
B
IRS2
RAB35
SLC2A4
TBC1D4
VPS45
C
ACER3
NPC1
UGCG
ABCA1
CERS2
RPKM (log2)
Time

Figure S2

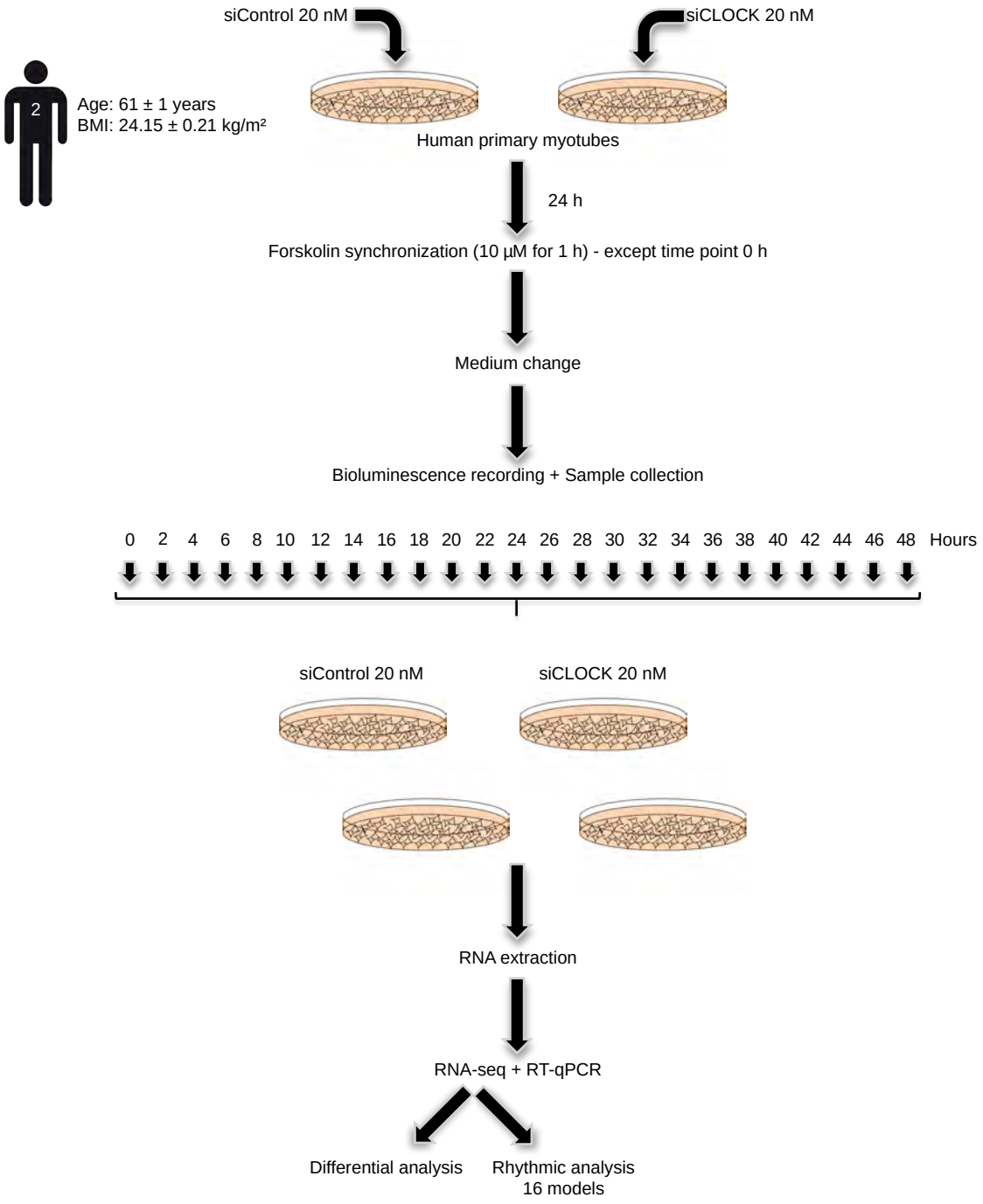
siControl 20 nM
siCLOCK 20 nM
2
Age: 61 ± 1 years
BMI: 24.15 ± 0.21 kg/m²
Human primary myotubes
24 h
Forskolin synchronization (10 µM for 1 h) - except time point 0 h
Medium change
Bioluminescence recording + Sample collection
0 2 4 6 8 10 12 14 16 18 20 22 24 26 28 30 32 34 36 38 40 42 44 46 48 Hours
siControl 20 nM
siCLOCK 20 nM
RNA extraction
RNA-seq + RT-qPCR
Differential analysis
Rhythmic analysis
16 models

Figure S3

A

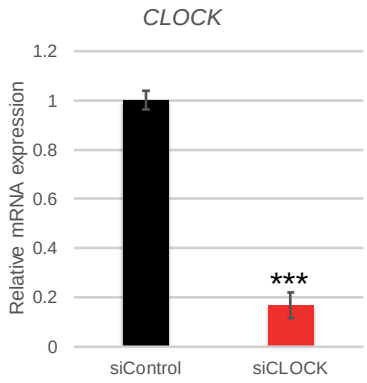
CLOCK
Relative mRNA expression
1.2
1
0.8
0.6
0.4
0.2
0
***
siControl
siCLOCK

B

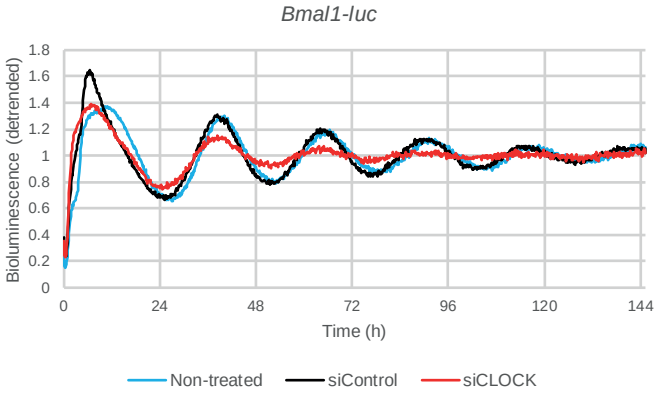
Bmal1-luc
Bioluminescence (detrended)
1.8
1.6
1.4
1.2
1
0.8
0.6
0.4
0.2
0
0
24
48
72
96
120
144
Time (h)
Non-treated
siControl
siCLOCK

Figure S4

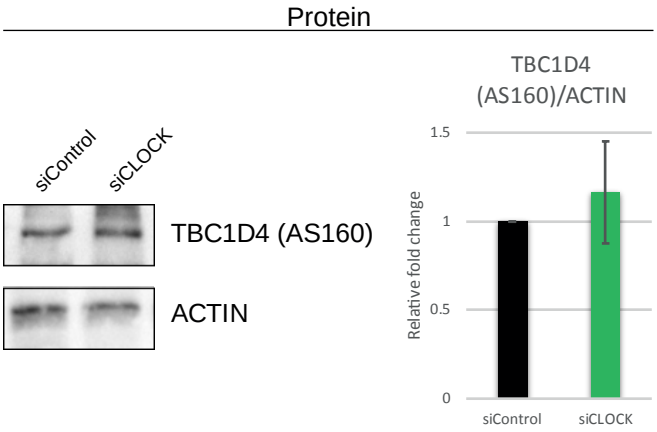
Protein
siControl
siCLOCK
TBC1D4 (AS160)
ACTIN
TBC1D4 (AS160)/ACTIN
Relative fold change
1.5
1
0.5
0
siControl
siCLOCK

Figure S5

A

Donor 1 siControl	Donor 1 siCLOCK	Donor 1 # of transcripts	Donor 2 siControl	Donor 2 siCLOCK	Donor 2 # of transcripts
∿	NR	230	∿	NR	305
NR	∿	120	NR	∿	267
∿	∿	167	∿	∿	199
NR	NR	477	NR	NR	223

B

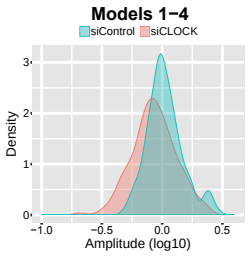

C

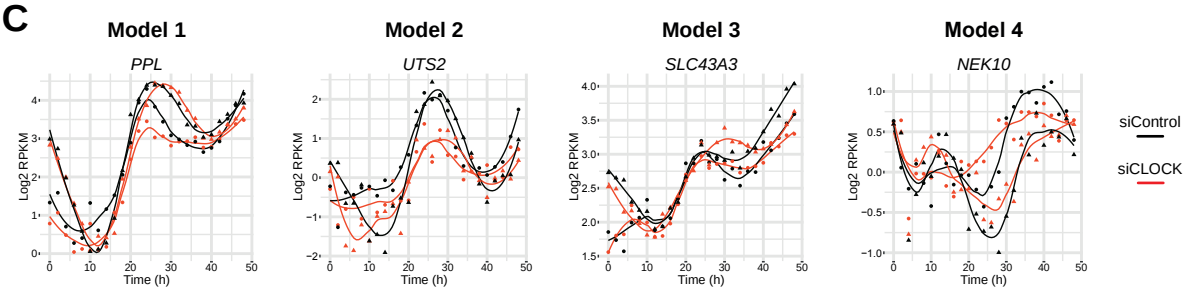

Figure S6

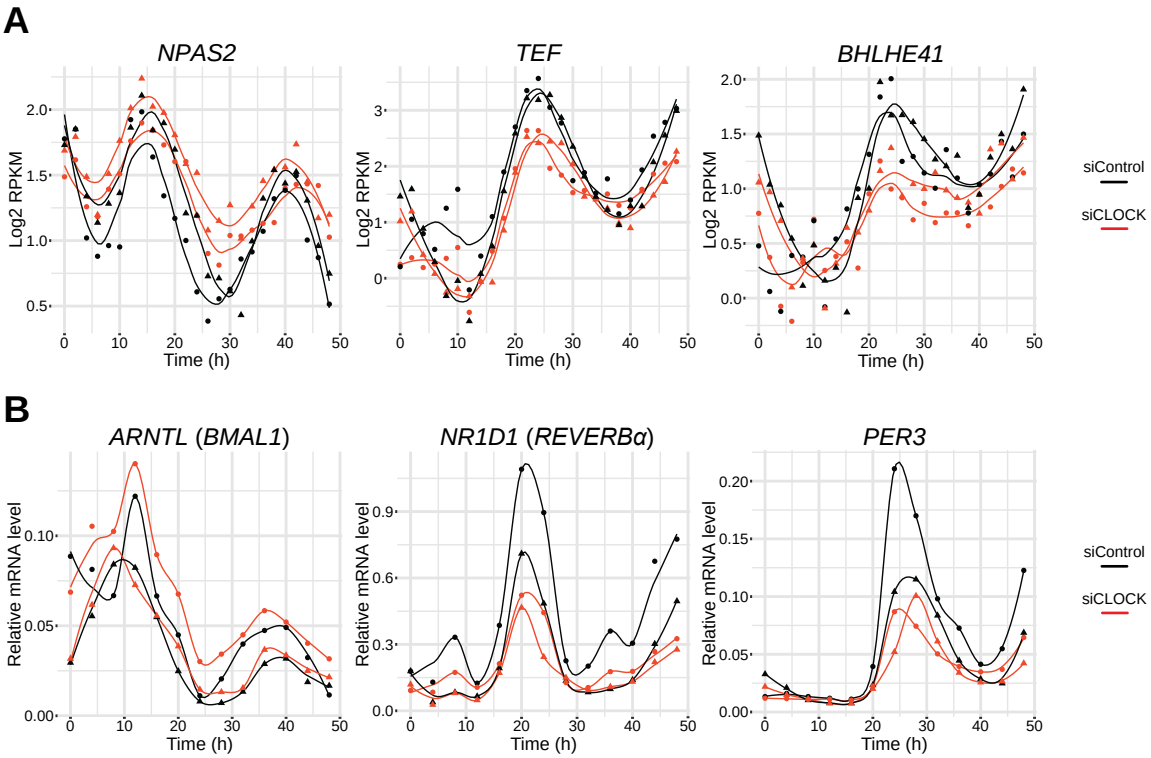
A
NPAS2
TEF
BHLHE41
Log2 RPKM
Time (h)
siControl
siCLOCK
B
ARNTL (BMAL1)
NR1D1 (REVERBα)
PER3
Relative mRNA level
Time (h)
siControl
siCLOCK

Figure S7

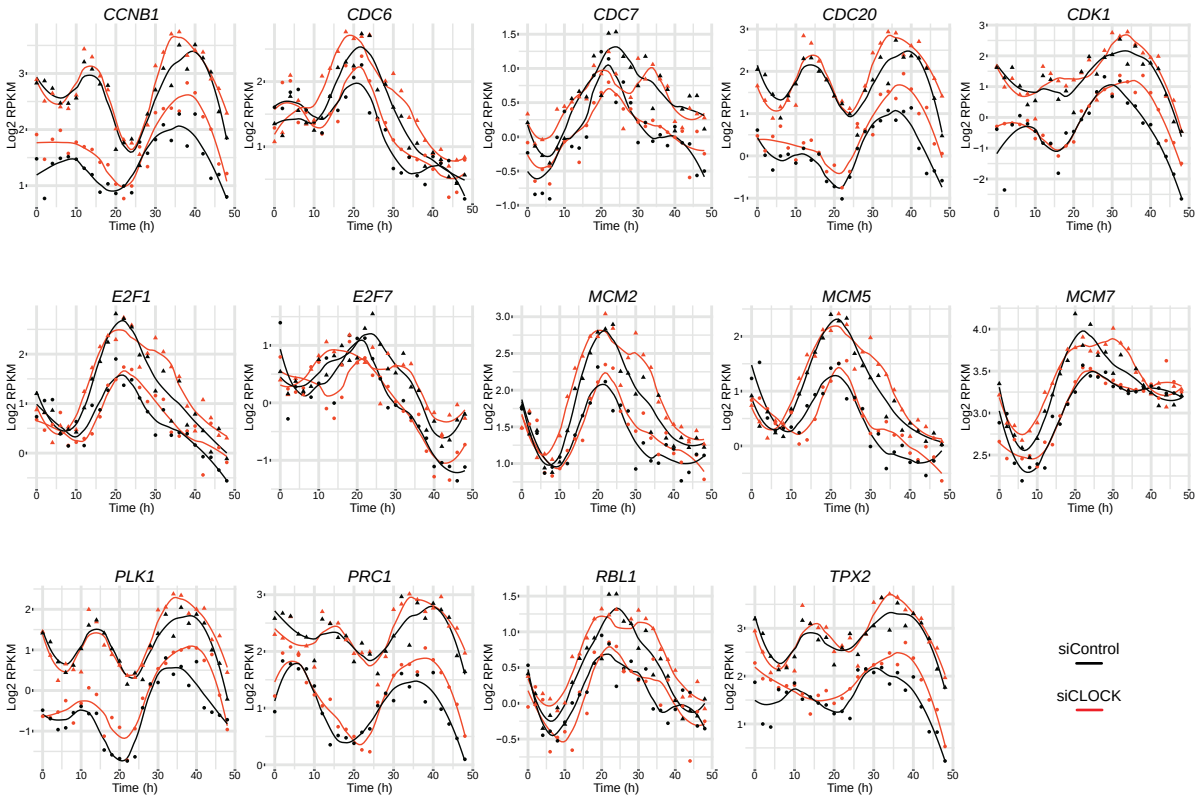
CCNB1
CDC6
CDC7
CDC20
CDK1
E2F1
E2F7
MCM2
MCM5
MCM7
PLK1
PRC1
RBL1
TPX2
Log2 RPKM
Time (h)
siControl
siCLOCK

5. ADDITIONAL RESULTS

An additional project for studying circadian rhythms in normal and pathological porcine SMCs was launched in collaboration with the group of the Dr. Marie-Luce Bochaton-Piallat at the University of Geneva.

Atherosclerosis is a chronic progressive inflammatory disease of the large arteries that can lead to ischemic heart disease and stroke (313). Atherosclerotic cardiovascular disease is the first cause of mortality worldwide with more than 16 million of deaths per year (314). One of the major steps in the progression of this disease is the migration of SMCs from the media toward the intima of the vessel wall. Origin of these pathological SMCs is still debated, however growing evidences suggest that the majority of SMCs found in the atherosclerotic plaque were already present in the vessel wall and a only few came from other locations or transdifferentiate (315). In normal conditions, mature SMCs in the vessel wall are characterized by the upregulation of specific genes such as α-smooth muscle actin (α-SMA), smooth muscle myosin heavy chains (*SMMHCs*) and smooth muscle protein 22-alpha (*SM22-α*), allowing proper contraction of the vessel wall (316), and with very low level of replication and death (317). However, it has been shown *in vivo*, that release of inflammatory mediators, mechanicals influences and growth factors stimulation, including by platelet-derived growth factor (PDGF)-BB and FGF-2, participate to the recruitment of SMCs and trigger their phenotypic switch (318, 319). Phenotypic modulation is the loss of SMC contractile property in part due to reduction in SMC markers, including α-SMA, acquirement of the capacity to migrate, proliferate and accumulate in the intima (320), followed by the ability to synthesize extracellular matrix contributing to the formation of the neointima after endothelial injury (321). *In vitro*, two types of SMCs can be isolated from carotid artery and aorta from rat, coronary artery from pig and carotid artery from man: the spindle-shaped (S) SMCs in rat and pig or large SMCs in man representative of the contractile phenotype and the epithelioid (E) SMCs in rat, rhomboid (R) SMCs in pig or small SMCs in man, corresponding to the synthetic phenotype, also found in cow pulmonary artery (322-326) (**Figure 9A**). The E, R and small phenotypes share common features, including an increased expression of S100A4 (324, 327), proliferation, migratory and proteolytic activities, and low levels of differentiation markers, such as α-SMA (328).

Compared to S-SMCs, R-SMCs present an upregulation of the calcium-binding protein S100A4, which regulates many cellular processes, such as proliferation and migration (329, 330). S100A4 is

strongly expressed in human and porcine SMCs of atheromatous and restenotic coronary artery lesions, including angioplasty and stent implantation, representing a novel marker of SMC activation during development of the atheromatous lesions (324, 327). Importantly, modulation of S100A4 expression has been shown to modulate the S- to R-SMCs phenotype switch (327), mediated through nuclear factor kappa B (NF-κB) signaling possibly *via* the receptor of advanced glycation endproducts (RAGE) (331). In addition to S100A4, several other genes and proteins are differently expressed in rhomboid SMCs compared to spindle SMCs, including members of the matrix metalloproteinases (MMPs) and the tissue inhibitors of metalloproteinases (TIMPs).

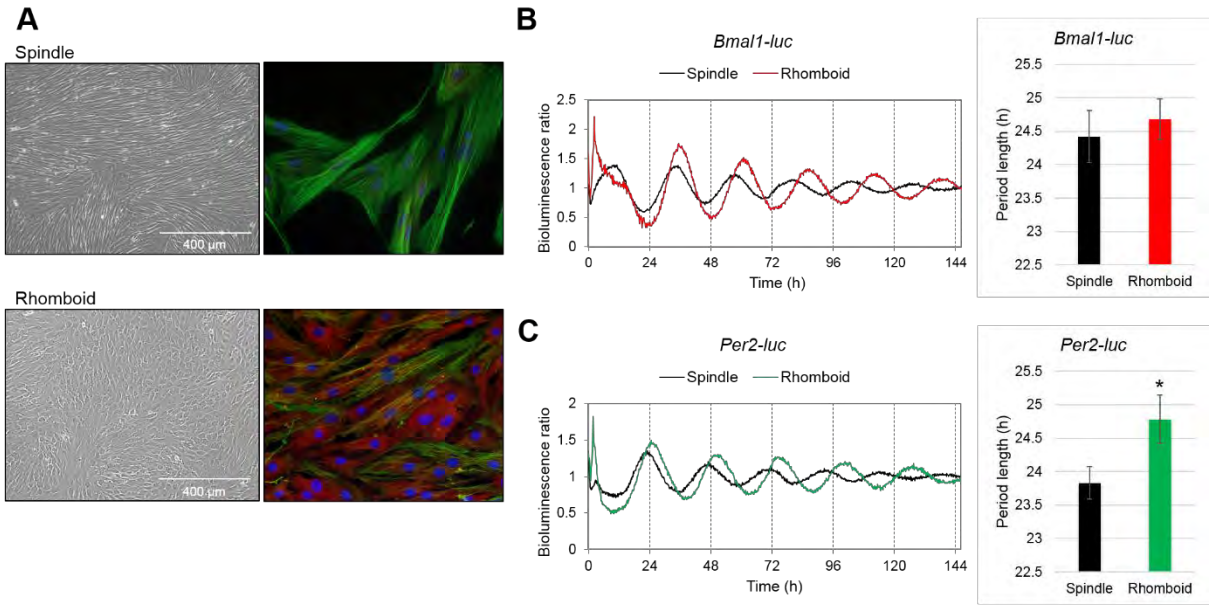

Figure 9. High-amplitude cell autonomous oscillators are functional in porcine coronary artery SMC spindle and rhomboid populations. (**A**) Phase-contrast micrographs showing spindle-shaped (S) and rhomboid (R) SMCs isolated from the normal media of porcine coronary artery. Immunofluorescence staining[#] for α-SMA expression (green), S100A4 (red) and DNA (blue). Higher S100A4 levels and lower α-SMA expression are observed in rhomboid phenotype compared to S-SMCs. Porcine S- or R-SMCs were transduced with lentiviral particles expressing *Bmal1-luc* or *Per2-luc*. Cells were synchronized with 10 µM forskolin for 60 min and transferred to an Actimetrics Lumicycle for bioluminescence recording. (**B**) Detrended *Bmal1-luc* oscillation profiles of S-SMCs (black line) and R-SMCs (red line) are representative of 7 and 5 independent experiments, respectively, done at least in duplicate. The period length of *Bmal1-luc* profiles is not significantly different between S-SMCs (24.42 ± 0.39 h, n=7) and R-SMCs (24.68 ± 0.30 h, n=5). (**C**) Detrended *Per2-luc* profiles of spindle (black line) or rhomboid (green line) are representative of 5 independent experiments, done at least in duplicate. The period length of *Per2-luc* is significantly longer for R-SMCs (24.78 ± 0.36 h, n=5) compared to S-SMCs (23.83 ± 0.25 h, n=5). Data represent the mean ± SEM, * p<0.05 by paired t-test. [#] *Courtesy of Luis Miguel Cardoso Dos Santos from the group of Dr. Bochaton-Piallat.*

Despite that circadian rhythms were already characterized in mouse aorta *in vivo* and Movas-1 cell line *in vitro* (332) as well as in human showing that plaque-derived SMCs exhibit different oscillation properties from normal carotid (333), the mechanism underlying these observations remains unknown. Therefore, we decided to employ porcine SMCs isolated from coronary arteries, as it was shown to be a reliable model of atherosclerosis development (325), combined with our expertise, to provide new insights on the role of the circadian system in the development of atherosclerosis. The use of continuous

recording of oscillation profiles for several days with high temporal resolution, has revealed high-amplitude self-sustained *Bmal1-luc* (**Figure 9B**) and *Per2-luc* (**Figure 9C**) expression with expected phase in spindle and rhomboid SMCs synchronized with a forskolin pulse (10 µM; 60 min). The period length was similar in *Bmal1-luc* transduced spindle and rhomboid SMCs, however significantly longer period length was observed in rhomboid cells expressing *Per2-luc* reporter (24.78 ± 0.36 h, n=5) compared to spindle cells (23.83 ± 0.25 h, n=5) (**Figure 9B-C**).

To confirm these results, we looked at the endogenous core clock expression using qRT-PCR (**Figure 10A** and **Table 1** for primer sequences). Spindle and rhomboid SMCs were synchronized by forskolin and harvested every 4 h during 24 h between time point 12 h and 36 h post synchronization. All core clock genes tested exhibit a circadian expression with expected phase but surprisingly in rhomboid cells, this expression present a phase delay from 2 h to 8 h for *BMAL1*, *CRY1*, *CRY2*, *PER1*, *PER2* and *REV-ERBβ*. Furthermore, the amplitude is significantly increased, except for *CLOCK* which did not show neither difference in amplitude nor of phase between spindle and rhomboids populations. We further evaluated the expression of selected genes involved in the SMC phenotype (**Figure 10B**). In line with the immunostaining experiments (**Figure 9A**), *S100A4* and *TIMP-3* present a significant upregulation, whereas *SMMHCs* and *SM22-α* are downregulated and *C-myc* expression remained stable in rhomboid cells compared to spindle, supporting a previous report (331). Moreover, *TIMP-3* and *C-myc* seem to follow a circadian pattern of expression with similar phase in rhomboid and spindle cells respectively. We also found a small but significant increase in *MMP-14* mRNA level which differs from results shown in a recent article (331).

Next, we investigated the impact on the circadian clock of treatment with PDGF-BB (30 ng/ml) and FGF-2 (10 ng/ml) for at least 7 days and 4 days, respectively, before bioluminescence recording. Both treatments induced a phenotype switch from spindle to rhomboid-like SMCs (**Figure 11A, D**). As expected, immunofluorescence staining showed profound modifications of protein expression, with a decrease of α-SMA and an increase of S100A4 in FGF-2-treated spindle cells (**Figure 11 D**). Experiments using circadian reporters *Bmal1-luc* and *Per2-luc* have shown that both treatments lead to a longer period despite that this increase was significant only for *Per2-luc* oscillation profiles with 24.34 ± 0.14 h period in PDGF-BB-treated SMCs compared to 23.72 ± 0.29 h in non-treated spindle cells, and 25.25 ± 0.07 h in FGF-2-treated SMCs compared to 24.93 ± 0.18 h in non-treated spindle cells (**Figure**

11B-C, E-F). Taken together, these results are in good agreement with those seen in native rhomboid SMCs (**Figure 9**).

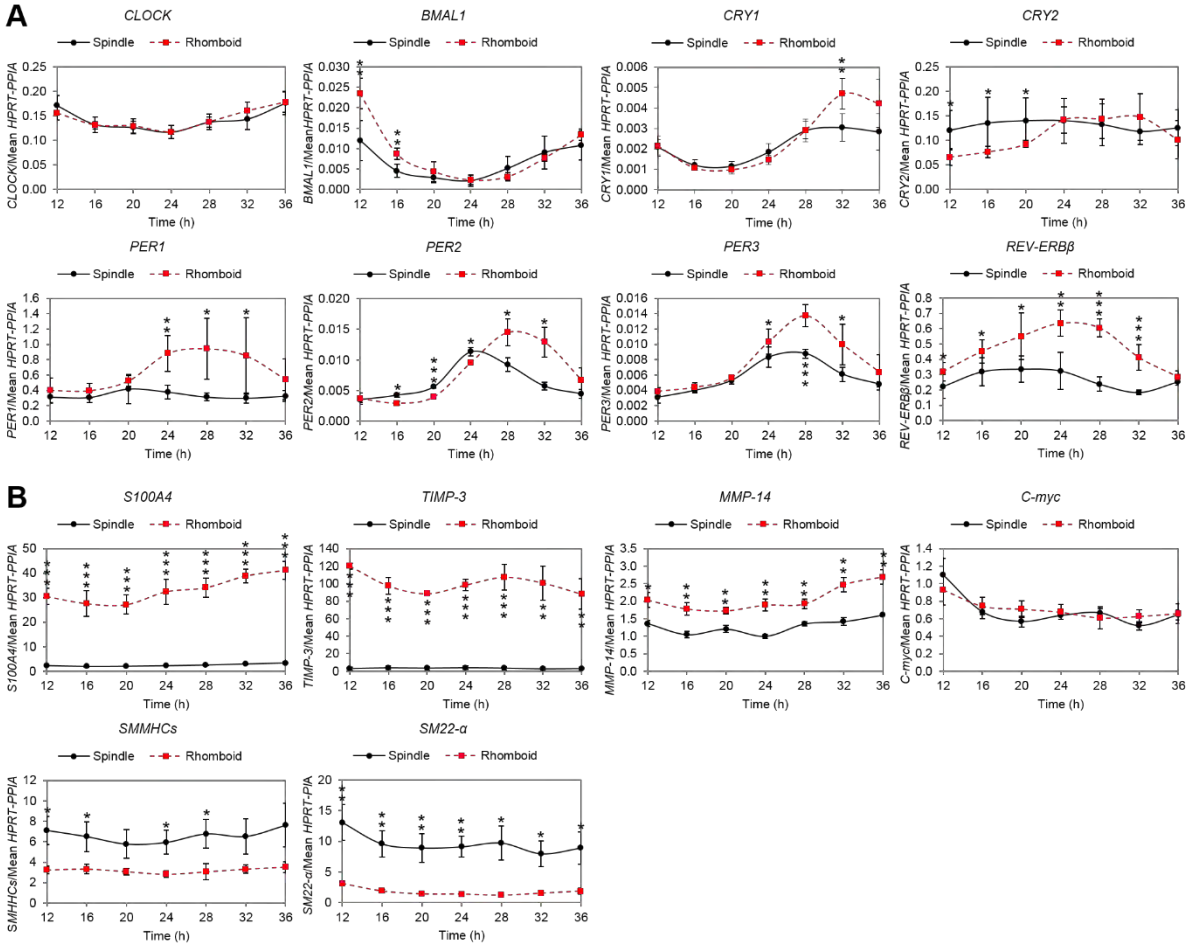

Figure 10. Endogenous gene expression in pig spindle and rhomboid cells. Cells were grown to confluence and subjected to synchronization by forskolin (10 µM; 60 min). Samples were deep frozen in liquid nitrogen every 4 h during 24 h between the time points 12 h and 36 h after synchronization, then RNA extraction, cDNA synthesis and quantitative real-time PCR (qRT-PCR) were performed. (**A**) mRNA expression levels of core clock genes *CLOCK*, *BMAL1*, *CRY1*, *CRY2*, *PER1*, *PER2*, *PER3* and *REV-ERBβ*. In R-SMCs (dash red line), all genes expect *CLOCK* and *PER3* present a phase delay between 2 h and 8 h compared to S-SMCs (full black line). In addition, all genes, expect *CLOCK* and *CRY2* exhibit a higher amplitude of their oscillations. (**B**) Selected target genes expression. *S100A4*, *TIMP-3* and *MMP-14* are significantly upregulated whereas *SMMHCs* and *SM22-α* are downregulated in R-SMCs compared to S-SMCs as expected (331). Moreover, *TIMP-3* and *C-myc* seem to be circadian in R- and S-SMCs, respectively. Data are normalized to the mean of *HPRT*/*PPIA*, * p<0.05, ** p<0.01, *** p<0.001 by paired t-test. Profiles are mean ± SEM of two independent experiments done in duplicate per time point for S- and R-SMCs, respectively.

Table 1. Sequences of porcine qRT-PCR primers

Gene name	Primer sequence		Amplicon size (bp)	Reference
BMAL1	Forward	5'-GGGCTGGATGAAGACAACGA-3'	117	
	Reverse	5'-CACCCTGATTTCCCCGTTCA -3'		
CLOCK	Forward	5'-CTGGGATCCATGCTTCCTGG-3'	111	
	Reverse	5'-AGCATCTGACTGTGCAGTGA-3'		
CRY1	Forward	5'-TTCTTGCGTCAGTGCCATCT-3'	107	
	Reverse	5'-TCCTTGAGGGCAACTTCCAC-3'		
CRY2	Forward	5'-TTCTACTACCGCCTGTGGGA-3'	108	
	Reverse	5'-GGCTGCCGTGTAGAAGAACT-3'		
PER1	Forward	5'-GCAGGCCAACCAGGAATACT-3'	113	
	Reverse	5'-TGTACTCGGACGTGATGTGC-3'		
PER2	Forward	5'-GCCATTACCCTGGTGCATCT-3'	110	
	Reverse	5'-CGAGCTGTCTTTTTCCGCAG-3'		
PER3	Forward	5'-GCAGCCACACTTTTCTCACG-3'	107	
	Reverse	5'-GCGGGAGTCATATCTGGGTG-3'		
REV-ERBβ	Forward	5'-GTGCAACACTGGAGGGAGAA-3'	116	
	Reverse	5'-CTGGGGTGAAGCTCATCGAA-3'		
C-myc	Forward	5'-GCTGGATTTCCTTCGGATAG-3'	66	(331)
	Reverse	5'-TTGGTGAAGCTGACGTTGAG-3'		
MMP-14	Forward	5'-TGCAGCAGTATGGCTACCTG-3'	110	(331)
	Reverse	5'-CTCGCAGACCGTAGAACCTC-3'		
S100A4	Forward	5'-GCGATGCAGGACAGGAAGAC-3'	227	(331)
	Reverse	5'-GGCCCTCGATGTGATGGTGT-3'		
SM22-α	Forward	5'-GGCTGAAGAATGGCGTGAT-3'	209	(331)
	Reverse	5'-CTGCCATGTCTTTGCCTTCA-3'		
SMMHCs	Forward	5'-AGGACCAGTCCATTTTGTGC-3'	115	(331)
	Reverse	5'-CCTGGTCCTTCTTGCTCTTG-3'		
TIMP-3	Forward	5'-CTTCACCAAGATGCCCCATG-3'	120	(331)
	Reverse	5'-CTTGCCATCATAGACACGGC-3'		
PPIA	Forward	5'-CACAAACGGTTCCCAGTTTT -3'	171	(334)
	Reverse	5'-TGTCCACAGTCAGCAATGGT-3'		
HPRT	Forward	5'-CCGAGGATTTGGAAAAGGT-3'	181	(334)
	Reverse	5'-CTATTTCTGTTCAGTGCTTTGATGT-3'		

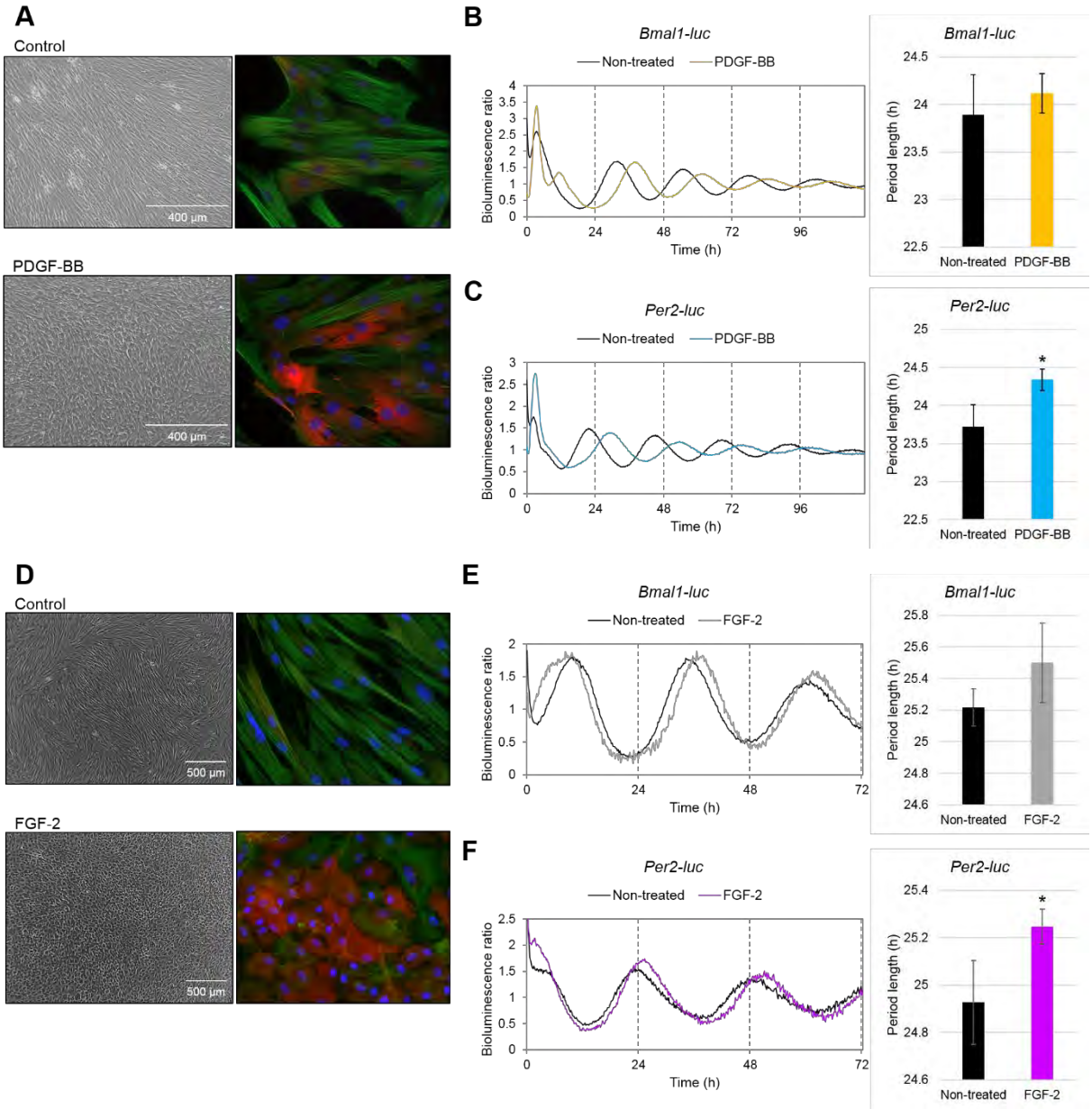

Figure 11. PDGF-BB and FGF-2 treatments trigger SMC phenotype switch from spindle to rhomboid and affect the circadian rhythm. (**A**) Phase-contrast micrographs showing S-SMCs (control) and S-SMCs harboring a rhomboid-like phenotype after PDGF-BB treatment (30 ng/ml for at least 7 days). Immunofluorescence staining[#] for α-SMA expression (green), S100A4 (red) and DNA in the nucleus (blue). Higher S100A4 levels are observed in PDGF-BB-treated cells compared to control, with subsequent reduction in α-SMA expression validating the rhomboid-like phenotype. Porcine S-SMCs were transduced with circadian lentivector *Bmal1-luc* or *Per2-luc* and cells were synchronized with 10 µM forskolin for 60 min and transferred to an Actimetrics Lumicycle for bioluminescence recording. (**B**) Detrended *Bmal1-luc* oscillation profiles of S-SMCs non-treated (black line) and S-SMCs treated with PDGF-BB (orange line) are representative of 2 and 3 independent experiments, respectively, done in duplicate. The period length of *Bmal1-luc* profiles is not significantly different between non-treated (23.89 ± 0.42 h, n=2) and PDGF-BB-treated S-SMCs (24.12 ± 0.21 h, n=3). (**C**) Detrended *Per2-luc* profiles of S-SMCs non-treated (black line) and S-SMCs treated with PDGF-BB (blue line) are representative of 2 and 3 independent experiments, respectively, done in duplicate. The period length of *Per2-luc* profiles is significantly longer in PDGF-BB-treated SMCs (24.34 ± 0.14 h, n=3) compared to non-treated S-SMCs (23.72 ± 0.29 h, n=2). (**D**) Phase-contrast pictures showing S-SMCs (control) and S-SMCs harboring a rhomboid-like phenotype after FGF-2 treatment (10 ng/ml for at least 4 days). Immunofluorescence staining[#] shows drastic changes in α-SMA expression (green) in FGF-2-treated cells compared to control. In addition, increased expression of S100A4 (red) corroborate the phenotype switch toward rhomboid-like SMCs after FGF-2 treatment. Nucleus were stained with DAPI (blue). (**E**) Detrended *Bmal1-luc* oscillation profiles of S-SMCs non-treated (black line) and S-SMCs treated with FGF-2 (grey line) are representative of 3 independent experiments, respectively, done at least in one plicate. The period length of *Bmal1-luc* profiles is not significantly different between non-treated (25.22 ± 0.12 h, n=3) and PDGF-BB-treated S-SMCs (25.5 ± 0.25 h, n=3). (**F**) Detrended *Per2-luc* profiles of S-SMCs non-treated (black line) and S-SMCs treated with FGF-2 (purple line) are representative of 2 and 3 independent experiments, respectively, done at least in one plicate. The period length of *Per2-luc* profiles is significantly longer in FGF-2-treated SMCs (25.25 ± 0.07 h, n=3) compared to non-treated S-SMCs (24.93 ± 0.18 h, n=2). Data represent the mean ± SEM, * p<0.05 by paired t-test. [#] *Courtesy of Luis Miguel Cardoso Dos Santos from the group of Dr. Bochaton-Piallat.*

6. DISCUSSION

6.1. Overview of the main findings

The present project has provided significant new insights into the understanding of the circadian clockwork in regulation of human skeletal muscle metabolism and physiology. We hereby characterized for the first time cell-autonomous self-sustained circadian oscillators operative in human primary skeletal myotubes *in vitro* (**Figure 1** from (10)).

We have set up an experimental design for efficient siRNA-mediated knockdown of *CLOCK* mRNA and protein levels, resulting in the disruption of the circadian clock in adult hSKM (**Figure 2** from (10)). Significant alteration in other core clock genes expression, including *REV-ERBα*, *PER3* and *DBP*, following *CLOCK* knockdown were in an agreement with the published works in mice (11, 12, 91, 93, 157).

Employing continuous perifusion system (312), we assessed the temporal profile of basal secretion of myokines by hSKM *in vitro* over 48 h following *in vitro* synchronization, in the presence of either functional or disrupted circadian oscillator. Among the 15 detected myokines, IL-6, IL-8 and MCP-1 were rhythmically secreted by siControl-, but not by siCLOCK-transfected human primary myotubes (**Figures 3** and **4** from (10)). In addition, absolute levels of IL-6, IL-8, CD44, FABP3, Galectin-3, TIMP-1 and VEGF were significantly lower in hSKM following the clock disruption (**Table 4** from (10)). Of note, total IL-6 secretion over 48 h was elevated in hSKM derived from obese individuals, as compared to the lean controls (**Table 3** from(10)), suggesting that high systemic levels of IL-6 measured in plasma from obese subjects (335) could, to a certain extent, coming from the skeletal muscle.

Most importantly, both basal and insulin-stimulated glucose uptake were decreased by about 30% in cultured hSKM under disrupted circadian clock condition (**Figure 3**, Perrin *et al.* submitted to eLife). To obtain mechanistic insights into the observed functional changes, large-scale circadian transcriptome analyses have been conducted in hSKM harboring or not a functional oscillator *in vitro*, and in human skeletal muscle biopsies *in vivo*. While rhythmic transcription is abundantly observed *in vivo*, a large part of this rhythmicity is lost at the mRNA accumulation level in the *in vitro* cell culture (**Figures 1**, **4**, **5** and **Table 2**, Perrin *et al.* submitted to eLife). *CLOCK* silencing significantly affected the expression levels of ~8% of all myotube genes, impacting glucose homeostasis and lipid metabolism (**Figure 2**, **Table 1**

and **Table S5**, Perrin *et al.* submitted to eLife). Altogether, our findings suggest an essential role for cell-autonomous circadian clocks in the regulation of muscle glucose homeostasis and lipid metabolism in humans.

Based on the same experimental settings, large-scale circadian lipidomics has been conducted *in vitro* in hSKM, and in human skeletal muscle biopsies collected *in vivo* (336). These analyses determined that about 20% of lipid metabolites exhibit rhythmic profiles *in vivo* and *in vitro* (**Figure 4** from (336)). Importantly, cellular lipid oscillations were clock-dependent, and were significantly dampened in the absence of a functional oscillator (**Figure 8** from (336)), agreeing with the important role played by the muscle clock in regulating lipid metabolism (336).

Developed here experimental settings have been successfully applied to different human and mammalian primary cell types, including human pancreatic islets (16, 158), and primary porcine SMCs (**chapter 5. Additional results**, collaboration with the group of Marie-Luce Bochaton-Piallat). As metabolic disorders are growing rapidly in modern societies (211) and cardiovascular diseases are causing millions of deaths worldwide (314), *in vitro* synchronized primary cells may therefore represent a good model to decipher the link between circadian oscillators and T2D, obesity and atherosclerosis etiologies.

6.2. Characterization of the molecular clock operative in human skeletal muscle

Molecular makeup of the hSKM circadian clock has been achieved employing *Bmal1-luc* or *Per2-luc* lentivectors, allowing recording of circadian bioluminescence in living cells with high temporal resolution for several days (**Figure 1** from (10)). hSKM synchronization *in vitro* has occurred independently of the entrainment pathway, as it was achieved by forskolin, an activator of the adenylyl cyclase (51), and by dexamethasone, a glucocorticoid analogue (52-54) (**Supplementary Figure 2** from (10)). Comparable circadian period length were obtained with both bioluminescent reporters (**Table 2** from (10)). These results have been further validated by analyzing temporal profiles of endogenous core clock genes expression following forskolin or dexamethasone synchronization by qRT-PCR (**Figure 2C** closed circles, **Supplementary Figure 3** from (10)). Overall, the provided here molecular characterization of the circadian oscillator operative in hSKM is in a good agreement with previous reports on the clock makeup in different human tissues employing similar methodology (8, 177, 337).

6.3. Temporal pattern of basal IL-6 secretion is regulated by the muscle clock

Human skeletal muscle represents the largest insulin sensitive organ in the body (240), producing and secreting cytokines, dubbed myokines, that act in an autocrine, paracrine and endocrine manner (268). The myokines participate in the inter-organ crosstalk with endocrine pancreas, adipose tissue and liver, which are in turn secreting islet hormones, adipo- and hepatokines, respectively, impacting critically on the body glucose homeostasis (338). Thus, further evaluation of the ability to synchronize the muscle clock by other stimuli, including glucose, insulin or myokine-induced signaling pathways, will be important, as was done in a parallel project assessing physiologically relevant synchronizers for the pancreatic islet cells (16).

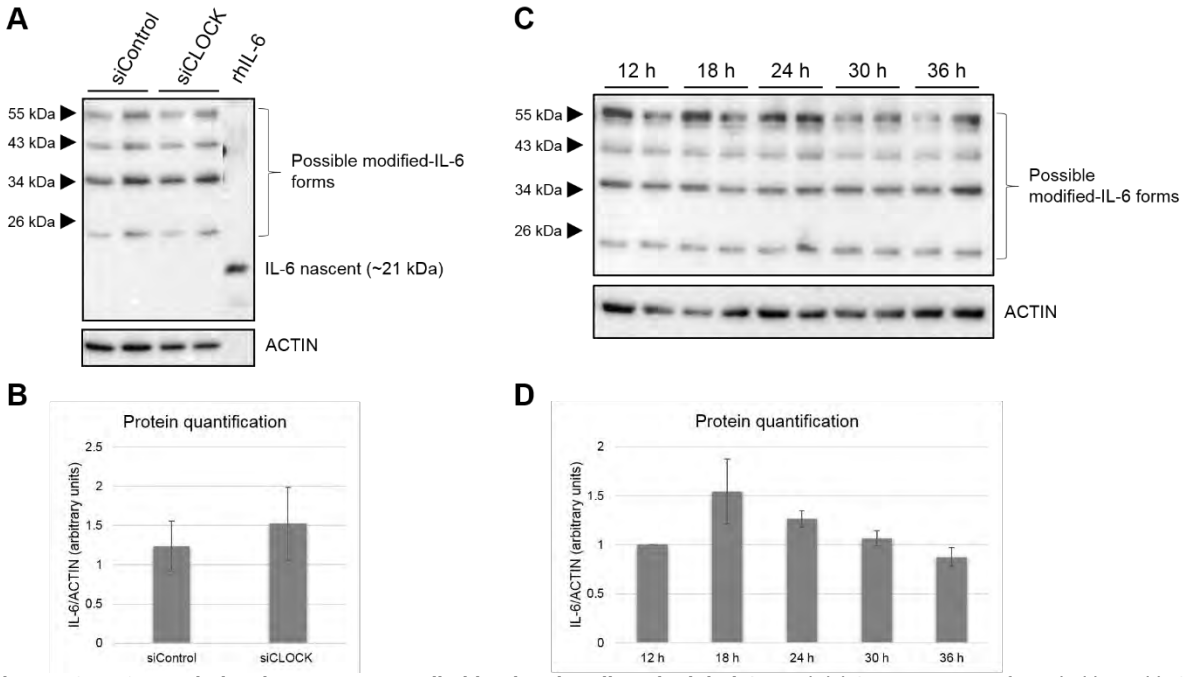

Figure 12. IL-6 protein levels are not controlled by the circadian clock in hSKM. (**A**) hSKM were transfected either with 20 nM of siControl or siCLOCK in duplicate for 24 h. Cell lysis was performed using RIPA buffer containing phosphate-buffered saline (PBS) calcium (Ca)/magnesium (Mg)-free, 1% NP 40, 0.5% sodium deoxycholate, 0.1% SDS, 1% ethylene diamine tetraacetic acid (EDTA) 5 mM, 1% Na_3VO_4 1 mM, 4% NaF 20 mM, 0.1% dithiothreitol (DTT) 1 mM and 0.1% protease inhibitor. Lysates were collected, vortexed, kept 10 min on ice, centrifuged at 10'000g at 4°C during 10 min and supernatant was kept at -80°C. Samples were loaded on a SDS-PAGE gel, transferred to a polyvinylidene difluoride (PVDF) membrane 0.2 µM and subjected to incubation with human IL-6 antibody. Recombinant human IL-6 (rhIL-6) was loaded as a positive control and the correspondent band is located at the expected size (~21 kDa). However, in hSKM extracts, 4 main bands were detected. Bands at ~25 and ~35 kDa might be IL-6 with post-translational modifications, the band at ~42 kDa could be IL-6 homodimers and the one at ~55 kDa could be homo- or heterodimers of modified-IL-6 as described in (339-341). Actin was used as a loading control. (**B**) Despite an efficient reduction of CLOCK protein of about 76% (data not shown), no differences were observed for IL-6 protein levels between siControl and siCLOCK. Data are mean of quantification values of the four detected bands at 25, 35, 42 and 55 kDa ± SD of one experiment done in duplicate. (**C**) We also looked at the rhythmic protein accumulation of IL-6. To this end, hSKM were synchronized by a forskolin pulse and harvested during a time span of 24 h, between time point 12 h and 36 h. (**D**) Protein quantification did not reveal a circadian pattern of IL-6 despite a slight increase at time point 18 h. Data are mean of quantification values for the four detected bands at 25, 35, 42 and 55 kDa ± SD of two experiments using one donor each done in duplicate.

The regulation of the basal secretion of IL-6 by the muscle clock represents one of the important conclusions of this work. However, the mechanism underlying this regulation stays to be unraveled. Indeed, we have demonstrated that the rhythmic profile of IL-6 basal secretion was not stemming from

changes in either *IL6* mRNA, measured by qRT-PCR, or in its protein levels (**Figure 12**). We did not find significant differences in IL-6 protein levels between siControl and siCLOCK samples (**Figure 12A-B**). This might explain the pattern of bands detected by western blot in our samples siControl/siCLOCK, with bands at ~25 and ~35 kDa possibly corresponding to modified-IL-6 by O-glycosylation or O- and N-glycosylation, respectively (339, 340) (**Figure 12A**). The band at ~42 kDa might represent IL-6 homodimers which is two times heavier than the band seen with the recombinant human IL-6 (rhIL-6) used as positive control and detected at ~21 kDa (**Figure 12A**). The band at ~55 kDa could be the O-glycosylated IL-6 form (~25 kDa) in complex with itself, or other proteins, as it was demonstrated in human foreskin fibroblasts FS-4 cell line (341). Quantification of the four bands (25, 35, 42 and 55 kDa) revealed a similar level between siControl- and siCLOCK-transfected hSKM (**Figure 12B**). Furthermore, IL-6 protein accumulation did not exhibit a circadian profile when measured across 24 h in synchronized hSKM (**Figure 12C-D**).

Previous reports have suggested circadian regulation of *IL6* and *MCP1* in both rodent and human immune cell models. Indeed, in mouse astrocytes, *Il6* is regulated by REV-ERBα/RORα and NF-κB (164), whereas in rat spinal astrocytes, *Il6* and *Mcp1* genes are modulated by PER1 acting through activation of NF-κB pathway (342). These results support that IL-6 and MCP-1 present a circadian pattern in the magnitude of their response to an endotoxin challenge at different times of the day, which is lost when the circadian system is disrupted either in *Bmal1*$^{-/-}$ or *Rev-Erbα* KO mice, and in human macrophages transfected with short hairpin RNA (shRNA) against *REV-ERBα* (163). Moreover, microglial cells isolated from *Bmal1*-deficient mice reduced *Il6* expression following lipopolysaccharide (LPS) stimulation. This effect was recapitulated when microglial cells from *Per2-luciferase* mice were treated with the REV-ERBα agonist SR9011 (218, 343). Furthermore, as *REV-ERBα* regulates *IL6* transcription in mouse and human macrophages (163, 164) and that *REV-ERBα* is the only gene differentially expressed between primary myotubes from healthy and T2D (344), determination of the rhythmic IL-6 secretion and other myokines using our experimental settings on hSKM derived from T2D would be of interest.

In summary, one plausible explanation for the observed here phenomenon of the regulation of myokine secretion by the local oscillators (**Figure 3, Table 3** from (10)) might be that such regulation

occurred at the myokine secretion process level. This hypothesis is further supported by the transcriptome data discussed below (see **chapter 6.5.2.**).

6.4. Roles of IL-6 in metabolism

Besides its role in inflammation, IL-6 plays important roles in physiology and metabolism (345). IL-6 was demonstrated to be important for regulating glucose homeostasis, as its single injection improved insulin-stimulated glucose uptake in young healthy human subjects (296), but not in T2D patients (298). Additional data suggested that it is rather the acute versus chronical character of elevated IL-6 levels, which will define whether the effects of IL-6 are beneficial or deleterious. An acute increase of IL-6 ameliorates insulin sensitivity, and impacts positively on glucose (346, 347) and fat metabolism (348), whereas chronic exposure causes insulin resistance in mice (299). Although *IL6* KO mice develop mature-onset obesity and glucose intolerance (293), recent evidences in muscle-specific *IL6* KO mice suggest that muscle IL-6 reduces utilization of carbohydrates during prolonged exercise by regulating pyruvate dehydrogenase activity (290).

IL-6 plasma levels are higher in obese people compared to non-obese, and we confirmed this *in vitro* (10). A recent article has shown that in obese mice fed on HFD, IL-6 acts independently of its receptor (IL-6R) *via* the trans-signaling pathway involving gp130 (also known as IL6ST), which activates STAT3 signaling in paraventricular nucleus of the hypothalamus (PVH), resulting in potent suppression of feeding and improvement of glucose homeostasis. Moreover, elevated levels of the soluble form of IL-6R and an increase of gp130 expression were specifically found in obese mice upon HFD, most likely to amplify IL-6 sensitivity of PVH (349). Thus, the identified signaling pathway in central nervous system might be an interesting potential target for drug to treat obesity and obesity-associated insulin resistance, as it exists for other pathologies, such as arthritis (350). A recent publication has revealed that myokine secretion is altered in cultured human myotubes established from T2D subject biopsies (302), agreeing with previous reports (351-359). However, in this study, authors measured only total secretion after 24 h or 48 h of culture, whereas our approach allows for obtaining continuous temporal secretion profile (302). Assessment of this conjunction in hSKM established from the tissue biopsies taken from obese and T2D individuals, by the developed here methodology, will represent an important direction for the continuation of this work (see **chapter 6.8.3.**), which we have already started to pursue. We hypothesize that the daily oscillation pattern of myokines might represent an advantage for their temporal

coordination with the rest/activity cycle, which will likely result in optimal myokine response to external cues (10).

6.5. RNA-seq analyses revealed candidate genes involved in vesicle trafficking, glucose and lipid metabolism in hSKM synchronized *in vitro,* and in human skeletal muscle biopsies collected *in vivo*

The here presented study is the first that is depicting gene expression by RNA-seq analysis from human skeletal muscle biopsies and primary human myotubes derived from healthy subjects in the presence or absence of a functional circadian clock (**Figure S1**, Perrin *et al.* submitted to eLife). This design allowed to dissect the effects of the cell-autonomous muscle clocks on the gene transcription from the central effects driven by external cues, including rest-activity and feeding-fasting cycles (303). Rhythmic mRNA oscillations have been observed for numerous functional gene groups, including cell cycle and DNA metabolic process (**Table S2**, Perrin L. *et al.* submitted to eLife). Of note, three major groups related to exocytosis, glucose uptake and lipid metabolism might provide explanation to our previous observations regarding the basal circadian myokine secretion and lipid metabolites oscillations in hSKM synchronized *in vitro* (**Figure 13**) (10, 336).

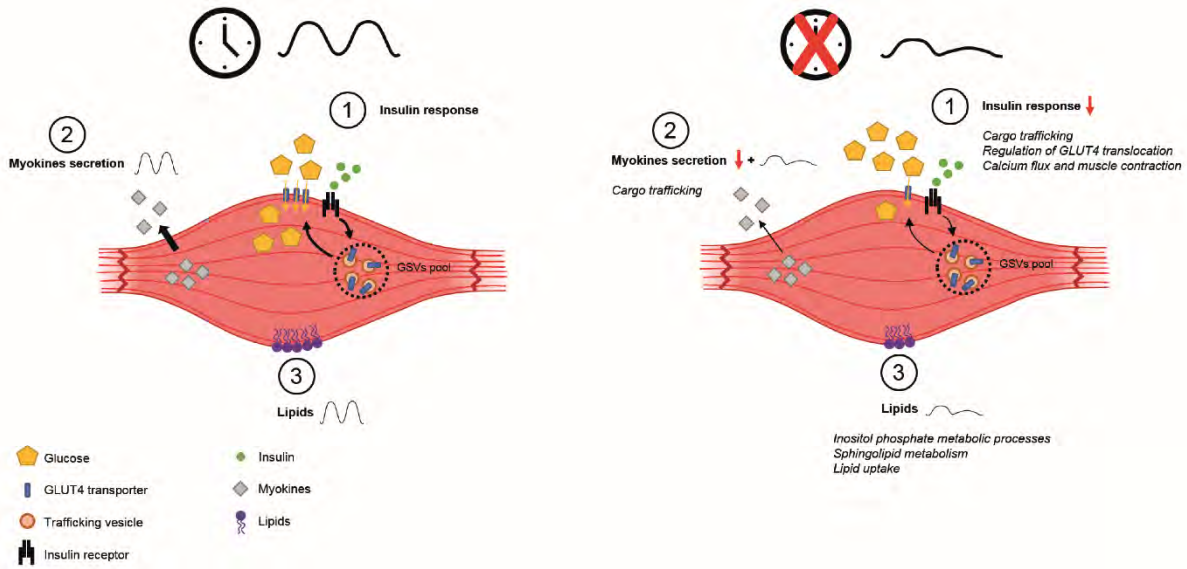

Figure 13. (Adopted from Perrin L. *et al.* submitted to eLife). **Schema summarizing the main conclusions of the RNA-seq analysis.** Clock disruption leads to an impaired insulin response and a decrease in glucose uptake (**1**), dysregulation of gene involved in vesicle trafficking (**2**) and lipid metabolism (**3**).

6.5.1. Muscle clock disruption impairs glucose uptake in response to insulin

We found that basal and insulin-stimulated glucose uptake were reduced by about 30% upon siCLOCK (**Figure 3D**, Perrin L. *et al.* submitted to eLife). *GLUT4* mRNA followed daily oscillation *in vivo* but not *in vitro*, (Perrin L. *et al.* submitted to eLife). Moreover, *14-3-3θ* (*YWHAQ*) was downregulated upon siCLOCK at the mRNA and protein level by 14.7% and 28%, respectively which might lead to a weaker inhibition of the two Rab-GTPase-activating proteins (Rab-GAPs) TBC1D1 and TBC1D4 (known as AS160) (**Figure 3C**, **Table 1**, Perrin L. *et al.* submitted to eLife), triggering the maintenance of Rabs in their inactive state, and thus blocking GLUT4 movement to the plasma membrane (360-364). Of note, *TBC1D4* (*AS160*) mRNA accumulation was found rhythmic in human skeletal muscle *in vivo* (Perrin L. *et al.* submitted to eLife). Our results are in good agreement with studies demonstrating in muscle-specific *Bmal1* KO or in *Clock*$^{\Delta 19}$ mutant mice, that dysregulation of the clock leads to an impaired insulin-stimulated glucose uptake and glucose metabolism (145, 154, 365).

Despite mice models with whole-body or organ specific core clock gene deletion/mutation induce typical phenotype of metabolic disorder, mostly obesity and/or T2D (157, 186, 188, 221), and that HFD itself disrupts core clock genes expression in mice (190), this direct relationship between clock ablation and the development of a metabolic syndrome has not been well established in human. Two recent studies have characterized the transcriptional program of hSKM isolated from T2D and/or obese subjects (265, 266). A third one has depicted the temporal expression of selected genes by conventional qRT-PCR in hSKM from T2D subjects (344). hSKM derived *in vitro* from muscle biopsies of untrained/trained lean and from T2D or healthy obese subjects, displayed comparable core clock genes expression, except for *REV-ERBα* which presents a reduced rhythmicity pattern, whereas genes involved in carbohydrates and lipid metabolism exhibit various expression profiles depending of the donor characteristics (344). Therefore, it might be relevant to perform deeper large-scale circadian transcriptomic analyses on hSKM taken from T2D and/or obese subjects in order to identify the effects of the pathology on the circadian clockwork.

6.5.2. A functional muscle clock is required for proper myokine secretion

We did not find myokine encoding genes rhythmically expressed *in vitro*, except *SERPINE1*, whereas *FABP3*, *TIMP-1* and *VEGFA* were oscillating *in vivo* (**Supplemental Datasets 1** and **5**, Perrin L. *et al.* submitted to eLife). We identified vesicle associated membrane protein 3 (*VAMP3*) and syntaxin

6 (*STX6*) as downregulated upon siCLOCK *in vitro* (**Table 1, Supplemental Dataset 1**, Perrin L. *et al.* submitted to eLife) in an agreement with the data obtained by us in human islets using a similar approach, and in mouse islets (157, 158). Importantly, VAMP3 and STX6 are required for proper IL-6 secretion by mouse macrophages (366) and by the synovial sarcoma cell line (367). Moreover, *VAMP3* exhibited a rhythmic expression in human skeletal muscle biopsies *in vivo* (Perrin L. *et al.* submitted to eLife). We found that phosphatidylinositol 4-kinase type 2 alpha (*PI4K2A*) was downregulated in siCLOCK-treated myotubes, suggesting that the VAMP3-mediated recycling from plasma membrane might be impaired (**Figure 2**, **Table 1**, Perrin L. *et al.* submitted to eLife). This corroborates a previous study reporting that *PI4K2A* knockdown inhibited VAMP3 trafficking to perinuclear membranes (368). Collectively, our RNA-seq data pinpoint on the exocytosis as a potential regulation site for clock regulation of myokine secretion. To validate this hypothesis, it will be important quantifying exocytosis events by total internal reflection fluorescence (TIRF) microscopy in this system around-the-clock, or in siCLOCK-transfected hSKM. Moreover, siRNA-mediated knockdown experiments for one or several of those genes, followed by perifusion and myokine assessment, could further provide insights into the mechanism of this regulation. Finally, as post-translational modifications can be subjected to circadian regulation, it would be of interest to visualize myokine secretion at the single cell level in synchronized human myotubes using time lapse microscopy, employing a combination of fluorescent dyes labelling the myokine and core clock gene in parallel. Immunofluorescence, co-immunoprecipitation and electronic microscopy might also be useful to assess this mechanism.

6.5.3. Circadian clock regulated lipid homeostasis in human skeletal muscle

Thanks to the developed *in vitro* hSKM model, our group has recently published that 18.6% of lipid metabolites oscillate in human primary myotubes *in vitro* and 20.3% *in vivo* (**Figure 4** from (336)). Employing our siRNA-mediated *CLOCK* knockdown assay, we demonstrated that this rhythmic pattern was abolished under not fully functional clock (**Figure 8** from (336)). Moreover, correlation between temporal expression of enzymes involved in lipid biosynthesis and lipid species, including *UGCG*, *SPTLC2*, *ELOVL5* and *ACSL4*, has been made (**Figures 6** and **7** from (336)).

Based on our RNA-seq data, we confirmed the *in vivo* rhythmic expression of enzymes, such as those mentioned above, and the dysregulation upon siCLOCK of numerous genes involved in lipid metabolism, including *SPTLC3* and *UCGC*, in fatty acid transport, such as *CD36* and *FABP3*, and in

lipolysis with *PNPLA3* (**Figure 2**, **Table S5**, **Supplemental Dataset 1**, Perrin L. *et al.* submitted to eLife). Importantly, these modifications in gene expression resulted in significant alterations in absolute lipid metabolite levels as analyzed by mass spectrometry based lipidomics, with total phosphatidylcholine levels being slightly downregulated, and glycosylceramide levels being upregulated (**Figure 2**, Perrin L. *et al.* submitted to eLife), agreeing with results obtained in *Bmal1*$^{-/-}$ skeletal muscle (146, 369) and liver (137). Altogether, these results suggest a change in energy consumption from glucose utilization toward lipolysis in siCLOCK muscle (140, 145, 146, 154).

6.6. Insulin sensitivity (IS) around-the-clock might suggest different rhythmic phenotypes among human subjects

Since it was demonstrated that the muscle IS and glucose metabolism are controlled by the muscle clock in mice (145), we assessed the ability of forskolin-synchronized hSKM derived from 5 male subjects with matched age and BMI to respond to insulin (100 nM; 10 min) over 24 h with 6 h resolution (**Figure 14A**). Western blots for total AKT and its Ser-473 phosphorylation form were performed (**Figure 14B**). Quantification of these 5 immunoblots revealed 3 patterns of response (**Figure 14C**): 1) IS gradually increased over the 24 h (subjects #1 and #2), reflected by the ratio pAKT/AKT normalized to tubulin; 2) IS decreased during first 12 h, followed by a return nearly to the baseline in the next 12 h (subject #3); and 3) a constant reduction of the IS during first 12 h, after which it remained stable (subjects #4 and #5). Of course, these are only preliminary data, which need careful validation by additional experiments. Interestingly, lipid oscillation patterns also vary among subjects *in vivo*, a phenomenon that persists *in vitro,* in an agreement with a previous report in human plasma (150) arguing for the existence of distinct diurnal metabolic phenotypes within the human population (336). Such diversity of metabolic responses observed even *in vitro,* where all conditions are controlled and core clock genes are well synchronized among the different cell cultures, as confirmed by qRT-PCR or RNA-seq, suggests an additional level of complexity for the regulation of metabolic outputs of the cell-autonomous clocks, that remains to be unraveled.

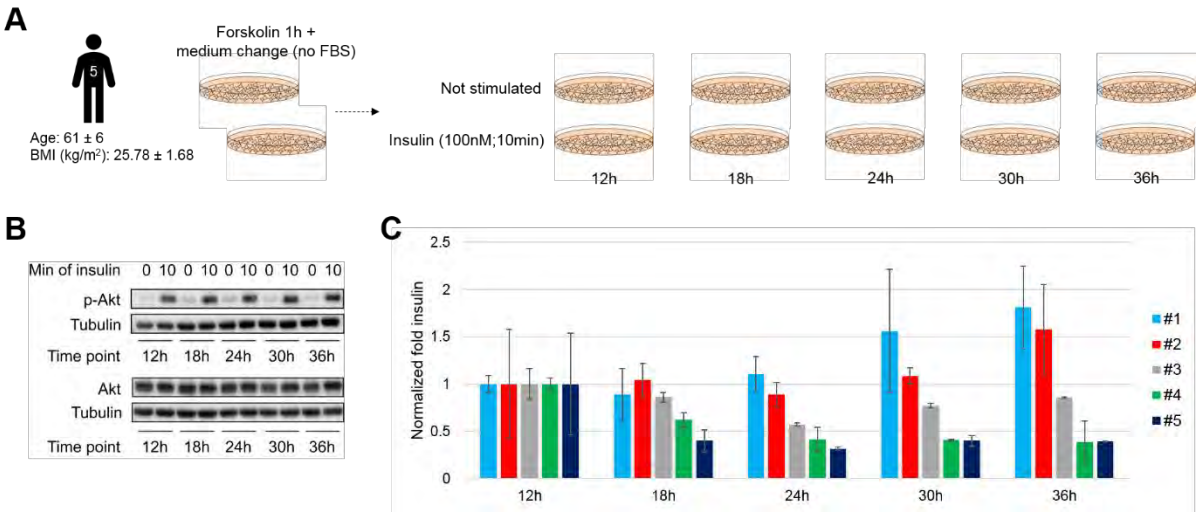

Figure 14. Insulin sensitivity assessed around-the-clock identified 3 metabolic phenotypes among the human subjects. (**A**) hSKM were derived from five male subjects with matched age and BMI (mean ± SD). After 7 to 10 days of differentiation, human primary myotubes were synchronized with a forskolin pulse for 1 h then medium was replaced by fresh one without FBS. Insulin stimulation (100 nM for 10 min) was applied on samples every 6 h over 24 h, from time point 12 h to 36 h. Duplicate dishes were used for each condition and proteins were collected by cell lysis in a RIPA buffer containing PBS Ca/Mg-free, 1% NP 40, 0.5% sodium deoxycholate, 0.1% SDS, 1% EDTA 5 mM, 1% Na_3VO_4 1 mM, 4% NaF 20 mM, 0.1% DTT 1 mM and 0.1% protease inhibitor. Lysates were collected, vortexed, kept 10 min on ice, centrifuged at 10'000g at 4°C during 10 min and supernatant was kept at -80°C. (**B**) Representative SDS-PAGE gel for pAKT and total AKT. Tubulin was used as a loading control. Insulin stimulation triggers phosphorylation of AKT on Ser-473, a downstream effector of the insulin signaling pathway. (**C**) Immunoblot quantification of the pAKT/AKT total ratio. Individual profiles of the 5 subjects show 3 types of response, with subjects #1 and #2 exhibiting an increased insulin sensitivity across 24 h, subject #3 presenting an intermediate phenotype with reduced response to insulin at time point 24 h followed by return to baseline. Finally, insulin response of subjects #4 and #5 was decreasing until time point 24 h, then remained stable. Data are mean ± SD, normalized to tubulin.

6.7. The circadian clock might be dysregulated in pathological R-SMCs

The present methodology has been employed for characterization of the circadian rhythm in primary porcine S-SMCs (normal condition) or pathological R-SMCs. Using bioluminescence recording, we have observed that the period length of *Per2-luc*-transduced R-SMCs was significantly longer than in normal S-SMCs (**Figure 9**). Our preliminary data further confirmed the dysregulation of almost all core clock genes expression (**Figure 10A**). Clear upregulation and/or phase shift were observed as principal differences between S- and R-SMCs. Some interesting candidates were also tested by qRT-PCR (331). Specific expression levels were found in each cell type, with *S100A4* and *TIMP-3* largely expressed in R-SMCs, and *SMMHC*s and *SM22-α* more expressed in S-SMCs (**Figure 10B**). *TIMP-3* and *C-myc* might follow daily rhythm at the mRNA level in rhomboid or spindle cells, respectively (**Figure 10B**). We used PDGF-BB or FGF-2 treatment of S-SMCs to induce phenotypical switch toward rhomboid-like SMCs as seen by immunofluorescence with the upregulation of S100A4 and the reduction of α-SMA (**Figure 11A** and **D**). *Per2-luc* period length was also significantly longer in cells treated by these two compounds, whereas *Bmal1-luc* period length exhibited a tendency to the same result without reaching statistical significance (**Figure 11B-C** and **E-F**).

Circadian core clock genes expression was already described in human SMCs derived from healthy carotid area or from atheromatous plaque, synchronized by a serum shock (333). The expression levels of these core clock genes were significantly attenuated in human plaque-derived SMCs as compared with normal human carotid SMCs, contrasting with our results (**Figure 10A**). For instance, *CRY1* mRNA expression was significantly decreased in atherosclerotic patients compared to the healthy subjects (370), whereas we found a significant increase of *CRY1* mRNA during its peak of expression in rhomboid SMCs. This might promote the process of atherosclerosis (333) as circadian oscillation in glucocorticoids, catecholamines, blood viscosity, and platelet reactivity correlate with plaque rupture and thrombus formation in the early morning hours in humans (371). Moreover, 15 years ago, several studies have reported the presence of a functional circadian clock in the vasculature with 5% to 10% of the transcriptome, exhibiting circadian expression patterns in mouse aorta (372). Diurnal core clock genes and target genes expression, including *Timp-1*, *Timp-3* and *Sm22α,* were found in mouse smooth muscle cell line Movas-1 and *in vivo* in mouse aortic tissue (332). In our model, *TIMP-3* expression appears to be rhythmic in R-SMCs but not in S-SMCs, whereas *SM22α* does not show circadian rhythm (**Figure 10B**). Furthermore, circadian clock dysfunction, induced in *Bmal1* KO and *Per*-triple KO mice, contributes to the hardening of arteries, possibly due to an increased expression and activity of matrix metalloproteinase (MMP)-2 and -9 and collagen deposit in the media of remodeled arteries (373).

Metabolic disorders including T2D and obesity impact the rhythmic expression of core clock genes and genes involved in contraction both *in vivo* and in cultured SMCs isolated from mouse aorta (374, 375). In addition, human plaque-derived SMCs have high intracellular cholesterol content that might lead to alteration in clock genes and CCGs rhythmic expressions (376). We also found that *C-myc* expression might follow rhythmic oscillations in S-SMCs but not in R-SMCs.

Numerous studies have shown that the circadian clock regulates the checkpoint transition during cell cycle (377-383). *C-myc* plays a critical role in cell proliferation and negatively regulates BMAL1 by binding to E-box domains, causing disruption of normal circadian gene expression (384). In addition, CRY2 was identified to induce degradation of *C-myc* (385). Therefore, future experiments are required to confirm the possible alteration of the circadian clockwork in porcine R-SMCs compared to S-SMCs, and to unravel the link between circadian clock, *C-myc* and atherosclerosis development by screening for additional target genes specific to each phenotype employing qRT-PCR or RNA-seq. As S100A4 is

also secreted and triggers phenotype switch toward rhomboid-like cells (331), examining additional secreted protein using the perifusion system would represent another serious interesting option. Our methodology would also be applied on porcine SMCs treated with PDGF-BB or FGF-2, as our preliminary data are in line with those obtained in native R-SMCs (**Figure 11**).

6.8. Significance of the developed methodology

6.8.1. *In vitro* models allow for studying peripheral clocks in human individuals

Growing evidences have been discovered linking the circadian clock perturbations and metabolic diseases as well as cancer in humans (177, 179, 184, 386, 387). Importantly, because correlation between the clock characteristics *in vitro* and the *in vivo* circadian phenotype has been observed (56), the use of human primary cultures to examine peripheral clock properties may represent the utmost approach for better understanding the potential clock connection to these diseases. Although *in vitro* study does not represent the complex regulation of circadian rhythm occurring at the whole-body level, as for instance we found 14-fold more rhythmic genes in human skeletal muscle *in vivo* than *in vitro,* suggesting that circadian expression is mainly due to rest/activity cycle, it allows to examine the function of an autonomous clock on cellular metabolism under controlled conditions.

6.8.2. siCLOCK knockdown as a model of perturbed circadian clock

The here established *in vitro* model for efficient *CLOCK* silencing based on siRNA technology, affects both bioluminescence profile, which results in its flattening, and endogenous gene expression (**Figure 2** from (10), **Figure 8A** from (336)). The difference of the promoter length between the *Bmal1-luc* reporter and the endogenous *BMAL1* gene, might explain the divergence observed between bioluminescence experiments, where the flattening of the *Bmal1-luc* profile occurred essentially after 48 h, and qRT-PCR results. Moreover, Baggs J. E. and colleagues have shown similar results, arguing in favor of redundant roles occurring at the core clock gene expression to maintain the clock functionality (91). Such compensatory mechanism has also been reported in *Clock*$^{-/-}$ mice, where the upregulation of *Npas2* in the SCN allowed maintenance of circadian rhythm at the behavioral and molecular level (92). Of note, CLOCK protein is unable to enter into the nucleus without binding to BMAL1 (388), nonetheless the reverse is false, as BMAL1 can translocate into the nucleus with very low efficiency even in the absence of CLOCK (93), possibly by binding to NPAS2 (165). Liver and lung of *Clock* mutant mice still

exhibit oscillations during the first 24 h followed by a fast desynchronization, suggesting that increased levels of *Npas2* are not sufficient for maintaining proper clock function in peripheral organs (93, 389).

Of note, this model allowed our group to published articles using human pancreatic islets cells and human skeletal muscle. The study of Saini C., Petrenko V., Pulimeno P. *et al.* (158) demonstrated that ablation of the circadian clock in human islets cells caused a significant decrease in both acute and chronic glucose-stimulated insulin secretion as well as a perturbed basal insulin secretion after *in vitro* synchronization, which presented a circadian profile in siControl condition. The recent study of Loizides-Mangold U. *et al.* (336) has shown that lipid metabolites exhibited a circadian pattern possibly due to the circadian control of several enzymes involved in lipid biosynthesis in human skeletal muscle *in vivo* and *in vitro*. Thus, siRNA-mediated *CLOCK* silencing is a powerful tool to disrupt the oscillator in primary cells or cell lines, since similar disruption is likely to occur in humans with the ageing process (184).

6.8.3. Perifusion system: a valuable tool for the hormone secretion studies

The here described methodology based on horizontal perifusion system connected to a Lumicycle allows for simultaneous and continuous analysis of circadian rhythm, paralleled by the hormone secretion profile assessment within the same cells. The perifusion system can be easily employed to analyze different secreted substances comprising proteins and miRNAs, such as insulin, glucagon, adipokines or thyroid hormones, by almost all cell types in culture *in vitro*, such as primary pancreatic islets cells, adipocytes or thyrocytes (312). Moreover, these settings could be adapted to the secretion study lasting for several days, independently of the circadian rhythm, and for studying kinetics and evaluating effects of a substance on a precise cell type. The impact of physiological and/or pharmacological compounds, as well as conditioned medium, on cellular circadian clock function and secretion could be examined as well as the compound of interest could be applied either continuously or at chosen time point for an acute application. Further technical improvements of this machine could be addition of a system allowing synchronization by temperature cycles, to avoid overstimulation of some pathways due to synchronization protocol by the pulses of distinct compounds (17, 34, 35). Also, an increase of the dishes number that can be proceeded at the same time would offer new perspectives, as multiple treatments can be assessed in parallel with adequate controls, limiting technical variations in the measures. *In vitro* system offers the advantage to work on isolated material under controlled conditions, which may help to identify precise mechanisms by which the circadian clock regulates the

metabolism, however results should be put in perspective of the whole-body complexity and regulation. Thus, our perifusion system represents a novel tool that allowed us interesting discoveries, and that has powerful abilities for a broad range of utilizations.

6.9. Conclusions and perspectives

The present study provides new insights into the circadian regulation of human skeletal muscle metabolism, which was allowed due to the development of powerful methodology, including circadian bioluminescence studies in cultured primary hSKM, horizontal perifusion system allowing for assessment profiles of myokine secretion, and employment of high throughput techniques for RNA and lipid analyses. Examining circadian clockwork on human and porcine tissues *in vivo* implies obvious limitations, due to requirement of serial sampling across 24 h, therefore our experimental approach of studying primary cultured cells synchronized *in vitro* represents a unique alternative for getting mechanistic comprehension into molecular clock and its functional outputs. Moreover, the experiments in *in vitro* cellular system are done in isolated cells and in controlled conditions, thus allowing to dissect the effects of cell-autonomous clocks from those related to feeding-fasting and rest/activity cycles, impossible endeavor when employing *in vivo* collected sets of tissue biopsies. Of note, hSKM derived from T2D donors have been shown to keep their *in vivo* phenotype of inflammation and insulin resistance even in culture *in vitro* (354). T2D seems to promote an altered myokine secretion *in vitro* and higher myokine plasma levels *in vivo* (302, 351-359). For instance, higher levels of SERPINE1 were found in diabetic patients (390, 391), and were associated with common vessel pathologies/complications linked to T2D progression (392). High levels of SERPINE1 were also linked to muscle atrophy (393) and SERPINE1 inhibition improved skeletal muscle regeneration in type 1 diabetes rodent models (394, 395). Employing our perifusion system, we would be able to provide additional knowledge regarding the basal myokines secretion of hSKM from normoglycemic and T2D subjects. These thoughts are valuable for hSKM isolated from obese donors. Therefore, human primary cells cultured *in vitro* would represent an excellent model and would be clinically relevant for studying human metabolism and diseases (239, 396).

Importantly, our methodology is not restricted to our hSKM system but can be easily applied to other cell types with other biological question, and the porcine SMC project illustrates well this aspect. Further experiments are required to precise the exact mechanism driving rhythmic basal myokine secretion,

glucose homeostasis, lipid metabolism and regulation of porcine SMC phenotype. Nonetheless, we opened new ways for future studies linking clockwork defects with etiology of T2D, obesity and atherosclerosis, pathologies that are spreading more and more in modern societies (211, 314), to one day provide better therapeutic approach and prevention.

7. APPENDIX

7.1. Lipidomics reveals diurnal lipid oscillations in human skeletal muscle persisting in cellular myotubes cultured *in vitro*

The work presented here allowed the Dr. Ursula Loizides-Mangold to conduct the study of circadian lipidomics in hSKM. I took part in this project during the last three years of my thesis where I performed the research for the *in vitro* part. This work led to a scientific paper in second author entitled "*Lipidomics reveals diurnal lipid oscillations in human skeletal muscle persisting in cellular myotubes cultured in vitro*" that has been published in the Proceedings of the National Academy of Sciences of the United States of America (PNAS) in September 2017 (336).

Lipidomics reveals diurnal lipid oscillations in human skeletal muscle persisting in cellular myotubes cultured in vitro

Ursula Loizides-Mangold[a,b,c], Laurent Perrin[a,b,c], Bart Vandereycken[d], James A. Betts[e], Jean-Philippe Walhin[e], Iain Templeman[e], Stéphanie Chanon[f], Benjamin D. Weger[g], Christine Durand[f], Maud Robert[h], Jonathan Paz Montoya[i], Marc Moniatte[i], Leonidas G. Karagounis[j,k], Jonathan D. Johnston[l], Frédéric Gachon[g,m], Etienne Lefai[f], Howard Riezman[n,o,1], and Charna Dibner[a,b,c,1]

[a]Division of Endocrinology, Diabetology, Hypertension and Nutrition, Department of Internal Medicine Specialties, University of Geneva, CH-1211 Geneva, Switzerland; [b]Department of Cell Physiology and Metabolism, University of Geneva, CH-1211 Geneva, Switzerland; [c]Faculty Diabetes Centre, Faculty of Medicine, University of Geneva, CH-1211 Geneva, Switzerland; [d]Section of Mathematics, University of Geneva, CH-1211 Geneva, Switzerland; [e]Department for Health, University of Bath, Bath BA2 7AY, United Kingdom; [f]CarMeN Laboratory, INSERM U1060, INRA 1397, University Lyon 1, 69600 Oullins, France; [g]Department of Diabetes and Circadian Rhythms, Nestlé Institute of Health Sciences, CH-1015 Lausanne, Switzerland; [h]Department of Digestive Surgery, Center of Bariatric Surgery, Edouard Herriot Hospital, 69003 Lyon, France; [i]Proteomics Core Facility, École Polytechnique Fédérale de Lausanne, CH-1015 Lausanne, Switzerland; [j]Experimental Myology and Integrative Biology Research Cluster, Faculty of Sport and Health Sciences, Plymouth Marjon University, Plymouth PL6 8BH, United Kingdom; [k]Institute of Nutritional Science, Nestlé Research Centre, CH-1015 Lausanne, Switzerland; [l]Faculty of Health and Medical Sciences, University of Surrey, Guildford, Surrey GU2 7XH, United Kingdom; [m]School of Life Sciences, École Polytechnique Fédérale de Lausanne, CH-1015 Lausanne, Switzerland; [n]Department of Biochemistry, University of Geneva, CH-1211 Geneva, Switzerland; and [o]National Centre of Competence in Research Chemical Biology, University of Geneva, CH-1211 Geneva, Switzerland

Edited by Joseph S. Takahashi, Howard Hughes Medical Institute, University of Texas Southwestern Medical Center, Dallas, TX, and approved August 31, 2017 (received for review April 10, 2017)

Circadian clocks play an important role in lipid homeostasis, with impact on various metabolic diseases. Due to the central role of skeletal muscle in whole-body metabolism, we aimed at studying muscle lipid profiles in a temporal manner. Moreover, it has not been shown whether lipid oscillations in peripheral tissues are driven by diurnal cycles of rest–activity and food intake or are able to persist in vitro in a cell-autonomous manner. To address this, we investigated lipid profiles over 24 h in human skeletal muscle in vivo and in primary human myotubes cultured in vitro. Glycerolipids, glycerophospholipids, and sphingolipids exhibited diurnal oscillations, suggesting a widespread circadian impact on muscle lipid metabolism. Notably, peak levels of lipid accumulation were in phase coherence with core clock gene expression in vivo and in vitro. The percentage of oscillating lipid metabolites was comparable between muscle tissue and cultured myotubes, and temporal lipid profiles correlated with transcript profiles of genes implicated in their biosynthesis. Lipids enriched in the outer leaflet of the plasma membrane oscillated in a highly coordinated manner in vivo and in vitro. Lipid metabolite oscillations were strongly attenuated upon siRNA-mediated clock disruption in human primary myotubes. Taken together, our data suggest an essential role for endogenous cell-autonomous human skeletal muscle oscillators in regulating lipid metabolism independent of external synchronizers, such as physical activity or food intake.

lipid metabolism | circadian clock | human skeletal muscle | human primary myotubes | lipidomics

Circadian oscillations are daily cycles in behavior and physiology that are driven by the existence of underlying intrinsic biological clocks with near 24-h periods. This anticipatory mechanism has evolved to ensure that all aspects of behavior and physiology, including metabolic pathways, are temporally coordinated with daily cycles of rest–activity and feeding to provide the organism with an adaptive advantage (1). In mammals, circadian oscillations are driven by a master pacemaker, located in the suprachiasmatic nucleus (SCN) of the hypothalamus, which orchestrates subsidiary oscillators in peripheral organs via neuronal, endocrine, and metabolic signaling pathways (2, 3).

Large-scale gene expression datasets suggest that, in mammals, the vast majority of circadian-gene expression is highly organ-specific (4–6). Key metabolic functions in peripheral organs are subject to daily oscillations, such as carbohydrate and lipid metabolism by the liver, skeletal muscle, and endocrine pancreas (7).

Skeletal muscle is a major contributor of whole-body metabolism and is the main site of glucose uptake in the postprandial state (8). Therefore, perturbations in glucose sensing and metabolism in skeletal muscle are strongly associated with insulin resistance in type 2 diabetes (T2D) (9). Recent data support a fundamental role for the circadian muscle clock in the regulation of glucose uptake, with a significant reduction in *Glut4* mRNA and protein levels in two muscle specific *Bmal1* knockout models (10, 11). In addition, rhythmic genes involved in carbohydrate metabolism were down-regulated while those involved in lipid metabolic processes were up-regulated in mice bearing a muscle-specific *Bmal1* KO (12). In line with these observations, it has been noted that disruption of

Significance

Our experiments provide the analysis of lipid metabolite circadian oscillations in a cellular system synchronized in vitro, suggesting cell-autonomous diurnal changes in lipid profiles independent of feeding. Moreover, our work represents a comprehensive comparison between the lipid composition of human skeletal muscle derived from sedentary healthy adults, receiving hourly isocaloric solutions, and human primary skeletal myotubes cultured in vitro. A substantial number of lipid metabolites, in particular membrane lipids, exhibited oscillatory patterns in muscle tissue and in myotube cells, where they were blunted upon cell-autonomous clock disruption. As lipid oscillations in skeletal muscle membrane lipids may impact on insulin signaling and on the development of insulin resistance, studying the temporal lipid composition of human muscle is therefore of utmost importance.

Author contributions: U.L.-M., J.A.B., J.D.J., F.G., E.L., H.R., and C. Dibner designed research; U.L.-M., L.P., J.-P.W., I.T., S.C., B.D.W., C. Durand, M.R., and J.P.M. performed research; J.P.M., M.M., and L.G.K. contributed new reagents/analytic tools; U.L.-M. and B.V. analyzed data; and U.L.-M. wrote the paper.

Conflict of interest statement: B.D.W. and F.G. are employees of Nestlé Institute of Health Sciences SA; L.G.K. is an employee of Nestec Ltd. J.A.B. has been a consultant for PepsiCo (Quaker) and Kellogg's. The other authors have no conflict of interest to declare.

This article is a PNAS Direct Submission.

Freely available online through the PNAS open access option.

[1]To whom correspondence may be addressed. Email: Howard.Riezman@unige.ch or charna.dibner@hcuge.ch.

This article contains supporting information online at www.pnas.org/lookup/suppl/doi:10.1073/pnas.1705821114/-/DCSupplemental.

circadian rhythmicity is associated with hyperlipidemia and hepatic steatosis in *Clock*Δ*19* mice (13), with obesity in mice that bear an adipocyte-specific deletion of *Bmal1* (14), and with reduced whole-body weight and reduction of total triglycerides and fatty acids in blood plasma of *Per2*-deficient mice (15).

Lipidomic analysis of liver from WT and clock-disrupted *Per1*/*Per2* KO mice demonstrated a comparable fraction of oscillating lipids in the presence or absence of a functional clock. However, substantial differences in their composition and peak phase of oscillation were observed, suggesting that both endogenous clocks and fasting–feeding cycles contribute to the observed profile (16). Furthermore, quantitative characterization of the nuclear and mitochondrial lipidome of mouse liver uncovered daily lipid oscillations with distinct phases in these intracellular organelles (17).

In humans, diurnal variations in glucose tolerance have long been described (18), and rhythmic profiles of plasma glucose, insulin, and triglycerides have been detected (19, 20). Furthermore, a lipidomic analysis of human plasma has shown that ∼18% of all lipid profiles oscillate in a circadian manner independent of sleep and food intake (19). Similarly, metabolomics studies of plasma, saliva, and urine revealed that around 20% of all identified metabolites, among them many fatty acids, were oscillating (21–23).

Fasting–feeding cycles accompanying rest–activity rhythms represent major timing cues in the synchronization of peripheral clocks (24). However, whether lipids in peripheral tissues oscillate in a cell-autonomous manner has not yet been resolved. As the existence of self-sustained circadian oscillators operative in human primary skeletal myotubes established from muscle biopsies, cultured and synchronized in vitro, has been recently demonstrated (25–27), we sought to address this question. In this study, we explored the regulation of lipid metabolite oscillations in human skeletal muscle in vivo and in vitro, focusing on lipids involved in membrane organization (phospholipids and sphingolipids) and those involved in energy metabolism, such as triglycerides. Serial human muscle biopsies were analyzed, using a controlled protocol designed to minimize the effect of confounding factors, and were compared with primary myotubes established from human donor biopsies. Using a large-scale lipidomic approach, we monitored the time course of skeletal muscle lipid metabolites under physiological conditions and under siRNA-mediated cellular clock disruption, allowing us to dissect the impact of the cell-autonomous muscle clock from external factors.

Results

The Temporal Lipidome of Human Skeletal Muscle in Vivo. To investigate the time course of lipid metabolites in human skeletal muscle, we analyzed serial biopsies from the *vastus lateralis* muscle, taken every 4 h across 24 h (Fig. 1*A*). Samples were obtained from 10 healthy volunteers (see *SI Appendix*, Table S1 for donor characteristics), using a controlled protocol designed to minimize the effect of confounding factors (*SI Appendix*, *SI Materials and Methods*). Blood samples were drawn every hour, starting on the testing day over a span of 24 h. Plasma concentration profiles of melatonin and cortisol were highly synchronized across subjects, with the melatonin zenith reached at 0300 hours ± 38 min (SD) and the cortisol nadir at 0000 hours ± 40 min (SD) (Fig. 1*B*).

Using a targeted lipidomics-based approach, we next examined the diurnal profiles of triacylglycerides (TAGs), glycerophospholipids (PLs), and sphingolipids (SLs) in human skeletal muscle. Out of

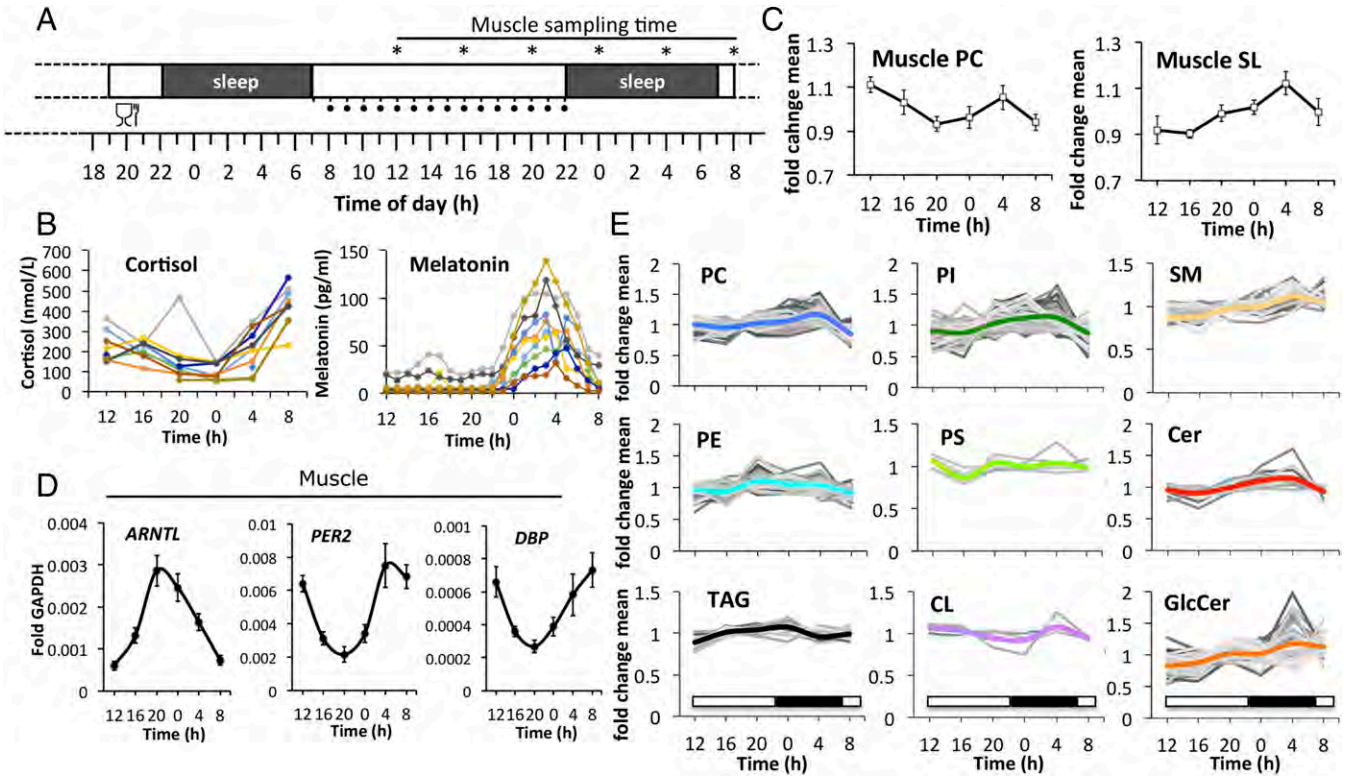

Fig. 1. Temporal analysis of human skeletal muscle lipids in vivo. (*A*) Experimental design for the collection of muscle tissue samples (*vastus lateralis*) from healthy human subjects (n = 10, asterisks indicate muscle-sampling times). One standardized meal was provided on the evening before the testing day, as illustrated. The hourly intake of isocaloric solutions during the testing day is indicated by black dots. For protocol details, see *Materials and Methods* and *SI Appendix, SI Materials and Methods*. (*B*) Time course of plasma cortisol (*Left*) and melatonin (*Right*). (*C*) Temporal profiles of major PC species (*Left*; mean ± SEM, n = 10) and major SLs (*Right*, mean of total GlcCer, SM, Cer ± SD). (*D*) RT-qPCR results for *ARNTL*, *PER2*, and *DBP* on mRNA samples extracted from human skeletal muscle biopsies. Data were normalized to *GAPDH* (mean ± SEM). (*E*) Temporal profiles of lipid metabolites clustered by lipid class. Only lipid species that were detected in all participants are shown. Values were normalized to the lipid mean value per individual analysis and then averaged across all subjects (n = 10) for each time point. The thick colored line represents the average of each lipid class.

1,058 lipid metabolites analyzed, 532 lipids were detected in all participants at all time points (32 TAGs, 181 SLs, and 319 PLs). Lipid raw data were normalized to the phosphorus content of each lipid extract to correct for differences in the amount of starting material. Each lipid value was then divided by its daily mean value, calculated individually for each biopsy. Examples of normalized and unnormalized lipid profiles are shown in *SI Appendix*, Fig. S1. Normalized lipid values were averaged for each time point across all donors (n = 10). The major phosphatidylcholine (PC) profile, representing the most abundant PC lipids, as well as the major SL profile, representing the most abundant sphingomyelins (SMs), ceramides (Cers), and glycosylceramides (GlcCers), showed enrichment at 0400 hours (Fig. 1*C*). The SL profile varied up to 20% in amplitude across 24 h, with the valley reached at 1600 hours and the peak reached at 0400 hours (Fig. 1*C*). In parallel to the lipidomic analysis, core clock transcript levels were monitored by quantitative reverse transcription PCR (RT-qPCR), with RNA extracted from the same human skeletal muscle biopsy material. As shown in Fig. 1*D*, core clock transcript expression was highly rhythmic, with *ARNTL* (*BMAL1*) exhibiting an oscillatory profile antiphasic to *PER2* and *DBP*. The zenith of *ARNTL* expression was reached around 2000 hours, preceding the 0400 hours peak of PC and SL lipid accumulation by about 8 h.

Next, all lipid metabolite profiles, including low abundant lipids, were clustered by lipid class (Fig. 1*E* and Dataset S1). Phosphatidylinositol (PI), PC, SM, GlcCer, and Cer lipids exhibited peak levels around 0400 hours while phosphatidylethanolamine (PE), phosphatidylserine (PS), and TAG levels peaked at earlier time points, with zeniths reached on average at 2000 hours and 0000 hours, respectively (Fig. 1*E* and Dataset S1). Overall, lipid levels changed more than 20% over the course of 24 h, with variability observed among lipid classes (Fig. 1*E* and Dataset S1).

Lipidomes of Human Skeletal Muscle and Primary Myotubes Are Comparable, with Main Differences Seen for CL and PS. We next aimed to assess whether the in vivo lipid oscillations, observed in skeletal muscle biopsies, persist in vitro. To this end, human primary myoblasts were established from skeletal muscle biopsies (*gluteus maximus*) obtained from 10 healthy donors (see *SI Appendix*, Table S2 for donor characteristics). Cells were synchronized in vitro with a pulse of forskolin, and samples were collected every 4 h over 24 h, as shown in Fig. 2*A*.

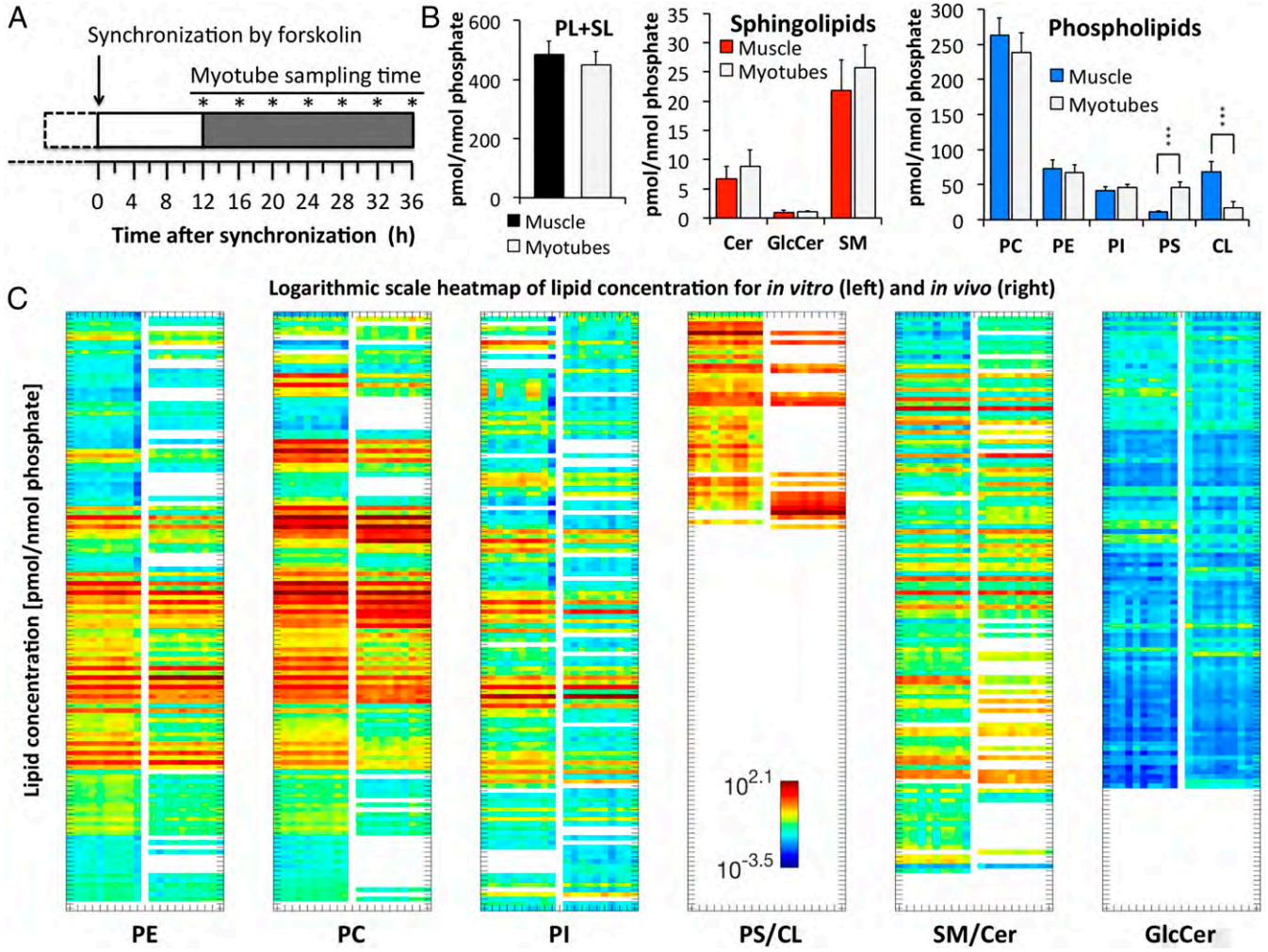

Fig. 2. Comparison between the lipidome of human skeletal muscle and primary myotubes. (*A*) Experimental design: Human primary myoblasts were differentiated into myotubes, synchronized with forskolin, and harvested at the indicated seven time points (asterisks). (*B*) Lipid concentrations of muscle tissue and myotubes; Sum of PL plus SL (*Left*), SL (*Middle*), PL (*Right*). Data represent the average across all time points. Mean ± SD; ***P < 0.001. (*C*) Logarithmic scale heat map of lipid concentration (pmol/nmol phosphate), shown for in vitro (n = 10) and in vivo (n = 10). Lipids were sorted by lipid class (PE, PC, PI, PS, CL, SM, Cer, and GlcCer) and lipid name, and separated for each lipid class into two columns (left columns, in vitro; right columns, in vivo). Data represent the mean concentration of each metabolite across all time points per individual participant. Colors indicate the log concentration of each metabolite.

Out of 1,058 analyzed lipid metabolites, 637 were detected in all myotube cultures at all time points (20 TAGs, 215 SLs, 402 PLs). When averaged across all time points, lipid levels were comparable between human skeletal muscle and primary myotubes. Combined PL and SL levels (Fig. 2 *B*, *Left*), as well as SL levels alone (Fig. 2 *B*, *Middle*), were not significantly different. However, a decrease in mitochondria-specific cardiolipin (CL) and an increase in PS were observed in human primary myotubes compared to muscle tissue (Fig. 2 *B*, *Right*). Overall, the lipid composition was highly homogenous among the 10 muscle and primary myotube samples but differed with regard to lipid chain length and degree of desaturation (Fig. 2*C* and Dataset S2). The strongest difference was observed for CLs, where the most abundant CL of skeletal muscle (CL72:8_C18:2) was not detected on average in primary myotubes (Fig. 2*C*, *SI Appendix*, Fig. S2, and Dataset S2). TAGs were not absolutely quantified but analyzed in a relative manner, and are therefore not included in Fig. 2 *B* and *C*.

Lipid Metabolite Oscillations Persist in Vitro in Synchronized Human Myotubes. Human primary myotube lipids were analyzed as described for the in vivo analysis (for normalization, see *SI Appendix*, Fig. S3). To monitor core clock properties in synchronized human primary myotubes, circadian bioluminescence was continuously recorded for several days, using a lentiviral *Bmal1-luc* reporter (27). *Bmal1-luc* reporter profiles recorded from all 10 myotube cultures demonstrated a high degree of alignment (Fig. 3*A*). The first peak of *Bmal1-luc* reporter activity was observed about 8 h after forskolin synchronization (Fig. 3 *A*, *Inset*), and as previously demonstrated for endogenous *BMAL1* in human primary myotubes (27). The *Bmal1-luc* reporter activity peak recorded 8 h after synchronization (Fig. 3*B*) was followed about 8 h later by a peak of the most abundant PL and SL lipids. This phase coherence was consistent with human skeletal muscle (Fig. 1 *C* and *D*). The most abundant PC lipids also exhibited enrichment at the 16-h time point; however, a second peak was observed 28 h following synchronization (*SI Appendix*, Fig. S4).

When temporal profiles of lipid metabolites were averaged across all myotube cultures, individual lipid profiles were oscillating for each lipid class (Fig. 3*C* and Dataset S3). However, the amplitude of the mean (colored lines in Figs. 1*E* and 3*C*) was smaller in vitro than in vivo for some lipid classes (compare PC and PI in Figs. 1*E* and 3*C* and Dataset S3). This observed reduction in fold change might be in part attributed to the weaker effect of in vitro synchronization of primary myotubes by a single forskolin pulse, compared with the combination of central and peripheral synchronizing stimuli driving the skeletal muscle clock in vivo. The average PE, TAG, and CL profiles displayed a single peak 16 to 20 h following synchronization whereas PC and GlcCer profiles peaked twice within a 24-h period, at 16 h and 28 h, respectively (Fig. 3*C* and Dataset S3).

A Similar Percentage of Lipid Metabolites Exhibit Circadian Oscillations in Vivo and in Vitro. We next identified rhythmic lipid metabolites in human skeletal muscle and primary myotubes based on individually analyzed lipid profiles, using a widely used nonparametric algorithm, JTK_CYCLE (28). As the in vivo sample collection was incomplete (55 out of 60 samples were available), the calculation could only be performed on the basis of seven subjects for whom complete datasets were available. The percentage of circadian lipids per lipid class was determined as the number of cycling lipids vs. the total number of lipids detected per lipid class, averaged across the seven participants (Fig. 4*A* and Dataset S4). Rhythmic lipids were identified for each lipid class, suggesting a widespread circadian regulation of lipid metabolism (Fig. 4*A* and Dataset S4). A similar analysis was performed for human primary myotubes. Here, the percentage of rhythmic lipids per lipid class was calculated based on seven time points (Fig. 4*B* and Dataset S5). Strikingly, the average percentage of rhythmic lipids across the nine lipid classes was comparable between skeletal muscle and myotubes (12.7% vs. 12.4%, respectively). With regard to specific lipid classes, SM was the most

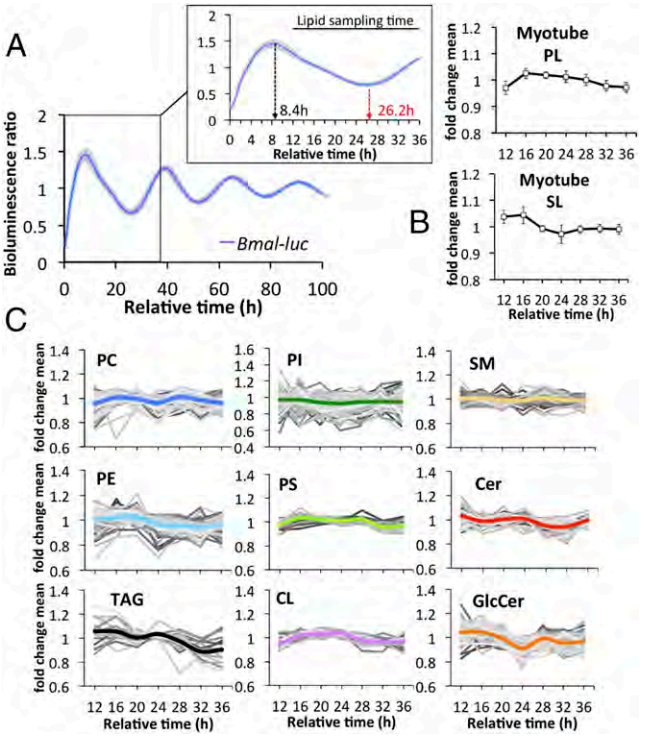

Fig. 3. Lipid oscillations are preserved in human skeletal myotubes. (*A*) Average detrended *Bmal1-luc* bioluminescence profile of all human myotube cultures (n = 10). Mean ± SEM. (*Inset*) *Bmal1-luc* bioluminescence profile between 0 and 36 h. (*B*) Average temporal profile of major phospholipid PC, PE, PI, PS, and CL species (*Upper*; mean ± SD), and major sphingolipid SM, GlcCer, and Cer species (*Lower*, mean ± SD). (*C*) Temporal profiles of lipid metabolites clustered by lipid class. Only lipid species that were detected in all cultures are shown. Values were normalized to the lipid mean value per individual analysis and then averaged across all for each time point. The thick colored line represents the average of each lipid class.

rhythmic one in vivo whereas TAGs were the most rhythmic lipids in vitro (Fig. 4 *A* and *B* and Datasets S4 and S5).

If oscillating lipids were sorted according to their peak phase and plotted for each individual participant separately, the inter-individual variability with regard to the total number of rhythmic metabolites and their phase preference became visible (Fig. 4 *C* and *D* and Datasets S4 and S5). Across all seven in vivo participants, the average percentage of rhythmic lipids in human skeletal muscle was 20.3% (based on the number of cycling lipids vs. detected lipids in each donor). For the in vitro study, the average percentage of rhythmic lipids was 18.6% (based on the number of cycling lipids vs. detected lipids per myotube culture).

The most rhythmic metabolites in vitro were TAG54:6 and GlcCer34:1, significantly oscillating in eight and seven myotube cultures, respectively (Fig. 4 *E*, *Lower*). However, if averaged across all 10 cultures, those lipids were not circadian (Fig. 4 *E*, *Upper*), due to phase differences between individual cultures (Fig. 4 *E*, *Lower*) and noncircadian oscillations in the remaining cultures. In contrast, PE lipids showed a higher degree of alignment, with PE34:4 being rhythmic on average across all myotube cultures and being one of the most rhythmic PE lipids on an individual level (Fig. 4*E* and Dataset S5). The most rhythmic lipids in human muscle and primary myotubes are listed in *SI Appendix*, Table S3.

Metabolic Clustering of Rhythmic Lipid Metabolites. Based on the observed variance within the in vivo and in vitro donor cohorts (Fig. 4 *C* and *D*), we next investigated whether rhythmic lipids can be clustered into different subgroups based on their temporal

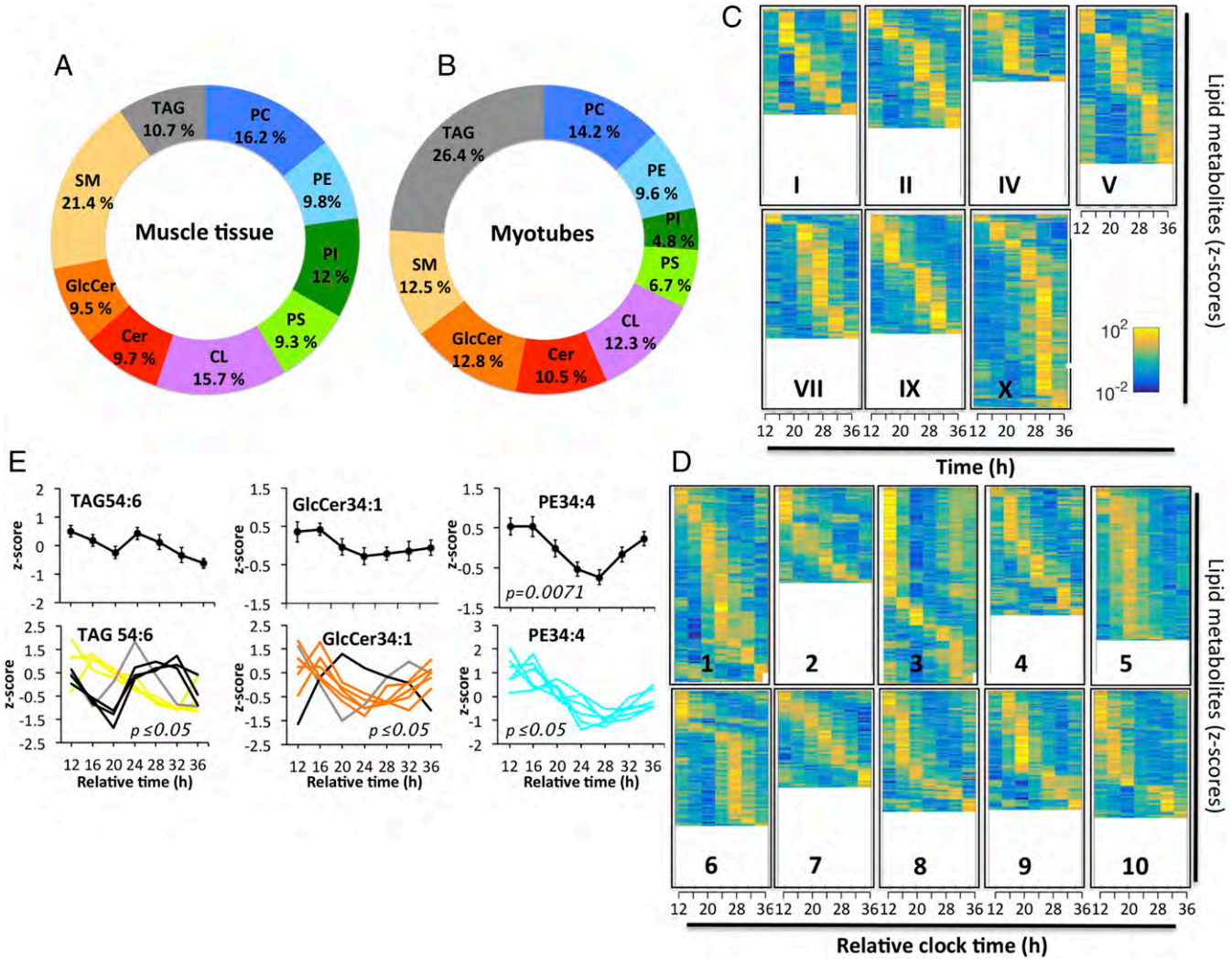

Fig. 4. Identification of rhythmic lipid metabolites in myotubes and skeletal muscle. (*A*) Percentage of diurnal lipid metabolites per lipid class in skeletal muscle ($n = 7$). (*B*) Percentage of circadian lipids per lipid class in primary myotubes ($n = 10$). The average across all lipid classes was 12.7% for skeletal muscle and 12.4% for primary myotubes. (*C*) Heat maps of rhythmic lipids in human skeletal muscle biopsies ($n = 7$). The average percentage of rhythmic lipids was 20.3% across all muscle donors based on the number of cycling lipids vs. detected lipids in each donor. (*D*) Heat maps of rhythmic lipid species in primary skeletal myotubes ($n = 10$). The average percentage of rhythmic lipids was 18.6%. Normalized z-scores of lipid metabolites are indicated in yellow (high) and blue (low). (*E*) Representative rhythmic lipids of skeletal myotube cultures: TAG54:6 (rhythmic in eight cultures), GlcCer34:1 (rhythmic in seven), and PE34:4 (rhythmic in six). (*Upper*) Average lipid profiles (mean ± SEM). (*Lower*) Individual lipid profiles, adjusted *P* value according to JTK_CYCLE.

profile. To assess this point, we applied nearest-neighbor clustering on the phase and amplitude of each profile to identify distinct lipid clusters within one lipid class both in vivo and in vitro. Following this approach, individual PC profiles of skeletal muscle (Fig. 5 *A*, *Left* and Dataset S6) could be separated into two clusters, with a single sinusoid fitted for all profiles in each cluster, exhibiting zenith levels at 1600 hours and 0400 hours, respectively (Fig. 5 *A*, *Right*). Lipid clusters were further dissected by investigating individual lipid metabolites (Fig. 5*B* and Dataset S6). PC32:2, which was identified as highly rhythmic in skeletal muscle upon JTK_CYCLE analysis (rhythmic in five out of seven muscle donors), was not significantly rhythmic if averaged across all participants, due to the phase variance between individual profiles (Fig. 5 *B*, *Top* and *Middle* and Dataset S6). However, individual profiles could be clustered into two major oscillatory subgroups with zeniths reached at 1600 hours and 0400 hours, respectively (Fig. 5 *B*, *Middle* and *Bottom* and Dataset S6).

Similarly, when PC lipids derived from human primary myotubes (Fig. 5 *C*, *Left* and Dataset S6) were analyzed using this algorithm, two major subgroups emerged with zenith levels reached at 16 to 20 h and 28 h after synchronization (Fig. 5 *C*, *Right*). Such clustering was further validated on a single lipid level for the highly rhythmic PC42:6 (Fig. 5*D* and Dataset S6). PC32:2 was less rhythmic in primary myotubes (cycling in 3 out of 10 cultures) but could also be sorted according to phase into two subclusters (*SI Appendix*, Fig. S5*A*).

Overlapping lipid profiles were also observed within other lipid classes, including TAGs. Indeed, the total TAG profile of primary myotubes clustered into two groups, with zenith levels reached at 20 h and 28 h after synchronization (Fig. 5*E* and Dataset S6). TAG52:2 was not rhythmic across all myotube cultures; however, it became rhythmic upon subgroup analysis, with zeniths reached at 20 h and 28 to 32 h after synchronization (Fig. 5*F* and Dataset S6). Due to limitations of the in vivo TAG dataset (lower number of technical replicates), those could not be sorted using the here-described clustering algorithm; however, certain TAG lipids, such as TAG58:9, displayed subgroup oscillations upon individual analysis (*SI Appendix*, Fig. S5*B*).

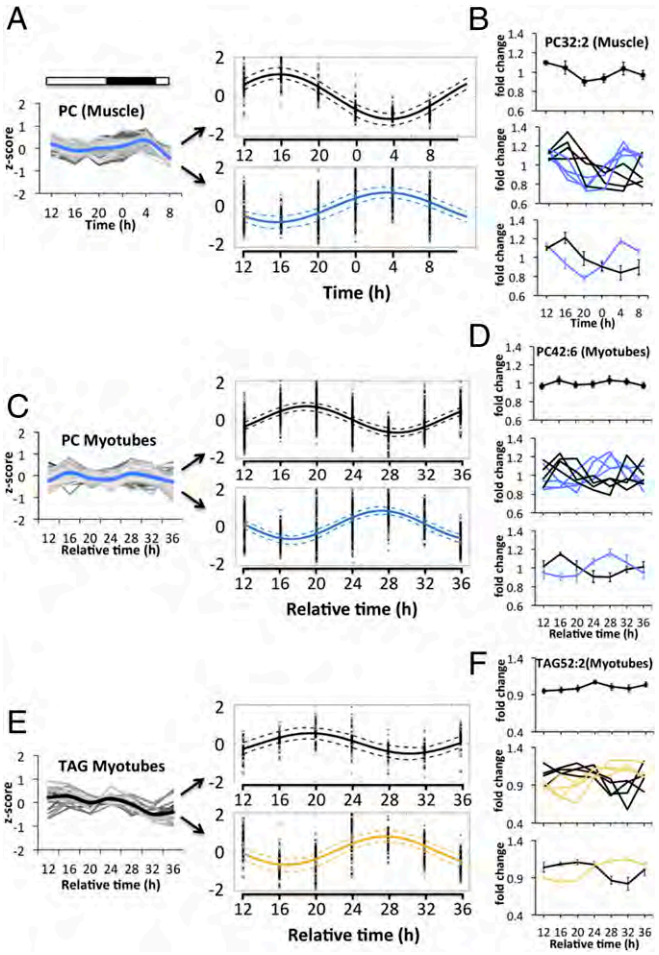

Fig. 5. Overlapping lipid clusters exist within different lipid classes in vivo and in vitro. (*A*) The total PC profile of skeletal muscle (*Left*) can be separated into two major PC clusters (*Right*) with zenith levels reached at 1600 hours and 0400 hours, respectively. The dashed line indicates the 95% confidence interval of the calculated fit. (*B*) PC32:2 is not rhythmic on average across all muscle donors (*Top*) but becomes rhythmic upon subcluster analysis (*Middle* and *Bottom*). (*C*) The total PC profile of human myotubes (*Left*) can be separated into two major PC clusters (*Right*) with zenith levels reached between 16 and 20 h and 28 h after synchronization, respectively. (*D*) PC42:6 is not rhythmic on average across all myotube cultures (*Top*) but becomes rhythmic upon subcluster analysis (*Middle* and *Bottom*). (*E*) The total TAG profile of myotubes (*Left*) can be separated into two major clusters (*Right*) with zenith levels reached at 20 h and 28 h, respectively. (*F*) TAG52:2 is not rhythmic on average across all myotube cultures (*Top*) but becomes rhythmic upon subcluster analysis (*Middle* and *Bottom*).

Diurnal Lipid Metabolite Levels Correlate with Transcript Profiles Encoding for Key Enzymes Involved in Their Biosynthesis. In human skeletal muscle, all three major SL classes (GlcCer, Cer, and SM) reached their zenith levels around 0400 hours (Figs. 1*E* and 6 *A*, *Left*). A similar accumulation pattern was found on a single metabolite level for GlcCer34:1, Cer42:2, and SM42:2 (Fig. 6 *A*, *Middle* and *Right*). Importantly, GlcCer34:1 was also one of the most rhythmic SLs in primary myotubes (Fig. 4*E* and *SI Appendix*, Table S3).

Next, we investigated the temporal gene expression profile of enzymes involved in de novo SL biosynthesis, using the same biopsy material used for the lipidomic analysis. Remarkably, the temporal expression profiles of *SPTLC2* and *UGCG*, coding for subunit 2 of serine palmitoyltransferase and UDP-Glucose ceramide glucosyltransferase, respectively, correlated with the diurnal profiles of the three major SL classes (Fig. 6*B*). The transcripts of both key enzymes of de novo SL biosynthesis reached their peak levels between 0000 hours and 0400 hours, similar to the profile of their corresponding lipid metabolites (Fig. 6 *A* and *B*).

Moreover, we assessed whether a similar correlation could also be made for other lipid classes by analyzing the temporal mRNA profile of choline phosphotransferase 1 (*CHPT1*), involved in PC biosynthesis. While, on average, transcript levels of *CHPT1* exhibited no clear oscillatory pattern (Fig. 6*C*), individually analyzed *CHPT1* transcript levels were oscillating in a subset of muscle biopsy donors with distinct phases (Fig. 6 *D*, *Upper*). Strikingly, the oscillatory transcript expression pattern of *CHPT1* and the diurnal profiles of the most rhythmic PC lipid (PC32:2) were highly similar in a subset of muscle donors (Fig. 6 *D*, *Lower*), with profile II and VIII being significantly correlated.

Chain Length, but Not the Degree of Desaturation, Influences the Circadian Profile of Lipid Metabolites. PC and SM lipid classes share the same head group, phosphocholine, and their biosynthesis pathways are interconnected. We noticed that temporal profiles of PC and SM showed similarities in vivo (Fig. 7*A* and Dataset S7) and in vitro (*SI Appendix*, Fig. S6*A*). When lipid profiles were clustered according to chain length, lipids that carried very long chain fatty acids (PC40-44, SM40-44) were oscillating in a synchronized manner, with zenith levels reached at 0400 hours (Fig. 7*A* and Dataset S7) compared with shorter chain PC an SM species. In contrast, PE lipids were not further synchronized upon lipid elongation. Shorter chain PEs (PE28-32) were well synchronized while very long chain PEs (PE40-44) were less synchronized and not enriched at the 0400 hours time point. Similar observations were made in vitro for PC, SM, and PE lipids of primary myotubes (*SI Appendix*, Fig. S6*A*).

Human long chain acyl-CoA synthetases activate fatty acids to form acyl-CoAs. The activated fatty acids can then be used for the biosynthesis of triglycerides and phospholipids, or for the generation

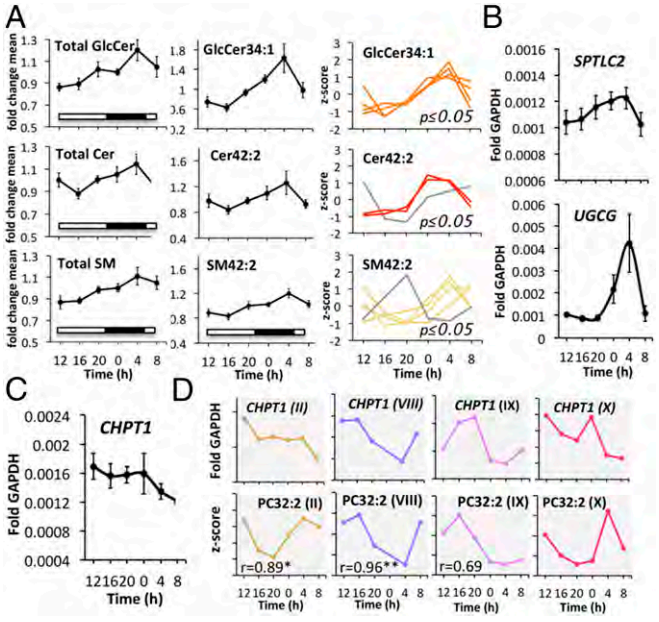

Fig. 6. Temporal lipid profiles and mRNA profiles of genes implicated in their biosynthesis are correlated in vivo. (*A*) Total profiles of GlcCer, Cer, SM (*Left*, mean ± SEM); profiles of GlcCer34:1, Cer42:2, and SM42:2 (mean ± SEM; *Middle*); individual profiles of GlcCer34:1, Cer42:2, and SM42:2 that were identified as circadian (*Right*). (*B*) RT-qPCR gene expression profile of *SPTLC2*, and *UGCG* normalized to *GAPDH* (mean ± SEM). (*C*) RT-qPCR gene expression profile of *CHPT1* normalized to *GAPDH* (mean ± SEM). (*D*) Individual gene expression profile of *CHPT1* normalized to *GAPDH* in four subjects and temporal profile of PC32:2 in the same four subjects. The r numerical value indicates the corresponding Pearson correlation coefficient; $^{*}P < 0.05$, $^{**}P < 0.01$.

of energy via β-oxidation. Moreover, these fatty acyl-CoAs can be elongated by fatty acid elongases (ELOVLs). We therefore investigated the temporal transcript levels of long chain fatty acyl-CoA synthetases (*ACSL3-5*), fatty acid elongase 5 (*ELOVL5*), and acyl-CoA dehydrogenases, responsible for the oxidation of long and very long chain fatty acids (*ACAD* and *ACADVL*). As shown in Fig. 7*B*, *ELOVL5*, *ACSL4*, and *ACSL5* transcript levels oscillate with zenith levels reached at 0400 hours, coinciding with the peak accumulation of very long chain PC and SM lipids (Fig. 7*A*), whereas *ACSL3*, *ACAD*, and *ACADVL* did not oscillate (*SI Appendix*, Fig. S6*B*).

In contrast, the degree of desaturation did not have an effect on lipid rhythmicity, both in vivo and in vitro. Completely saturated lipids, or lipids bearing one or multiple double bonds in their fatty acyl chains, were equally aligned in skeletal muscle and in primary myotubes (Fig. 7*C*, *SI Appendix*, Fig. S6*C*, and Datasets S7 and S9).

Lipid Rhythms Are Driven by the Cell-Autonomous Molecular Circadian Clock. Finally, to investigate the effect of a functional molecular clock operative in human skeletal myotubes on lipid metabolism, we applied an efficient *siClock* transfection protocol, resulting in ∼80% knockdown of *CLOCK* transcript levels (Fig. 8 *A*, *Left*). Circadian amplitude of the *Bmal1-luc* reporter activity profile was strongly blunted in *siClock*-transfected myotubes, compared with cells transfected with nontargeting sequences (*siControl*) in four independent experiments, validating clock disruption (Fig. 8 *A*, *Right*). Following siRNA transfection, human primary myotubes were synchronized in vitro with a pulse of forskolin, and samples were collected every 4 h over 24 h in four independent experiments to monitor the effect of *CLOCK* depletion on lipid metabolite oscillations (see *SI Appendix*, Table S2 for donor characteristics). Importantly, the number of oscillating lipid metabolites was reduced on average for all four myotube cultures by 39.4 ± 7.8% (mean ± SEM) upon *CLOCK* depletion, and as individually shown by heat map analysis (Fig. 8*B* and Dataset S8). The analysis of lipidomic data from three major lipid classes (PC, PE, and SM) by ARSER algorithm (29) suggested a significant reduction in the frequency of oscillations with a period between 20 and 28 h upon *siClock*, as shown by period density plotted against the period length (Fig. 8*C*). Moreover, the mean amplitude of all circadian lipids was reduced in clock-disrupted myotubes, compared with their control counterparts for PC, PE, and SM (Fig. 8*D*).

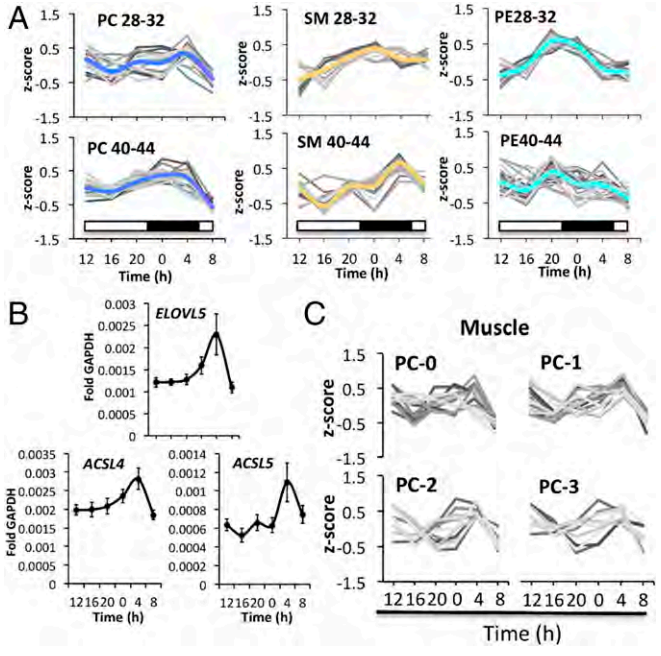

Fig. 7. Lipid chain length but not desaturation influences the circadian profile of PC and SM lipid metabolites. (*A*) Average temporal profile of PC, SM, and PE lipids, sorted by chain length in skeletal muscle ($n = 10$). PC, PE: 28-32 and 40-44 represents the sum of carbon atoms in both fatty acyl chains; SM lipids: 28-32 and 40-44 represents the sum of carbon atoms in the sphingoid base (C18) plus fatty acyl chain. (*B*) RT-qPCR results for *ELOVL5*, *ACSL4*, and *ACSL5* on mRNA samples extracted from human skeletal muscle biopsies. Data were normalized to *GAPDH* (mean ± SEM). (*C*) Average PC lipid profiles (skeletal muscle) sorted by their degree of desaturation. The number of double bonds is indicated by the suffix 0, 1, 2, and 3.

Discussion

This study provides a systematic analysis of lipid metabolite oscillations in human skeletal muscle and in human primary myotubes. Moreover, it represents a comprehensive comparison between the lipid composition of human skeletal muscle in vivo and human primary myotube cells cultured in vitro. Importantly, rhythmic profiles of the lipid metabolites were blunted in myotubes upon clock perturbation, suggesting an essential role of the cell-autonomous oscillators for orchestrating circadian lipidomics.

Globally, lipid quantities were highly comparable between skeletal muscle and human primary myotubes (Fig. 2*B*), with the exception of CL and PS levels (Fig. 2 *B*, *Right*). Muscle biopsy donors were similar with regard to body mass index (BMI) but differed in age and muscle fiber type composition between the in vivo and in vitro cohorts (*SI Appendix*, Tables S1 and S2), as confirmed by myosin isoform analysis (*SI Appendix*, Fig. S7). While biopsies for the in vivo study originated from the *vastus lateralis* muscle (∼43% slow-twitch type I fibers) (30), samples for the in vitro study were established from the *gluteus maximus* that has a higher percentage of slow-twitch type I fibers (52 to 60%) (31).

CL, a lipid exclusively found in mitochondrial membranes, was reduced in human skeletal myotubes compared with muscle tissue (Fig. 2 *B*, *Right*), implying that the overall number of mitochondria is diminished in cell culture compared with muscle tissue, similar to mouse skeletal muscle and C2C12 myotubes (32). This effect might have been further enhanced by aging (33), due to the significant age difference between the older in vitro and younger in vivo cohorts in our study. Moreover, cells in culture rely mostly on glycolysis, leading to a further reduction in mitochondrial respiration (34). Additionally, a significant increase in PS was observed in primary myotubes compared with muscle tissue (Fig. 2 *B*, *Right*). Mammalian skeletal muscle is formed by the proliferation, differentiation, and fusion of myogenic precursor myoblast cells into multinucleated myotubes, and PS greatly enhances this fusion event (35, 36).

Overall, the lipid composition was more complex in primary myotubes (637 species) compared with skeletal muscle (532 metabolites), in particular for the lipid class of PCs (Fig. 2*C*). The fatty acid composition of skeletal muscle is reflected by the dietary intake of lipids in humans (37). The same holds true for the fatty acid composition of cells in culture where changes in serum influence the lipid composition of established cell lines. Of note, FBS is enriched in arachidonic (C20) and docosahexanoic (C22) acid (38) whereas a standard western diet mostly relies on C16- and C18-containing lipids. Consistently, very long chain PCs (PC40-44), containing C20 and C22 fatty acids in their fatty acyl chains, were highly abundant in primary myotubes, but less abundant or not detected in skeletal muscle (in Fig. 2*C*, compare the left and right columns of the PC heat map).

The data presented here demonstrate diurnal lipid oscillations of 20.3% in human skeletal muscle (Fig. 4). This value is similar to a study in human plasma, which showed 17.8% of oscillating lipid metabolites when analyzed on an individual basis (19). To unravel whether these metabolite oscillations are solely driven by diurnal cycles of rest–activity and food intake, or are controlled in a cell-autonomous manner, we conducted a similar temporal analysis in primary human skeletal myotubes synchronized in vitro. Recent studies conducted in other types of isolated human primary cells have demonstrated that peripheral clocks are functional in vitro, as shown for skin fibroblasts (39), thyrocytes (40), and pancreatic islets

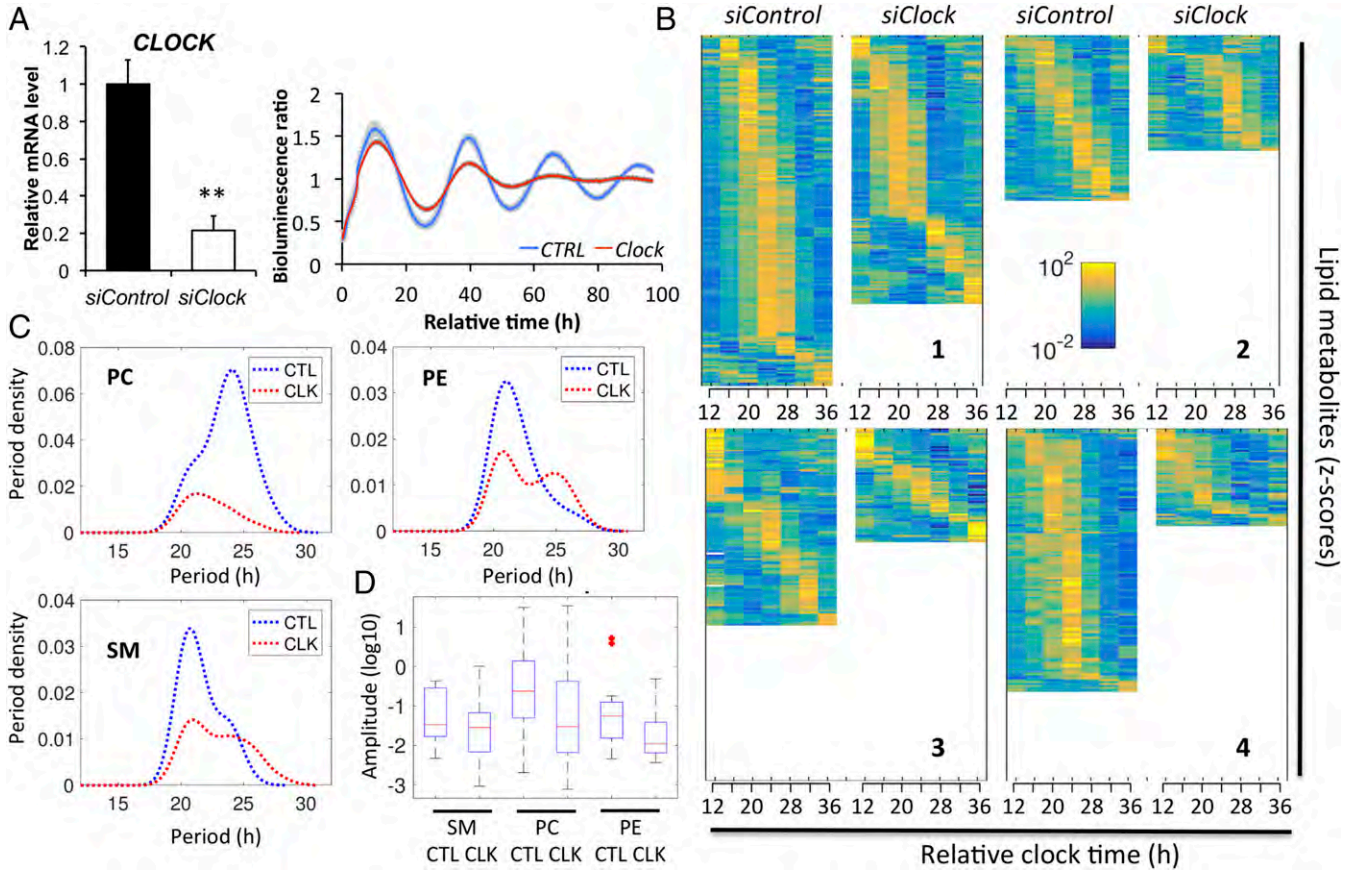

Fig. 8. si*Clock*-mediated clock disruption attenuates circadian lipid oscillations in human skeletal myotubes. (*A*, *Left*) *CLOCK* mRNA was measured in human myotubes transfected with *siControl* or *siClock* by RT-qPCR and normalized to the mean of *9S* and *HPRT* (mean ± SEM, $n = 4$; $^{**}P < 0.01$). (*Right*) Average detrended *Bmal1-luc* bioluminescence profile ($n = 4$, mean ± SEM). Average *Bmal1-luc* oscillation profiles are shown for *siControl* (blue line) and *siClock* (red line) transfected myotubes. (*B*) Heat maps of rhythmic lipid species in primary skeletal myotubes transfected with either *siControl* or *siClock* in donors 1, 2, 3, and 4. Normalized z-scores of lipid metabolites are indicated in yellow (high) and blue (low). (*C*) Distribution of periodicity of oscillating PC, PE, and SM lipids for *siControl* (CTL) and *siClock* (CLK) (ARSER analysis, P value < 0.05). *CLOCK* knockdown induces a shift to include longer periods but mostly reduces the number of cycling lipids overall. (*D*) Box plot of amplitudes for PC, PE and SM raw lipid data for *siControl* and *siClock* of cycling lipids with a period between 22 and 26 (ARSER, P value < 0.05) after log transform. Knockdown lowers the amplitudes, with PC having the most pronounced effect.

(41–43). Moreover, cell-autonomous oscillators of human primary skeletal myotubes have been recently assessed (25–27). Remarkably, we observed that lipid oscillations persisted in human primary myotubes synchronized in vitro, with a comparable percentage of oscillating lipid species (18.6%) (Fig. 4). However, as the in vivo biopsy collection was incomplete, with samples collected at six time points compared with seven time points in vitro, the percentage of oscillating metabolites in muscle tissue might be higher if analyzed in an identical manner. Furthermore, we cannot exclude that the results presented here are in part influenced by differences in fiber type composition between *vastus lateralis* and *gluteus maximus*, as demonstrated by myosin isoform analysis (*SI Appendix*, Fig. S7).

Globally, the percentage of lipid oscillations might even be underestimated as whole-cell lipid measurements can mask oscillations within subcellular compartments. Recent studies by Asher and coworkers identified that 17% of lipid metabolites oscillate when assessed in whole liver (16) whereas separate analyses of liver nuclei and mitochondria identified 34% and 31% of oscillating lipids, respectively, with distinct circadian phases between these organelles (17). However, it should be noted that participants in this study were confined to a semirecumbent position throughout the testing day while, in the mouse liver study, the data were collected from mice freely moving until the sampling point. Given that physical activity can modulate the level and oscillatory parameters of lipids, this may partly account for the observed differences.

The oscillation amplitude of individual lipid metabolite profiles was up to 30% across 24 h both in vivo and in vitro (Fig. 5), similar to previous analyses in mouse liver (17). Whereas such changes in amplitude are smaller than for diurnal transcript oscillations, they represent substantial differences in membrane homeostasis across 24 h.

How transcriptional rhythms are translated into lipid metabolites oscillations has not been addressed so far. Notably, peak levels of major PLs and SLs correlated with *ARNTL* (*BMAL1*) gene expression both in vivo (Fig. 1 *C* and *D*) and in vitro (Fig. 3 *A* and *B*), with phase coherence kept between core clock gene expression and lipid profiles indicating a potential role for the endogenous skeletal muscle clock in the regulation of lipid metabolism. In vivo, lipid levels peaked in the early morning hours, near the usual wake time, supporting a major role for the muscle clock in anticipating sleep-to-wake transition as has been proposed previously (44). To directly test the effect of cell-autonomous oscillators on lipid metabolic changes, we subsequently disrupted the endogenous clock, operative in human skeletal myotubes (27). Clock disruption had a strong impact on lipid metabolite oscillations. The number of oscillating lipid species was significantly reduced upon *CLOCK* depletion, as confirmed by JTK_CYCLE (Fig. 8*B*) and ARSER (Fig. 8*C*) analyses, with a strong impact on both PL and SL metabolites. Furthermore, amplitudes of the remaining oscillating lipid species were reduced (Fig. 8*D*), suggesting an overall blunting of the circadian rhythmicity in the absence of a functional cell-autonomous myotube clock.

Remarkably, zenith levels of enzymes involved in de novo SL biosynthesis (*SPTLC2*, *UGCG*) correlated well with the accumulation of SL species at the early morning hours in human skeletal muscle (Fig. 6). This correlation was not restricted to SLs alone as also the transcriptional regulation of PL biosynthesis showed enrichment at the early morning hours, with peak levels of *ELOVL5*, *ACSL4*, and *ACSL5* transcripts correlating with peak levels of very long chain PC lipids (Fig. 7 *A* and *B*). Although the gene expression profile of choline phosphotransferase 1 (*CHPT1*), which catalyzes PC biosynthesis from CDP-choline, was not rhythmic on average, individual *CHPT1* transcripts oscillated with profiles similar to the most rhythmic PC lipid metabolite in skeletal muscle (PC32:2) in a subset of biopsy donors (Fig. 6*D* and *SI Appendix*, Table S3).

Interestingly, we observed an effect of the circadian clock on lipid chain length but not on desaturation (Fig. 7 and *SI Appendix*, Fig. S6). This effect was characteristic for long and very long chain PC and SM lipids, which were highly synchronized in both skeletal muscle and primary myotubes, whereas other PLs like PE did not show this preference. Remarkably, a correlation based on chain length was also observed for long and very long chain PC and SM species in WT and *Per1/2* KO mice whereas the contribution of desaturation was less prominent (17). Consistent with this observation is the rhythmic gene expression of *ELOVL5*, *ACSL4*, and *ACSL5* in human skeletal muscle tissue, whose peak of expression correlated with peak levels of very long chain PC and SM lipids (Fig. 7 *A* and *B*). Importantly, all seven mammalian elongase family members are either rhythmically expressed or their expression is affected by core clock gene alterations in peripheral mouse tissues, with *Elovl1*, *Elovl5*, and *Elovl6* being circadian in mouse skeletal muscle (5, 12, 45). Moreover, *ACSL4* was shown to be rhythmic in mouse liver, and its rhythmicity was attenuated in *Clock*Δ*19* mutant mice (46). We therefore hypothesize that enzymes involved in long chain fatty acid activation and elongation are important drivers of lipid oscillations. As very long chain PC and SM lipids make up a significant proportion of the outer leaflet of the plasma membrane (47, 48), these data suggest that the circadian clock might impact on plasma membrane function, with important consequences on receptor signaling and membrane glucose uptake.

Fasting–feeding and rest–activity cycles are major timing cues in the synchronization of peripheral clocks (24). The SCN molecular clock communicates with peripheral tissues, such as skeletal muscle, using neurohumoral, metabolic, and temperature signals (49–51). In our in vivo study, core clock alignment was demonstrated by plasma cortisol and melatonin profiles, as well as by muscle core clock gene expression (Fig. 1). In human primary myotubes, highly synchronized *Bmal1-luc* activity profiles showed alignment of the molecular clock also in the absence of the SCN (Fig. 3*A*). However, despite core clock alignment, we observed extensive variability among the individual participants with regard to lipid oscillations. This heterogeneity persisted in vitro, allowing us to identify oscillatory subgroups within different lipid classes (Fig. 5). Such variability with regard to lipid profiles has been previously observed in human plasma (19) and supports the existence of distinct diurnal metabolic phenotypes within the human population, possibly controlled on an epigenetic level.

Taken together, this work is a detailed characterization of the temporal human skeletal muscle lipidome, highlighting the essential role of the molecular oscillator in the circadian orchestration of muscle lipid metabolism. The observed substantial lipid oscillations further contribute to lipid complexity and could affect membrane properties and signaling. Given the current gap in understanding the enormous complexity of cellular lipids, circadian lipidomics may allow deciphering networks of coregulated lipids, due to their temporal regulation. Genetic animal models of clock disruption as well as nutritional studies have shown that the circadian clockwork is associated with altered lipid homeostasis, fatty liver, and obesity (52). Although various clock mutant mouse models exhibit altered lipid metabolism (53), it is challenging to dissect the contribution of the circadian clock on lipid metabolism from the impact of fasting–feeding cycles and rest–activity. In vitro synchronized primary cells may therefore pave the way for future studies that link circadian clock defects to insulin resistance, obesity, and T2D, and constitute a powerful model for studying peripheral oscillators in other human tissues. Of note, human primary myotubes established from donor muscle biopsies preserve their metabolic phenotype with regard to glucose metabolism (54) and insulin signaling (55, 56). As metabolic disorders, including obesity and T2D, are growing rapidly in modern societies (57), future studies aimed at deciphering clock functions in the regulation of lipid metabolism in context of these pathologies are therefore urgently warranted.

Materials and Methods

Human Skeletal Muscle Biopsies for the in Vivo Study. Ten healthy volunteers were recruited for the in vivo study (see *SI Appendix*, Table S1 for donor characteristics). One week before the scheduled laboratory visit, participants had to adhere to a consistent daily feeding and sleeping routine.

Six 100-mg biopsy samples were acquired from the *vastus lateralis* muscle at 4-h intervals (1200, 1600, 2000, 0000, 0400, and 0800 hours) and immediately snap frozen under liquid nitrogen. The study was conducted in accordance with the Declaration of Helsinki and with the approval of the Health Research Authority [National Research Ethics Service (NRES) Committee South West; 14/SW/0123] and the Commission cantonale (Canton de Vaud) d'Éthique de la Recherche (Cer-VD). See *SI Appendix, SI Materials and Methods* for further details of study procedure.

Human Skeletal Muscle Biopsies for the in Vitro Study and Primary Myotube Cell Culture. Muscle biopsies were derived from healthy donors with informed consent obtained from all participants (see *SI Appendix*, Table S2 for donor characteristics). The study conformed to the Declaration of Helsinki and the experimental protocol ("DIOMEDE") was approved by the Ethical Committee SUD EST IV (Agreement 12/111) and performed according to the French legislation (Huriet's law). All donors had HbAc1 levels inferior to 6.0% and fasting glycemia inferior to 7 mmol/L, were not diagnosed for T2D, neoplasia, or chronic inflammatory diseases, and were not doing shift work. Biopsies were taken from the *gluteus maximus* (n = 10) during planned surgeries. Human myoblasts were cultured in growth medium composed of HAM F-10 supplemented with 20% FBS, and 1% penicillin–streptomycin at 37 °C. After reaching confluence, myoblasts were differentiated into myotubes during 7 to 10 d in differentiation medium (DMEM supplemented with 2% FBS). Muscle differentiation was characterized by the fusion of myoblasts into polynucleated myotubes as previously described (27).

In Vitro Skeletal Myotube Synchronization, siRNA Transfection, and Real-Time Bioluminescence Recording. Myotube cells were synchronized by 10 μM forskolin (Sigma) for 1 h once differentiation was achieved. Differentiated human myotubes were transfected with 20 nM siRNA targeting *CLOCK* (*siClock*) or with nontargeting *siControl* (Dharmacon; GE Healthcare), using HiPerFect transfection reagent (Qiagen) 24 h before synchronization, following the manufacturer's protocol. Myotube bioluminescence recording was performed as described in ref. 27 and detailed in *SI Appendix, SI Materials and Methods*.

Quantitative RT-PCR. RNA from human skeletal muscle samples (550 ng) was reverse-transcribed using a SuperScript VILO cDNA Synthesis Kit (Thermo Scientific). mRNA levels were determined by TaqMan real-time qPCR using a LightCycler 480 (Roche) following the manufacturer's instructions. Copy numbers were normalized using *GAPDH*. The following TaqMan probes were used: *PER2*, Hs00256143_m1; *ARNTL*, Hs00253876_m1; *DBP*, Hs00609747_m1; *CHPT1*, Hs01012468_m1; *ELOVL5*, Hs01094711_m1; *SPTLC2*, Hs01027014_m1; *UGCG*, Hs00916612_m1; *GAPDH*, Hs02758991_m1; *ACSL3*, Hs00244853_m1; *ACSL4*, Hs00244871_m1; *ACSL5*, Hs01061754_m1; *ACAD*, Hs00155630_m1; *ACADVL*, Hs00825606_g1; *MYH1*, Hs00428600_m1; *MYH2*, Hs00430042_m1; *MYH4*, Hs00757977_m1; and *MYH7*, Hs01110632_m1.

RNA from human primary myotubes was reverse-transcribed, using SuperScript III reverse transcriptase (Thermo Scientific) and random hexamers, and then PCR-amplified on a LightCycler 480 (Roche). Values were normalized to the mean of two housekeeping genes (*HPRT* and *9S*) as described previously (27).

Lipidomics Analysis. The lipidomics analysis was performed as described in ref. 58 and detailed in *SI Appendix, SI Materials and Methods*.

Data Analysis. Actimetrics LumiCycle analysis software (Actimetrics LTD) was used for bioluminescence data analysis. Normalized lipid values (fold change mean) were defined as the lipid value (phosphate normalized) for each time point divided by the lipid mean value, calculated separately for each donor. To identify circadian variations within the lipidomic dataset, phosphate values were z-scored within subjects and then further analyzed using the JTK_CYCLE (28) and ARSER (29) algorithms. The period width for the JTK_CYCLE analysis was set to fit a time frame of 20 to 28 h and a P value of $\leq$0.05 was considered statistically significant.

Statistical analyses concerning absolute lipid quantities were performed using a paired Student's t test. Differences were considered significant for $P \leq 0.05$ (*), $P \leq 0.01$ (**), and $P \leq 0.001$ (***) if not noted otherwise.

To determine the clustering, k-NN (nearest neighbors with k clusters) was applied to the phases and amplitudes in polar coordinates of all circadian signals for k = 1, 2, and 3 clusters. For further details, see *SI Appendix, SI Materials and Methods*.

ACKNOWLEDGMENTS. We thank Jacques Philippe and Anton Alekseev (University of Geneva) for constructive discussions, Dylan Thompson and Keith Stokes (University of Bath) for their assistance with data collection, and Isabelle Riezman (University of Geneva) for sample processing. This work was funded by Sinergia Swiss National Science Foundation Grant CRSII3-154405 (to H.R., C. Dibner, and E.L.); by Swiss National Science Foundation Grants 31003A-166700 (to C. Dibner) and 310030B_166686 (to H.R.); by SystemsX.ch (evaluated by the Swiss National Science Foundation) (H.R.); by the National Centre of Competence in Research Chemical Biology (H.R.); by the Fondation Romande pour la Recherche sur le Diabète; by the Fondation Ernst et Lucie Schmidheiny; by the Société Académique de Genève (C. Dibner); and by United Kingdom Biotechnology and Biological Sciences Research Council Grant BB/I008470/1 (to J.D.J.).

1. Asher G, Sassone-Corsi P (2015) Time for food: The intimate interplay between nutrition, metabolism, and the circadian clock. *Cell* 161:84–92.
2. Albrecht U (2012) Timing to perfection: The biology of central and peripheral circadian clocks. *Neuron* 74:246–260.
3. Dibner C, Schibler U, Albrecht U (2010) The mammalian circadian timing system: Organization and coordination of central and peripheral clocks. *Annu Rev Physiol* 72:517–549.
4. Storch KF, et al. (2002) Extensive and divergent circadian gene expression in liver and heart. *Nature* 417:78–83.
5. Zhang R, Lahens NF, Ballance HI, Hughes ME, Hogenesch JB (2014) A circadian gene expression atlas in mammals: Implications for biology and medicine. *Proc Natl Acad Sci USA* 111:16219–16224.
6. Panda S, et al. (2002) Coordinated transcription of key pathways in the mouse by the circadian clock. *Cell* 109:307–320.
7. Gachon F, Loizides-Mangold U, Petrenko V, Dibner C (2017) Glucose homeostasis: Regulation by peripheral circadian clocks in rodents and humans. *Endocrinology*, 10.1210/en.2017-00218.
8. DeFronzo RA, et al. (1981) The effect of insulin on the disposal of intravenous glucose. Results from indirect calorimetry and hepatic and femoral venous catheterization. *Diabetes* 30:1000–1007.
9. Muoio DM, Newgard CB (2008) Mechanisms of disease: Molecular and metabolic mechanisms of insulin resistance and beta-cell failure in type 2 diabetes. *Nat Rev Mol Cell Biol* 9:193–205.
10. Dyar KA, et al. (2013) Muscle insulin sensitivity and glucose metabolism are controlled by the intrinsic muscle clock. *Mol Metab* 3:29–41.
11. Harfmann BD, et al. (2016) Muscle-specific loss of Bmal1 leads to disrupted tissue glucose metabolism and systemic glucose homeostasis. *Skelet Muscle* 6:12.
12. Hodge BA, et al. (2015) The endogenous molecular clock orchestrates the temporal separation of substrate metabolism in skeletal muscle. *Skelet Muscle* 5:17.
13. Turek FW, et al. (2005) Obesity and metabolic syndrome in circadian clock mutant mice. *Science* 308:1043–1045.
14. Paschos GK, et al. (2012) Obesity in mice with adipocyte-specific deletion of clock component Arntl. *Nat Med* 18:1768–1777.
15. Grimaldi B, et al. (2010) PER2 controls lipid metabolism by direct regulation of PPARγ. *Cell Metab* 12:509–520.
16. Adamovich Y, et al. (2014) Circadian clocks and feeding time regulate the oscillations and levels of hepatic triglycerides. *Cell Metab* 19:319–330.
17. Aviram R, et al. (2016) Lipidomics analyses reveal temporal and spatial lipid organization and uncover daily oscillations in intracellular organelles. *Mol Cell* 62:636–648.
18. Kalsbeek A, la Fleur S, Fliers E (2014) Circadian control of glucose metabolism. *Mol Metab* 3:372–383.
19. Chua EC, et al. (2013) Extensive diversity in circadian regulation of plasma lipids and evidence for different circadian metabolic phenotypes in humans. *Proc Natl Acad Sci USA* 110:14468–14473.
20. Morgan L, Hampton S, Gibbs M, Arendt J (2003) Circadian aspects of postprandial metabolism. *Chronobiol Int* 20:795–808.
21. Dallmann R, Viola AU, Tarokh L, Cajochen C, Brown SA (2012) The human circadian metabolome. *Proc Natl Acad Sci USA* 109:2625–2629.
22. Davies SK, et al. (2014) Effect of sleep deprivation on the human metabolome. *Proc Natl Acad Sci USA* 111:10761–10766.
23. Giskeødegård GF, Davies SK, Revell VL, Keun H, Skene DJ (2015) Diurnal rhythms in the human urine metabolome during sleep and total sleep deprivation. *Sci Rep* 5:14843.
24. Dibner C, Schibler U (2015) Circadian timing of metabolism in animal models and humans. *J Intern Med* 277:513–527.
25. Hansen J, et al. (2016) Synchronized human skeletal myotubes of lean, obese and type 2 diabetic patients maintain circadian oscillation of clock genes. *Sci Rep* 6:35047.
26. Loizides-Mangold U, et al. (2016) Paraoxonase 1 (PON1) and pomegranate influence circadian gene expression and period length. *Chronobiol Int* 33:453–461.
27. Perrin L, et al. (2015) Human skeletal myotubes display a cell-autonomous circadian clock implicated in basal myokine secretion. *Mol Metab* 4:834–845.
28. Hughes ME, Hogenesch JB, Kornacker K (2010) JTK_CYCLE: An efficient nonparametric algorithm for detecting rhythmic components in genome-scale data sets. *J Biol Rhythms* 25:372–380.
29. Yang R, Su Z (2010) Analyzing circadian expression data by harmonic regression based on autoregressive spectral estimation. *Bioinformatics* 26:i168–i174.
30. Staron RS, et al. (2000) Fiber type composition of the vastus lateralis muscle of young men and women. *J Histochem Cytochem* 48:623–629.
31. Johnson MA, Polgar J, Weightman D, Appleton D (1973) Data on the distribution of fibre types in thirty-six human muscles. An autopsy study. *J Neurol Sci* 18:111–129.
32. Deshmukh AS, et al. (2015) Deep proteomics of mouse skeletal muscle enables quantitation of protein isoforms, metabolic pathways, and transcription factors. *Mol Cell Proteomics* 14:841–853.
33. Murgia M, et al. (2017) Single muscle fiber proteomics reveals fibertype-specific features of human muscle aging. *Cell Rep* 19:2396–2409.
34. Aguer C, et al. (2011) Galactose enhances oxidative metabolism and reveals mitochondrial dysfunction in human primary muscle cells. *PLoS One* 6:e28536.
35. Jeong J, Conboy IM (2011) Phosphatidylserine directly and positively regulates fusion of myoblasts into myotubes. *Biochem Biophys Res Commun* 414:9–13.
36. van den Eijnde SM, et al. (2001) Transient expression of phosphatidylserine at cell-cell contact areas is required for myotube formation. *J Cell Sci* 114:3631–3642.
37. Andersson A, Nälsén C, Tengblad S, Vessby B (2002) Fatty acid composition of skeletal muscle reflects dietary fat composition in humans. *Am J Clin Nutr* 76:1222–1229.
38. Stoll LL, Spector AA (1984) Changes in serum influence the fatty acid composition of established cell lines. *In Vitro* 20:732–738.
39. Brown SA, et al. (2005) The period length of fibroblast circadian gene expression varies widely among human individuals. *PLoS Biol* 3:e338.
40. Mannic T, et al. (2013) Circadian clock characteristics are altered in human thyroid malignant nodules. *J Clin Endocrinol Metab* 98:4446–4456.
41. Perelis M, et al. (2015) Pancreatic β cell enhancers regulate rhythmic transcription of genes controlling insulin secretion. *Science* 350:aac4250.
42. Pulimeno P, et al. (2013) Autonomous and self-sustained circadian oscillators displayed in human islet cells. *Diabetologia* 56:497–507.
43. Saini C, et al. (2016) A functional circadian clock is required for proper insulin secretion by human pancreatic islet cells. *Diabetes Obes Metab* 18:355–365.
44. Schiaffino S, Blaauw B, Dyar KA (2016) The functional significance of the skeletal muscle clock: Lessons from Bmal1 knockout models. *Skelet Muscle* 6:33.
45. Dyar KA, et al. (2015) The calcineurin-NFAT pathway controls activity-dependent circadian gene expression in slow skeletal muscle. *Mol Metab* 4:823–833.
46. Kudo T, Tamagawa T, Kawashima M, Mito N, Shibata S (2007) Attenuating effect of clock mutation on triglyceride contents in the ICR mouse liver under a high-fat diet. *J Biol Rhythms* 22:312–323.
47. Li G, et al. (2016) Efficient replacement of plasma membrane outer leaflet phospholipids and sphingolipids in cells with exogenous lipids. *Proc Natl Acad Sci USA* 113:14025–14030.
48. van Meer G, Voelker DR, Feigenson GW (2008) Membrane lipids: Where they are and how they behave. *Nat Rev Mol Cell Biol* 9:112–124.
49. Abraham U, et al. (2010) Coupling governs entrainment range of circadian clocks. *Mol Syst Biol* 6:438.
50. Balsalobre A, Marcacci L, Schibler U (2000) Multiple signaling pathways elicit circadian gene expression in cultured Rat-1 fibroblasts. *Curr Biol* 10:1291–1294.
51. Brown SA, Zumbrunn G, Fleury-Olela F, Preitner N, Schibler U (2002) Rhythms of mammalian body temperature can sustain peripheral circadian clocks. *Curr Biol* 12:1574–1583.
52. Adamovich Y, Aviram R, Asher G (2015) The emerging roles of lipids in circadian control. *Biochim Biophys Acta* 1851:1017–1025.
53. Panda S (2016) Circadian physiology of metabolism. *Science* 354:1008–1015.
54. Bourlier V, et al. (2013) Enhanced glucose metabolism is preserved in cultured primary myotubes from obese donors in response to exercise training. *J Clin Endocrinol Metab* 98:3739–3747.
55. Bouzakri K, et al. (2003) Reduced activation of phosphatidylinositol-3 kinase and increased serine 636 phosphorylation of insulin receptor substrate-1 in primary culture of skeletal muscle cells from patients with type 2 diabetes. *Diabetes* 52:1319–1325.
56. Green CJ, Pedersen M, Pedersen BK, Scheele C (2011) Elevated NF-κB activation is conserved in human myocytes cultured from obese type 2 diabetic patients and attenuated by AMP-activated protein kinase. *Diabetes* 60:2810–2819.
57. Krug EG (2016) Trends in diabetes: Sounding the alarm. *Lancet* 387:1485–1486.
58. Loizides-Mangold U, David FP, Nesatyy VJ, Kinoshita T, Riezman H (2012) Glycosylphosphatidylinositol anchors regulate glycosphingolipid levels. *J Lipid Res* 53:1522–1534.

SUPPORTING INFORMATION to:

Lipidomics reveals diurnal lipid oscillations in human skeletal muscle persisting in cellular myotubes cultured *in vitro*

Ursula Loizides-Mangold[a,b,c], Laurent Perrin[a,b,c], Bart Vandereycken[d], James A. Betts[e], Jean-Philippe Walhin[e], Iain Templeman[e], Stéphanie Chanon[f], Benjamin D. Weger[g], Christine Durand[f], Maud Robert[h], Jonathan Paz Montoya[i], Marc Moniatte[i], Leonidas G. Karagounis[j,k], Jonathan D. Johnston[l], Frédéric Gachon[g,m], Etienne Lefai[f], Howard Riezman[n,o,1], and Charna Dibner[a,b,c,1]

[a]Division of Endocrinology, Diabetology, Hypertension and Nutrition, Department of Internal Medicine Specialties, University of Geneva, CH-1211 Geneva, Switzerland;
[b]Department of Cell Physiology and Metabolism, University of Geneva, CH-1211 Geneva, Switzerland;
[c]Faculty Diabetes Centre, Faculty of Medicine, University of Geneva, CH-1211 Geneva, Switzerland;
[d]Section of Mathematics, University of Geneva, CH-1211 Geneva, Switzerland;
[e]Department for Health, University of Bath, Bath BA2 7AY, United Kingdom;
[f]CarMeN Laboratory, INSERM U1060, INRA 1397, University Lyon 1, 69600 Oullins, France;
[g]Department of Diabetes and Circadian Rhythms, Nestlé Institute of Health Sciences, CH-1015 Lausanne, Switzerland;
[h]Department of Digestive Surgery, Center of Bariatric Surgery, Edouard Herriot Hospital, 69003 Lyon, France;
[i]Proteomics Core Facility, École Polytechnique Fédérale de Lausanne, CH-1015 Lausanne, Switzerland;
[j]Experimental Myology and Integrative Biology Research Cluster, Faculty of Sport and Health Sciences, Plymouth Marjon University, Plymouth PL6 8BH, United Kingdom;

[k]Institute of Nutritional Science, Nestlé Research Centre, CH-1015 Lausanne, Switzerland;
[l]Faculty of Health and Medical Sciences, University of Surrey, Guildford, Surrey GU2 7XH, United Kingdom;
[m]School of Life Sciences, École Polytechnique Fédérale de Lausanne, CH-1015 Lausanne, Switzerland;
[n]Department of Biochemistry, University of Geneva, Geneva, Switzerland;
[o]National Centre of Competence in Research Chemical Biology, University of Geneva, CH-1211 Geneva, Switzerland

[1]Co-corresponding authors

[1]Charna Dibner, lead contact

Division of Endocrinology, Diabetes, Hypertension and Nutrition, Department of Internal Medicine Specialties, Department of Cell Physiology and Metabolism, Faculty of Medicine, University of Geneva, Rue Michel-Servet, 1, CH-1211 Geneva 4, Switzerland

email: Charna.Dibner@hcuge.ch

Phone: +41 22 379 59 34

[1]Howard Riezman

University of Geneva, Department of Biochemistry, 30 Quai Ernest-Ansermet, CH-1211 Geneva, Switzerland

email: Howard.Riezman@unige.ch

Phone: +41 22 379 64 69

SI Materials and Methods

Human skeletal muscle biopsies for the in vivo study

The volunteers of the *in vivo* study had neither history of sleep disorder as confirmed by pre-study questionnaires MCTQ (1), Horne-Ostberg (2) and PSQI (3) (see Tables S4-S6), nor did they participate in a shifted work schedule, or travelled across more than two time zones within three weeks preceding the study. Each participant adhered to a consistent daily feeding and sleeping routine. Specifically, participants woke between 06:00 and 07:00 h and went to bed between 22:00 and 23:00 h (with individual wake-up and sleep times recorded during the week and verified via time-stamped voicemails) - resulting in an average of 8 h sleep opportunity. In addition, participants exposed themselves to 15 min natural light within 1.5 h of waking, as verified by wearable light sensors (ActiWatch™). Self-selected meals were scheduled at 08:00 h, 12:00 h and 18:00 h, with defined snacks at 10:00 h, 15:00 h and 20:00 h daily. Participants arrived in the laboratory at 19:00 h on the day prior to the testing day and ingested a standardized meal and snack (6405 kJ, 132 g carbohydrate, 76 g fat, 70 g protein) that first evening and remained for the duration of their stay in a semi-recumbent position. The resting metabolic rate was measured via indirect calorimetry the next morning according to best practice and used to calculate individual energy requirements at rest, which were then precisely met on an individual basis by prescribing hourly ingestion during waking hours of a mixed-macronutrient meal-replacement solution (Resource, Nestlé, CH) containing 5270 kJ/L, 140 g/L carbohydrate, 35 g/L fat, 94 g/L protein in small volumes relative to metabolic requirements (i.e. 92 ± 17 ml) to ensure energy and nutrient balance. The laboratory was free from natural light and with artificial lighting standardized to 800 lux in the direction of gaze, ambient temperature maintained between 20-25°C (23.6 ± 3.62°C; mean ± SD) and noise levels tightly regulated. Participants were not permitted to sleep during waking hours when

lights were on (07:00-22:00 h) and wore eye masks whilst trying to sleep during lights-out (22:00-07:00 h). Participants remained asleep during hourly blood sampling throughout the night but were woken briefly for acquisition of the nighttime muscle biopsy samples but without removing their eye masks. Anesthetic administration (1% lidocaine w/o epinephrine) and skin/fascia incisions for this procedure (4) were completed within the hour prior to sleep such that night-time samples could be acquired within several minutes from pre-prepared sites with minimal discomfort. Three samples were taken from each leg in alternating and ascending order (starting with the non/dominant limb counterbalanced between participants), with skin incisions separated by 2-3 cm.

Melatonin and cortisol analyses

Blood samples were drawn every hour, starting on the testing day throughout both the waking and sleeping periods. Samples were obtained using an intravenous cannula fitted to the antecubital vein. The first 2 ml was drawn and discarded as waste before a further 10 ml was extracted. Of this 10 ml, 2 ml was dispensed in to a centrifuge tube containing lithium heparin, 4 ml was allocated to a plain serum tube and the remaining 4 ml was deposited in a tube coated with EDTA. The lithium heparin and EDTA tubes were both immediately centrifuged for 10 minutes (3466 g, 4°C) after which the supernatants were removed and stored at -80°C. Melatonin was measured as previously described (5) and cortisol was measured by COBAS (Roche).

In vitro skeletal myotube synchronization and real-time bioluminescence recording

Myoblasts were transduced with a *Bmal1* luciferase (*Bmal1-luc*) (6) containing lentiviral reporter with a multiplicity of infection (MOI) = 3, grown to confluence, and subsequently differentiated into myotubes, as previously described by us in (7). For lentiviral production

see (8). To synchronize primary myotubes, 10 μM forskolin (Sigma) was added to the culture medium for 1 h, followed by a medium change. For bioluminescence recording the culture medium was changed to the phenol red-free recording medium containing 100 μM luciferin (D-luciferin 306-250, NanoLight Technology) and cells were transferred to a 37°C light-tight incubator (Prolume LTD), as previously described by us (8). Bioluminescence from each dish was continuously monitored using a Hamamatsu photomultiplier tube (PMT) detector assembly. Photon counts were integrated over 1 min intervals. Bioluminescence profiles are shown as detrended data. For detrended time series, luminescence signals were smoothened by a moving average with a window of 24 h. For this, each data point was divided by the average of data points in an interval of 24 h (12 h before and 12 h after the analyzed data point).

Materials for lipid extraction

Synthetic lipid standards [PC 12:0/12:0 (850335), PE 17:0/14:1 (LM-1104), PI 17:0/14:1 (LM-1504), PS 17:0/14:1 (LM-1304), Cer d18:1/17:0 (860517), SM d18:1/12:0 (860583), GlcCer d18:1/8:0 (860540)] were from Avanti Polar Lipids Inc. MTBE and methylamine (33% in absolute ethanol) were purchased from Sigma. Chloroform, methanol, n-butanol and ammonium molybdate were from Acros Organics. LC-MS grade methanol, water and ammonium acetate were from Fluka. HPLC grade chloroform was purchased from Acros Organics. Monopotassium phosphate and L-ascorbic acid were from Sigma. 70% perchloric acid was from Merck.

Lipid extraction procedure

Lipid extracts were prepared using the MTBE protocol (9). Briefly, ~30 mg ground skeletal muscle tissue or human primary myotubes harvested from one confluent 10 cm dish (~1.5 x

10^6 cells) were resuspended in 100 µl H_2O. 360 µl methanol and a mix of internal standards were added (400 pmol PC 12:0/12:0, 1000 pmol PE 17:0/14:1, 1000 pmol PI 17:0/14:1, 3300 pmol PS 17:0/14:1, 2500 pmol SM d18:1/12:0, 500 pmol Cer d18:1/17:0 and 100 pmol GlcCer d18:1/8:0). After addition of 1.2 ml of MTBE, samples were placed for 10 min on a multitube vortexer at 4°C followed by incubation for 1 h at room temperature (RT) on a shaker. Phase separation was induced by addition of 200 µl MS-grade water. After 10 min at RT samples were centrifuged at 1000 g for 10 min. The upper (organic) phase was transferred into a 13 mm glass tube and the lower phase was re-extracted with 400 µl artificial upper phase [MTBE/methanol/H_2O (10:3:1.5, v/v/v)]. The combined organic phases were dried in a vacuum concentrator (CentriVap, Labconco). Lipids were dissolved in chloroform/methanol and divided into three aliquots. One aliquot was treated by alkaline hydrolysis to enrich for sphingolipids and the other two aliquots were used for glycerophospholipid and phosphorus assay, respectively. Glycerophospholipids were deacylated according to the method by Clarke (10). Briefly, 1 ml freshly prepared monomethylamine reagent [methylamine/H_2O/n-butanol/methanol (5:3:1:4, (v/v/v/v)] was added to the dried lipid extract and then incubated at 53°C for 1 h in a water bath. Lipids were cooled to RT and then dried. For desalting, the dried lipid extract was resuspended in 300 µl water-saturated n-butanol and then extracted with 150 µl H_2O. The organic phase was collected, and the aqueous phase was re-extracted twice with 300 µl water-saturated n-butanol. The organic phases were pooled and dried in a vacuum concentrator.

Determination of total phosphorus

100 µl of the total lipid extract, resuspended in chloroform/methanol (1:1), were placed into 13 mm disposable pyrex tubes and dried in a vacuum concentrator. 0, 2, 5, 10, 20 µl of a 3 mM KH_2PO_4 standard solution were placed into separate pyrex tubes. To each tube 20 µl of

water and 140 µl of 70% perchloric acid were added. Samples were heated at 180°C for 1 h in a chemical hood. Then, 800 µl of a freshly prepared solution of water, ammonium molybdate (100 mg/8 ml H_2O) and ascorbic acid (100 mg/6 ml H_2O) in a ratio of 5:2:1 (v/v/v) were added. Tubes were heated at 100°C for 5 min with a marble on each tube to prevent evaporation. Tubes were cooled at RT for 5 min. 100 µl of each sample was then transferred into a 96-well microplate and the absorbance at 820 nm was measured.

Phospho- and sphingolipid analysis by mass spectrometry

Mass spectrometry analysis for the identification and quantification of phospho- and sphingolipid species was performed on a TSQ Vantage Triple Stage Quadrupole Mass Spectrometer (Thermo Fisher Scientific) equipped with a robotic nanoflow ion source (Nanomate HD, Advion Biosciences), using multiple reaction monitoring (MRM). Each individual ion dissociation pathway was optimized with regard to collision energy. Dried lipid extracts were resuspended in 250 µl MS grade chloroform/methanol (1:1) and further diluted in either chloroform/methanol (1:2) plus 5 mM ammonium acetate (negative ion mode) or in chloroform/methanol/H_2O (2:7:1) plus 5 mM ammonium acetate (positive ion mode). Lipid concentrations were calculated relative to the relevant internal standards and then normalized to the total phosphate content of each total lipid extract.

Triacylglyceride analysis

Mass spectrometry analysis for triacylglycerides (TAG) was performed on a hybrid ion trap LTQ-Orbitrap XL mass spectrometer (Thermo Fisher Scientific, San Jose, CA, USA) equipped with a micro LC binary pump UFLC-XR (Shimadzu). The equivalent of 0.4 nmol of total phosphate content in 20mM ammonium hydroxide was injected onto a 2.6 µm, 50 x 2.1 mm Kinetex Hilic column (Phenomenex). Lipid extracts (2 µL injection volume) were

separated over an 8 minute gradient at a flow rate of 200 µL/min. Mobile phase composition and gradient were as follow: 0 min, 5% A; 1.7 min, 12%A, 3.5 min, 25% A and 4.5 min, 0% A where A was deionized water containing 10 mM ammonium formate and 0.5% formic acid and B was acetonitrile/methanol 10:1 (v/v) containing 10 mM ammonium formate and 0.5% formic acid. TAG ions were analyzed in positive mode in full scan experiment (m/z 200-2000) and detected as ammonium adducts $[M+NH4]^+$. MS survey scans were acquired with a resolution set at 60'000 (FWHM at m/z = 400) with an AGC set at 5.0E5, one microscan and maximum injection time set at 250 ms. The heated electrospray source HESI II was operated at a temperature of 100°C and a source voltage at 4.0KV. Sheath, auxiliary and sweep nitrogen gas arbitrary units were set at 15, 5, 1 respectively, while the transfer capillary temperature was set to 275°C. Data analysis: Mass spectrometry data were acquired with the LTQ Tuneplus 2.5 and treated with Xcalibur 2.1 (Thermo Fisher Scientific). Lipid identification was carried out with the Lipid Data Analyzer II (LDA v. 2.5.1, IGB-TUG Graz University) (11). Care was taken to calibrate the instrument regularly to ensure a mass accuracy consistently lower than 3 ppm thereby leaving only few theoretical possibilities for elemental assignment.

Data analysis

The clustering of the circadian lipid data into two groups was computed with a custom made procedure in MATLAB as follows. Step 1: the z scores were computed from raw lipid concentration data for each lipid/subject and after removal of outliers. Step 2: for each subject/lipid/biological replicate, the z-scores were detrended with the mean over 6 (*in vivo*) or 7 (*in vitro*) time points. Step 3: for each subject/lipid, the phase and amplitude for period 22 h (*in vitro*) and 24 h (*in vivo*) of a sinusoidal fit was computed using ordinary least squares using the two biological replicates per time point. P values of the coefficients were computed

assuming normality of the data. Step 4: for clustering, the signals were retained if they had a *p* value of the fit with FDR less than 0.05 (*in vitro*) or 0.10 (*in vivo*) using the Benjamini-Hochberg procedure applied over all lipids and subjects. The data were then clustered into two groups using k means in MATLAB (using 20 replicates). Step 5: two different sinusoids with fixed periods 22 h (*in vitro*) and 24 h (*in vivo*) were fit using ordinary least squares through all the data respecting the earlier determined clustering. The clustering was encoded with a standard 0/1 categorical variable. P values on the coefficients of the fit were calculated assuming normality of the data and verified to be significant (≤ 0.05) for each fitted sinusoid. Step 6: for visualizing the 95% confidence intervals of the fit, the standard errors on the coefficients were used in a Monte Carlo procedure to generate 500 fits.

Time-series for lipid data were analyzed by ARSER (12) through meta2d in MetaCycle R package (13). Period length was set between 20 and 28 h. Distribution plots were made by kernel smoothing as implemented by ksdensity in MATLAB with standard options. Boxplots were made with MATLAB (standard options) on the raw lipid concentration data (7 time points per lipid). Amplitude was calculated as difference of max and mix over the 7 time points.

REFERENCES

1. Roenneberg T, Wirz-Justice A, & Merrow M (2003) Life between clocks: daily temporal patterns of human chronotypes. *Journal of biological rhythms* 18(1):80-90.
2. Horne JA & Ostberg O (1976) A self-assessment questionnaire to determine morningness-eveningness in human circadian rhythms. *International journal of chronobiology* 4(2):97-110.
3. Buysse DJ, Reynolds CF, 3rd, Monk TH, Berman SR, & Kupfer DJ (1989) The Pittsburgh Sleep Quality Index: a new instrument for psychiatric practice and research. *Psychiatry Res* 28(2):193-213.

4. Bergstrom J (1962) Muscle Electrolytes in Man - Determined by Neutron Activation Analysis on Needle Biopsy Specimens - Study on Normal Subjects, Kidney Patients, and Patients with Chronic Diarrhoea. *Scand J Clin Lab Inv* 14:1-&.
5. Middleton B (2013) Measurement of melatonin and 6-sulphatoxymelatonin. *Methods Mol Biol* 1065:171-199.
6. Liu AC, *et al.* (2008) Redundant function of REV-ERBalpha and beta and non-essential role for Bmal1 cycling in transcriptional regulation of intracellular circadian rhythms. *PLoS genetics* 4(2):e1000023.
7. Perrin L, *et al.* (2015) Human skeletal myotubes display a cell-autonomous circadian clock implicated in basal myokine secretion. *Molecular metabolism* 4(11):834-845.
8. Pulimeno P, *et al.* (2013) Autonomous and self-sustained circadian oscillators displayed in human islet cells. *Diabetologia* 56(3):497-507.
9. Matyash V, Liebisch G, Kurzchalia TV, Shevchenko A, & Schwudke D (2008) Lipid extraction by methyl-tert-butyl ether for high-throughput lipidomics. *J Lipid Res* 49(5):1137-1146.
10. Clarke NG & Dawson RM (1981) Alkaline O leads to N-transacylation. A new method for the quantitative deacylation of phospholipids. *Biochem J* 195(1):301-306.
11. Hartler J, *et al.* (2011) Lipid Data Analyzer: unattended identification and quantitation of lipids in LC-MS data. *Bioinformatics* 27(4):572-577.
12. Yang R & Su Z (2010) Analyzing circadian expression data by harmonic regression based on autoregressive spectral estimation. *Bioinformatics* 26(12):i168-174.
13. Wu G, Anafi RC, Hughes ME, Kornacker K, & Hogenesch JB (2016) MetaCycle: an integrated R package to evaluate periodicity in large scale data. *Bioinformatics* 32(21):3351-3353.

FIGURE LEGENDS

Figure S1. Representative PC metabolite profiles of phosphate normalized and unnormalized data *in vivo*. PC metabolite profiles for donor VII and donor X are shown. Lipid values were either not normalized to phosphate (upper panel) or normalized to total phosphate (lower panel). Normalized and unnormalized temporal lipid values were divided by each lipid mean value. Only lipids that were detected at all time points are shown.

Figure S2. Logarithmic scale heatmap of lipid abundance shown for phosphatidylserine (PS) and cardiolipin (CL). CL72:8_C18:2 is not detected *in vitro* (left column) but is highly abundant *in vivo* (right column). Colors show the log concentration for each metabolite. PS nomenclature: the total number of acyl carbons and double bonds is indicated. CL nomenclature: total number of acyl carbons in the four fatty acyl chains with presence of at least one fatty acid with a carbon number as indicated by underscore.

Figure S3. Representative PC metabolite profiles of phosphate normalized and unnormalized data *in vitro*. PC metabolite profiles for myotube cultures established from donor #5 and donor #9 are shown. Lipid values were either not normalized to phosphate (upper panel) or normalized to total phosphate (lower panel). Each lipid value (normalized or unnormalized) was divided by its lipid mean value.

Figure S4. Around-the-clock profile of the most abundant PC lipids in primary myotubes. The most abundant PC lipids exhibit enrichment 16 h and 28 h after synchronization.

Figure S5. Temporal lipid profile of PC32:2 in human skeletal myotubes. (A) The total profile of PC32:2 is not rhythmic in human primary myotubes (left panel). Individual lipid profiles are displaying oscillations albeit with different phase (middle panel). Lipid oscillations can be clustered into two major subgroups that reach their zenith 16 h or 24-28 h after synchronization, respectively (right panel). **(B)** TAG58:9 is not rhythmic in skeletal muscle across all subjects but displays subgroup oscillations upon individual analysis.

Figure S6. Lipid chain length but not the degree of desaturation influences the circadian profile of PC and SM lipid metabolites. (A) Temporal profile of PC, SM, and PE lipids, sorted by chain length in human primary myotubes. PC/SM lipids: only a subgroup of donors is shown that peak 28 h after forskolin synchronization (n=4). For PE, the average profile across all ten subjects is shown (n=10). PC, PE: the number represents the sum of carbon atoms in both fatty acyl chains; SM lipids: the number represents the sum of carbon atoms in the sphingoid base (C18) plus fatty acyl chain. **(B)** RT-qPCR results for *ACADL*, *ACADVL* and *ACSL3* on mRNA samples extracted from human skeletal muscle biopsies. Data were normalized to *GAPDH* (mean ± SEM). **(C)** PC lipid profiles (primary myotubes) sorted by their degree of desaturation. The number of double bonds is indicated.

Figure S7. Myosin isoform analysis. (A) RT-qPCR results for *MYH1*, *MYH2*, *MYH4* and *MYH7* on mRNA samples extracted from human skeletal muscle biopsies derived from two different origins (*vastus lateralis* or *gluteus maximus*). For donor characteristics see Table S1 and S2. Data were normalized to *GAPDH* (mean ± SEM). **(B)** Myosin isoform expression levels relative to *MYH1*.

Supplementary Tables

Table S1. Donor characteristics *vastus lateralis* (*in vivo* study)

Subject	Sex	Age (years)	BMI (kg/m^2)	Muscle biopsy
I	M	22	28.3	*vastus lateralis*
II	F	37	28.3	*vastus lateralis*
III	M	27	20.4	*vastus lateralis*
IV	M	33	23.6	*vastus lateralis*
V	M	54	25.6	*vastus lateralis*
VI	M	24	24.6	*vastus lateralis*
VII	M	25	23.8	*vastus lateralis*
VIII	M	30	20.3	*vastus lateralis*
IX	M	22	23.2	*vastus lateralis*
X	M	25	23.4	*vastus lateralis*
AVERAGE	**9/1**	**29.9 ± 9.8**	**24.1 ± 2.7**	***vastus lateralis***

Table S2. Donor characteristics *gluteus maximus* (*in vitro* study)

Subject	Sex	Age (years)	BMI (kg/m^2)	Fasting blood glucose (mmol/L)	Muscle biopsy
1	F	66	24.77	5.0	*gluteus maximus*
2	M	62	24.30	5.44	*gluteus maximus*
3*,#	F	77	25.56	5.98	*gluteus maximus*
4*	M	65	23.41	6.9	*gluteus maximus*
5*	F	65	25.85	5.06	*gluteus maximus*
6*	M	58	23.88	6.0	*gluteus maximus*
7*	M	59	24.62	4.88	*gluteus maximus*
8*	F	65	21.99	6.2	*gluteus maximus*
9#	F	65	22.77	4.95	*gluteus maximus*
10	M	48	24.30	5.5	*gluteus maximus*
AVERAGE 5/5		**63 ± 7.36**	**24.15 ± 1.19**	**5.59 ± 0.66**	***gluteus maximus***
11*,#	F	53	22.41	5.1	*gluteus maximus*
12*,#	M	57	26.3	6.2	*gluteus maximus*
13*	M	65	22.53	5.6	*gluteus maximus*
14*	M	64	22.04	5.4	*gluteus maximus*

Myotube cells of donors 1-10 were used for the *in vitro* lipidomic analysis.
* cDNA of these donor biopsies was used for myosin isoform analysis.
# Donors used for siRNA-mediated clock disruption experiment.

Table S3. Most significantly rhythmic lipids in human skeletal muscle and primary myotubes

Ion	Rhythmic *in vitro*	Ion	Rhythmic *in vivo*
TAG54:6	8/9	GlcCer42:2	5/7
GlcCer34:1	**7/10**	**SM38:1**	**5/7**
TAG50:4	6/10	SM42:2	5/7
TAG52:2	6/9	LysoPI	5/7
TAG54:3	6/9	PC(O)36:4	5/7
TAG56:7	6/9	PC(O)36:6	5/7
TAG56:8	6/9	PC32:2	5/7
TAG58:7	6/9	PC34:4	5/7
DHCer32:0	6/10	**GlcCer34:1**	**4/7**
PE30:1	6/10	GlcDHCer34:1	4/7
PE34:4	**6/10**	PC(O)32:0	4/7
SM32:1	6/10	PC(O)32:6	4/7
Cer42:1	5/10	PC(O)34:4	4/7
Cer36:1	5/10	PC(O)36:2	4/7
GlcCer34:1-OH	5/10	PC(O)36:3	4/7
GlcCer40:1	5/10	PC(O)36:5	4/7
GlcCer40:1-OH	5/10	PC30:0	4/7
GlcCer42:1	5/10	PC32:1	4/7
GlcDHCer40:0	5/10	PC34:2	4/7
PC42:1	5/10	PC36:3	4/7
PC42:3	5/10	PC36:5	4/7
PC42:6	5/10	PE(O)34:4	4/7
PC44:4	5/10	**PE34:4**	**4/7**
PE(O)34:1	5/10	PE36:0	4/7
PE(O)44:1	5/10	PE38:1	4/7
PE34:0	5/10	PI42:1	4/7
SM34:1	5/10	PI42:2	4/7
SM38:1	**5/10**	PS40:6	4/7
SM42:1	5/10	SM40:2	4/7
SM44:3	5/10	TAG44:6	4/7

Table S4. Munich Chronotype Questionaire

Munich Chronotype Questionnaire

Statement	Participant									
	1	2	3	4	5	6	7	8	9	10
On Workdays:										
I have to get up at:	08:00	06:00	06:45	06:30	06:30	06:30	08:00	06:00		06:30
I need … minutes to wake up	5	0	15	5	20	5	1	5		1
I regularly wake up … minutes before my alarm	0	15	0	10	0	2	5	0		5
I am fully awake from …	08:05	06:00	08:00	07:15	08:30	06:45	08:30	06:30		07:00
I have an energy dip at around …	16:00	14:00	14:00	15:30	14:00	11:30	17:00	15:00		14:00
On nights before workdays I go to bed at …	00:00	22:00	23:30	22:00	23:00	23:00	00:00	21:30		22:30
It then takes me … minutes to fall asleep	3	15	15	10	10	10	30	30		15
If I can, I like to take a nap (Y/N)	N	N	N	N	Y	N	N	N		N
If Y then I sleep for …	-	-	-	-	7	-	-	-		-
I would feel terrible afterwards (Y/N)	-	-	Y	-	-	-	-	-		-
On free days:										
My dream would be to sleep until …	09:00	08:00	09:00	08:30	09:00	09:30	10:00	07:00		08:30
I normally wake up at …	09:00	06:00	10:30	06:30	07:50	09:00	09:00	06:30		08:00
If I wake up at my workday time I try to get back to sleep (Y/N)	N	N	Y	Y	Y	Y	N	N		Y
If I get back to sleep I will usually sleep for another … minutes	-	-	210	60	60	150	-	20		60
I need … minutes to wake up	5	-	30	5	20	5	-	5		10
I am fully awake from …	09:05	-	11:00	07:15	08:30	09:15	-	07:00		08:30
I have an energy dip at around …	16:00	-	18:00	15:30	14:00	18:00	-	-		-
On nights before free days I go to bed at …	00:30	23:00	01:30	22:30	23:00	00:00	01:00	22:00		23:00
It then takes me … minutes to fall asleep	3	15	30	10	10	15	10	10		30
If I can, I like to take a nap (Y/N)	N	N	N	N	Y	N	N	N		N
If Y then I sleep for …	-	-	-	-	10	-	-	-		-
If Y then I would feel terrible afterwards (Y/N)	-	-	Y	-	-	-	-	-		-
Preferences:										
Once I am in bed, I would like to read for … minutes	0	0	30	30	0	30	20	30		15
… but generally fall asleep after no more than … minutes	-	-	10	20	-	5	20	30		20
I prefer to sleep in a completely dark room (Y/N)	N	Y	Y	Y	Y	Y	Y	Y		Y
I wake up more easily when morning light shines in to my room (Y/N)	Y	Y	Y	Y	Y	Y	Y	Y		Y
How long per day do you spend on average outside exposed to daylight?										
On workdays (hh:mm)	01:30	02:00	1.5	01:00	02:00	03:00	01:30	01:10		01:00
On free days (hh:mm)	02:00	05:30	1.5	03:00	03:30	07:00	03:00	02:00		04:00
Self Assessment										
I am …	3	1	4	1	4	5	5	1		1
As a child I was …	1	2	1	1	4	2	3	0		2
As a teenager I was …	3	4	3	5	5	6	5	6		2
If over 65, in the middle of my life I was …	-	-	-	-	-	-	-	-		-
My mother is/was …	1	1	3	2	3	4	1	4		1
My father is/was …	1	4	6	0	2	5	2	0		0
My sister (1) is/was …	UKW	4	5	-	4	5	6	-		-
My sister (2) is/was …	-	-	6	-	2	4	3	-		-
My sister (3) is/was …	-	-	6	-	-	-	2	-		-
My brother (1) is/was …	-	-	6	4	-	-	5	4		4
My brother (2) is/was …	-	-	6	-	-	-	1	-		3
My brother (3) is/was …	-	-	6	-	-	-	-	-		-
My brother (4) is/was …	-	-	3	-	-	-	-	-		-
My partner (girlfriend/boyfriend, spouse, significant other) is/was …	2	4	0	5	4	5	5	1		-

Computed Variables	Participant									
	1	2	3	4	5	6	7	8	9	10
Sleep onset (WD):	00:03	22:15	23:45	22:10	23:10	23:10	00:30	22:00		22:45
Out of bed (WD):	08:05	06:00	07:00	06:35	06:50	06:35	08:01	06:05		06:31
Sleep duration (WD):	07:57	07:45	07:00	08:20	07:20	07:20	07:30	08:00		07:45
Time in bed (WD):	08:05	08:00	07:30	08:35	07:50	07:35	08:01	08:35		08:01
Mid-sleep (WD):	03:59	02:08	03:15	02:20	02:50	02:50	04:15	02:00		02:38
Sleep onset (FD):	00:33	23:15	02:00	22:40	23:10	00:15	01:10	22:10		23:30
Out of bed (FD):	09:05	06:00	11:00	06:35	08:10	09:05	09:00	06:35		08:10
Sleep duration (FD):	08:27	06:45	08:30	07:50	08:40	08:45	07:50	08:20		08:30
Time in bed (FD):	08:35	07:00	09:30	08:05	09:10	09:05	08:00	08:35		09:10
Mid-sleep (FD):	4:51:00 AM	2:38:00 AM	6:15:00 AM	2:35:00 AM	3:30:00 AM	4:38:00 AM	5:05:00 AM	2:20:00 AM		3:45:00 AM
WD Duration	07:57	07:45	07:00	08:20	07:20	07:20	07:30	08:00		07:45
WD hours	7	7	7	8	7	7	7	8		7
WD mins	57	45	0	20	20	20	30	0		45
WD Weekly Sleep	39.75	38.75	35	41.666667	36.666667	36.666667	37.5	40		38.75
FD Duration	08:27	06:45	08:30	07:50	08:40	08:45	07:50	08:20		08:30
FD hours	8	6	8	7	8	8	7	8		8
FD mins	27	45	30	50	40	45	50	20		30
FD Weekly Sleep	16.9	13.5	17	15.666667	17.333333	17.5	15.666667	16.666667		17
Total Weekly Sleep Time	56.65	52.25	52	57.333333	54	54.166667	53.166667	56.666667		55.75
Total Weekly Sleep Hours	56	52	52	57	54	54	53	56		55
Remainder	0.65	0.25	0	0.33333	0	0.16667	0.16667	0.66667		0.75
Total Sleep Mins	39	15	0	20	0	10	10	40		45
Total Weekly Sleep Time (hh:mm:ss)	56:39:00	52:15:00	52:00:00	57:20:00	54:00:00	54:10:00	53:10:00	56:40:00		55:45:00
Average Daily Sleep duration (hh:mm:ss):	8:05:34	7:27:51	7:25:43	8:11:26	7:42:51	7:44:17	7:35:43	8:05:43		7:57:51
Equation:	1	2	1	2	1	1	1	1		1
Chronotype:	**04:40**	**02:38**	**05:42**	**02:35**	**03:01**	**04:07**	**04:57**	**02:12**		**03:28**

Table S5. Horne-Ostberg Questionnaire

Horne-Ostberg Questionnaire

No.	Statement	Participant Number									
		1	**2**	**3**	**4**	**5**	**6**	**7**	**8**	**9**	**10**
1	Considering only your own "feeling best" rhythm, at what time would you get up if you were entirely free to plan your day?	3	3	3	4	3	3	3	4		3
2	Considering only your own "feeling best" rhythm, at what time would you go to bed if you were entirely free to plan your evening?	3	4	3	3	3	3	2	4		3
3	If there is a specific time you have to get up in the morning, to what extent are you dependent on being woken up by an alarm clock?	2	3	1	3	2	3	2	3		2
4	Assuming adequate environmental conditions, how easy do you find getting up in the morning?	3	4	3	4	3	3	3	3		4
5	How alert do you feel during the first half hour after having woken in the morning?	3	3	3	3	1	2	2	3		3
6	How is your appetite during the first half hour after having woken in the morning?	2	3	2	4	3	2	3	2		3
7	During the first half hour after having woken in the morning, how tired do you feel?	3	3	2	4	2	2	3	3		3
8	When you have no commitments the next day, at what time do you go to bed compared to your usual bedtime?	3	2	2	3	3	2	2	3		3
9	You have decided to engage in some physical exercise. A friend suggests that you do this one hour twice a week and the best time for him is between 0700 and 0800h. Bearing in mind nothing else but your own inclinations, how do you think you would perform?	4	4	3	3	2	2	2	4		3
10	At what time in the evening do you feel tired and as a result in need of sleep?	3	4	3	4	3	3	3	4		3
11	You wish to be at your peak for a test which you know is going to be mentally exhausting and lasting for two hours. You are entirely free to plan your day and considering only your own "feeling best" rhythm, which ONE of the four testing times would you choose?	4	6	6	4	4	2	4	6		4
12	If you went to bed at 2300h at what level of tiredness would you be?	3	2	2	5	3	2	2	5		2
13	For some reason you have gone to bed several hours later than usual, but there is no need to get up at any particular time the next morning. Which ONE of the following events are you most likely to experience:	1	3	3	4	3	2	2	4		3
14	One night you have to remain awake between 0400 and 0600h. You have no commitments the next day. Which ONE of the following suits you best:	3	4	4	3	3	1	3	4		4
15	You have to do two hours of hard physical work. You are entirely free to plan your day and considering only your own "feeling best" rhythm which ONE of the following times would you choose?	3	4	3	3	3	1	2	4		3
16	You have decided to engage in some physical exercise. A friend suggests that you do this between 2200 and 2300h twice a week. Bearing in mind nothing else but your own "feeling best" rhythm how well do you think you would perform?	1	4	2	4	2	1	2	3		3
17	Suppose that you can choose your own work hours. Assume that you worked a FIVE hour day (including breaks)) and that your job was interesting and paid by results. Which FIVE CONSECUTIVE HOURS would you select:	2	3	2	3	2	2	2	3		3
18	At what time of day do you think that you reach your "feeling best" peak?	3	4	5	3	3	2	3	4		3
19	One hears of "morning" and "evening" types. Which do you consider yourself to be?	4	4	2	6	4	0	2	6		6
	Total Score	53	67	54	70	52	38	47	72		61
	Category	Neither	M. Morn	Neither	D. Morn	Neither	M. Even	Neither	D. Morn		M. Morn

Table S6. Pittsburgh Sleep Quality Index

Pittsburgh Sleep Quality Index

			Participant									
Question			**1**	**2**	**3**	**4**	**5**	**6**	**7**	**8**	**9**	**10**
	1	a	12:20:00 AM	10:00:00 PM	11:00:00 PM	10:00:00 PM	11:10:00 PM	11:00:00 PM	12:00:00 AM	10:00:00 PM		10:30:00 PM
	2	a	3	15	12.5	10	10	5	30	5		15
LATEN		score	0	0	0	0	0	0	1	0		0
	3	a	9:00:00 AM	6:30:00 AM	7:00:00 AM	6:30:00 AM	6:35:00 AM	9:15:00 AM	8:00:00 AM	6:00:00 AM		6:20:00 AM
		diff	08:40	08:30	08:00	08:30	07:25	10:15	08:00	08:00		07:50
		hr	8	8	8	8	7	10	8	8		7
		min	40	30	0	30	25	15	0	0		50
		sec	31200	30600	28800	30600	26700	36900	28800	28800		28200
		diffhour	8.67	8.50	8.00	8.50	7.42	10.25	8.00	8.00		7.83
		newtib	8.67	8.50	8.00	8.50	7.42	10.25	8.00	8.00		7.83
		tmphse	99	82	81	82	94	98	94	100		89
4	**HSE**	**score**	**0**	**1**	**1**	**1**	**0**	**0**	**0**	**0**		**0**
	4	a	08:37	07:00	06:30	07:00	07:00	10:00	07:30	08:00		07:00
		hr	8	7	6	7	7	10	7	8		7
		min	37	0	30	0	0	0	30	0		0
		sec	31020	25200	23400	25200	25200	36000	27000	28800		25200
			8.62	7.00	6.50	7.00	7.00	10.00	7.50	8.00		7.00
3	**DURAT**	**score**	**0**	**0**	**1**	**0**	**0**	**0**	**0**	**0**		**0**
	5	a	0	1	0	1	1	0	2	1		0
		2a + 5a	0	1	0	1	1	0	3	1		0
2	**LATEN**	**score**	**0**	**1**	**0**	**1**	**1**	**0**	**2**	**1**		**0**
		b	3	2	0	3	3	2	1	0		2
		c	0	2	0	1	3	1	2	0		2
		d	0	0	0	0	0	0	1	0		0
		e	0	0	0	0	0	0	1	0		0
		f	0	0	0	0	0	1	1	0		0
		g	0	2	0	2	1	1	0	1		2
		h	0	0	2	1	0	0	0	0		0
		i	0	1	0	0	0	0	0	0		0
		j	0	0	0	0	0	2	0	0		0
		sum b-j	3	7	2	7	7	7	6	1		6
5	**DISTB**	**score**	**1**	**1**	**1**	**1**	**1**	**1**	**1**	**1**		**1**
1	**6**	**a**	**0**	**1**	**1**	**1**	**1**	**1**	**1**	**0**		**1**
6	**7**	**a**	**0**	**0**	**0**	**0**	**0**	**0**	**0**	**0**		**0**
	8	a	0	1	0	0	0	0	0	0		0
	9	a	0	1	1	0	0	0	2	0		0
		8 + 9	0	2	1	0	0	0	2	0		0
7	**DAYDYS**	**score**	**0**	**1**	**1**	**0**	**0**	**0**	**1**	**0**		**0**
	10		3	3	0	0	0	3	0	3		1
		a	0	0	0	0	0	0	0	0		0
		b	0	0	0	0	0	0	0	0		0
		c	0	0	0	0	0	0	0	0		0
		d	0	0	0	0	0	0	0	0		0
		e	0	0	0	0	1	2	0	0		0
PSQI		**Score**	**1**	**5**	**5**	**4**	**3**	**2**	**5**	**2**	-	**2**
		Interp	**Good**	**Good**	**Good**	**Good**	**Good**	**Good**	**Good**	**Good**	-	**Good**

Supplementary Figures

Figure S1

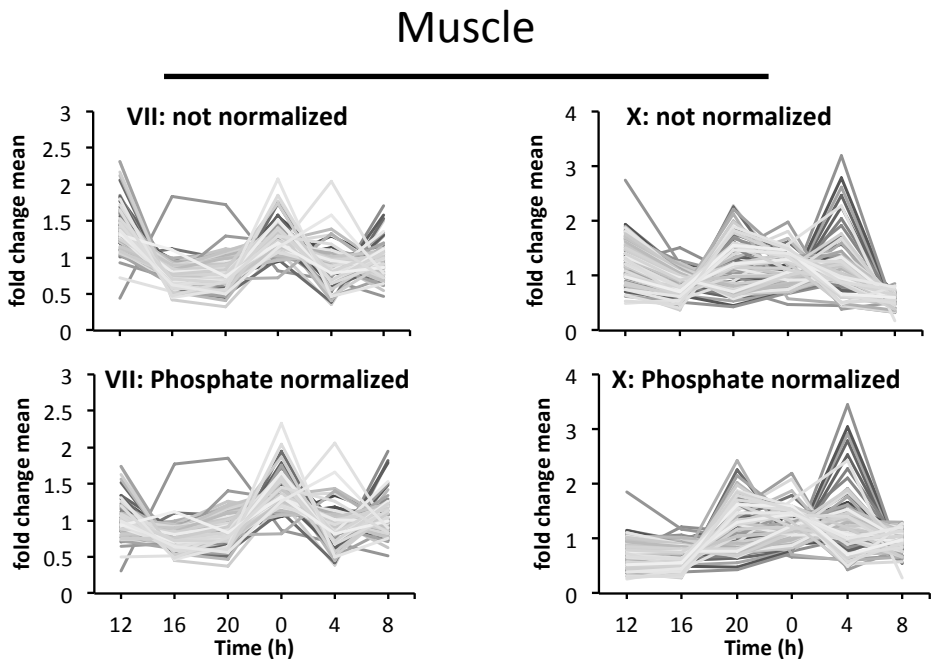

Figure S2

Logarithmic scale heatmap of lipid concentration for *in vitro* (left) and *in vivo* (right)

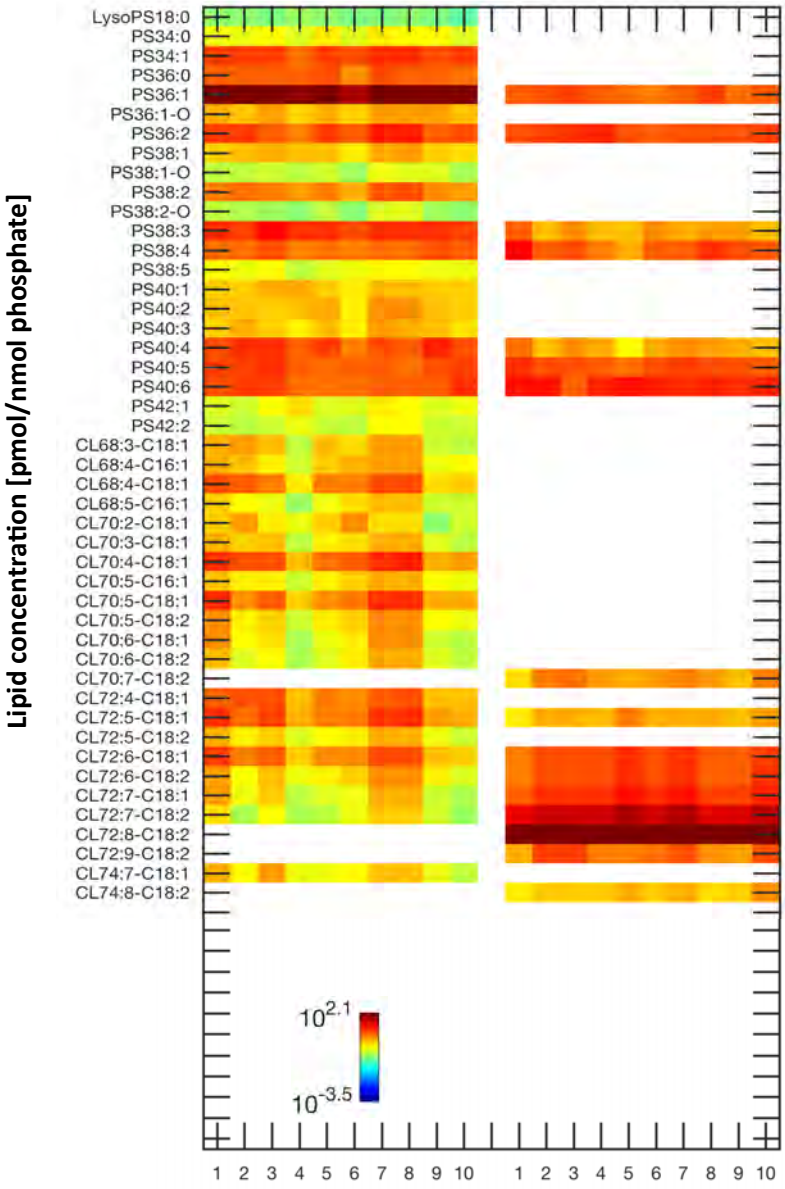

Figure S3

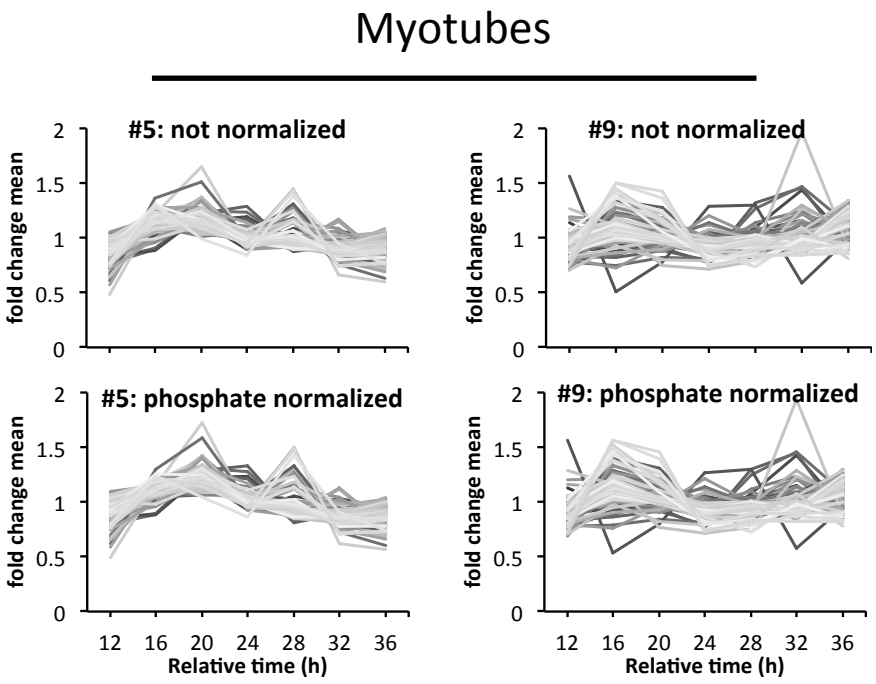
Myotubes
#5: not normalized
#9: not normalized
#5: phosphate normalized
#9: phosphate normalized
fold change mean
Relative time (h)
0
0.5
1
1.5
2
12
16
20
24
28
32
36

Figure S4

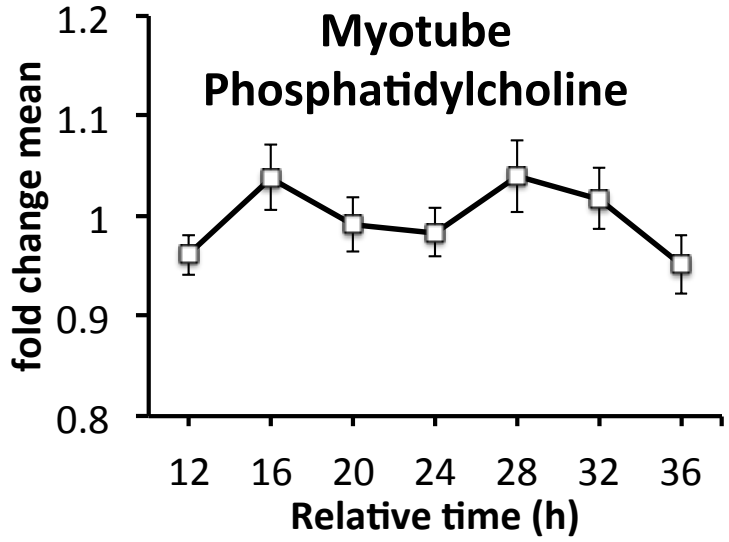
Myotube
Phosphatidylcholine
fold change mean
1.2
1.1
1
0.9
0.8
12
16
20
24
28
32
36
Relative time (h)

Figure S5

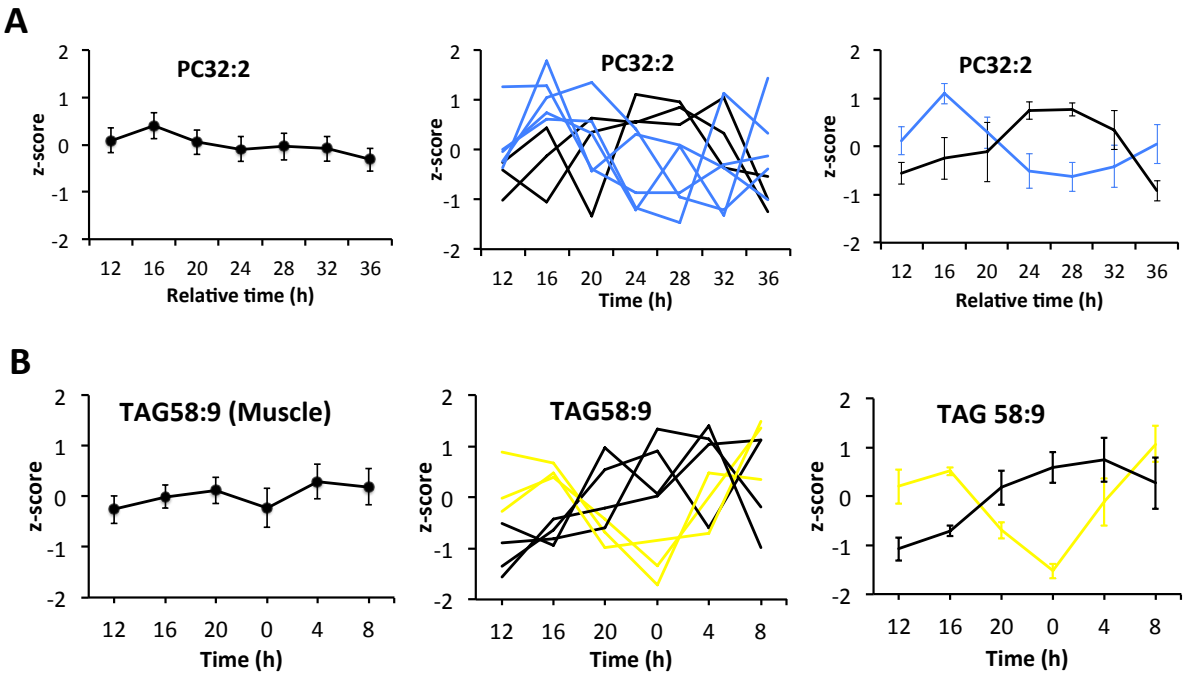
A
PC32:2
z-score
Relative time (h)
PC32:2
Time (h)
PC32:2
Relative time (h)
B
TAG58:9 (Muscle)
Time (h)
TAG58:9
Time (h)
TAG 58:9
Time (h)

Figure S6

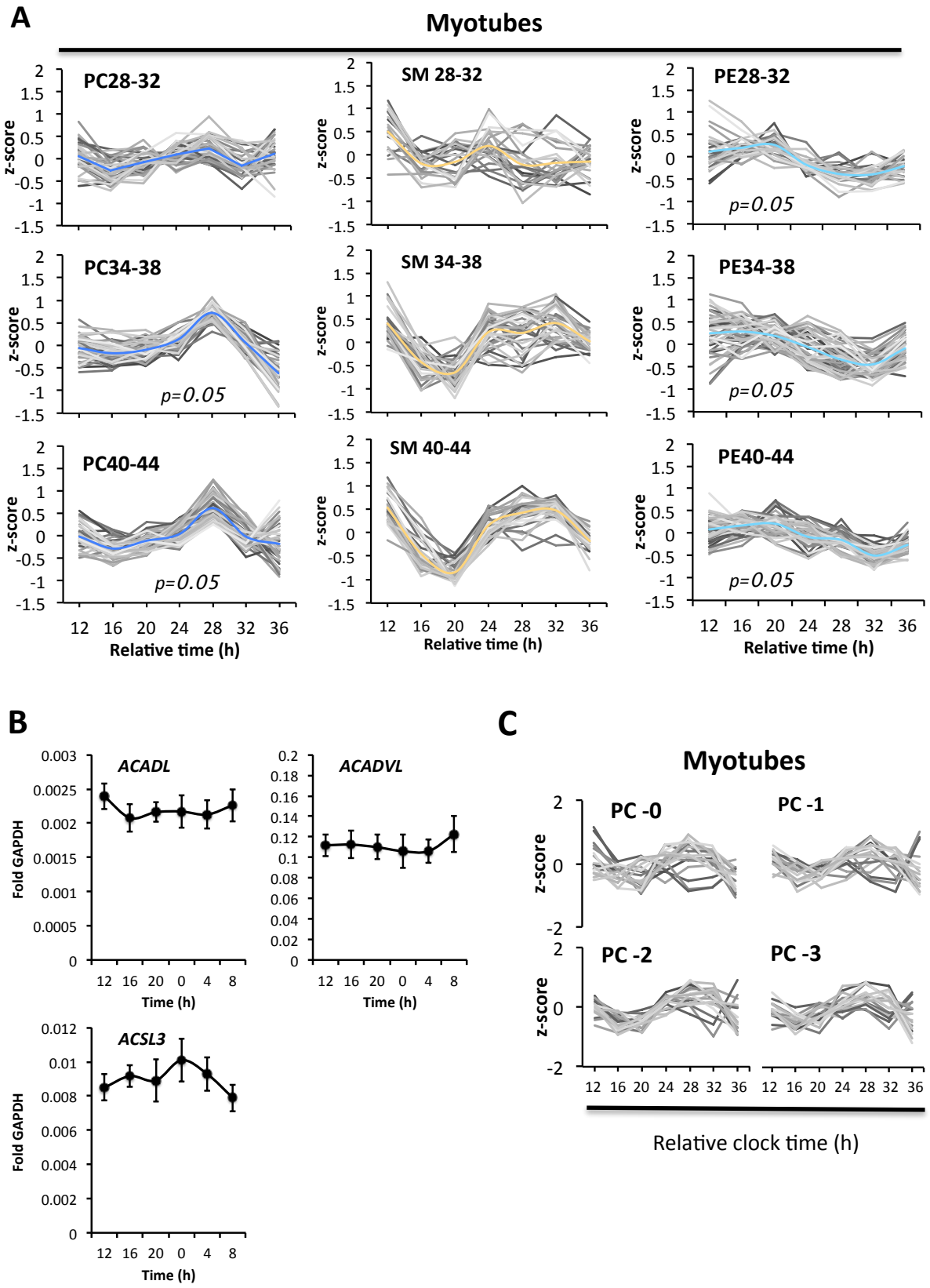
A
Myotubes
PC28-32
SM 28-32
PE28-32
PC34-38
SM 34-38
PE34-38
PC40-44
SM 40-44
PE40-44
p=0.05
z-score
Relative time (h)
B
ACADL
ACADVL
ACSL3
Fold GAPDH
Time (h)
C
Myotubes
PC -0
PC -1
PC -2
PC -3
z-score
Relative clock time (h)

Figure S7

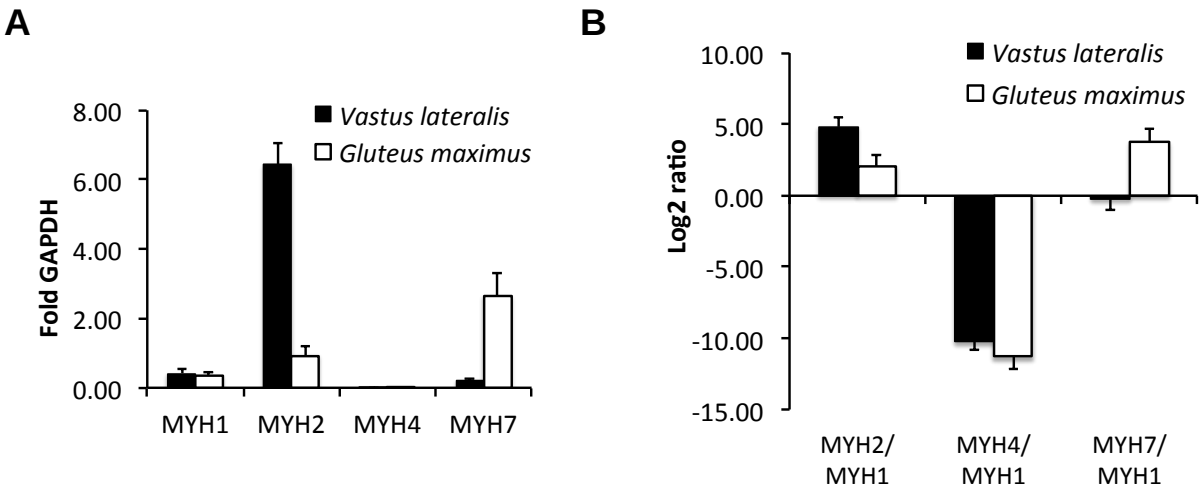
A
8.00
6.00
4.00
2.00
0.00
Fold GAPDH
Vastus lateralis
Gluteus maximus
MYH1
MYH2
MYH4
MYH7
B
10.00
5.00
0.00
-5.00
-10.00
-15.00
Log2 ratio
Vastus lateralis
Gluteus maximus
MYH2/ MYH1
MYH4/ MYH1
MYH7/ MYH1

8. REFERENCES

1. **Aschoff J.** 1965. CIRCADIAN RHYTHMS IN MAN. *Science* **148:**1427-1432.
2. **Bass J, Lazar MA.** 2016. Circadian time signatures of fitness and disease. *Science* **354:**994-999.
3. **Welsh DK, Takahashi JS, Kay SA.** 2010. Suprachiasmatic nucleus: cell autonomy and network properties. *Annu Rev Physiol* **72:**551-577.
4. **Schmutz I, Albrecht U, Ripperger JA.** 2012. The role of clock genes and rhythmicity in the liver. *Mol Cell Endocrinol* **349:**38-44.
5. **Stow LR, Gumz ML.** 2011. The circadian clock in the kidney. *J Am Soc Nephrol* **22:**598-604.
6. **Takeda N, Maemura K.** 2011. Circadian clock and cardiovascular disease. *J Cardiol* **57:**249-256.
7. **Zvonic S, Ptitsyn AA, Conrad SA, Scott LK, Floyd ZE, Kilroy G, Wu X, Goh BC, Mynatt RL, Gimble JM.** 2006. Characterization of peripheral circadian clocks in adipose tissues. *Diabetes* **55:**962-970.
8. **Pulimeno P, Mannic T, Sage D, Giovannoni L, Salmon P, Lemeille S, Giry-Laterriere M, Unser M, Bosco D, Bauer C, Morf J, Halban P, Philippe J, Dibner C.** 2013. Autonomous and self-sustained circadian oscillators displayed in human islet cells. *Diabetologia* **56:**497-507.
9. **Sadacca LA, Lamia KA, deLemos AS, Blum B, Weitz CJ.** 2011. An intrinsic circadian clock of the pancreas is required for normal insulin release and glucose homeostasis in mice. *Diabetologia* **54:**120-124.
10. **Perrin L, Loizides-Mangold U, Skarupelova S, Pulimeno P, Chanon S, Robert M, Bouzakri K, Modoux C, Roux-Lombard P, Vidal H, Lefai E, Dibner C.** 2015. Human skeletal myotubes display a cell-autonomous circadian clock implicated in basal myokine secretion. *Mol Metab* **4:**834-845.
11. **McCarthy JJ, Andrews JL, McDearmon EL, Campbell KS, Barber BK, Miller BH, Walker JR, Hogenesch JB, Takahashi JS, Esser KA.** 2007. Identification of the circadian transcriptome in adult mouse skeletal muscle. *Physiol Genomics* **31:**86-95.
12. **Miller BH, McDearmon EL, Panda S, Hayes KR, Zhang J, Andrews JL, Antoch MP, Walker JR, Esser KA, Hogenesch JB, Takahashi JS.** 2007. Circadian and CLOCK-controlled regulation of the mouse transcriptome and cell proliferation. *Proc Natl Acad Sci U S A* **104:**3342-3347.
13. **Balsalobre A, Damiola F, Schibler U.** 1998. A serum shock induces circadian gene expression in mammalian tissue culture cells. *Cell* **93:**929-937.
14. **Nagoshi E, Saini C, Bauer C, Laroche T, Naef F, Schibler U.** 2004. Circadian gene expression in individual fibroblasts: cell-autonomous and self-sustained oscillators pass time to daughter cells. *Cell* **119:**693-705.
15. **Welsh DK, Yoo SH, Liu AC, Takahashi JS, Kay SA.** 2004. Bioluminescence imaging of individual fibroblasts reveals persistent, independently phased circadian rhythms of clock gene expression. *Curr Biol* **14:**2289-2295.
16. **Petrenko V, Saini C, Giovannoni L, Gobet C, Sage D, Unser M, Heddad Masson M, Gu G, Bosco D, Gachon F, Philippe J, Dibner C.** 2017. Pancreatic alpha- and beta-cellular clocks have distinct molecular properties and impact on islet hormone secretion and gene expression. *Genes Dev* **31:**383-398.
17. **Dibner C, Sage D, Unser M, Bauer C, d'Eysmond T, Naef F, Schibler U.** 2009. Circadian gene expression is resilient to large fluctuations in overall transcription rates. *EMBO J* **28:**123-134.
18. **Dibner C, Schibler U, Albrecht U.** 2010. The mammalian circadian timing system: organization and coordination of central and peripheral clocks. *Annu Rev Physiol* **72:**517-549.
19. **Rimmer DW, Boivin DB, Shanahan TL, Kronauer RE, Duffy JF, Czeisler CA.** 2000. Dynamic resetting of the human circadian pacemaker by intermittent bright light. *Am J Physiol Regul Integr Comp Physiol* **279:**R1574-1579.
20. **Hatori M, Panda S.** 2010. The emerging roles of melanopsin in behavioral adaptation to light. *Trends Mol Med* **16:**435-446.
21. **Schroeder AM, Colwell CS.** 2013. How to fix a broken clock. *Trends Pharmacol Sci* **34:**605-619.
22. **Hara R, Wan K, Wakamatsu H, Aida R, Moriya T, Akiyama M, Shibata S.** 2001. Restricted feeding entrains liver clock without participation of the suprachiasmatic nucleus. *Genes Cells* **6:**269-278.
23. **Stokkan KA, Yamazaki S, Tei H, Sakaki Y, Menaker M.** 2001. Entrainment of the circadian clock in the liver by feeding. *Science* **291:**490-493.
24. **Wu T, Ni Y, Zhuge F, Fu Z.** 2010. Resetting process of peripheral circadian gene expression after the combined reversal of feeding schedule and light/dark cycle *via* a 24-h light period transition in rats. *Physiol Res* **59:**581-590.
25. **Sujino M, Furukawa K, Koinuma S, Fujioka A, Nagano M, Iigo M, Shigeyoshi Y.** 2012. Differential entrainment of peripheral clocks in the rat by glucocorticoid and feeding. *Endocrinology* **153:**2277-2286.
26. **Tahara Y, Hirao A, Moriya T, Kudo T, Shibata S.** 2010. Effects of medial hypothalamic lesions on feeding-induced entrainment of locomotor activity and liver Per2 expression in Per2::luc mice. *J Biol Rhythms* **25:**9-18.
27. **Izumo M, Pejchal M, Schook AC, Lange RP, Walisser JA, Sato TR, Wang X, Bradfield CA, Takahashi JS.** 2014. Differential effects of light and feeding on circadian organization of peripheral clocks in a forebrain Bmal1 mutant. *Elife* **3**.
28. **Ikeda Y, Sasaki H, Ohtsu T, Shiraishi T, Tahara Y, Shibata S.** 2015. Feeding and adrenal entrainment stimuli are both necessary for normal circadian oscillation of peripheral clocks in mice housed under different photoperiods. *Chronobiol Int* **32:**195-210.
29. **Stephan FK, Swann JM, Sisk CL.** 1979. Entrainment of circadian rhythms by feeding schedules in rats with suprachiasmatic lesions. *Behav Neural Biol* **25:**545-554.
30. **Damiola F, Le Minh N, Preitner N, Kornmann B, Fleury-Olela F, Schibler U.** 2000. Restricted feeding uncouples circadian oscillators in peripheral tissues from the central pacemaker in the suprachiasmatic nucleus. *Genes Dev* **14:**2950-2961.
31. **Kornmann B, Schaad O, Bujard H, Takahashi JS, Schibler U.** 2007. System-driven and oscillator-dependent circadian transcription in mice with a conditionally active liver clock. *PLoS Biol* **5:**e34.
32. **Vollmers C, Gill S, DiTacchio L, Pulivarthy SR, Le HD, Panda S.** 2009. Time of feeding and the intrinsic circadian clock drive rhythms in hepatic gene expression. *Proc Natl Acad Sci U S A* **106:**21453-21458.
33. **Ohnishi N, Tahara Y, Kuriki D, Haraguchi A, Shibata S.** 2014. Warm water bath stimulates phase-shifts of the peripheral circadian clocks in PER2::LUCIFERASE mouse. *PLoS One* **9:**e100272.
34. **Saini C, Morf J, Stratmann M, Gos P, Schibler U.** 2012. Simulated body temperature rhythms reveal the phase-shifting behavior and plasticity of mammalian circadian oscillators. *Genes Dev* **26:**567-580.

35. **Brown SA, Zumbrunn G, Fleury-Olela F, Preitner N, Schibler U.** 2002. Rhythms of mammalian body temperature can sustain peripheral circadian clocks. *Curr Biol* **12:**1574-1583.
36. **Buhr ED, Yoo SH, Takahashi JS.** 2010. Temperature as a universal resetting cue for mammalian circadian oscillators. *Science* **330:**379-385.
37. **Chappuis S, Ripperger JA, Schnell A, Rando G, Jud C, Wahli W, Albrecht U.** 2013. Role of the circadian clock gene Per2 in adaptation to cold temperature. *Mol Metab* **2:**184-193.
38. **Wehr TA, Aeschbach D, Duncan WC.** 2001. Evidence for a biological dawn and dusk in the human circadian timing system. *The Journal of Physiology* **535:**937-951.
39. **Sasaki H, Hattori Y, Ikeda Y, Kamagata M, Iwami S, Yasuda S, Shibata S.** 2016. Phase shifts in circadian peripheral clocks caused by exercise are dependent on the feeding schedule in PER2::LUC mice. *Chronobiol Int* **33:**849-862.
40. **Yamanaka Y, Honma S, Honma K.** 2008. Scheduled exposures to a novel environment with a running-wheel differentially accelerate re-entrainment of mice peripheral clocks to new light-dark cycles. *Genes Cells* **13:**497-507.
41. **Schroeder AM, Truong D, Loh DH, Jordan MC, Roos KP, Colwell CS.** 2012. Voluntary scheduled exercise alters diurnal rhythms of behaviour, physiology and gene expression in wild-type and vasoactive intestinal peptide-deficient mice. *J Physiol* **590:**6213-6226.
42. **Wolff G, Esser KA.** 2012. Scheduled exercise phase shifts the circadian clock in skeletal muscle. *Med Sci Sports Exerc* **44:**1663-1670.
43. **Morf J, Rey G, Schneider K, Stratmann M, Fujita J, Naef F, Schibler U.** 2012. Cold-inducible RNA-binding protein modulates circadian gene expression posttranscriptionally. *Science* **338:**379-383.
44. **Preussner M, Goldammer G, Neumann A, Haltenhof T, Rautenstrauch P, Muller-McNicoll M, Heyd F.** 2017. Body Temperature Cycles Control Rhythmic Alternative Splicing in Mammals. *Mol Cell* **67:**433-446 e434.
45. **Almon RR, Yang E, Lai W, Androulakis IP, Ghimbovschi S, Hoffman EP, Jusko WJ, Dubois DC.** 2008. Relationships between circadian rhythms and modulation of gene expression by glucocorticoids in skeletal muscle. *Am J Physiol Regul Integr Comp Physiol* **295:**R1031-1047.
46. **Pezuk P, Mohawk JA, Wang LA, Menaker M.** 2012. Glucocorticoids as entraining signals for peripheral circadian oscillators. *Endocrinology* **153:**4775-4783.
47. **Balsalobre A, Brown SA, Marcacci L, Tronche F, Kellendonk C, Reichardt HM, Schutz G, Schibler U.** 2000. Resetting of circadian time in peripheral tissues by glucocorticoid signaling. *Science* **289:**2344-2347.
48. **Nader N, Chrousos GP, Kino T.** 2009. Circadian rhythm transcription factor CLOCK regulates the transcriptional activity of the glucocorticoid receptor by acetylating its hinge region lysine cluster: potential physiological implications. *FASEB J* **23:**1572-1583.
49. **Reddy AB, Maywood ES, Karp NA, King VM, Inoue Y, Gonzalez FJ, Lilley KS, Kyriacou CP, Hastings MH.** 2007. Glucocorticoid signaling synchronizes the liver circadian transcriptome. *Hepatology* **45:**1478-1488.
50. **Balsalobre A, Marcacci L, Schibler U.** 2000. Multiple signaling pathways elicit circadian gene expression in cultured Rat-1 fibroblasts. *Curr Biol* **10:**1291-1294.
51. **Yagita K, Okamura H.** 2000. Forskolin induces circadian gene expression of rPer1, rPer2 and dbp in mammalian rat-1 fibroblasts. *FEBS Lett* **465:**79-82.
52. **Grontved L, John S, Baek S, Liu Y, Buckley JR, Vinson C, Aguilera G, Hager GL.** 2013. C/EBP maintains chromatin accessibility in liver and facilitates glucocorticoid receptor recruitment to steroid response elements. *EMBO J* **32:**1568-1583.
53. **Heitzer MD, Wolf IM, Sanchez ER, Witchel SF, DeFranco DB.** 2007. Glucocorticoid receptor physiology. *Rev Endocr Metab Disord* **8:**321-330.
54. **Han DH, Lee YJ, Kim K, Kim CJ, Cho S.** 2014. Modulation of glucocorticoid receptor induction properties by core circadian clock proteins. *Mol Cell Endocrinol* **383:**170-180.
55. **Hirota T, Okano T, Kokame K, Shirotani-Ikejima H, Miyata T, Fukada Y.** 2002. Glucose down-regulates Per1 and Per2 mRNA levels and induces circadian gene expression in cultured Rat-1 fibroblasts. *J Biol Chem* **277:**44244-44251.
56. **Pagani L, Semenova EA, Moriggi E, Revell VL, Hack LM, Lockley SW, Arendt J, Skene DJ, Meier F, Izakovic J, Wirz-Justice A, Cajochen C, Sergeeva OJ, Cheresiz SV, Danilenko KV, Eckert A, Brown SA.** 2010. The physiological period length of the human circadian clock in vivo is directly proportional to period in human fibroblasts. *PLoS One* **5:**e13376.
57. **Brown SA, Ripperger J, Kadener S, Fleury-Olela F, Vilbois F, Rosbash M, Schibler U.** 2005. PERIOD1-associated proteins modulate the negative limb of the mammalian circadian oscillator. *Science* **308:**693-696.
58. **Vitaterna MH, King DP, Chang AM, Kornhauser JM, Lowrey PL, McDonald JD, Dove WF, Pinto LH, Turek FW, Takahashi JS.** 1994. Mutagenesis and mapping of a mouse gene, Clock, essential for circadian behavior. *Science* **264:**719-725.
59. **Gekakis N, Staknis D, Nguyen HB, Davis FC, Wilsbacher LD, King DP, Takahashi JS, Weitz CJ.** 1998. Role of the CLOCK protein in the mammalian circadian mechanism. *Science* **280:**1564-1569.
60. **Yoshitane H, Ozaki H, Terajima H, Du NH, Suzuki Y, Fujimori T, Kosaka N, Shimba S, Sugano S, Takagi T, Iwasaki W, Fukada Y.** 2014. CLOCK-controlled polyphonic regulation of circadian rhythms through canonical and noncanonical E-boxes. *Mol Cell Biol* **34:**1776-1787.
61. **Kwon I, Lee J, Chang SH, Jung NC, Lee BJ, Son GH, Kim K, Lee KH.** 2006. BMAL1 shuttling controls transactivation and degradation of the CLOCK/BMAL1 heterodimer. *Mol Cell Biol* **26:**7318-7330.
62. **Langmesser S, Tallone T, Bordon A, Rusconi S, Albrecht U.** 2008. Interaction of circadian clock proteins PER2 and CRY with BMAL1 and CLOCK. *BMC Mol Biol* **9:**41.
63. **Kim JY, Kwak PB, Weitz CJ.** 2014. Specificity in circadian clock feedback from targeted reconstitution of the NuRD corepressor. *Mol Cell* **56:**738-748.
64. **Padmanabhan K, Robles MS, Westerling T, Weitz CJ.** 2012. Feedback regulation of transcriptional termination by the mammalian circadian clock PERIOD complex. *Science* **337:**599-602.
65. **Griffin EA, Jr., Staknis D, Weitz CJ.** 1999. Light-independent role of CRY1 and CRY2 in the mammalian circadian clock. *Science* **286:**768-771.
66. **Kume K, Zylka MJ, Sriram S, Shearman LP, Weaver DR, Jin X, Maywood ES, Hastings MH, Reppert SM.** 1999. mCRY1 and mCRY2 are essential components of the negative limb of the circadian clock feedback loop. *Cell* **98:**193-205.

67. **Sangoram AM, Saez L, Antoch MP, Gekakis N, Staknis D, Whiteley A, Fruechte EM, Vitaterna MH, Shimomura K, King DP, Young MW, Weitz CJ, Takahashi JS.** 1998. Mammalian circadian autoregulatory loop: a timeless ortholog and mPer1 interact and negatively regulate CLOCK-BMAL1-induced transcription. *Neuron* **21:**1101-1113.
68. **Zheng B, Albrecht U, Kaasik K, Sage M, Lu W, Vaishnav S, Li Q, Sun ZS, Eichele G, Bradley A, Lee CC.** 2001. Nonredundant roles of the mPer1 and mPer2 genes in the mammalian circadian clock. *Cell* **105:**683-694.
69. **Sato TK, Yamada RG, Ukai H, Baggs JE, Miraglia LJ, Kobayashi TJ, Welsh DK, Kay SA, Ueda HR, Hogenesch JB.** 2006. Feedback repression is required for mammalian circadian clock function. *Nat Genet* **38:**312-319.
70. **Godinho SI, Maywood ES, Shaw L, Tucci V, Barnard AR, Busino L, Pagano M, Kendall R, Quwailid MM, Romero MR, O'Neill J, Chesham JE, Brooker D, Lalanne Z, Hastings MH, Nolan PM.** 2007. The after-hours mutant reveals a role for Fbxl3 in determining mammalian circadian period. *Science* **316:**897-900.
71. **Busino L, Bassermann F, Maiolica A, Lee C, Nolan PM, Godinho SI, Draetta GF, Pagano M.** 2007. SCFFbxl3 controls the oscillation of the circadian clock by directing the degradation of cryptochrome proteins. *Science* **316:**900-904.
72. **Siepka SM, Yoo SH, Park J, Song W, Kumar V, Hu Y, Lee C, Takahashi JS.** 2007. Circadian mutant Overtime reveals F-box protein FBXL3 regulation of cryptochrome and period gene expression. *Cell* **129:**1011-1023.
73. **Tamayo AG, Duong HA, Robles MS, Mann M, Weitz CJ.** 2015. Histone monoubiquitination by Clock-Bmal1 complex marks Per1 and Per2 genes for circadian feedback. *Nat Struct Mol Biol* **22:**759-766.
74. **Duong HA, Robles MS, Knutti D, Weitz CJ.** 2011. A molecular mechanism for circadian clock negative feedback. *Science* **332:**1436-1439.
75. **Lande-Diner L, Boyault C, Kim JY, Weitz CJ.** 2013. A positive feedback loop links circadian clock factor CLOCK-BMAL1 to the basic transcriptional machinery. *Proc Natl Acad Sci U S A* **110:**16021-16026.
76. **Fang B, Everett LJ, Jager J, Briggs E, Armour SM, Feng D, Roy A, Gerhart-Hines Z, Sun Z, Lazar MA.** 2014. Circadian enhancers coordinate multiple phases of rhythmic gene transcription in vivo. *Cell* **159:**1140-1152.
77. **Robles MS, Boyault C, Knutti D, Padmanabhan K, Weitz CJ.** 2010. Identification of RACK1 and protein kinase Calpha as integral components of the mammalian circadian clock. *Science* **327:**463-466.
78. **Anafi RC, Lee Y, Sato TK, Venkataraman A, Ramanathan C, Kavakli IH, Hughes ME, Baggs JE, Growe J, Liu AC, Kim J, Hogenesch JB.** 2014. Machine learning helps identify CHRONO as a circadian clock component. *PLoS Biol* **12:**e1001840.
79. **Zhao WN, Malinin N, Yang FC, Staknis D, Gekakis N, Maier B, Reischl S, Kramer A, Weitz CJ.** 2007. CIPC is a mammalian circadian clock protein without invertebrate homologues. *Nat Cell Biol* **9:**268-275.
80. **Guillaumond F, Dardente H, Giguere V, Cermakian N.** 2005. Differential control of Bmal1 circadian transcription by REV-ERB and ROR nuclear receptors. *J Biol Rhythms* **20:**391-403.
81. **Raghuram S, Stayrook KR, Huang P, Rogers PM, Nosie AK, McClure DB, Burris LL, Khorasanizadeh S, Burris TP, Rastinejad F.** 2007. Identification of heme as the ligand for the orphan nuclear receptors REV-ERBalpha and REV-ERBbeta. *Nat Struct Mol Biol* **14:**1207-1213.
82. **Yin L, Lazar MA.** 2005. The orphan nuclear receptor Rev-erbalpha recruits the N-CoR/histone deacetylase 3 corepressor to regulate the circadian Bmal1 gene. *Mol Endocrinol* **19:**1452-1459.
83. **Ramakrishnan SN, Lau P, Crowther LM, Cleasby ME, Millard S, Leong GM, Cooney GJ, Muscat GE.** 2009. Rev-erb beta regulates the Srebp-1c promoter and mRNA expression in skeletal muscle cells. *Biochem Biophys Res Commun* **388:**654-659.
84. **Preitner N, Damiola F, Lopez-Molina L, Zakany J, Duboule D, Albrecht U, Schibler U.** 2002. The orphan nuclear receptor REV-ERBalpha controls circadian transcription within the positive limb of the mammalian circadian oscillator. *Cell* **110:**251-260.
85. **Phelan CA, Gampe RT, Jr., Lambert MH, Parks DJ, Montana V, Bynum J, Broderick TM, Hu X, Williams SP, Nolte RT, Lazar MA.** 2010. Structure of Rev-erbalpha bound to N-CoR reveals a unique mechanism of nuclear receptor-co-repressor interaction. *Nat Struct Mol Biol* **17:**808-814.
86. **Wu N, Yin L, Hanniman EA, Joshi S, Lazar MA.** 2009. Negative feedback maintenance of heme homeostasis by its receptor, Rev-erbalpha. *Genes Dev* **23:**2201-2209.
87. **Stratmann M, Suter DM, Molina N, Naef F, Schibler U.** 2012. Circadian Dbp transcription relies on highly dynamic BMAL1-CLOCK interaction with E boxes and requires the proteasome. *Mol Cell* **48:**277-287.
88. **Ripperger JA, Schibler U.** 2006. Rhythmic CLOCK-BMAL1 binding to multiple E-box motifs drives circadian Dbp transcription and chromatin transitions. *Nat Genet* **38:**369-374.
89. **Yamaguchi S, Mitsui S, Yan L, Yagita K, Miyake S, Okamura H.** 2000. Role of DBP in the circadian oscillatory mechanism. *Mol Cell Biol* **20:**4773-4781.
90. **Maury E, Ramsey KM, Bass J.** 2010. Circadian rhythms and metabolic syndrome: from experimental genetics to human disease. *Circ Res* **106:**447-462.
91. **Baggs JE, Price TS, DiTacchio L, Panda S, Fitzgerald GA, Hogenesch JB.** 2009. Network features of the mammalian circadian clock. *PLoS Biol* **7:**e52.
92. **DeBruyne JP, Weaver DR, Reppert SM.** 2007. CLOCK and NPAS2 have overlapping roles in the suprachiasmatic circadian clock. *Nat Neurosci* **10:**543-545.
93. **Debruyne JP, Noton E, Lambert CM, Maywood ES, Weaver DR, Reppert SM.** 2006. A clock shock: mouse CLOCK is not required for circadian oscillator function. *Neuron* **50:**465-477.
94. **Shi S, Hida A, McGuinness OP, Wasserman DH, Yamazaki S, Johnson CH.** 2010. Circadian clock gene Bmal1 is not essential; functional replacement with its paralog, Bmal2. *Curr Biol* **20:**316-321.
95. **Liu AC, Tran HG, Zhang EE, Priest AA, Welsh DK, Kay SA.** 2008. Redundant function of REV-ERBalpha and beta and non-essential role for Bmal1 cycling in transcriptional regulation of intracellular circadian rhythms. *PLoS Genet* **4:**e1000023.
96. **Yang F, Inoue I, Kumagai M, Takahashi S, Nakajima Y, Ikeda M.** 2013. Real-time analysis of the circadian oscillation of the Rev-Erb beta promoter. *J Atheroscler Thromb* **20:**267-276.
97. **Lee C, Etchegaray JP, Cagampang FR, Loudon AS, Reppert SM.** 2001. Posttranslational mechanisms regulate the mammalian circadian clock. *Cell* **107:**855-867.
98. **Hirota T, Lewis WG, Liu AC, Lee JW, Schultz PG, Kay SA.** 2008. A chemical biology approach reveals period shortening of the mammalian circadian clock by specific inhibition of GSK-3beta. *Proc Natl Acad Sci U S A* **105:**20746-20751.

99. **Besing RC, Paul JR, Hablitz LM, Rogers CO, Johnson RL, Young ME, Gamble KL.** 2015. Circadian rhythmicity of active GSK3 isoforms modulates molecular clock gene rhythms in the suprachiasmatic nucleus. *J Biol Rhythms* **30:**155-160.
100. **Iitaka C, Miyazaki K, Akaike T, Ishida N.** 2005. A role for glycogen synthase kinase-3beta in the mammalian circadian clock. *J Biol Chem* **280:**29397-29402.
101. **Harada Y, Sakai M, Kurabayashi N, Hirota T, Fukada Y.** 2005. Ser-557-phosphorylated mCRY2 is degraded upon synergistic phosphorylation by glycogen synthase kinase-3 beta. *J Biol Chem* **280:**31714-31721.
102. **Sahar S, Zocchi L, Kinoshita C, Borrelli E, Sassone-Corsi P.** 2010. Regulation of BMAL1 protein stability and circadian function by GSK3beta-mediated phosphorylation. *PLoS One* **5:**e8561.
103. **Spengler ML, Kuropatwinski KK, Schumer M, Antoch MP.** 2009. A serine cluster mediates BMAL1-dependent CLOCK phosphorylation and degradation. *Cell Cycle* **8:**4138-4146.
104. **Yoshitane H, Takao T, Satomi Y, Du NH, Okano T, Fukada Y.** 2009. Roles of CLOCK phosphorylation in suppression of E-box-dependent transcription. *Mol Cell Biol* **29:**3675-3686.
105. **Kurabayashi N, Hirota T, Sakai M, Sanada K, Fukada Y.** 2010. DYRK1A and glycogen synthase kinase 3beta, a dual-kinase mechanism directing proteasomal degradation of CRY2 for circadian timekeeping. *Mol Cell Biol* **30:**1757-1768.
106. **Yin L, Wang J, Klein PS, Lazar MA.** 2006. Nuclear receptor Rev-erbalpha is a critical lithium-sensitive component of the circadian clock. *Science* **311:**1002-1005.
107. **Sanada K, Okano T, Fukada Y.** 2002. Mitogen-activated protein kinase phosphorylates and negatively regulates basic helix-loop-helix-PAS transcription factor BMAL1. *J Biol Chem* **277:**267-271.
108. **Sanada K, Harada Y, Sakai M, Todo T, Fukada Y.** 2004. Serine phosphorylation of mCRY1 and mCRY2 by mitogen-activated protein kinase. *Genes Cells* **9:**697-708.
109. **Eide EJ, Woolf MF, Kang H, Woolf P, Hurst W, Camacho F, Vielhaber EL, Giovanni A, Virshup DM.** 2005. Control of mammalian circadian rhythm by CKIepsilon-regulated proteasome-mediated PER2 degradation. *Mol Cell Biol* **25:**2795-2807.
110. **Eide EJ, Vielhaber EL, Hinz WA, Virshup DM.** 2002. The circadian regulatory proteins BMAL1 and cryptochromes are substrates of casein kinase Iepsilon. *J Biol Chem* **277:**17248-17254.
111. **Takano A, Isojima Y, Nagai K.** 2004. Identification of mPer1 phosphorylation sites responsible for the nuclear entry. *J Biol Chem* **279:**32578-32585.
112. **Loudon AS, Meng QJ, Maywood ES, Bechtold DA, Boot-Handford RP, Hastings MH.** 2007. The biology of the circadian Ck1epsilon tau mutation in mice and Syrian hamsters: a tale of two species. *Cold Spring Harb Symp Quant Biol* **72:**261-271.
113. **Akashi M, Tsuchiya Y, Yoshino T, Nishida E.** 2002. Control of intracellular dynamics of mammalian period proteins by casein kinase I epsilon (CKIepsilon) and CKIdelta in cultured cells. *Mol Cell Biol* **22:**1693-1703.
114. **Tamaru T, Hattori M, Honda K, Nakahata Y, Sassone-Corsi P, van der Horst GT, Ozawa T, Takamatsu K.** 2015. CRY Drives Cyclic CK2-Mediated BMAL1 Phosphorylation to Control the Mammalian Circadian Clock. *PLoS Biol* **13:**e1002293.
115. **Lamia KA, Sachdeva UM, DiTacchio L, Williams EC, Alvarez JG, Egan DF, Vasquez DS, Juguilon H, Panda S, Shaw RJ, Thompson CB, Evans RM.** 2009. AMPK regulates the circadian clock by cryptochrome phosphorylation and degradation. *Science* **326:**437-440.
116. **Ramsey KM, Yoshino J, Brace CS, Abrassart D, Kobayashi Y, Marcheva B, Hong HK, Chong JL, Buhr ED, Lee C, Takahashi JS, Imai S, Bass J.** 2009. Circadian clock feedback cycle through NAMPT-mediated NAD+ biosynthesis. *Science* **324:**651-654.
117. **Nakahata Y, Sahar S, Astarita G, Kaluzova M, Sassone-Corsi P.** 2009. Circadian control of the NAD+ salvage pathway by CLOCK-SIRT1. *Science* **324:**654-657.
118. **Asher G, Gatfield D, Stratmann M, Reinke H, Dibner C, Kreppel F, Mostoslavsky R, Alt FW, Schibler U.** 2008. SIRT1 regulates circadian clock gene expression through PER2 deacetylation. *Cell* **134:**317-328.
119. **Wang RH, Zhao T, Cui K, Hu G, Chen Q, Chen W, Wang XW, Soto-Gutierrez A, Zhao K, Deng CX.** 2016. Negative reciprocal regulation between Sirt1 and Per2 modulates the circadian clock and aging. *Sci Rep* **6:**28633.
120. **Nakahata Y, Kaluzova M, Grimaldi B, Sahar S, Hirayama J, Chen D, Guarente LP, Sassone-Corsi P.** 2008. The NAD+-dependent deacetylase SIRT1 modulates CLOCK-mediated chromatin remodeling and circadian control. *Cell* **134:**329-340.
121. **Bellet MM, Sassone-Corsi P.** 2010. Mammalian circadian clock and metabolism – the epigenetic link. *J Cell Sci* **123:**3837-3848.
122. **Cardone L, Hirayama J, Giordano F, Tamaru T, Palvimo JJ, Sassone-Corsi P.** 2005. Circadian clock control by SUMOylation of BMAL1. *Science* **309:**1390-1394.
123. **Lee J, Lee Y, Lee MJ, Park E, Kang SH, Chung CH, Lee KH, Kim K.** 2008. Dual modification of BMAL1 by SUMO2/3 and ubiquitin promotes circadian activation of the CLOCK/BMAL1 complex. *Mol Cell Biol* **28:**6056-6065.
124. **Yagita K, Tamanini F, Yasuda M, Hoeijmakers JH, van der Horst GT, Okamura H.** 2002. Nucleocytoplasmic shuttling and mCRY-dependent inhibition of ubiquitylation of the mPER2 clock protein. *Embo j* **21:**1301-1314.
125. **DeBruyne JP, Baggs JE, Sato TK, Hogenesch JB.** 2015. Ubiquitin ligase Siah2 regulates RevErbalpha degradation and the mammalian circadian clock. *Proc Natl Acad Sci U S A* **112:**12420-12425.
126. **Durgan DJ, Pat BM, Laczy B, Bradley JA, Tsai JY, Grenett MH, Ratcliffe WF, Brewer RA, Nagendran J, Villegas-Montoya C, Zou C, Zou L, Johnson RL, Jr., Dyck JR, Bray MS, Gamble KL, Chatham JC, Young ME.** 2011. O-GlcNAcylation, novel post-translational modification linking myocardial metabolism and cardiomyocyte circadian clock. *J Biol Chem* **286:**44606-44619.
127. **Kim EY, Jeong EH, Park S, Jeong HJ, Edery I, Cho JW.** 2012. A role for O-GlcNAcylation in setting circadian clock speed. *Genes Dev* **26:**490-502.
128. **Kaasik K, Kivimae S, Allen JJ, Chalkley RJ, Huang Y, Baer K, Kissel H, Burlingame AL, Shokat KM, Ptacek LJ, Fu YH.** 2013. Glucose sensor O-GlcNAcylation coordinates with phosphorylation to regulate circadian clock. *Cell Metab* **17:**291-302.
129. **Li MD, Ruan HB, Hughes ME, Lee JS, Singh JP, Jones SP, Nitabach MN, Yang X.** 2013. O-GlcNAc signaling entrains the circadian clock by inhibiting BMAL1/CLOCK ubiquitination. *Cell Metab* **17:**303-310.
130. **Ma YT, Luo H, Guan WJ, Zhang H, Chen C, Wang Z, Li JD.** 2013. O-GlcNAcylation of BMAL1 regulates circadian rhythms in NIH3T3 fibroblasts. *Biochem Biophys Res Commun* **431:**382-387.

131. **Gachon F, Loizides-Mangold U, Petrenko V, Dibner C.** 2017. Glucose Homeostasis: Regulation by Peripheral Circadian Clocks in Rodents and Humans. *Endocrinology* **158:**1074-1084.
132. **Atger F, Gobet C, Marquis J, Martin E, Wang J, Weger B, Lefebvre G, Descombes P, Naef F, Gachon F.** 2015. Circadian and feeding rhythms differentially affect rhythmic mRNA transcription and translation in mouse liver. *Proc Natl Acad Sci U S A* **112:**E6579-6588.
133. **Jouffe C, Cretenet G, Symul L, Martin E, Atger F, Naef F, Gachon F.** 2013. The circadian clock coordinates ribosome biogenesis. *PLoS Biol* **11:**e1001455.
134. **Liu X, Dang Y, Matsu-Ura T, He Y, He Q, Hong CI, Liu Y.** 2017. DNA Replication Is Required for Circadian Clock Function by Regulating Rhythmic Nucleosome Composition. *Mol Cell* **67:**203-213.e204.
135. **Sinturel F, Gerber A, Mauvoisin D, Wang J, Gatfield D, Stubblefield JJ, Green CB, Gachon F, Schibler U.** 2017. Diurnal Oscillations in Liver Mass and Cell Size Accompany Ribosome Assembly Cycles. *Cell* **169:**651-663.e614.
136. **Zhang R, Lahens NF, Ballance HI, Hughes ME, Hogenesch JB.** 2014. A circadian gene expression atlas in mammals: implications for biology and medicine. *Proc Natl Acad Sci U S A* **111:**16219-16224.
137. **Adamovich Y, Rousso-Noori L, Zwighaft Z, Neufeld-Cohen A, Golik M, Kraut-Cohen J, Wang M, Han X, Asher G.** 2014. Circadian clocks and feeding time regulate the oscillations and levels of hepatic triglycerides. *Cell Metab* **19:**319-330.
138. **Muhlbauer E, Wolgast S, Finckh U, Peschke D, Peschke E.** 2004. Indication of circadian oscillations in the rat pancreas. *FEBS Lett* **564:**91-96.
139. **Perelis M, Marcheva B, Ramsey KM, Schipma MJ, Hutchison AL, Taguchi A, Peek CB, Hong H, Huang W, Omura C, Allred AL, Bradfield CA, Dinner AR, Barish GD, Bass J.** 2015. Pancreatic beta cell enhancers regulate rhythmic transcription of genes controlling insulin secretion. *Science* **350:**aac4250.
140. **Dyar KA, Ciciliot S, Tagliazucchi GM, Pallafacchina G, Tothova J, Argentini C, Agatea L, Abraham R, Ahdesmaki M, Forcato M, Bicciato S, Schiaffino S, Blaauw B.** 2015. The calcineurin-NFAT pathway controls activity-dependent circadian gene expression in slow skeletal muscle. *Mol Metab* **4:**823-833.
141. **Ando H, Yanagihara H, Hayashi Y, Obi Y, Tsuruoka S, Takamura T, Kaneko S, Fujimura A.** 2005. Rhythmic messenger ribonucleic acid expression of clock genes and adipocytokines in mouse visceral adipose tissue. *Endocrinology* **146:**5631-5636.
142. **Menet JS, Rodriguez J, Abruzzi KC, Rosbash M.** 2012. Nascent-Seq reveals novel features of mouse circadian transcriptional regulation. *Elife* **1:**e00011.
143. **Le Martelot G, Canella D, Symul L, Migliavacca E, Gilardi F, Liechti R, Martin O, Harshman K, Delorenzi M, Desvergne B, Herr W, Deplancke B, Schibler U, Rougemont J, Guex N, Hernandez N, Naef F.** 2012. Genome-wide RNA polymerase II profiles and RNA accumulation reveal kinetics of transcription and associated epigenetic changes during diurnal cycles. *PLoS Biol* **10:**e1001442.
144. **Koike N, Yoo SH, Huang HC, Kumar V, Lee C, Kim TK, Takahashi JS.** 2012. Transcriptional architecture and chromatin landscape of the core circadian clock in mammals. *Science* **338:**349-354.
145. **Dyar KA, Ciciliot S, Wright LE, Bienso RS, Tagliazucchi GM, Patel VR, Forcato M, Paz MI, Gudiksen A, Solagna F, Albiero M, Moretti I, Eckel-Mahan KL, Baldi P, Sassone-Corsi P, Rizzuto R, Bicciato S, Pilegaard H, Blaauw B, Schiaffino S.** 2014. Muscle insulin sensitivity and glucose metabolism are controlled by the intrinsic muscle clock. *Mol Metab* **3:**29-41.
146. **Hodge BA, Wen Y, Riley LA, Zhang X, England JH, Harfmann BD, Schroder EA, Esser KA.** 2015. The endogenous molecular clock orchestrates the temporal separation of substrate metabolism in skeletal muscle. *Skelet Muscle* **5:**17.
147. **Mauvoisin D, Dayon L, Gachon F, Kussmann M.** 2015. Proteomics and circadian rhythms: it's all about signaling! *Proteomics* **15:**310-317.
148. **Mauvoisin D, Wang J, Jouffe C, Martin E, Atger F, Waridel P, Quadroni M, Gachon F, Naef F.** 2014. Circadian clock-dependent and -independent rhythmic proteomes implement distinct diurnal functions in mouse liver. *Proc Natl Acad Sci U S A* **111:**167-172.
149. **Aviram R, Manella G, Kopelman N, Neufeld-Cohen A, Zwighaft Z, Elimelech M, Adamovich Y, Golik M, Wang C, Han X, Asher G.** 2016. Lipidomics Analyses Reveal Temporal and Spatial Lipid Organization and Uncover Daily Oscillations in Intracellular Organelles. *Mol Cell* **62:**636-648.
150. **Chua EC, Shui G, Lee IT, Lau P, Tan LC, Yeo SC, Lam BD, Bulchand S, Summers SA, Puvanendran K, Rozen SG, Wenk MR, Gooley JJ.** 2013. Extensive diversity in circadian regulation of plasma lipids and evidence for different circadian metabolic phenotypes in humans. *Proc Natl Acad Sci U S A* **110:**14468-14473.
151. **Dallmann R, Viola AU, Tarokh L, Cajochen C, Brown SA.** 2012. The human circadian metabolome. *Proc Natl Acad Sci U S A* **109:**2625-2629.
152. **Krishnaiah SY, Wu G, Altman BJ, Growe J, Rhoades SD, Coldren F, Venkataraman A, Olarerin-George AO, Francey LJ, Mukherjee S, Girish S, Selby CP, Cal S, Er U, Sianati B, Sengupta A, Anafi RC, Kavakli IH, Sancar A, Baur JA, Dang CV, Hogenesch JB, Weljie AM.** 2017. Clock Regulation of Metabolites Reveals Coupling between Transcription and Metabolism. *Cell Metab* **25:**961-974.e964.
153. **Hughes ME, DiTacchio L, Hayes KR, Vollmers C, Pulivarthy S, Baggs JE, Panda S, Hogenesch JB.** 2009. Harmonics of circadian gene transcription in mammals. *PLoS Genet* **5:**e1000442.
154. **Harfmann BD, Schroder EA, Kachman MT, Hodge BA, Zhang X, Esser KA.** 2016. Muscle-specific loss of Bmal1 leads to disrupted tissue glucose metabolism and systemic glucose homeostasis. *Skelet Muscle* **6:**12.
155. **Le Martelot G, Claudel T, Gatfield D, Schaad O, Kornmann B, Lo Sasso G, Moschetta A, Schibler U.** 2009. REV-ERBalpha participates in circadian SREBP signaling and bile acid homeostasis. *PLoS Biol* **7:**e1000181.
156. **Reinke H, Asher G.** 2016. Circadian Clock Control of Liver Metabolic Functions. *Gastroenterology* **150:**574-580.
157. **Marcheva B, Ramsey KM, Buhr ED, Kobayashi Y, Su H, Ko CH, Ivanova G, Omura C, Mo S, Vitaterna MH, Lopez JP, Philipson LH, Bradfield CA, Crosby SD, JeBailey L, Wang X, Takahashi JS, Bass J.** 2010. Disruption of the clock components CLOCK and BMAL1 leads to hypoinsulinaemia and diabetes. *Nature* **466:**627-631.
158. **Saini C, Petrenko V, Pulimeno P, Giovannoni L, Berney T, Hebrok M, Howald C, Dermitzakis ET, Dibner C.** 2016. A functional circadian clock is required for proper insulin secretion by human pancreatic islet cells. *Diabetes Obes Metab* **18:**355-365.
159. **Andrews JL, Zhang X, McCarthy JJ, McDearmon EL, Hornberger TA, Russell B, Campbell KS, Arbogast S, Reid MB, Walker JR, Hogenesch JB, Takahashi JS, Esser KA.** 2010. CLOCK and BMAL1 regulate MyoD and are necessary for maintenance of skeletal muscle phenotype and function. *Proc Natl Acad Sci U S A* **107:**19090-19095.

160. **Kiehn JT, Tsang AH, Heyde I, Leinweber B, Kolbe I, Leliavski A, Oster H.** 2017. Circadian Rhythms in Adipose Tissue Physiology. *Compr Physiol* **7:**383-427.
161. **Gachon F, Olela FF, Schaad O, Descombes P, Schibler U.** 2006. The circadian PAR-domain basic leucine zipper transcription factors DBP, TEF, and HLF modulate basal and inducible xenobiotic detoxification. *Cell Metab* **4:**25-36.
162. **Man K, Loudon A, Chawla A.** 2016. Immunity around the clock. *Science* **354:**999-1003.
163. **Gibbs JE, Blaikley J, Beesley S, Matthews L, Simpson KD, Boyce SH, Farrow SN, Else KJ, Singh D, Ray DW, Loudon AS.** 2012. The nuclear receptor REV-ERBalpha mediates circadian regulation of innate immunity through selective regulation of inflammatory cytokines. *Proc Natl Acad Sci U S A* **109:**582-587.
164. **Journiac N, Jolly S, Jarvis C, Gautheron V, Rogard M, Trembleau A, Blondeau JP, Mariani J, Vernet-der Garabedian B.** 2009. The nuclear receptor ROR(alpha) exerts a bi-directional regulation of IL-6 in resting and reactive astrocytes. *Proc Natl Acad Sci U S A* **106:**21365-21370.
165. **Rutter J, Reick M, Wu LC, McKnight SL.** 2001. Regulation of clock and NPAS2 DNA binding by the redox state of NAD cofactors. *Science* **293:**510-514.
166. **Cajochen C, Frey S, Anders D, Spati J, Bues M, Pross A, Mager R, Wirz-Justice A, Stefani O.** 2011. Evening exposure to a light-emitting diodes (LED)-backlit computer screen affects circadian physiology and cognitive performance. *J Appl Physiol (1985)* **110:**1432-1438.
167. **Walmsley L, Hanna L, Mouland J, Martial F, West A, Smedley AR, Bechtold DA, Webb AR, Lucas RJ, Brown TM.** 2015. Colour as a signal for entraining the mammalian circadian clock. *PLoS Biol* **13:**e1002127.
168. **van der Lely S, Frey S, Garbazza C, Wirz-Justice A, Jenni OG, Steiner R, Wolf S, Cajochen C, Bromundt V, Schmidt C.** 2015. Blue blocker glasses as a countermeasure for alerting effects of evening light-emitting diode screen exposure in male teenagers. *J Adolesc Health* **56:**113-119.
169. **Scheer FAJL, Hilton MF, Mantzoros CS, Shea SA.** 2009. Adverse metabolic and cardiovascular consequences of circadian misalignment. *Proceedings of the National Academy of Sciences* **106:**4453-4458.
170. **Altman BJ.** 2016. Cancer Clocks Out for Lunch: Disruption of Circadian Rhythm and Metabolic Oscillation in Cancer. *Front Cell Dev Biol* **4:**62.
171. **Blakeman V, Williams JL, Meng QJ, Streuli CH.** 2016. Circadian clocks and breast cancer. *Breast Cancer Res* **18:**89.
172. **Hansen J.** 2017. Night Shift Work and Risk of Breast Cancer. *Curr Environ Health Rep*.
173. **Padmanabhan K, Billaud M.** 2017. Desynchronization of Circadian Clocks in Cancer: A Metabolic and Epigenetic Connection. *Front Endocrinol (Lausanne)* **8:**136.
174. **Reszka E, Przybek M, Muurlink O, Peplonska B.** 2017. Circadian gene variants and breast cancer. *Cancer Lett* **390:**137-145.
175. **Fu L, Pelicano H, Liu J, Huang P, Lee C.** 2002. The circadian gene Period2 plays an important role in tumor suppression and DNA damage response in vivo. *Cell* **111:**41-50.
176. **Hua H, Wang Y, Wan C, Liu Y, Zhu B, Yang C, Wang X, Wang Z, Cornelissen-Guillaume G, Halberg F.** 2006. Circadian gene mPer2 overexpression induces cancer cell apoptosis. *Cancer Sci* **97:**589-596.
177. **Mannic T, Meyer P, Triponez F, Pusztaszeri M, Le Martelot G, Mariani O, Schmitter D, Sage D, Philippe J, Dibner C.** 2013. Circadian clock characteristics are altered in human thyroid malignant nodules. *J Clin Endocrinol Metab* **98:**4446-4456.
178. **Makhlouf AM, Chitikova Z, Pusztaszeri M, Berczy M, Delucinge-Vivier C, Triponez F, Meyer P, Philippe J, Dibner C.** 2016. Identification of CHEK1, SLC26A4, c-KIT, TPO and TG as new biomarkers for human follicular thyroid carcinoma. *Oncotarget* **7:**45776-45788.
179. **Chitikova Z, Pusztaszeri M, Makhlouf AM, Berczy M, Delucinge-Vivier C, Triponez F, Meyer P, Philippe J, Dibner C.** 2015. Identification of new biomarkers for human papillary thyroid carcinoma employing NanoString analysis. *Oncotarget* **6:**10978-10993.
180. **Toh KL, Jones CR, He Y, Eide EJ, Hinz WA, Virshup DM, Ptacek LJ, Fu YH.** 2001. An hPer2 phosphorylation site mutation in familial advanced sleep phase syndrome. *Science* **291:**1040-1043.
181. **Pandi-Perumal SR, Trakht I, Spence DW, Srinivasan V, Dagan Y, Cardinali DP.** 2008. The roles of melatonin and light in the pathophysiology and treatment of circadian rhythm sleep disorders. *Nat Clin Pract Neurol* **4:**436-447.
182. **Archer SN, Robilliard DL, Skene DJ, Smits M, Williams A, Arendt J, von Schantz M.** 2003. A length polymorphism in the circadian clock gene Per3 is linked to delayed sleep phase syndrome and extreme diurnal preference. *Sleep* **26:**413-415.
183. **Sanchez-Garrido MA, Brandt SJ, Clemmensen C, Muller TD, DiMarchi RD, Tschop MH.** 2017. GLP-1/glucagon receptor co-agonism for treatment of obesity. *Diabetologia*.
184. **Dibner C, Schibler U.** 2015. Circadian timing of metabolism in animal models and humans. *J Intern Med* **277:**513-527.
185. **Albrecht U.** 2017. The circadian clock, metabolism and obesity. *Obes Rev* **18 Suppl 1:**25-33.
186. **Turek FW, Joshu C, Kohsaka A, Lin E, Ivanova G, McDearmon E, Laposky A, Losee-Olson S, Easton A, Jensen DR, Eckel RH, Takahashi JS, Bass J.** 2005. Obesity and metabolic syndrome in circadian Clock mutant mice. *Science* **308:**1043-1045.
187. **Shimba S, Ishii N, Ohta Y, Ohno T, Watabe Y, Hayashi M, Wada T, Aoyagi T, Tezuka M.** 2005. Brain and muscle Arnt-like protein-1 (BMAL1), a component of the molecular clock, regulates adipogenesis. *Proc Natl Acad Sci U S A* **102:**12071-12076.
188. **Paschos GK, Ibrahim S, Song WL, Kunieda T, Grant G, Reyes TM, Bradfield CA, Vaughan CH, Eiden M, Masoodi M, Griffin JL, Wang F, Lawson JA, Fitzgerald GA.** 2012. Obesity in mice with adipocyte-specific deletion of clock component Arntl. *Nat Med* **18:**1768-1777.
189. **Hemmeryckx B, Himmelreich U, Hoylaerts MF, Lijnen HR.** 2011. Impact of clock gene Bmal1 deficiency on nutritionally induced obesity in mice. *Obesity (Silver Spring)* **19:**659-661.
190. **Kohsaka A, Laposky AD, Ramsey KM, Estrada C, Joshu C, Kobayashi Y, Turek FW, Bass J.** 2007. High-fat diet disrupts behavioral and molecular circadian rhythms in mice. *Cell Metab* **6:**414-421.
191. **Ramkisoensing A, Meijer JH.** 2015. Synchronization of Biological Clock Neurons by Light and Peripheral Feedback Systems Promotes Circadian Rhythms and Health. *Front Neurol* **6:**128.
192. **Kettner NM, Mayo SA, Hua J, Lee C, Moore DD, Fu L.** 2015. Circadian Dysfunction Induces Leptin Resistance in Mice. *Cell metabolism* **22:**448-459.
193. **Wang H, van Spyk E, Liu Q, Geyfman M, Salmans ML, Kumar V, Ihler A, Li N, Takahashi JS, Andersen B.** 2017. Time-Restricted Feeding Shifts the Skin Circadian Clock and Alters UVB-Induced DNA Damage. *Cell Rep* **20:**1061-1072.

194. **Wu T, Fu O, Yao L, Sun L, Zhuge F, Fu Z.** 2012. Differential responses of peripheral circadian clocks to a short-term feeding stimulus. *Mol Biol Rep* **39:**9783-9789.
195. **Shavlakadze T, Anwari T, Soffe Z, Cozens G, Mark PJ, Gondro C, Grounds MD.** 2013. Impact of fasting on the rhythmic expression of myogenic and metabolic factors in skeletal muscle of adult mice. *Am J Physiol Cell Physiol* **305:**C26-35.
196. **Reznick J, Preston E, Wilks DL, Beale SM, Turner N, Cooney GJ.** 2013. Altered feeding differentially regulates circadian rhythms and energy metabolism in liver and muscle of rats. *Biochimica et Biophysica Acta (BBA) - Molecular Basis of Disease* **1832:**228-238.
197. **Lin YC, Hsiao TJ, Chen PC.** 2009. Persistent rotating shift-work exposure accelerates development of metabolic syndrome among middle-aged female employees: a five-year follow-up. *Chronobiol Int* **26:**740-755.
198. **Ellingsen T, Bener A, Gehani AA.** 2007. Study of shift work and risk of coronary events. *J R Soc Promot Health* **127:**265-267.
199. **Lin YC, Hsiao TJ, Chen PC.** 2009. Shift work aggravates metabolic syndrome development among early-middle-aged males with elevated ALT. *World J Gastroenterol* **15:**5654-5661.
200. **Silva-Costa A, Rotenberg L, Coeli CM, Nobre AA, Griep RH.** 2016. Night work is associated with glycemic levels and anthropometric alterations preceding diabetes: Baseline results from ELSA-Brasil. *Chronobiol Int* **33:**64-72.
201. **Sharma A, Laurenti MC, Dalla Man C, Varghese RT, Cobelli C, Rizza RA, Matveyenko A, Vella A.** 2017. Glucose metabolism during rotational shift-work in healthcare workers. *Diabetologia* **60:**1483-1490.
202. **Pivovarova O, Jurchott K, Rudovich N, Hornemann S, Ye L, Mockel S, Murahovschi V, Kessler K, Seltmann AC, Maser-Gluth C, Mazuch J, Kruse M, Busjahn A, Kramer A, Pfeiffer AF.** 2015. Changes of Dietary Fat and Carbohydrate Content Alter Central and Peripheral Clock in Humans. *J Clin Endocrinol Metab* **100:**2291-2302.
203. **Pivovarova O, Gogebakan O, Sucher S, Groth J, Murahovschi V, Kessler K, Osterhoff M, Rudovich N, Kramer A, Pfeiffer AF.** 2016. Regulation of the clock gene expression in human adipose tissue by weight loss. *Int J Obes (Lond)* **40:**899-906.
204. **Garaulet M, Sanchez-Moreno C, Smith CE, Lee YC, Nicolas F, Ordovas JM.** 2011. Ghrelin, sleep reduction and evening preference: relationships to CLOCK 3111 T/C SNP and weight loss. *PLoS One* **6:**e17435.
205. **Bandin C, Martinez-Nicolas A, Ordovas JM, Ros Lucas JA, Castell P, Silvente T, Madrid JA, Garaulet M.** 2013. Differences in circadian rhythmicity in CLOCK 3111T/C genetic variants in moderate obese women as assessed by thermometry, actimetry and body position. *Int J Obes (Lond)* **37:**1044-1050.
206. **Sookoian S, Gemma C, Gianotti TF, Burgueno A, Castano G, Pirola CJ.** 2008. Genetic variants of Clock transcription factor are associated with individual susceptibility to obesity. *Am J Clin Nutr* **87:**1606-1615.
207. **Scott EM, Carter AM, Grant PJ.** 2008. Association between polymorphisms in the Clock gene, obesity and the metabolic syndrome in man. *Int J Obes (Lond)* **32:**658-662.
208. **Ruano EG, Canivell S, Vieira E.** 2014. REV-ERB ALPHA polymorphism is associated with obesity in the Spanish obese male population. *PLoS One* **9:**e104065.
209. **Garaulet M, Smith CE, Gomez-Abellan P, Ordovas-Montanes M, Lee YC, Parnell LD, Arnett DK, Ordovas JM.** 2014. REV-ERB-ALPHA circadian gene variant associates with obesity in two independent populations: Mediterranean and North American. *Mol Nutr Food Res* **58:**821-829.
210. **Arble DM, Sandoval DA.** 2013. CNS control of glucose metabolism: response to environmental challenges. *Front Neurosci* **7:**20.
211. **Chatterjee S, Khunti K, Davies MJ.** 2017. Type 2 diabetes. *Lancet* **389:**2239-2251.
212. **Samuel VT, Shulman GI.** 2012. Mechanisms for insulin resistance: common threads and missing links. *Cell* **148:**852-871.
213. **NCD-RisC NRFC.** 2016. Worldwide trends in diabetes since 1980: a pooled analysis of 751 population-based studies with 4.4 million participants. *Lancet* **387:**1513-1530.
214. **Wilmot E, Idris I.** 2014. Early onset type 2 diabetes: risk factors, clinical impact and management. *Therapeutic Advances in Chronic Disease* **5:**234-244.
215. **Song SH, Hardisty CA.** 2009. Early onset type 2 diabetes mellitus: a harbinger for complications in later years--clinical observation from a secondary care cohort. *Qjm* **102:**799-806.
216. **Stamenkovic JA, Olsson AH, Nagorny CL, Malmgren S, Dekker-Nitert M, Ling C, Mulder H.** 2012. Regulation of core clock genes in human islets. *Metabolism* **61:**978-985.
217. **Ando H, Takamura T, Matsuzawa-Nagata N, Shima KR, Eto T, Misu H, Shiramoto M, Tsuru T, Irie S, Fujimura A, Kaneko S.** 2009. Clock gene expression in peripheral leucocytes of patients with type 2 diabetes. *Diabetologia* **52:**329-335.
218. **Solt LA, Wang Y, Banerjee S, Hughes T, Kojetin DJ, Lundasen T, Shin Y, Liu J, Cameron MD, Noel R, Yoo SH, Takahashi JS, Butler AA, Kamenecka TM, Burris TP.** 2012. Regulation of circadian behaviour and metabolism by synthetic REV-ERB agonists. *Nature* **485:**62-68.
219. **Kumar N, Solt LA, Wang Y, Rogers PM, Bhattacharyya G, Kamenecka TM, Stayrook KR, Crumbley C, Floyd ZE, Gimble JM, Griffin PR, Burris TP.** 2010. Regulation of adipogenesis by natural and synthetic REV-ERB ligands. *Endocrinology* **151:**3015-3025.
220. **Lamia KA, Storch KF, Weitz CJ.** 2008. Physiological significance of a peripheral tissue circadian clock. *Proc Natl Acad Sci U S A* **105:**15172-15177.
221. **Shi SQ, Ansari TS, McGuinness OP, Wasserman DH, Johnson CH.** 2013. Circadian disruption leads to insulin resistance and obesity. *Curr Biol* **23:**372-381.
222. **Honma K, Hikosaka M, Mochizuki K, Goda T.** 2016. Loss of circadian rhythm of circulating insulin concentration induced by high-fat diet intake is associated with disrupted rhythmic expression of circadian clock genes in the liver. *Metabolism* **65:**482-491.
223. **Zhang EE, Liu Y, Dentin R, Pongsawakul PY, Liu AC, Hirota T, Nusinow DA, Sun X, Landais S, Kodama Y, Brenner DA, Montminy M, Kay SA.** 2010. Cryptochrome mediates circadian regulation of cAMP signaling and hepatic gluconeogenesis. *Nat Med* **16:**1152-1156.
224. **Kumar Jha P, Challet E, Kalsbeek A.** 2015. Circadian rhythms in glucose and lipid metabolism in nocturnal and diurnal mammals. *Mol Cell Endocrinol* **418 Pt 1:**74-88.
225. **Woon PY, Kaisaki PJ, Braganca J, Bihoreau MT, Levy JC, Farrall M, Gauguier D.** 2007. Aryl hydrocarbon receptor nuclear translocator-like (BMAL1) is associated with susceptibility to hypertension and type 2 diabetes. *Proc Natl Acad Sci U S A* **104:**14412-14417.

226. **Dupuis J, Langenberg C, Prokopenko I, Saxena R, Soranzo N, Jackson AU, Wheeler E, Glazer NL, Bouatia-Naji N, Gloyn AL, Lindgren CM, Magi R, Morris AP, Randall J, Johnson T, Elliott P, Rybin D, Thorleifsson G, Steinthorsdottir V, Henneman P, Grallert H, Dehghan A, Hottenga JJ, Franklin CS, Navarro P, Song K, Goel A, Perry JR, Egan JM, Lajunen T, Grarup N, Sparso T, Doney A, Voight BF, Stringham HM, Li M, Kanoni S, Shrader P, Cavalcanti-Proenca C, Kumari M, Qi L, Timpson NJ, Gieger C, Zabena C, Rocheleau G, Ingelsson E, An P, O'Connell J, Luan J, Elliott A, et al.** 2010. New genetic loci implicated in fasting glucose homeostasis and their impact on type 2 diabetes risk. *Nat Genet* **42:**105-116.
227. **Englund A, Kovanen L, Saarikoski ST, Haukka J, Reunanen A, Aromaa A, Lonnqvist J, Partonen T.** 2009. NPAS2 and PER2 are linked to risk factors of the metabolic syndrome. *J Circadian Rhythms* **7:**5.
228. **Viollet B, Guigas B, Sanz Garcia N, Leclerc J, Foretz M, Andreelli F.** 2012. Cellular and molecular mechanisms of metformin: an overview. *Clinical Science (London, England : 1979)* **122:**253-270.
229. **Zhou G, Myers R, Li Y, Chen Y, Shen X, Fenyk-Melody J, Wu M, Ventre J, Doebber T, Fujii N, Musi N, Hirshman MF, Goodyear LJ, Moller DE.** 2001. Role of AMP-activated protein kinase in mechanism of metformin action. *J Clin Invest* **108:**1167-1174.
230. **Barnea M, Haviv L, Gutman R, Chapnik N, Madar Z, Froy O.** 2012. Metformin affects the circadian clock and metabolic rhythms in a tissue-specific manner. *Biochim Biophys Acta* **1822:**1796-1806.
231. **Barnea M, Cohen-Yogev T, Chapnik N, Madar Z, Froy O.** 2014. Effect of metformin and lipid emulsion on the circadian gene expression in muscle cells. *Int J Biochem Cell Biol* **53:**151-161.
232. **Caton PW, Kieswich J, Yaqoob MM, Holness MJ, Sugden MC.** 2011. Metformin opposes impaired AMPK and SIRT1 function and deleterious changes in core clock protein expression in white adipose tissue of genetically-obese db/db mice. *Diabetes Obes Metab* **13:**1097-1104.
233. **Um JH, Yang S, Yamazaki S, Kang H, Viollet B, Foretz M, Chung JH.** 2007. Activation of 5'-AMP-activated kinase with diabetes drug metformin induces casein kinase Iepsilon (CKIepsilon)-dependent degradation of clock protein mPer2. *J Biol Chem* **282:**20794-20798.
234. **Chal J, Pourquie O.** 2017. Making muscle: skeletal myogenesis in vivo and in vitro. *Development* **144:**2104-2122.
235. **Marieb EN, Hoehn K.** 2013. Human anatomy & physiology. Pearson, Boston.
236. **Talbot J, Maves L.** 2016. Skeletal muscle fiber type: using insights from muscle developmental biology to dissect targets for susceptibility and resistance to muscle disease. *Wiley Interdiscip Rev Dev Biol* **5:**518-534.
237. **McKinley MP, O'Loughlin VD.** 2011. Human anatomy. Mcgraw Hill Higher, New York.
238. **Abmayr SM, Pavlath GK.** 2012. Myoblast fusion: lessons from flies and mice. *Development* **139:**641-656.
239. **Aas V, Bakke SS, Feng YZ, Kase ET, Jensen J, Bajpeyi S, Thoresen GH, Rustan AC.** 2013. Are cultured human myotubes far from home? *Cell Tissue Res* **354:**671-682.
240. **DeFronzo RA, Tripathy D.** 2009. Skeletal muscle insulin resistance is the primary defect in type 2 diabetes. *Diabetes Care* **32 Suppl 2:**S157-163.
241. **Gaster M, Petersen I, Hojlund K, Poulsen P, Beck-Nielsen H.** 2002. The diabetic phenotype is conserved in myotubes established from diabetic subjects: evidence for primary defects in glucose transport and glycogen synthase activity. *Diabetes* **51:**921-927.
242. **Jackson S, Bagstaff SM, Lynn S, Yeaman SJ, Turnbull DM, Walker M.** 2000. Decreased insulin responsiveness of glucose uptake in cultured human skeletal muscle cells from insulin-resistant nondiabetic relatives of type 2 diabetic families. *Diabetes* **49:**1169-1177.
243. **Ciaraldi TP, Abrams L, Nikoulina S, Mudaliar S, Henry RR.** 1995. Glucose transport in cultured human skeletal muscle cells. Regulation by insulin and glucose in nondiabetic and non-insulin-dependent diabetes mellitus subjects. *J Clin Invest* **96:**2820-2827.
244. **Henry RR, Abrams L, Nikoulina S, Ciaraldi TP.** 1995. Insulin action and glucose metabolism in nondiabetic control and NIDDM subjects. Comparison using human skeletal muscle cell cultures. *Diabetes* **44:**936-946.
245. **Bonadonna RC, Del Prato S, Saccomani MP, Bonora E, Gulli G, Ferrannini E, Bier D, Cobelli C, DeFronzo RA.** 1993. Transmembrane glucose transport in skeletal muscle of patients with non-insulin-dependent diabetes. *J Clin Invest* **92:**486-494.
246. **Bonadonna RC, Saccomani MP, Seely L, Zych KS, Ferrannini E, Cobelli C, DeFronzo RA.** 1993. Glucose transport in human skeletal muscle. The in vivo response to insulin. *Diabetes* **42:**191-198.
247. **Bouzakri K, Roques M, Gual P, Espinosa S, Guebre-Egziabher F, Riou JP, Laville M, Le Marchand-Brustel Y, Tanti JF, Vidal H.** 2003. Reduced activation of phosphatidylinositol-3 kinase and increased serine 636 phosphorylation of insulin receptor substrate-1 in primary culture of skeletal muscle cells from patients with type 2 diabetes. *Diabetes* **52:**1319-1325.
248. **Nikoulina SE, Ciaraldi TP, Carter L, Mudaliar S, Park KS, Henry RR.** 2001. Impaired muscle glycogen synthase in type 2 diabetes is associated with diminished phosphatidylinositol 3-kinase activation. *J Clin Endocrinol Metab* **86:**4307-4314.
249. **Pratipanawatr W, Pratipanawatr T, Cusi K, Berria R, Adams JM, Jenkinson CP, Maezono K, DeFronzo RA, Mandarino LJ.** 2001. Skeletal muscle insulin resistance in normoglycemic subjects with a strong family history of type 2 diabetes is associated with decreased insulin-stimulated insulin receptor substrate-1 tyrosine phosphorylation. *Diabetes* **50:**2572-2578.
250. **Kim YB, Nikoulina SE, Ciaraldi TP, Henry RR, Kahn BB.** 1999. Normal insulin-dependent activation of Akt/protein kinase B, with diminished activation of phosphoinositide 3-kinase, in muscle in type 2 diabetes. *J Clin Invest* **104:**733-741.
251. **Cusi K, Maezono K, Osman A, Pendergrass M, Patti ME, Pratipanawatr T, DeFronzo RA, Kahn CR, Mandarino LJ.** 2000. Insulin resistance differentially affects the PI 3-kinase- and MAP kinase-mediated signaling in human muscle. *J Clin Invest* **105:**311-320.
252. **Bjornholm M, Kawano Y, Lehtihet M, Zierath JR.** 1997. Insulin receptor substrate-1 phosphorylation and phosphatidylinositol 3-kinase activity in skeletal muscle from NIDDM subjects after in vivo insulin stimulation. *Diabetes* **46:**524-527.
253. **Ciaraldi TP, Carter L, Nikoulina S, Mudaliar S, McClain DA, Henry RR.** 1999. Glucosamine regulation of glucose metabolism in cultured human skeletal muscle cells: divergent effects on glucose transport/phosphorylation and glycogen synthase in non-diabetic and type 2 diabetic subjects. *Endocrinology* **140:**3971-3980.

254. **Krook A, Bjornholm M, Galuska D, Jiang XJ, Fahlman R, Myers MG, Jr., Wallberg-Henriksson H, Zierath JR.** 2000. Characterization of signal transduction and glucose transport in skeletal muscle from type 2 diabetic patients. *Diabetes* **49:**284-292.
255. **Mashili F, Chibalin AV, Krook A, Zierath JR.** 2013. Constitutive STAT3 phosphorylation contributes to skeletal muscle insulin resistance in type 2 diabetes. *Diabetes* **62:**457-465.
256. **Lefta M, Wolff G, Esser KA.** 2011. Circadian rhythms, the molecular clock, and skeletal muscle. *Curr Top Dev Biol* **96:**231-271.
257. **Kitzmann M, Lantier L, Hebrard S, Mercier J, Foretz M, Aguer C.** 2011. Abnormal metabolism flexibility in response to high palmitate concentrations in myotubes derived from obese type 2 diabetic patients. *Biochim Biophys Acta* **1812:**423-430.
258. **Sakamoto K, Holman GD.** 2008. Emerging role for AS160/TBC1D4 and TBC1D1 in the regulation of GLUT4 traffic. *Am J Physiol Endocrinol Metab* **295:**E29-37.
259. **Sano H, Kane S, Sano E, Miinea CP, Asara JM, Lane WS, Garner CW, Lienhard GE.** 2003. Insulin-stimulated phosphorylation of a Rab GTPase-activating protein regulates GLUT4 translocation. *J Biol Chem* **278:**14599-14602.
260. **Kramer HF, Witczak CA, Taylor EB, Fujii N, Hirshman MF, Goodyear LJ.** 2006. AS160 regulates insulin- and contraction-stimulated glucose uptake in mouse skeletal muscle. *J Biol Chem* **281:**31478-31485.
261. **Karlsson HK, Zierath JR, Kane S, Krook A, Lienhard GE, Wallberg-Henriksson H.** 2005. Insulin-stimulated phosphorylation of the Akt substrate AS160 is impaired in skeletal muscle of type 2 diabetic subjects. *Diabetes* **54:**1692-1697.
262. **Cha BS, Ciaraldi TP, Park KS, Carter L, Mudaliar SR, Henry RR.** 2005. Impaired fatty acid metabolism in type 2 diabetic skeletal muscle cells is reversed by PPARgamma agonists. *Am J Physiol Endocrinol Metab* **289:**E151-159.
263. **Bravard A, Lefai E, Meugnier E, Pesenti S, Disse E, Vouillarmet J, Peretti N, Rabasa-Lhoret R, Laville M, Vidal H, Rieusset J.** 2011. FTO is increased in muscle during type 2 diabetes, and its overexpression in myotubes alters insulin signaling, enhances lipogenesis and ROS production, and induces mitochondrial dysfunction. *Diabetes* **60:**258-268.
264. **Albers PH, Pedersen AJ, Birk JB, Kristensen DE, Vind BF, Baba O, Nohr J, Hojlund K, Wojtaszewski JF.** 2015. Human muscle fiber type-specific insulin signaling: impact of obesity and type 2 diabetes. *Diabetes* **64:**485-497.
265. **Scott LJ, Erdos MR, Huyghe JR, Welch RP, Beck AT, Wolford BN, Chines PS, Didion JP, Narisu N, Stringham HM, Taylor DL, Jackson AU, Vadlamudi S, Bonnycastle LL, Kinnunen L, Saramies J, Sundvall J, Albanus RD, Kiseleva A, Hensley J, Crawford GE, Jiang H, Wen X, Watanabe RM, Lakka TA, Mohlke KL, Laakso M, Tuomilehto J, Koistinen HA, Boehnke M, Collins FS, Parker SC.** 2016. The genetic regulatory signature of type 2 diabetes in human skeletal muscle. *Nat Commun* **7:**11764.
266. **Varemo L, Henriksen TI, Scheele C, Broholm C, Pedersen M, Uhlen M, Pedersen BK, Nielsen J.** 2017. Type 2 diabetes and obesity induce similar transcriptional reprogramming in human myocytes. *Genome Med* **9:**47.
267. **McPherron AC, Lawler AM, Lee SJ.** 1997. Regulation of skeletal muscle mass in mice by a new TGF-beta superfamily member. *Nature* **387:**83-90.
268. **Pedersen BK.** 2011. Muscles and their myokines. *J Exp Biol* **214:**337-346.
269. **Keller P, Keller C, Carey AL, Jauffred S, Fischer CP, Steensberg A, Pedersen BK.** 2003. Interleukin-6 production by contracting human skeletal muscle: autocrine regulation by IL-6. *Biochem Biophys Res Commun* **310:**550-554.
270. **Bustamante M, Fernandez-Verdejo R, Jaimovich E, Buvinic S.** 2014. Electrical stimulation induces IL-6 in skeletal muscle through extracellular ATP by activating Ca(2+) signals and an IL-6 autocrine loop. *Am J Physiol Endocrinol Metab* **306:**E869-882.
271. **Haugen F, Norheim F, Lian H, Wensaas AJ, Dueland S, Berg O, Funderud A, Skalhegg BS, Raastad T, Drevon CA.** 2010. IL-7 is expressed and secreted by human skeletal muscle cells. *Am J Physiol Cell Physiol* **298:**C807-816.
272. **Trayhurn P, Drevon CA, Eckel J.** 2011. Secreted proteins from adipose tissue and skeletal muscle - adipokines, myokines and adipose/muscle cross-talk. *Arch Physiol Biochem* **117:**47-56.
273. **Nielsen AR, Mounier R, Plomgaard P, Mortensen OH, Penkowa M, Speerschneider T, Pilegaard H, Pedersen BK.** 2007. Expression of interleukin-15 in human skeletal muscle effect of exercise and muscle fibre type composition. *J Physiol* **584:**305-312.
274. **Pedersen BK, Febbraio MA.** 2008. Muscle as an endocrine organ: focus on muscle-derived interleukin-6. *Physiol Rev* **88:**1379-1406.
275. **Akerstrom T, Steensberg A, Keller P, Keller C, Penkowa M, Pedersen BK.** 2005. Exercise induces interleukin-8 expression in human skeletal muscle. *J Physiol* **563:**507-516.
276. **Li F, Li Y, Tang Y, Lin B, Kong X, Oladele OA, Yin Y.** 2014. Protective effect of myokine IL-15 against H2O2-mediated oxidative stress in skeletal muscle cells. *Mol Biol Rep* **41:**7715-7722.
277. **Plomgaard P, Penkowa M, Pedersen BK.** 2005. Fiber type specific expression of TNF-alpha, IL-6 and IL-18 in human skeletal muscles. *Exerc Immunol Rev* **11:**53-63.
278. **Penkowa M, Keller C, Keller P, Jauffred S, Pedersen BK.** 2003. Immunohistochemical detection of interleukin-6 in human skeletal muscle fibers following exercise. *FASEB J* **17:**2166-2168.
279. **Hiscock N, Chan MH, Bisucci T, Darby IA, Febbraio MA.** 2004. Skeletal myocytes are a source of interleukin-6 mRNA expression and protein release during contraction: evidence of fiber type specificity. *Faseb j* **18:**992-994.
280. **Fischer CP, Hiscock NJ, Penkowa M, Basu S, Vessby B, Kallner A, Sjoberg LB, Pedersen BK.** 2004. Supplementation with vitamins C and E inhibits the release of interleukin-6 from contracting human skeletal muscle. *J Physiol* **558:**633-645.
281. **Keller ET, Wanagat J, Ershler WB.** 1996. Molecular and cellular biology of interleukin-6 and its receptor. *Front Biosci* **1:**d340-357.
282. **Wolvekamp MC, Marquet RL.** 1990. Interleukin-6: historical background, genetics and biological significance. *Immunol Lett* **24:**1-9.
283. **Ostrowski K, Rohde T, Zacho M, Asp S, Pedersen BK.** 1998. Evidence that interleukin-6 is produced in human skeletal muscle during prolonged running. *J Physiol* **508 (Pt 3):**949-953.
284. **Steensberg A, Keller C, Starkie RL, Osada T, Febbraio MA, Pedersen BK.** 2002. IL-6 and TNF-alpha expression in, and release from, contracting human skeletal muscle. *Am J Physiol Endocrinol Metab* **283:**E1272-1278.
285. **Pedersen BK, Steensberg A, Schjerling P.** 2001. Exercise and interleukin-6. *Curr Opin Hematol* **8:**137-141.
286. **Febbraio MA, Pedersen BK.** 2002. Muscle-derived interleukin-6: mechanisms for activation and possible biological roles. *FASEB J* **16:**1335-1347.

287. **Starkie RL, Rolland J, Angus DJ, Anderson MJ, Febbraio MA.** 2001. Circulating monocytes are not the source of elevations in plasma IL-6 and TNF-alpha levels after prolonged running. *Am J Physiol Cell Physiol* **280:**C769-774.
288. **Al-Khalili L, Bouzakri K, Glund S, Lonnqvist F, Koistinen HA, Krook A.** 2006. Signaling specificity of interleukin-6 action on glucose and lipid metabolism in skeletal muscle. *Mol Endocrinol* **20:**3364-3375.
289. **Chan MH, Carey AL, Watt MJ, Febbraio MA.** 2004. Cytokine gene expression in human skeletal muscle during concentric contraction: evidence that IL-8, like IL-6, is influenced by glycogen availability. *Am J Physiol Regul Integr Comp Physiol* **287:**R322-327.
290. **Gudiksen A, Schwartz CL, Bertholdt L, Joensen E, Knudsen JG, Pilegaard H.** 2016. Lack of Skeletal Muscle IL-6 Affects Pyruvate Dehydrogenase Activity at Rest and during Prolonged Exercise. *PLoS One* **11:**e0156460.
291. **Starkie RL, Arkinstall MJ, Koukoulas I, Hawley JA, Febbraio MA.** 2001. Carbohydrate ingestion attenuates the increase in plasma interleukin-6, but not skeletal muscle interleukin-6 mRNA, during exercise in humans. *J Physiol* **533:**585-591.
292. **Nieman DC, Davis JM, Brown VA, Henson DA, Dumke CL, Utter AC, Vinci DM, Downs MF, Smith JC, Carson J, Brown A, McAnulty SR, McAnulty LS.** 2004. Influence of carbohydrate ingestion on immune changes after 2 h of intensive resistance training. *J Appl Physiol* **96:**1292-1298.
293. **Wallenius V, Wallenius K, Ahren B, Rudling M, Carlsten H, Dickson SL, Ohlsson C, Jansson JO.** 2002. Interleukin-6-deficient mice develop mature-onset obesity. *Nat Med* **8:**75-79.
294. **Franckhauser S, Elias I, Rotter Sopasakis V, Ferre T, Nagaev I, Andersson CX, Agudo J, Ruberte J, Bosch F, Smith U.** 2008. Overexpression of Il6 leads to hyperinsulinaemia, liver inflammation and reduced body weight in mice. *Diabetologia* **51:**1306-1316.
295. **Spranger J, Kroke A, Mohlig M, Hoffmann K, Bergmann MM, Ristow M, Boeing H, Pfeiffer AF.** 2003. Inflammatory cytokines and the risk to develop type 2 diabetes: results of the prospective population-based European Prospective Investigation into Cancer and Nutrition (EPIC)-Potsdam Study. *Diabetes* **52:**812-817.
296. **Carey AL, Steinberg GR, Macaulay SL, Thomas WG, Holmes AG, Ramm G, Prelovsek O, Hohnen-Behrens C, Watt MJ, James DE, Kemp BE, Pedersen BK, Febbraio MA.** 2006. Interleukin-6 increases insulin-stimulated glucose disposal in humans and glucose uptake and fatty acid oxidation in vitro *via* AMP-activated protein kinase. *Diabetes* **55:**2688-2697.
297. **Jiang LQ, Duque-Guimaraes DE, Machado UF, Zierath JR, Krook A.** 2013. Altered response of skeletal muscle to IL-6 in type 2 diabetic patients. *Diabetes* **62:**355-361.
298. **Harder-Lauridsen NM, Krogh-Madsen R, Holst JJ, Plomgaard P, Leick L, Pedersen BK, Fischer CP.** 2014. Effect of IL-6 on the insulin sensitivity in patients with type 2 diabetes. *Am J Physiol Endocrinol Metab* **306:**E769-778.
299. **Nieto-Vazquez I, Fernandez-Veledo S, de Alvaro C, Lorenzo M.** 2008. Dual role of interleukin-6 in regulating insulin sensitivity in murine skeletal muscle. *Diabetes* **57:**3211-3221.
300. **Amir Levy Y, Ciaraldi TP, Mudaliar SR, Phillips SA, Henry RR.** 2015. Excessive secretion of IL-8 by skeletal muscle in type 2 diabetes impairs tube growth: potential role of PI3K and the Tie2 receptor. *Am J Physiol Endocrinol Metab* **309:**E22-34.
301. **Plomgaard P, Nielsen AR, Fischer CP, Mortensen OH, Broholm C, Penkowa M, Krogh-Madsen R, Erikstrup C, Lindegaard B, Petersen AM, Taudorf S, Pedersen BK.** 2007. Associations between insulin resistance and TNF-alpha in plasma, skeletal muscle and adipose tissue in humans with and without type 2 diabetes. *Diabetologia* **50:**2562-2571.
302. **Ciaraldi TP, Ryan AJ, Mudaliar SR, Henry RR.** 2016. Altered Myokine Secretion Is an Intrinsic Property of Skeletal Muscle in Type 2 Diabetes. *PLoS One* **11:**e0158209.
303. **Harfmann BD, Schroder EA, Esser KA.** 2015. Circadian rhythms, the molecular clock, and skeletal muscle. *J Biol Rhythms* **30:**84-94.
304. **Bunger MK, Wilsbacher LD, Moran SM, Clendenin C, Radcliffe LA, Hogenesch JB, Simon MC, Takahashi JS, Bradfield CA.** 2000. Mop3 is an essential component of the master circadian pacemaker in mammals. *Cell* **103:**1009-1017.
305. **Chatterjee S, Yin H, Nam D, Li Y, Ma K.** 2015. Brain and muscle Arnt-like 1 promotes skeletal muscle regeneration through satellite cell expansion. *Exp Cell Res* **331:**200-210.
306. **Chatterjee S, Nam D, Guo B, Kim JM, Winnier GE, Lee J, Berdeaux R, Yechoor VK, Ma K.** 2013. Brain and muscle Arnt-like 1 is a key regulator of myogenesis. *J Cell Sci* **126:**2213-2224.
307. **Vinciguerra M, Fulco M, Ladurner A, Sartorelli V, Rosenthal N.** 2010. SirT1 in muscle physiology and disease: lessons from mouse models. *Dis Model Mech* **3:**298-303.
308. **Fulco M, Schiltz RL, Iezzi S, King MT, Zhao P, Kashiwaya Y, Hoffman E, Veech RL, Sartorelli V.** 2003. Sir2 regulates skeletal muscle differentiation as a potential sensor of the redox state. *Mol Cell* **12:**51-62.
309. **Muoio DM, Koves TR.** 2007. Skeletal muscle adaptation to fatty acid depends on coordinated actions of the PPARs and PGC1 alpha: implications for metabolic disease. *Appl Physiol Nutr Metab* **32:**874-883.
310. **Liu C, Li S, Liu T, Borjigin J, Lin JD.** 2007. Transcriptional coactivator PGC-1alpha integrates the mammalian clock and energy metabolism. *Nature* **447:**477-481.
311. **Um JH, Pendergast JS, Springer DA, Foretz M, Viollet B, Brown A, Kim MK, Yamazaki S, Chung JH.** 2011. AMPK regulates circadian rhythms in a tissue- and isoform-specific manner. *PLoS One* **6:**e18450.
312. **Petrenko V, Saini C, Perrin L, Dibner C.** 2016. Parallel Measurement of Circadian Clock Gene Expression and Hormone Secretion in Human Primary Cell Cultures. *J Vis Exp*.
313. **Hansson GK, Libby P, Tabas I.** 2015. Inflammation and plaque vulnerability. *J Intern Med* **278:**483-493.
314. **Khavandi M, Duarte F, Ginsberg HN, Reyes-Soffer G.** 2017. Treatment of Dyslipidemias to Prevent Cardiovascular Disease in Patients with Type 2 Diabetes. *Curr Cardiol Rep* **19:**7.
315. **Bennett MR, Sinha S, Owens GK.** 2016. Vascular Smooth Muscle Cells in Atherosclerosis. *Circ Res* **118:**692-702.
316. **Wang G, Jacquet L, Karamariti E, Xu Q.** 2015. Origin and differentiation of vascular smooth muscle cells. *J Physiol* **593:**3013-3030.
317. **Gordon D, Schwartz SM.** 1987. Replication of arterial smooth muscle cells in hypertension and atherosclerosis. *Am J Cardiol* **59:**44A-48A.
318. **Nemenoff RA, Horita H, Ostriker AC, Furgeson SB, Simpson PA, VanPutten V, Crossno J, Offermanns S, Weiser-Evans MC.** 2011. SDF-1alpha induction in mature smooth muscle cells by inactivation of PTEN is a critical mediator of exacerbated injury-induced neointima formation. *Arterioscler Thromb Vasc Biol* **31:**1300-1308.
319. **Herring BP, Hoggatt AM, Burlak C, Offermanns S.** 2014. Previously differentiated medial vascular smooth muscle cells contribute to neointima formation following vascular injury. *Vasc Cell* **6:**21.

320. **House SJ, Potier M, Bisaillon J, Singer HA, Trebak M.** 2008. The non-excitable smooth muscle: calcium signaling and phenotypic switching during vascular disease. *Pflugers Arch* **456:**769-785.
321. **Owens GK.** 1995. Regulation of differentiation of vascular smooth muscle cells. *Physiol Rev* **75:**487-517.
322. **Yan Z, Hansson GK.** 1998. Overexpression of inducible nitric oxide synthase by neointimal smooth muscle cells. *Circ Res* **82:**21-29.
323. **Walker LN, Bowen-Pope DF, Ross R, Reidy MA.** 1986. Production of platelet-derived growth factor-like molecules by cultured arterial smooth muscle cells accompanies proliferation after arterial injury. *Proc Natl Acad Sci U S A* **83:**7311-7315.
324. **Coen M, Marchetti G, Palagi PM, Zerbinati C, Guastella G, Gagliano T, Bernardi F, Mascoli F, Bochaton-Piallat ML.** 2013. Calmodulin expression distinguishes the smooth muscle cell population of human carotid plaque. *Am J Pathol* **183:**996-1009.
325. **Hao H, Ropraz P, Verin V, Camenzind E, Geinoz A, Pepper MS, Gabbiani G, Bochaton-Piallat ML.** 2002. Heterogeneity of smooth muscle cell populations cultured from pig coronary artery. *Arterioscler Thromb Vasc Biol* **22:**1093-1099.
326. **Stenmark KR, Frid MG.** 1998. Smooth muscle cell heterogeneity: role of specific smooth muscle cell subpopulations in pulmonary vascular disease. *Chest* **114:**82s-90s.
327. **Brisset AC, Hao H, Camenzind E, Bacchetta M, Geinoz A, Sanchez JC, Chaponnier C, Gabbiani G, Bochaton-Piallat ML.** 2007. Intimal smooth muscle cells of porcine and human coronary artery express S100A4, a marker of the rhomboid phenotype in vitro. *Circ Res* **100:**1055-1062.
328. **Hao H, Gabbiani G, Bochaton-Piallat ML.** 2003. Arterial smooth muscle cell heterogeneity: implications for atherosclerosis and restenosis development. *Arterioscler Thromb Vasc Biol* **23:**1510-1520.
329. **Chappell J, Harman JL, Narasimhan VM, Yu H, Foote K, Simons BD, Bennett MR, Jorgensen HF.** 2016. Extensive Proliferation of a Subset of Differentiated, yet Plastic, Medial Vascular Smooth Muscle Cells Contributes to Neointimal Formation in Mouse Injury and Atherosclerosis Models. *Circ Res* **119:**1313-1323.
330. **Feil S, Fehrenbacher B, Lukowski R, Essmann F, Schulze-Osthoff K, Schaller M, Feil R.** 2014. Transdifferentiation of vascular smooth muscle cells to macrophage-like cells during atherogenesis. *Circ Res* **115:**662-667.
331. **Chaabane C, Heizmann CW, Bochaton-Piallat ML.** 2015. Extracellular S100A4 induces smooth muscle cell phenotypic transition mediated by RAGE. *Biochim Biophys Acta* **1853:**2144-2157.
332. **Chalmers JA, Martino TA, Tata N, Ralph MR, Sole MJ, Belsham DD.** 2008. Vascular circadian rhythms in a mouse vascular smooth muscle cell line (Movas-1). *Am J Physiol Regul Integr Comp Physiol* **295:**R1529-1538.
333. **Lin C, Tang X, Zhu Z, Liao X, Zhao R, Fu W, Chen B, Jiang J, Qian R, Guo D.** 2014. The rhythmic expression of clock genes attenuated in human plaque-derived vascular smooth muscle cells. *Lipids Health Dis* **13:**14.
334. **Park SJ, Kwon SG, Hwang JH, Park da H, Kim TW, Kim CW.** 2015. Selection of appropriate reference genes for RT-qPCR analysis in Berkshire, Duroc, Landrace, and Yorkshire pigs. *Gene* **558:**152-158.
335. **Eder K, Baffy N, Falus A, Fulop AK.** 2009. The major inflammatory mediator interleukin-6 and obesity. *Inflamm Res* **58:**727-736.
336. **Loizides-Mangold U, Perrin L, Vandereycken B, Betts JA, Walhin JP, Templeman I, Chanon S, Weger BD, Durand C, Robert M, Paz Montoya J, Moniatte M, Karagounis LG, Johnston JD, Gachon F, Lefai E, Riezman H, Dibner C.** 2017. Lipidomics reveals diurnal lipid oscillations in human skeletal muscle persisting in cellular myotubes cultured in vitro. *Proc Natl Acad Sci U S A*.
337. **Brown SA, Kunz D, Dumas A, Westermark PO, Vanselow K, Tilmann-Wahnschaffe A, Herzel H, Kramer A.** 2008. Molecular insights into human daily behavior. *Proc Natl Acad Sci U S A* **105:**1602-1607.
338. **Pedersen BK, Febbraio MA.** 2012. Muscles, exercise and obesity: skeletal muscle as a secretory organ. *Nat Rev Endocrinol* **8:**457-465.
339. **Santhanam U, Ghrayeb J, Sehgal PB, May LT.** 1989. Post-translational modifications of human interleukin-6. *Arch Biochem Biophys* **274:**161-170.
340. **Simpson RJ, Hammacher A, Smith DK, Matthews JM, Ward LD.** 1997. Interleukin-6: structure-function relationships. *Protein Sci* **6:**929-955.
341. **May LT, Santhanam U, Sehgal PB.** 1991. On the multimeric nature of natural human interleukin-6. *J Biol Chem* **266:**9950-9955.
342. **Sugimoto T, Morioka N, Zhang FF, Sato K, Abe H, Hisaoka-Nakashima K, Nakata Y.** 2014. Clock gene Per1 regulates the production of CCL2 and interleukin-6 through p38, JNK1 and NF-kappaB activation in spinal astrocytes. *Mol Cell Neurosci* **59:**37-46.
343. **Nakazato R, Hotta S, Yamada D, Kou M, Nakamura S, Takahata Y, Tei H, Numano R, Hida A, Shimba S, Mieda M, Hinoi E, Yoneda Y, Takarada T.** 2017. The intrinsic microglial clock system regulates interleukin-6 expression. *Glia* **65:**198-208.
344. **Hansen J, Timmers S, Moonen-Kornips E, Duez H, Staels B, Hesselink MK, Schrauwen P.** 2016. Synchronized human skeletal myotubes of lean, obese and type 2 diabetic patients maintain circadian oscillation of clock genes. *Sci Rep* **6:**35047.
345. **Mauer J, Denson JL, Brüning JC.** 2015. Versatile functions for IL-6 in metabolism and cancer. *Trends in Immunology* **36:**92-101.
346. **Ellingsgaard H, Hauselmann I, Schuler B, Habib AM, Baggio LL, Meier DT, Eppler E, Bouzakri K, Wueest S, Muller YD, Hansen AM, Reinecke M, Konrad D, Gassmann M, Reimann F, Halban PA, Gromada J, Drucker DJ, Gribble FM, Ehses JA, Donath MY.** 2011. Interleukin-6 enhances insulin secretion by increasing glucagon-like peptide-1 secretion from L cells and alpha cells. *Nat Med* **17:**1481-1489.
347. **Weigert C, Hennige AM, Lehmann R, Brodbeck K, Baumgartner F, Schauble M, Haring HU, Schleicher ED.** 2006. Direct cross-talk of interleukin-6 and insulin signal transduction *via* insulin receptor substrate-1 in skeletal muscle cells. *J Biol Chem* **281:**7060-7067.
348. **Wueest S, Item F, Boyle CN, Jirkof P, Cesarovic N, Ellingsgaard H, Boni-Schnetzler M, Timper K, Arras M, Donath MY, Lutz TA, Schoenle EJ, Konrad D.** 2014. Interleukin-6 contributes to early fasting-induced free fatty acid mobilization in mice. *Am J Physiol Regul Integr Comp Physiol* **306:**R861-867.
349. **Timper K, Denson JL, Steculorum SM, Heilinger C, Engstrom-Ruud L, Wunderlich CM, Rose-John S, Wunderlich FT, Bruning JC.** 2017. IL-6 Improves Energy and Glucose Homeostasis in Obesity *via* Enhanced Central IL-6 trans-Signaling. *Cell Rep* **19:**267-280.

350. **Jones SA, Scheller J, Rose-John S.** 2011. Therapeutic strategies for the clinical blockade of IL-6/gp130 signaling. *The Journal of Clinical Investigation* **121:**3375-3383.
351. **Zozulinska D, Majchrzak A, Sobieska M, Wiktorowicz K, Wierusz-Wysocka B.** 1999. Serum interleukin-8 level is increased in diabetic patients. *Diabetologia* **42:**117-118.
352. **Hermann C, von Aulock S, Dehus O, Keller M, Okigami H, Gantner F, Wendel A, Hartung T.** 2006. Endogenous cortisol determines the circadian rhythm of lipopolysaccharide-- but not lipoteichoic acid--inducible cytokine release. *Eur J Immunol* **36:**371-379.
353. **Bouzakri K, Plomgaard P, Berney T, Donath MY, Pedersen BK, Halban PA.** 2011. Bimodal effect on pancreatic beta-cells of secretory products from normal or insulin-resistant human skeletal muscle. *Diabetes* **60:**1111-1121.
354. **Patsouris D, Cao JJ, Vial G, Bravard A, Lefai E, Durand A, Durand C, Chauvin MA, Laugerette F, Debard C, Michalski MC, Laville M, Vidal H, Rieusset J.** 2014. Insulin resistance is associated with MCP1-mediated macrophage accumulation in skeletal muscle in mice and humans. *PLoS One* **9:**e110653.
355. **Elias I, Franckhauser S, Ferre T, Vila L, Tafuro S, Munoz S, Roca C, Ramos D, Pujol A, Riu E, Ruberte J, Bosch F.** 2012. Adipose tissue overexpression of vascular endothelial growth factor protects against diet-induced obesity and insulin resistance. *Diabetes* **61:**1801-1813.
356. **Kodama K, Horikoshi M, Toda K, Yamada S, Hara K, Irie J, Sirota M, Morgan AA, Chen R, Ohtsu H, Maeda S, Kadowaki T, Butte AJ.** 2012. Expression-based genome-wide association study links the receptor CD44 in adipose tissue with type 2 diabetes. *Proc Natl Acad Sci U S A* **109:**7049-7054.
357. **Kodama K, Toda K, Morinaga S, Yamada S, Butte AJ.** 2015. Anti-CD44 antibody treatment lowers hyperglycemia and improves insulin resistance, adipose inflammation, and hepatic steatosis in diet-induced obese mice. *Diabetes* **64:**867-875.
358. **Liu LF, Kodama K, Wei K, Tolentino LL, Choi O, Engleman EG, Butte AJ, McLaughlin T.** 2015. The receptor CD44 is associated with systemic insulin resistance and proinflammatory macrophages in human adipose tissue. *Diabetologia* **58:**1579-1586.
359. **Hagberg CE, Mehlem A, Falkevall A, Muhl L, Fam BC, Ortsater H, Scotney P, Nyqvist D, Samen E, Lu L, Stone-Elander S, Proietto J, Andrikopoulos S, Sjoholm A, Nash A, Eriksson U.** 2012. Targeting VEGF-B as a novel treatment for insulin resistance and type 2 diabetes. *Nature* **490:**426-430.
360. **Kleppe R, Martinez A, Doskeland SO, Haavik J.** 2011. The 14-3-3 proteins in regulation of cellular metabolism. *Semin Cell Dev Biol* **22:**713-719.
361. **Ramm G, Larance M, Guilhaus M, James DE.** 2006. A role for 14-3-3 in insulin-stimulated GLUT4 translocation through its interaction with the RabGAP AS160. *J Biol Chem* **281:**29174-29180.
362. **Szekeres F, Chadt A, Tom RZ, Deshmukh AS, Chibalin AV, Bjornholm M, Al-Hasani H, Zierath JR.** 2012. The Rab-GTPase-activating protein TBC1D1 regulates skeletal muscle glucose metabolism. *Am J Physiol Endocrinol Metab* **303:**E524-533.
363. **Roach WG, Chavez JA, Miinea CP, Lienhard GE.** 2007. Substrate specificity and effect on GLUT4 translocation of the Rab GTPase-activating protein Tbc1d1. *Biochem J* **403:**353-358.
364. **An D, Toyoda T, Taylor EB, Yu H, Fujii N, Hirshman MF, Goodyear LJ.** 2010. TBC1D1 regulates insulin- and contraction-induced glucose transport in mouse skeletal muscle. *Diabetes* **59:**1358-1365.
365. **Kennaway DJ, Owens JA, Voultsios A, Boden MJ, Varcoe TJ.** 2007. Metabolic homeostasis in mice with disrupted Clock gene expression in peripheral tissues. *American Journal of Physiology - Regulatory, Integrative and Comparative Physiology* **293:**R1528-R1537.
366. **Manderson AP, Kay JG, Hammond LA, Brown DL, Stow JL.** 2007. Subcompartments of the macrophage recycling endosome direct the differential secretion of IL-6 and TNFalpha. *J Cell Biol* **178:**57-69.
367. **Boddul SV, Meng J, Dolly JO, Wang J.** 2014. SNAP-23 and VAMP-3 contribute to the release of IL-6 and TNFalpha from a human synovial sarcoma cell line. *FEBS J* **281:**750-765.
368. **Jovic M, Kean MJ, Dubankova A, Boura E, Gingras AC, Brill JA, Balla T.** 2014. Endosomal sorting of VAMP3 is regulated by PI4K2A. *J Cell Sci* **127:**3745-3756.
369. **Schiaffino S, Blaauw B, Dyar KA.** 2016. The functional significance of the skeletal muscle clock: lessons from Bmal1 knockout models. *Skelet Muscle* **6:**33.
370. **Yang L, Chu Y, Wang L, Wang Y, Zhao X, He W, Zhang P, Yang X, Liu X, Tian L, Li B, Dong S, Gao C.** 2015. Overexpression of CRY1 protects against the development of atherosclerosis *via* the TLR/NF-kappaB pathway. *Int Immunopharmacol* **28:**525-530.
371. **Steffens S, Winter C, Schloss MJ, Hidalgo A, Weber C, Soehnlein O.** 2017. Circadian Control of Inflammatory Processes in Atherosclerosis and Its Complications. *Arterioscler Thromb Vasc Biol* **37:**1022-1028.
372. **McAlpine CS, Swirski FK.** 2016. Circadian Influence on Metabolism and Inflammation in Atherosclerosis. *Circ Res* **119:**131-141.
373. **Anea CB, Ali MI, Osmond JM, Sullivan JC, Stepp DW, Merloiu AM, Rudic RD.** 2010. Matrix metalloproteinase 2 and 9 dysfunction underlie vascular stiffness in circadian clock mutant mice. *Arterioscler Thromb Vasc Biol* **30:**2535-2543.
374. **Su W, Xie Z, Guo Z, Duncan MJ, Lutshumba J, Gong MC.** 2012. Altered clock gene expression and vascular smooth muscle diurnal contractile variations in type 2 diabetic db/db mice. *Am J Physiol Heart Circ Physiol* **302:**H621-633.
375. **Chen S, Ding Y, Zhang Z, Wang H, Liu C.** 2014. Hyperlipidaemia impairs the circadian clock and physiological homeostasis of vascular smooth muscle cells *via* the suppression of Smarcd1. *J Pathol* **233:**159-169.
376. **Lin C, Tang X, Xu L, Qian R, Shi Z, Wang L, Cai T, Yan D, Fu W, Guo D.** 2017. Intracellular high cholesterol content disorders the clock genes, apoptosis-related genes and fibrinolytic-related genes rhythmic expressions in human plaque-derived vascular smooth muscle cells. *Lipids Health Dis* **16:**135.
377. **Kang TH, Leem SH.** 2014. Modulation of ATR-mediated DNA damage checkpoint response by cryptochrome 1. *Nucleic Acids Res* **42:**4427-4434.
378. **Unsal-Kacmaz K, Mullen TE, Kaufmann WK, Sancar A.** 2005. Coupling of human circadian and cell cycles by the timeless protein. *Mol Cell Biol* **25:**3109-3116.
379. **Yang X, Wood PA, Hrushesky WJ.** 2010. Mammalian TIMELESS is required for ATM-dependent CHK2 activation and G2/M checkpoint control. *J Biol Chem* **285:**3030-3034.
380. **Kowalska E, Ripperger JA, Hoegger DC, Bruegger P, Buch T, Birchler T, Mueller A, Albrecht U, Contaldo C, Brown SA.** 2013. NONO couples the circadian clock to the cell cycle. *Proc Natl Acad Sci U S A* **110:**1592-1599.

381. **Kim SY, Ferrell JE, Jr.** 2007. Substrate competition as a source of ultrasensitivity in the inactivation of Wee1. *Cell* **128:**1133-1145.
382. **Matsuo T, Yamaguchi S, Mitsui S, Emi A, Shimoda F, Okamura H.** 2003. Control mechanism of the circadian clock for timing of cell division in vivo. *Science* **302:**255-259.
383. **Matsu-Ura T, Dovzhenok A, Aihara E, Rood J, Le H, Ren Y, Rosselot AE, Zhang T, Lee C, Obrietan K, Montrose MH, Lim S, Moore SR, Hong CI.** 2016. Intercellular Coupling of the Cell Cycle and Circadian Clock in Adult Stem Cell Culture. *Mol Cell* **64:**900-912.
384. **Lau AN, Vander Heiden MG.** 2015. Stopping the Clock with MYC. *Mol Cell* **60:**511-513.
385. **Huber AL, Papp SJ, Chan AB, Henriksson E, Jordan SD, Kriebs A, Nguyen M, Wallace M, Li Z, Metallo CM, Lamia KA.** 2016. CRY2 and FBXL3 Cooperatively Degrade c-MYC. *Mol Cell* **64:**774-789.
386. **Innominato PF, Roche VP, Palesh OG, Ulusakarya A, Spiegel D, Levi FA.** 2014. The circadian timing system in clinical oncology. *Ann Med* **46:**191-207.
387. **Marcheva B, Ramsey KM, Peek CB, Affinati A, Maury E, Bass J.** 2013. Circadian clocks and metabolism. *Handb Exp Pharmacol***:**127-155.
388. **Kondratov RV, Chernov MV, Kondratova AA, Gorbacheva VY, Gudkov AV, Antoch MP.** 2003. BMAL1-dependent circadian oscillation of nuclear CLOCK: posttranslational events induced by dimerization of transcriptional activators of the mammalian clock system. *Genes Dev* **17:**1921-1932.
389. **DeBruyne JP, Weaver DR, Reppert SM.** 2007. Peripheral circadian oscillators require CLOCK. *Curr Biol* **17:**R538-539.
390. **Schneider DJ, Nordt TK, Sobel BE.** 1993. Attenuated fibrinolysis and accelerated atherogenesis in type II diabetic patients. *Diabetes* **42:**1-7.
391. **Juhan-Vague I, Roul C, Alessi MC, Ardissone JP, Heim M, Vague P.** 1989. Increased plasminogen activator inhibitor activity in non insulin dependent diabetic patients--relationship with plasma insulin. *Thromb Haemost* **61:**370-373.
392. **Domingueti CP, Dusse LM, Carvalho M, de Sousa LP, Gomes KB, Fernandes AP.** 2016. Diabetes mellitus: The linkage between oxidative stress, inflammation, hypercoagulability and vascular complications. *J Diabetes Complications* **30:**738-745.
393. **Naderi J, Bernreuther C, Grabinski N, Putman CT, Henkel B, Bell G, Glatzel M, Sultan KR.** 2009. Plasminogen activator inhibitor type 1 up-regulation is associated with skeletal muscle atrophy and associated fibrosis. *Am J Pathol* **175:**763-771.
394. **Krause MP, Moradi J, Nissar AA, Riddell MC, Hawke TJ.** 2011. Inhibition of plasminogen activator inhibitor-1 restores skeletal muscle regeneration in untreated type 1 diabetic mice. *Diabetes* **60:**1964-1972.
395. **Krause MP, Al-Sajee D, D'Souza DM, Rebalka IA, Moradi J, Riddell MC, Hawke TJ.** 2013. Impaired macrophage and satellite cell infiltration occurs in a muscle-specific fashion following injury in diabetic skeletal muscle. *PLoS One* **8:**e70971.
396. **Saini C, Brown SA, Dibner C.** 2015. Human peripheral clocks: applications for studying circadian phenotypes in physiology and pathophysiology. *Front Neurol* **6:**95.